

Brain parenchymal changes on magnetic resonance imaging in cerebrovascular diseases

Rashid Ghaznawi

Brain parenchymal changes on magnetic resonance imaging in cerebrovascular diseases

PhD thesis, Utrecht University, The Netherlands

Copyright © Rashid Ghaznawi, 2022

ISBN: 978-94-6469-103-0

Cover design and lay-out: ProefschriftMaken || www.proefschriftmaken.nl

Printed by: ProefschriftMaken || www.proefschriftmaken.nl

All rights reserved. No part of this thesis may be reproduced or transmitted in any form or by any means without prior written permission from the author. The copyright of the articles that have been published or accepted for publication has been transferred to the respective journals.

This research was supported by the European Research Council (grant agreement numbers 637024 and 66681) and the Netherlands Organization for Scientific Research (NWO) under grant agreement number 904-65-095

Financial support by the Dutch Heart Foundation for the publication of this thesis is gratefully acknowledged

Additional financial support was provided by Alzheimer Nederland

Brain parenchymal changes on magnetic resonance imaging in cerebrovascular diseases

Veranderingen in het hersenparenchym op magnetische resonantie beeldvorming in cerebrovasculaire ziekten

(met een samenvatting in het Nederlands)

Proefschrift

ter verkrijging van de graad van doctor aan de
Universiteit Utrecht
op gezag van de
rector magnificus, prof.dr. H.R.B.M. Kummeling,
ingevolge het besluit van het college voor promoties
in het openbaar te verdedigen op

dinsdag 13 december 2022 des middags te 12.15 uur

door

Rashid Ghaznawi

geboren op 6 augustus 1988
te Kabul, Afghanistan

Promotoren:

Prof. dr. J. Hendrikse
Prof. dr. Y. van der Graaf

Copromotoren:

Dr. M.I. Geerlings
Dr. J.H.J.M. de Bresser

Voor mijn moeder...

"A gem cannot be polished without friction, nor a man perfected without trials"

Lucius Annaeus Seneca (Roman philosopher)

CONTENTS

Chapter 1	General introduction	9
PART I QUANTITATIVE BRAIN PARENCHYMAL MRI MARKERS		
Chapter 2	The association between lacunes and white matter hyperintensity features on MRI: The SMART-MR Study	21
Chapter 3	Association of white matter hyperintensity markers on MRI and long-term risk of mortality and ischemic stroke. The SMART-MR Study	47
Chapter 4	MRI phenotypes of the brain are related to future stroke and mortality in patients with manifest arterial disease: The SMART-MR study	69
PART II MICROINFARCTS IN THE DEEP GRAY MATTER ON MRI		
Chapter 5	Detection and characterization of small infarcts in the caudate nucleus on 7 Tesla MRI: The SMART-MR study	95
Chapter 6	Microinfarcts in the deep gray matter on 7 tesla MRI: Risk factors, MRI correlates and relation to cognitive functioning. The SMART-MR study	115
PART III DETERMINANTS OF BRAIN ATROPHY PROGRESSION ON MRI		
Chapter 7	Low-grade carotid artery stenosis is associated with progression of brain atrophy and cognitive decline. The SMART-MR study	139
Chapter 8	Carotid artery stenosis and progression of hemispheric brain atrophy. The SMART-MR study	161
Chapter 9	Reduced parenchymal cerebral blood flow is associated with greater progression of brain atrophy. The SMART-MR study	179
Chapter 10	General discussion	201

Appendices

Dutch summary (Nederlandse samenvatting)	214
Acknowledgements (Dankwoord)	217
Curriculum Vitae	219
List of publications	220

CHAPTER 1

1

General introduction

Cerebrovascular disease refers to a wide variety of conditions that lead to pathological changes in the blood vessels of the brain.¹ These blood vessel abnormalities can result in brain parenchymal changes that can be detected on imaging or neuropathology.¹ Two common forms of cerebrovascular disease are cerebral small vessel disease and large vessel disease.²

Cerebral small vessel disease (CSVD) refers to a group of pathological changes affecting the cerebral small arteries, arterioles, venules and capillaries.³ Age-related CSVD, hypertension-related CSVD, and cerebral amyloid angiopathy are thought to represent the most common subtypes.³ Several brain parenchymal changes can be seen in CSVD on imaging, including white matter hyperintensities (WMH) of presumed vascular origin, lacunes, cerebral microbleeds, brain atrophy and enlarged perivascular spaces.⁴ From a clinical perspective, CSVD is a leading cause of ischemic stroke, cognitive decline and dementia.⁴

Large vessel disease (LVD) refers to the formation of atheromatous plaque along the lining of large and medium-sized arteries that are located inside or outside of the brain.⁵ Carotid artery stenosis (CAS) is an example of the latter and represents a common form of LVD.⁶ From a clinical perspective, LVD can lead to ischemic stroke through several mechanisms. First, advanced atheromatous plaque can encroach on the arterial lumen and occlude an artery, resulting in infarction of the parenchyma in subserved brain regions.⁵ Second, encroachment of the plaque on the arterial lumen can lead to severe stenosis with reduced blood flow through an artery, potentially resulting in ischemia or infarction of subserved brain regions.⁷ Third, small fragments or blood clots can detach from the atheromatous plaque, travel through the bloodstream, and occlude cerebral arteries resulting in infarction (i.e., embolic stroke).⁸ The latter two mechanisms are especially relevant in the relationship between CAS and ischemic stroke.⁶

Magnetic resonance imaging in cerebrovascular disease

The advent and clinical application of magnetic resonance imaging (MRI) in the early 1980s has substantially increased the knowledge on cerebrovascular diseases and their impact on the brain parenchyma.⁹ MRI is a technique based on the physical principle of nuclear magnetic resonance.⁹ Over time, MRI has become the imaging modality of choice in clinical neuroimaging. Aside from its clinical application, MRI has also proven valuable in visualizing brain parenchymal changes in a research setting. Image segmentation techniques applied to MRI scans, for example, allow quantification of brain volumes and thereby enable researchers to measure the exact progression of brain atrophy in individual patients and in prospective cohort studies.¹⁰ In addition, volumes of WMH of presumed vascular origin can be accurately determined using MRI segmentation techniques.¹¹ Recently, the use of ultra-high field 7T MRI has enabled researchers to visualize the smallest pathological changes in the brain parenchyma.¹² Cerebral microinfarcts, which represent

small ischemic lesions until recently only visible on histopathologic examination, can now be reliably detected on 7T brain MRI.¹³

Brain parenchymal changes on MRI and clinical outcomes

In the last decades, extensive research in the field of cerebrovascular diseases has been performed on the relationship between pathologic brain parenchymal changes on MRI and clinical outcomes. These studies have shown that lacunes, extensive WMH of presumed vascular origin, and accelerated brain atrophy on MRI relate to a considerably increased risk of mortality and ischemic stroke.^{14, 15} Moreover, studies indicate that brain parenchymal changes associated with CSVD and LVD on brain MRI correlate with worse cognitive performance, dementia, and cognitive decline.¹⁶ Together, these results underline the importance of MRI in detecting brain parenchymal changes that can lead to future detrimental clinical outcomes.

Although great progress has been made in determining the clinical value of brain parenchymal changes on MRI, the relationship between several novel MRI markers of cerebrovascular disease and clinical outcomes remains unknown. For example, as noted previously, microinfarcts in the cerebral cortex can now be detected using 7T MRI, and these lesions have been shown to correlate with worse cognitive performance.¹³ *In vivo* data on the relationship between microinfarcts in the deep gray matter and cognitive functioning, however, is not available. Similarly, previous studies showed that increasing volume of WMH of presumed vascular origin on MRI relates to an increased risk of mortality¹⁴, however it is not known whether this is also the case for other WMH markers such as shape or subtype. Lastly, until recently, brain parenchymal changes on MRI such as infarcts, lacunes and WMH have been analysed separately with respect to their relationship to clinical outcomes.¹⁷⁻²⁰ As these lesions frequently coincide with each other, an alternative approach would be to perform a combined analysis of brain MRI abnormalities. In this approach, patients with similar brain parenchymal changes on MRI are first classified into clusters (i.e., MRI phenotypes) using a machine learning method, after which the relation between these MRI phenotypes and clinical outcomes is determined. This approach, which has led to a greater understanding of the etiologic relationship between determinants and detrimental clinical outcomes in other research fields such as asthma^{21, 22}, has not been previously applied in the field of cerebrovascular disease.

Determinants of brain parenchymal changes on MRI

In addition to examining the relation between brain parenchymal changes and clinical outcomes, it is also important to identify their determinants (i.e., risk factors), as these may represent potential targets for intervention.

With respect to cerebral cortical microinfarcts on MRI, recent studies showed that their risk factors are heterogeneous, and their occurrence has been associated with MRI

correlates of CSVD and LVD.¹³ Data on microinfarcts in the deep gray matter, however, are scarce and are primarily derived from post-mortem studies^{23, 24}, whereas *in vivo* MRI studies examining their prevalence and risk factors are currently lacking.

Similar to cerebral microinfarcts, brain atrophy also represents a brain parenchymal change that is associated with poor clinical outcomes including occurrence of dementia.²⁵ The determinants of brain atrophy are not entirely clear, however it is thought that CSVD may play an important role in progression of brain atrophy.⁴ Recent studies suggests that presence of CAS may also represent a risk factor for greater brain volume loss over time.²⁷ Several aspects of this relationship, however, are not understood. First, previous studies reported that only severe CAS was related to greater progression of brain atrophy²⁷, however a recent cross-sectional analysis in a population-based cohort demonstrated that even low-grade (i.e., mild) CAS was associated with smaller brain volumes.²⁹ To our knowledge, no studies have yet examined whether there also exists a temporal relation between low-grade CAS and progression of brain atrophy over time. Second, it remains to be determined whether CAS impacts both cerebral hemispheres, or whether the effect is primarily on the cerebral hemisphere ipsilateral to the side of stenosis. A cross-sectional study suggests the latter³⁰, however longitudinal data on the impact of CAS on cerebral hemispheric volumes are lacking.

Another potential risk factor for progression of brain atrophy is reduced cerebral blood flow. In cross-sectional analyses, reduced cerebral blood flow correlated with smaller brain volumes.³¹⁻³³ However, in the only longitudinal study with a relatively short follow-up period, it was shown that smaller brain volumes at baseline were associated with a greater decrease in cerebral blood flow over time, rather than vice versa.³⁴ These contradictory findings warrant long-term longitudinal studies on this topic. Such studies are of particular importance as cerebral blood flow can be modified, and may therefore pose a potential target for future prevention strategies of brain atrophy progression.^{35, 36}

SMART-MR study

In this thesis, we used data from the Second Manifestations of ARterial disease-Magnetic Resonance (SMART-MR) study, a prospective cohort study at the University Medical Center Utrecht with the aim to investigate risk factors and consequences of brain changes on MRI in patients with symptomatic atherosclerotic disease.³⁷ Between 2001 and 2005, 1309 middle-aged and older adult persons newly referred to the University Medical Center Utrecht for treatment of symptomatic atherosclerotic disease (coronary artery disease, cerebrovascular disease, peripheral arterial disease or abdominal aortic aneurysm) were included for vascular risk factor and cognitive functioning assessment, and a 1.5T brain MRI. Of the 1309 persons included at baseline, 754 had follow-up measurements after an average of four years between January 2006 and May 2009. Between November 2013 and October 2017, 329 persons were included for second follow-up measurements, of which 213 also underwent a 7T brain MRI.

Outline of this thesis

The aim of this thesis is to investigate the detection, determinants and relation to clinical outcomes of several brain parenchymal changes on MRI. These brain parenchymal changes include WMH of presumed vascular origin, cerebral microinfarcts in the deep gray matter, and brain atrophy.

In **part I**, we will focus on WMH. Specifically, in **Chapter 2**, we examine whether quantitative WMH markers (volume, shape and type) can be obtained from 1.5T brain MRI scans and whether these markers are related to presence of lacunes (together with WMH a hallmark feature of CSVD). Next, in **Chapter 3**, we examine whether these quantitative WMH markers are related to future adverse clinical outcomes, including mortality and occurrence of ischemic stroke. Finally, in **Chapter 4**, we investigate whether MRI phenotypes (in part based on quantitative WMH markers) can be obtained using a machine learning method, and whether these phenotypes are related to risk of future mortality and ischemic stroke.

In **part II**, we focus on microinfarcts in the deep gray matter on 7T brain MRI. Specifically, in **Chapter 5**, we examine whether small infarcts and microinfarcts can be detected reliably in the caudate nucleus on 7T brain MRI scans. Next, in **Chapter 6**, we report on the determinants (i.e., risk factors) of microinfarcts in the deep gray matter and their relation to cognitive functioning.

In **part III**, we focus on CAS and cerebral blood flow as potential determinants of brain atrophy. In **Chapter 7**, we examine whether low-grade CAS on baseline ultrasound is associated with greater progression of brain atrophy on MRI. In **Chapter 8**, we investigate whether increasing degrees of CAS on baseline ultrasound is associated with greater hemispheric brain atrophy on MRI. The bidirectional relationship between parenchymal cerebral blood and brain atrophy, both measured on MRI, is examined in **Chapter 9**.

Lastly, in **Chapter 10**, we will discuss the main findings of this thesis and future prospects of research.

References

1. Donahue MJ, Achten E, Cogswell PM, et al. Consensus statement on current and emerging methods for the diagnosis and evaluation of cerebrovascular disease. *J Cereb Blood Flow Metab* 2018; 38: 1391-1417.
2. Brisset M, Boutouyrie P, Pico F, et al. Large-vessel correlates of cerebral small-vessel disease. *Neurology* 2013; 80: 662-669.
3. Pantoni L. Cerebral small vessel disease: from pathogenesis and clinical characteristics to therapeutic challenges. *Lancet Neurol* 2010; 9: 689-701.
4. Wardlaw JM, Smith C and Dichgans M. Mechanisms of sporadic cerebral small vessel disease: insights from neuroimaging. *Lancet Neurol* 2013; 12: 483-497.
5. Campbell BCV and Khatiri P. Stroke. *The Lancet* 2020; 396: 129-142.
6. Barnett HJM, Taylor DW, Haynes RB, et al. Beneficial effect of carotid endarterectomy in symptomatic patients with high-grade carotid stenosis. *N Engl J Med* 1991; 325: 445-453.
7. Caplan LR, Wong KS, Gao S, et al. Is Hypoperfusion an Important Cause of Strokes? If So, How? *Cerebrovascular Diseases* 2006; 21: 145-153.
8. Futrell N. Pathophysiology of Acute Ischemic Stroke: New Concepts in Cerebral Embolism. *Cerebrovascular Diseases* 1998; 8(suppl 1): 2-5.
9. Doyle FH, Gore JC, Pennock JM, et al. Imaging of the brain by nuclear magnetic resonance. *Lancet* 1981; 2: 53-57.
10. de Bresser J, Portegies MP, Leemans A, et al. A comparison of MR based segmentation methods for measuring brain atrophy progression. *Neuroimage* 2011; 54: 760-768.
11. Kuijf HJ, Biesbroek JM, De Bresser J, et al. Standardized Assessment of Automatic Segmentation of White Matter Hyperintensities and Results of the WMH Segmentation Challenge. *IEEE Trans Med Imaging* 2019; 38: 2556-2568.
12. Harteveld AA, van der Kolk AG, Zwanenburg JJ, et al. 7-T MRI in Cerebrovascular Diseases: Challenges to Overcome and Initial Results. *Top Magn Reson Imaging* 2016; 25: 89-100.
13. van Veluw SJ, Shih AY, Smith EE, et al. Detection, risk factors, and functional consequences of cerebral microinfarcts. *Lancet Neurol* 2017; 16: 730-740.
14. Debette S, Beiser A, DeCarli C, et al. Association of MRI markers of vascular brain injury with incident stroke, mild cognitive impairment, dementia, and mortality: the Framingham Offspring Study. *Stroke* 2010; 41: 600-606.
15. Henneman WJ, Sluimer JD, Cordonnier C, et al. MRI biomarkers of vascular damage and atrophy predicting mortality in a memory clinic population. *Stroke* 2009; 40: 492-498.
16. Kuller LH, Lopez OL, Newman A, et al. Risk factors for dementia in the cardiovascular health cognition study. *Neuroepidemiology* 2003; 22: 13-22.
17. Kuller LH, Longstreth WT, Jr., Arnold AM, et al. White matter hyperintensity on cranial magnetic resonance imaging: a predictor of stroke. *Stroke* 2004; 35: 1821-1825.
18. Chen X, Wen W, Anstey KJ, et al. Prevalence, incidence, and risk factors of lacunar infarcts in a community sample. *Neurology* 2009; 73: 266-272.

19. Gouw AA, van der Flier WM, Fazekas F, et al. Progression of white matter hyperintensities and incidence of new lacunes over a 3-year period: the Leukoaraiosis and Disability study. *Stroke* 2008; 39: 1414-1420.
20. Gouw AA, van der Flier WM, Pantoni L, et al. On the etiology of incident brain lacunes: longitudinal observations from the LADIS study. *Stroke* 2008; 39: 3083-3085.
21. Moore WC, Meyers DA, Wenzel SE, et al. Identification of asthma phenotypes using cluster analysis in the Severe Asthma Research Program. *Am J Respir Crit Care Med* 2010; 181: 315-323.
22. Haldar P, Pavord ID, Shaw DE, et al. Cluster analysis and clinical asthma phenotypes. *Am J Respir Crit Care Med* 2008; 178: 218-224.
23. White L, Petrovitch H, Hardman J, et al. Cerebrovascular pathology and dementia in autopsied Honolulu-Asia Aging Study participants. *Ann N Y Acad Sci* 2002; 977: 9-23.
24. Troncoso JC, Zonderman AB, Resnick SM, et al. Effect of infarcts on dementia in the Baltimore longitudinal study of aging. *Ann Neurol* 2008; 64: 168-176.
25. Jack CR, Jr., Shiung MM, Gunter JL, et al. Comparison of different MRI brain atrophy rate measures with clinical disease progression in AD. *Neurology* 2004; 62: 591-600.
26. Jack CR, Jr., Shiung MM, Weigand SD, et al. Brain atrophy rates predict subsequent clinical conversion in normal elderly and amnesic MCI. *Neurology* 2005; 65: 1227-1231.
27. Muller M, van der Graaf Y, Algra A, et al. Carotid atherosclerosis and progression of brain atrophy: the SMART-MR study. *Ann Neurol* 2011; 70: 237-244.
28. Romero JR, Beiser A, Seshadri S, et al. Carotid artery atherosclerosis, MRI indices of brain ischemia, aging, and cognitive impairment: the Framingham study. *Stroke* 2009; 40: 1590-1596.
29. Alhusaini S, Karama S, Nguyen TV, et al. Association between carotid atheroma and cerebral cortex structure at age 73 years. *Ann Neurol* 2018; 84: 576-587.
30. Enzinger C, Ropele S, Gatteringer T, et al. High-grade internal carotid artery stenosis and chronic brain damage: a volumetric magnetic resonance imaging study. *Cerebrovasc Dis* 2010; 30: 540-546.
31. Alosco ML, Gunstad J, Jerskey BA, et al. The adverse effects of reduced cerebral perfusion on cognition and brain structure in older adults with cardiovascular disease. *Brain Behav* 2013; 3: 626-636.
32. van Es AC, van der Grond J, ten Dam VH, et al. Associations between total cerebral blood flow and age related changes of the brain. *PLoS One* 2010; 5: e9825.
33. Benedictus MR, Binnewijzend MAA, Kuijjer JPA, et al. Brain volume and white matter hyperintensities as determinants of cerebral blood flow in Alzheimer's disease. *Neurobiol Aging* 2014; 35: 2665-2670.
34. Zonneveld HI, Loehrer EA, Hofman A, et al. The bidirectional association between reduced cerebral blood flow and brain atrophy in the general population. *J Cereb Blood Flow Metab* 2015; 35: 1882-1887.
35. Espeland MA, Luchsinger JA, Neiberg RH, et al. Long Term Effect of Intensive Lifestyle Intervention on Cerebral Blood Flow. *J Am Geriatr Soc* 2018; 66: 120-126.

36. de la Torre JC. Cerebral Perfusion Enhancing Interventions: A New Strategy for the Prevention of Alzheimer Dementia. *Brain Pathol* 2016; 26: 618-631.
37. Geerlings MI, Appelman AP, Vincken KL, et al. Brain volumes and cerebrovascular lesions on MRI in patients with atherosclerotic disease. The SMART-MR study. *Atherosclerosis* 2010; 210: 130-136.

PART I



Quantitative brain parenchymal MRI markers

CHAPTER 2

2

The association between lacunes and white matter hyperintensity features on MRI. The SMART-MR study

Rashid Ghaznawi ^{1,2}, Mirjam I. Geerlings ², Myriam G. Jaarsma-Coes ^{1,3}, Maarten H.T. Zwartbol ¹, Hugo J. Kuijff ⁴, Yolanda van der Graaf ², Theo D. Witkamp ¹, Jeroen Hendrikse ¹, Jeroen de Bresser ^{1,3}; on behalf of the SMART Study Group

¹Department of Radiology, University Medical Center Utrecht, Netherlands; ²Julius Center for Health Sciences and Primary Care, University Medical Center Utrecht, Netherlands; ³Department of Radiology, Leiden University Medical Center, Netherlands; ⁴Image Sciences Institute, University Medical Center Utrecht, Netherlands

Lacunae and white matter hyperintensities (WMH) are features of cerebral small vessel disease (CSVD) that are associated with poor functional outcomes. However, how the two are related remains unclear. In this study, we examined the association between lacunae and several WMH features in patients with a history of vascular disease. A total of 999 patients (mean age 59 ± 10 years) with a 1.5 T brain MRI scan were included from the SMART-MR study. Lacunae were scored visually and WMH features (volume, subtype and shape) were automatically determined. Analyses consisted of linear and Poisson regression adjusted for age, sex and total intracranial volume. Patients with lacunae ($n=188$; 19%) had greater total ($B=1.03$, 95%CI=0.86 to 1.21), periventricular/confluent ($B=1.08$, 95%CI=0.89 to 1.27) and deep ($B=0.71$, 95%CI=0.44 to 0.97) natural log-transformed WMH volumes than patients without lacunae. Patients with lacunae had an increased risk of confluent type WMH (RR=2.41, 95%CI=1.98 to 2.92) and deep WMH (RR=1.41, 95%CI=1.22 to 1.62), and had a more irregular shape of confluent WMH than patients without lacunae, independent of total WMH volume. In conclusion, we found that lacunae on MRI were associated with WMH features that correspond to more severe small vessel changes, mortality and poor functional outcomes.

Introduction

Cerebral small vessel disease (CSVD) is a major cause of cognitive decline and dementia¹⁻³. Lacunes and white matter hyperintensities of presumed vascular origin (WMH) are considered hallmark MRI features of CSVD and are frequently observed in older individuals⁴. WMH appear as hyperintense lesions on MRI in fluid attenuated inversion recovery (FLAIR) images⁵. Lacunes are round or ovoid, subcortical, fluid filled cavities of between 3 mm and 15 mm in diameter with a signal intensity similar to cerebrospinal fluid⁵.

CSVD is a highly prevalent disease in which the clinical spectrum that can range from asymptomatic disease through to vascular dementia⁶. Previous histopathological studies have shown that WMH correspond to different underlying brain parenchymal changes⁷. Smooth, periventricular lesions are associated with mild, non-ischemic parenchymal changes⁸. In contrast, irregular and confluent WMH are associated with more severe brain parenchymal changes, including loss of myelin and incomplete parenchymal destruction⁸⁻¹⁰. Functionally, confluent and deep WMH are associated with cognitive impairment, gait disturbances, mortality and a higher risk of stroke, while these associations have not been found for periventricular lesions¹¹⁻¹⁴. Lacunes, previously thought to arise solely from lacunar infarcts, are now considered lesions that may result from different causes, such as small hemorrhages, infarcts microembolism and amyloid angiopathy⁵. Importantly, there is increasing evidence that presence of lacunes on MRI is associated with cognitive impairment and poor clinical outcomes after stroke¹⁵⁻¹⁷. The relationship between lacunes and WMH features, however, remains unclear. As lacunes can have profound clinical consequences, examining the relationship between the two may aid in identifying patients with certain WMH characteristics that are prone to develop lacunes.

To better define the relationship between lacunes and WMH features, we developed an automated method to assess different WMH features (volume, subtype and shape) on brain MRI¹⁸. With this method, we investigated the relationship between lacunes and WMH features in a large group of patients with a history of vascular disease.

Material and methods

Study population and study sample

Data were used from the Second Manifestations of ARterial disease-Magnetic Resonance (SMART-MR) study, a prospective cohort study at the University Medical Center Utrecht with the aim to investigate risk factors and consequences of brain changes on MRI in patients with symptomatic atherosclerotic disease¹⁹. In brief, between 2001 and 2005, 1309 middle-aged and older adult persons newly referred to the University Medical Center Utrecht for treatment of symptomatic atherosclerotic disease (manifest coronary artery disease, cerebrovascular disease, peripheral arterial disease or abdominal aortic aneurysm)

were included for baseline measurements. During a one day visit to our medical center, a physical examination, ultrasonography of the carotid arteries to measure the intima-media thickness (mm), blood and urine samplings, neuropsychological assessment and a 1.5 T brain MRI scan were performed. The height and weight of patients were measured, and the body mass index (kg/m^2) was calculated. Questionnaires were used for the assessment of demographics, risk factors, medical history, medication use and cognitive and physical functioning. The SMART-MR study was approved by the medical ethics committee of the University Medical Center Utrecht according to the guidelines of the Declaration of Helsinki of 1975 and written informed consent was obtained from all participants.

Of the 1309 patients included in the SMART-MR study, MRI data were irretrievable for 19 patients and 239 patients had missing data of one or more MRI sequences due to motion artefacts or logistic reasons. Of the remaining 1051 patients, 44 had unreliable brain volume data due to motion artefacts in all three MRI sequences, and four patients were excluded due to severe undersegmentation of WMH by the automated segmentation program. Four patients were excluded because they did not have any WMH greater than five voxels. As a result, 999 patients were included in the current study.

Cardiovascular risk factors

Smoking habits and alcohol intake were assessed with questionnaires, and were categorized as never, former or current. Height and weight were measured, and the body mass index (BMI) was calculated (kg/m^2). Systolic blood pressure (mmHg) and diastolic blood pressure (mmHg) were measured three times with a sphygmomanometer, and the average of these measures was calculated. Hypertension was defined as a mean SBP of ≥ 160 mmHg, a mean DBP of ≥ 95 mmHg, self-reported use of antihypertensive drugs, or a known history of hypertension at inclusion. An overnight fasting venous blood sample was taken to determine glucose and lipid levels. Diabetes mellitus was defined as the use of glucose-lowering drugs, a known history of diabetes mellitus, or a fasting plasma glucose level of >11.1 mmol/l. Hyperlipidemia was defined as a total cholesterol of >5.0 mmol/l, a low-density lipoprotein cholesterol of >3.2 mmol/l, use of lipid-lowering drugs, or a known history of hyperlipidemia. Mean carotid intima-media thickness (in mm) was calculated for the left and right common carotid arteries based on six far-wall measurements on ultrasound.

Magnetic resonance imaging

MR imaging of the brain was performed on a 1.5 T whole-body system (Gyrosan ACS-NT, Philips Medical Systems, Best, the Netherlands) using a standardized scan protocol consisting of two-dimensional multi-slice sequences. Transversal T1-weighted [gradient-echo; repetition time (TR) = 235 ms; echo time (TE) = 2 ms], T2-weighted [turbo spin-echo; TR = 2200 ms; TE = 11 ms], fluid-attenuated inversion recovery (FLAIR) [turbo spin-echo; TR = 6000 m; TE = 100 ms; inversion time (TI) = 2000 ms] and T1-weighted inversion

recovery images [turbo spin-echo ; TR = 2900 ms; TE = 22 ms; TI = 410 ms] were acquired. All MR sequences had a resolution of $1.0 \times 1.0 \times 4.0 \text{ mm}^3$ and consisted of 38 contiguous slices (field of view 230 mm x 230 mm; matrix size 180 x 256, slice gap 0 mm).

Lacunes were visually rated by a neuroradiologist (TW) blinded to patient characteristics on the T1-weighted, T2-weighted and FLAIR images. We defined lacunes as focal lesions between 3 to 15 mm according to the STRIVE criteria⁵. Brain infarcts were visually rated by a neuroradiologist (TW) blinded to patient characteristics on the T1-weighted, T2-weighted and FLAIR images.

Assessment of WMH volumes and other brain volumes

WMH volumes were obtained using an automated segmentation program on the T1-weighted, FLAIR and T1-weighted inversion recovery sequences of the MR scans. A probabilistic segmentation technique was performed with k -nearest neighbor classification²⁰, distinguishing gray matter, white matter, cerebrospinal fluid and lesions. Cerebral infarcts, including lacunes and their hyperintense rim, were manually segmented. WMH segmentations were visually checked by an investigator (RG) using an image processing framework (MeVisLab 2.7.1., MeVis Medical Solutions AG, Bremen, Germany) to ensure that all cerebral infarcts were correctly removed from the WMH segmentations. Incorrectly segmented voxels were automatically added to the correct segmentation volumes. Next, ventricle segmentation was performed using the fully automated lateral ventricle delineation (ALVIN) algorithm²¹ in Statistical Parametric Mapping 8 (SPM8, Wellcome Trust Centre for Neuroimaging, University College London, London, UK) for Matlab (The MathWorks, Inc., Natick, Massachusetts, United States). The ALVIN mask was used to determine the margins of the lateral ventricles. A threshold of 10% was applied to the WMH probability maps to obtain binary data. A group of voxels was considered a WMH lesion if their faces, edges or corners touched along either one, two or all three of the primary axes (26-connectivity rule). WMH were labelled based on their continuity with the margins of the lateral ventricle and the extension from the lateral ventricle into the white matter. We defined periventricular WMH as lesions contiguous with the margins of the lateral ventricles and extending up to and including 10 mm from the lateral ventricle into the white matter. Confluent WMH were defined as lesions contiguous with the margins of the lateral ventricles and extending more than 10 mm from the lateral ventricles into the white matter. Deep WMH were defined as lesions that were separated from the margins of the lateral ventricles, regardless of their distance to the margins of the lateral ventricles. Total WMH volume was defined as the sum of periventricular or confluent WMH and all deep WMH. Examples of periventricular, confluent and deep WMH visualized in our algorithm are shown in Figure 1. The automatically assigned lesion labels were visually checked by an investigator (MJC) and manually corrected if necessary.

Total brain volume was calculated by summing the volumes of gray matter, white matter, total WMH and, if present, the volumes of brain infarcts¹⁹. Total intracranial volume (ICV) was calculated by summing the cerebrospinal fluid volume and total brain volume.

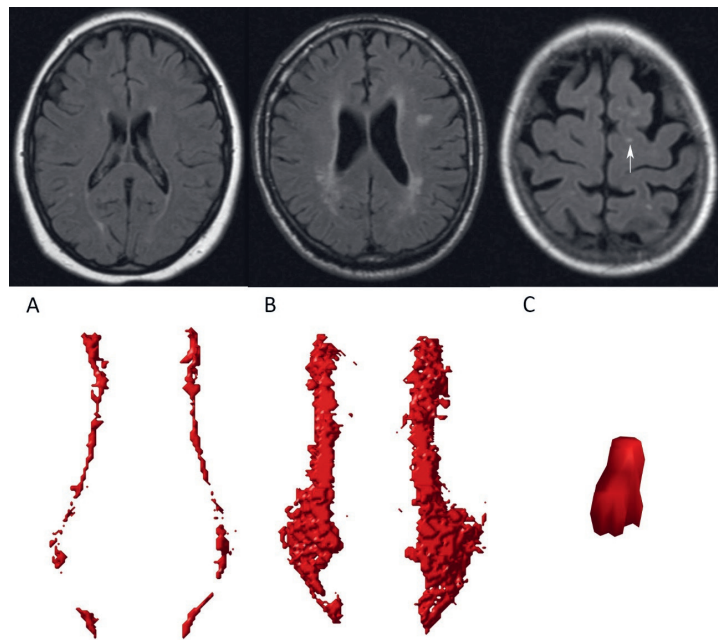


Figure 1. Examples of periventricular (A), confluent (B) and deep (C) WMH visualized in our algorithm. The corresponding FLAIR images are shown above. The deep WMH lesion (arrow) is reconstructed in the coronal view, while the periventricular and confluent WMH are viewed from a transverse perspective.

Assessment of WMH subtypes

To assess whether different WMH subtypes were associated with lacunes, patients were categorized into the following three WMH subtypes; periventricular WMH without deep WMH, periventricular WMH with deep WMH and confluent WMH. The rationale behind the WMH subtype definitions is described in the Supplementary Material.

Assessment of WMH shape

We assessed WMH shape using shape features¹⁸. WMH shape features were calculated from the binary segmentation data for all patients. Definitions and selection of shape features are described in the Supplementary Material and Supplementary Table 1. In short, we analyzed periventricular and confluent WMH by reconstructing convex hulls and calculating volume and surface area ratios. Solidity was obtained by dividing lesion volume by the volume of its convex hull, while convexity was obtained by dividing the convex hull surface area by the lesion's surface area. The concavity index²² was calculated from the solidity and convexity. A mean value for solidity, convexity and concavity index was calculated for each patient. For deep WMH, we calculated eccentricity by dividing the minor axis of a lesion by its major axis. In case of multiple deep WMH, a mean value

for eccentricity was calculated across all deep WMH per patient. Fractal dimension was calculated for periventricular, confluent and deep WMH using the box counting method. A mean value for fractal dimension was calculated for periventricular or confluent WMH and deep WMH for each patient. Examples of WMH that correspond to a low or high value of WMH shape features are shown in Supplementary Table 2.

Statistical analysis

First, baseline characteristics and WMH features (volume, subtype and shape) of patients with lacunes and patients without lacunes were compared using an independent samples t-test or Chi-square test.

Second, linear regression analyses were performed to compare total, periventricular or confluent, and deep WMH volumes (natural log-transformed) in patients with lacunes versus patients without lacunes, adjusted for age, sex and ICV. These analyses were repeated in patients with one lacune versus patients with multiple lacunes.

Third, relative risks for a confluent WMH subtype or a periventricular WMH subtype with deep WMH were estimated using Poisson regression with robust error variance for patients with lacunes compared to patients without lacunes, adjusted for age, sex and ICV. These analyses were repeated in patients with one lacune versus patients with multiple lacunes. A periventricular WMH subtype without deep WMH was chosen as the reference category.

Fourth, we assessed the association between lacunes and WMH shape features. Due to inherent shape differences between periventricular and confluent WMH visible on MRI, analyses were performed across strata of three WMH subtypes (periventricular without deep WMH (n=360), periventricular with deep WMH (n=424) and confluent WMH (n=215)). Z-scores were calculated for the WMH shape features to facilitate the comparison between these features. Linear regression analyses were performed with presence of lacunes as independent variable and shape descriptor Z-scores as dependent variable. In the first model, we adjusted for age and sex. In the second model, we additionally adjusted for total WMH volume (%ICV) to assess to what extent the observed relationships were explained by WMH volume. The linear regression analyses were repeated in patients with one lacune versus patients with multiple lacunes.

A *p*-value of < 0.05 was considered to be statistically significant. SAS 9.4 (SAS Institute, Cary, NC, USA) and SPSS 21.0 (Chicago, IL, USA) were used to analyze our data.

Results

Baseline characteristics for patients with lacunes (n=188; 19%) and without lacunes (n=811; 81%), and for the total study sample (n=999) are shown in Table 1. A total number of 439 lacunes were scored in 188 patients (range: 1 to 12 lacunes per patient). Eighty-six patients (9%) showed one lacune on MRI, while 102 patients (10%) showed multiple

lacunes on MRI. Of the patients with multiple lacunes, the majority (72%) showed two or three lacunes on MRI.

Patients with lacunes were older ($p < 0.0001$), more often had diabetes mellitus ($p = 0.006$) and hypertension ($p < 0.0001$), had a higher IMT ($p < 0.0001$), but also had a lower BMI compared to patients without lacunes ($p = 0.02$). WMH features of patients with lacunes, patients without lacunes and of the total study population are shown in Table 2. Patients with lacunes showed greater WMH volumes and were more likely to have a confluent WMH subtype than patients without lacunes ($p < 0.0001$). In patients with lacunes, periventricular and confluent WMH showed a lower solidity ($p < 0.0001$) and higher fractal dimension ($p < 0.0001$) than patients without lacunes.

Association between lacunes and WMH volumes

Results of the linear regression analyses with total, periventricular or confluent, and deep WMH volumes (natural log transformed) as dependent variables and lacunes as independent variable are shown in Table 3. After adjusting for age, sex and total intracranial volume, patients with lacunes had greater total ($B = 1.03$, 95% CI 0.86 to 1.21), periventricular or confluent ($B = 1.08$, 95% CI 0.89 to 1.27) and deep ($B = 0.71$, 95% CI 0.44 to 0.97) WMH volumes than patients without lacunes. Patients with multiple lacunes had greater total ($B = 0.36$, 95% CI 0.05 to 0.67) and periventricular or confluent ($B = 0.37$, 95% CI 0.03 to 0.70) WMH volumes than patients with one lacune, however no significant difference was found for deep WMH volumes ($B = -0.08$, 95% CI -0.54 to 0.39).

Table 1. Baseline characteristics of the patients with lacunes, patients without lacunes and the total study population.

	Patients with lacunes (n=188)	Patients without lacunes (n=811)	All patients (n=999)	<i>p</i> -value ^a
Age (years)	63 ± 10	58 ± 10	59 ± 10	<0.001
Sex, % men	81	78	79	0.37
Cardiovascular risk factors				
BMI (kg/m ²)	26.2 ± 3.5	26.9 ± 3.8	26.7 ± 3.7	0.02
Smoking, % current	28	25	25	0.34
Alcohol intake, % current	76	74	74	0.72
Hypertension, %	67	48	51	<0.001
Hyperlipidemia, %	79	78	79	0.99
Diabetes mellitus, %	27	18	20	0.006
IMT (mm)	1.04 ± 0.36	0.91 ± 0.29	0.93 ± 0.31	<0.001 ^b

Characteristics are presented as mean ± SD or %.

^a *p*-value of independent samples t-test or Chi-square test (if proportions) for comparison between patients with lacunes versus those without lacunes.

^b Between group analysis was performed on natural log transformed values due to a non-normal distribution of this characteristic.

BMI: body mass index.

IMT: intima-media thickness.

Association between lacunes and WMH subtypes

Patients with lacunes had an increased risk of a confluent WMH subtype or a periventricular WMH subtype with deep WMH than patients without lacunes (RR = 2.41, 95% CI 1.98 to 2.92, RR = 1.41, 95% CI 1.22 to 1.62, respectively), after adjusting for age, sex and total ICV (Table 4). Patients with multiple lacunes did not show an increased risk of a confluent WMH subtype or a periventricular WMH subtype with deep WMH than patients with one lacune (RR = 1.13, 95% CI 0.93 to 1.36, RR = 1.20, 95% CI 0.92 to 1.57, respectively).

Table 2. WMH features of patients with lacunes, patients without lacunes and the total study population.

	Patients with lacunes (n=188)	Patients without lacunes (n=811)	All patients (n=999)	p-value ^a
WMH volumes, ml^b				
Total	2.9 (0.5, 18.1)	0.8 (0.2, 4.0)	0.9 (0.2, 6.4)	<0.0001 ^c
Periventricular or confluent	2.3 (0.4, 17.4)	0.6 (0.1, 3.3)	0.8 (0.1, 5.4)	<0.0001 ^c
Deep	0.2 (0.0, 1.2)	0.1 (0.0, 0.7)	0.1 (0.0, 0.8)	<0.0001 ^c
WMH subtypes on MRI, %^d				
Periventricular	45	86	78	<0.0001
With deep	34	44	42	0.01
Without deep	11	42	36	<0.0001
Confluent	55	14	22	<0.0001
With deep	54	13	21	<0.0001
Without deep	1	1	1	0.22
WMH shape descriptors^e				
Periventricular or confluent				
Solidity	0.40 ± 0.20	0.61 ± 0.25	0.57 ± 0.25	<0.0001
Convexity	1.07 ± 0.17	1.08 ± 0.16	1.07 ± 0.16	0.48
Concavity index	1.13 ± 0.16	1.04 ± 0.09	1.06 ± 0.11	<0.0001
Fractal dimension	1.41 ± 0.22	1.20 ± 0.20	1.24 ± 0.22	<0.0001
Deep				
Eccentricity	0.46 ± 0.12	0.49 ± 0.15	0.48 ± 0.14	0.004
Fractal dimension	1.45 ± 0.12	1.45 ± 0.16	1.45 ± 0.15	0.77

Characteristics are presented as mean ± SD or %.

^a p-value of independent samples t-test or Chi-square test (if proportions) for comparison between the group with lacunes versus those without lacunes.

^b Median (10th percentile, 90th percentile).

^c Between group analysis was performed on natural log transformed values due to a non-normal distribution of this characteristic.

^d Percentage of patients with the WMH subtype on MRI in the group of patients with lacunes, without lacunes and in the total study population.

^e In periventricular or confluent WMH, a lower convexity, and a higher solidity, concavity index or fractal dimension correspond to a more complex lesion. In deep WMH, a higher eccentricity corresponds to a more round lesion, while a lower eccentricity corresponds to a more elongated lesion. A higher fractal dimension of a deep lesion corresponds to a more complex lesion.

Table 3. Results of linear regression analyses with lacunes on MRI as independent variable and total, periventricular or confluent WMH, and deep WMH volumes as dependent variables (all natural log transformed).

	Total	Periventricular or confluent	Deep
	B (95% CI) ^a	B (95% CI) ^a	B (95% CI) ^a
No lacunes on MRI	0 (reference)	0 (reference)	0 (reference)
Lacunes on MRI	1.03 (0.86 to 1.21) ^b	1.08 (0.89 to 1.27) ^b	0.71 (0.44 to 0.97) ^b

^a Adjusted for age, sex and total intracranial volume. B represents the natural log-transformed difference in volume between patients with and without lacunes on MRI.

^b $p < 0.0001$.

WMH: white matter hyperintensities.

Table 4. Results of Poisson regression with WMH subtype groups as dependent variable and lacunes on MRI as independent variable (n=188).

	Patients with a periventricular WMH subtype without deep WMH (n=360)	Patients with a periventricular WMH subtype with deep WMH (n=424)	Patients with a confluent WMH subtype (n=215)
	RR (95% CI)	RR (95% CI) ^a	RR (95% CI) ^a
Lacunes vs. no lacunes	1 (reference)	1.41 (1.22 to 1.62)	2.41 (1.98 to 2.92)

^a Adjusted for age, sex and total intracranial volume.

WMH: white matter hyperintensities.

RR: relative risk.

Association between lacunes and WMH shape features

Results of the linear regression analyses of the associations between lacunes and WMH shape features are shown in Table 5.

In patients with a confluent WMH subtype, presence of lacunes was associated with a more complex WMH shape (lower convexity Z score (B = -0.46, 95% CI -0.74 to -0.19) and a higher concavity index Z-score (B = 0.65, 95% CI: 0.33 to 0.97)) after adjusting for age and sex. These associations remained statistically significant after additionally adjusting for total WMH volume (B = -0.29, 95% CI: -0.55 to -0.04; B = 0.30, 95% CI: 0.10 to 0.50, respectively), indicating that patients with lacunes had a more complex WMH shape independent of WMH volume. Patients with multiple lacunes did not show a different WMH shape compared to patients with one lacune (convexity Z score B = 0.03, 95% CI: -0.34 to 0.40, concavity index Z score B = 0.17, 95% CI: -0.13 to 0.46), after adjusting for age, sex and total WMH volume. No differences were found for the remaining WMH shape features between patients with one lacune and patients with multiple lacunes. Presence of lacunes was associated with higher fractal dimension Z-scores (B = 0.28, 95% CI: 0.09

to 0.47) compared to absence of lacunes, after adjusting for age and sex. However, this association attenuated and lost statistical significance after additionally adjusting for total WMH volume ($B = 0.04$, 95% CI: -0.05 to 0.13). No statistically significant associations were found between presence of lacunes, and eccentricity and fractal dimension of deep WMH in patients with a confluent WMH subtype.

In patients with a periventricular WMH subtype with deep WMH, presence of lacunes was associated with lower solidity Z-scores ($B = -0.25$, 95% CI -0.47 to -0.02) and higher fractal dimension Z-scores ($B = 0.18$, 95% CI 0.01 to 0.36) compared to absence of lacunes, after adjusting for age and sex. This indicates more irregular shaped WMH in patients with lacunes, however the associations lost statistical significance after additionally adjusting for total WMH volume ($B = -0.04$, 95% CI -0.20 to 0.11, $B = -0.01$, 95% CI -0.09 to 0.08, respectively). Presence of lacunes was not associated with eccentricity and fractal dimension of deep WMH in these patients. WMH shape features did not differ between patients with one lacune and patients with multiple lacunes in this group.

Presence of lacunes was associated with lower solidity Z-scores ($B = -0.48$, 95% CI: -0.83 to -0.13) in patients with a periventricular WMH subtype without deep WMH, after adjusting for age and sex. After additionally adjusting for total WMH volume, this relationship attenuated and lost statistical significance ($B = -0.20$, 95% CI -0.44 to 0.05). WMH shape features did not differ between patients with one lacune and patients with multiple lacunes in this group.

Table 5. Linear regression analyses of WMH shape parameters as dependent variables and lacunes on MRI as independent variable.

WMH subtype groups ^b	Solidity periventricular or confluent WMH (Z score) ^a		Convexity periventricular or confluent WMH (Z score) ^a		Concavity index periventricular or confluent WMH (Z score) ^a		Fractal dimension periventricular or confluent WMH (Z score) ^a		Fractal dimension deep WMH (Z score) ^a	
	B (95% CI) ^c	B (95% CI) ^c	B (95% CI) ^c	B (95% CI) ^c	B (95% CI) ^c	B (95% CI) ^c	B (95% CI) ^c	B (95% CI) ^c	B (95% CI) ^c	
Patients with a periventricular WMH subtype with deep WMH (n=424)	Model 1 -0.25 (-0.47 to -0.02)*		0.17 (-0.09 to 0.44)		-0.03 (-0.19 to 0.14)		0.18 (0.01 to 0.36)*		-0.22 (-0.52 to 0.07)	
	Model 2 -0.04 (-0.20 to 0.11)		0.01 (-0.22 to 0.24)		-0.01 (-0.17 to 0.16)		-0.01 (-0.09 to 0.08)		-0.19 (-0.49 to 0.11)	
Patients with a periventricular WMH subtype without deep WMH (n=360)	Model 1 -0.48 (-0.83 to -0.13)*		0.35 (-0.06 to 0.75)		-0.15 (-0.44 to 0.13)		0.32 (-0.02 to 0.65)		NA	
	Model 2 -0.20 (-0.44 to 0.05)		0.09 (-0.24 to 0.42)		-0.03 (-0.30 to 0.26)		-0.01 (-0.18 to 0.17)		NA	
Patients with a confluent WMH subtype (n=215)	Model 1 -0.11 (-0.26 to 0.04)		-0.46 (-0.74 to -0.19)*		0.65 (0.33 to 0.97)*		0.28 (0.09 to 0.47)*		-0.02 (-0.20 to 0.16)	
	Model 2 0.02 (-0.10 to 0.13)		-0.29 (-0.55 to -0.04)*		0.30 (0.10 to 0.50)*		0.04 (-0.05 to 0.13)		-0.03 (-0.21 to 0.16)	

^a In periventricular or confluent WMH, a lower convexity, and a higher solidity, and a higher solidity, concavity index or fractal dimension correspond to a more complex lesion. In deep WMH, a higher eccentricity corresponds to a more round lesion, while a lower eccentricity corresponds to a more elongated lesion. A higher fractal dimension of a deep lesion corresponds to a more complex lesion.

^b Linear regression analyses were performed separately in each WMH subtype group.

^c B represents difference in WMH shape parameter for patients with lacunes versus those without lacunes.

Model 1: Adjusted for age and sex. Model 2: Additionally adjusted for natural log transformed total WMH volume (% ICV).

* $p < 0.05$.

WMH: white matter hyperintensities. ICV: intracranial volume. NA: not applicable.

Discussion

In this cohort of patients with a history of vascular disease, we observed that patients with lacunes on MRI had greater total, periventricular or confluent, and deep WMH volumes than patients without lacunes. Patients with lacunes also had an increased risk of confluent type WMH and deep WMH. Finally, patients with lacunes had a more irregular shape of confluent WMH than patients without lacunes, independent of total WMH volume.

Our results regarding WMH volume are in line with the findings of a prior cross-sectional MR study that used quantitative WMH volume measurements²³. In this study, greater total WMH volumes were found in patients with lacunar stroke than in non-lacunar stroke subtypes in two independent cohorts of patients with ischemic stroke²³. However, more recent studies have shown that lacunar stroke is not synonymous with lacunes and conversely, not all lacunes are due to lacunar stroke^{5, 24-27}. Therefore, it is likely that patients with lacunes in our study represent a more heterogeneous group of small vessel pathologies than solely lacunar stroke, and the results should be interpreted accordingly. In addition to the previous study²³, we showed that WMH subtype and WMH shape features are also associated with lacunes. To the best of our knowledge, these WMH features have not been previously linked to the presence of lacunes on brain MRI.

Although small vessel pathologies are considered the culprit for both lacunes and WMH, previous studies have shown that the pathological processes leading to WMH and lacunes are diverse²⁸⁻³⁰. For example, it is thought that not all lacunes are due to lacunar infarcts⁵. Rather, a lacune most likely represents damage to the brain from different etiologies, such as small hemorrhages, infarcts, microembolism, amyloid angiopathy or arteritis^{2, 26}. While it is currently impossible to determine the specific underlying small vessel pathologies in individual patients using brain MRI, several possibilities can be proposed that may explain the association between lacunes and WMH volume and subtype. First, it may be that lacunes and WMH share a common pathogenesis, while at the same time not affecting each other^{5, 24}. Alternatively, WMH may lead to the formation of lacunes through secondary hypoperfusion and ischemia in the surrounding brain parenchyma³¹. This notion has been supported by a recent study in patients with an inherited form of CSVD in which the edges of WMH were identified as a predilection site for lacunes³². Also, lacunes may promote formation of WMH, possibly through affecting white matter tract integrity³³. With regard to WMH shape, we found that lacunes are associated with more irregular WMH in patients with confluent lesions independent of WMH volume. Previous histopathological studies have demonstrated that more irregular periventricular and confluent WMH correspond to more severe small vessel changes⁷⁻⁹. While it may be that lacunes in the presence of irregular confluent WMH indicate increasing CSVD severity, it should be acknowledged that the relationship between WMH shape features as measured in our study and clinical outcomes is currently not known. To the best of our knowledge, our study is the first to quantify periventricular, confluent and deep WMH shape features

on brain MRI and further work is needed to examine whether WMH shape features are associated with clinical outcomes.

Our findings might have clinical relevance. Previous studies have shown that WMH and lacunes have consistently been associated with cognitive and functional impairment^{11, 15, 16}. The strong association between lacunes and WMH in our study suggests that lacunes may affect clinical outcomes not only through their own presence¹³, but also through the concomitant presence of WMH and vice versa. In addition, our results indicate that WMH volume and subtype should be considered as possible confounders in analyses investigating the relationship between lacunes and clinical outcomes.

We found in our study that patients with lacunes were older, more often had diabetes mellitus and hypertension, and had a higher IMT than patients without lacunes. These observations support findings of two large population-based studies in which increased age, hypertension and diabetes mellitus were found to be associated with presence of lacunes on MRI^{34, 35}. It has been hypothesized that diabetes mellitus and hypertension may lead to lipohyalinosis and microatheroma formation, respectively, in the microvasculature of the brain^{4, 24}. As discussed above, these processes can lead to acute lacunar infarcts, large acute infarcts or small hemorrhages, which eventually can lead to formation of lacunes^{4, 5, 26}. Thus, our findings add to the notion that certain vascular risk factors may be associated with lacunes, and future research is warranted to investigate whether diabetes mellitus and/or hypertension may act as possible targets for prevention or treatment of CSVD²⁴.

Although in our study patients with multiple lacunes showed a greater WMH volume than patients with only one lacune, we did not find differences for WMH subtype or WMH shape. Taken together, our data suggests that the association between lacunes and WMH is largely determined by the presence of lacunes, rather than the number of lacunes. While this finding may support the notion that WMH and lacunes result from the same underlying mechanism, future studies in different cohorts are needed to validate our findings with respect to the impact of the amount of lacunes on WMH features.

The strengths of our study are the use of a large cohort of patients in which we used quantitative WMH volume measurements and automated image processing techniques to examine multiple features of WMH and their relation to lacunes. Also, we adjusted our shape analyses for total WMH volume to determine to what extent a more irregular shape of WMH was explained by a greater WMH volume.

A limitation of our study is the cross-sectional design, which did not allow us to assess the relationship between lacunes and WMH features over time. Another limitation might be the use of a somewhat arbitrary distance of 10 mm from the margins of the lateral ventricles to differentiate periventricular from confluent WMH. It should be noted, however, that there are currently no unambiguous, non-disputable approaches to differentiate periventricular from confluent WMH and some authors have proposed a distance of 10 mm³⁶. Lastly, our study consisted of patients with a history of vascular

disease, which may limit the generalizability of the results. However, this characteristic of our study cohort may also have led to a higher prevalence of lacunes and greater total WMH volumes³⁷, which facilitated the analyses.

In conclusion, we found that lacunes on MRI were associated with several WMH features that correspond to more severe small vessel changes, mortality and poor functional outcomes.

References

1. Makin SD, Turpin S, Dennis MS and Wardlaw JM. Cognitive impairment after lacunar stroke: systematic review and meta-analysis of incidence, prevalence and comparison with other stroke subtypes. *J Neurol Neurosurg Psychiatry* 2013; 84: 893-900.
2. Ostergaard L, Engedal TS, Moreton F, et al. Cerebral small vessel disease: Capillary pathways to stroke and cognitive decline. *J Cereb Blood Flow Metab* 2016; 36: 302-325.
3. Pantoni L, Poggesi A and Inzitari D. Cognitive decline and dementia related to cerebrovascular diseases: some evidence and concepts. *Cerebrovasc Dis* 2009; 27 Suppl 1: 191-196.
4. Wardlaw JM, Smith C and Dichgans M. Mechanisms of sporadic cerebral small vessel disease: insights from neuroimaging. *Lancet Neurol* 2013; 12: 483-497.
5. Wardlaw JM, Smith EE, Biessels GJ, et al. Neuroimaging standards for research into small vessel disease and its contribution to ageing and neurodegeneration. *Lancet Neurol* 2013; 12: 822-838.
6. Lambert C, Benjamin P, Zeestraten E, Lawrence AJ, Barrick TR and Markus HS. Longitudinal patterns of leukoaraiosis and brain atrophy in symptomatic small vessel disease. *Brain* 2016; 139: 1136-1151.
7. Gouw AA, Seewann A, van der Flier WM, et al. Heterogeneity of small vessel disease: a systematic review of MRI and histopathology correlations. *J Neurol Neurosurg Psychiatry* 2011; 82: 126-135.
8. Fazekas F, Kleinert R, Offenbacher H, et al. Pathologic correlates of incidental MRI white matter signal hyperintensities. *Neurology* 1993; 43: 1683-1689.
9. Kim KW, MacFall JR and Payne ME. Classification of White Matter Lesions on Magnetic Resonance Imaging in Elderly Persons. *Biological Psychiatry* 2008; 64: 273-280.
10. Fazekas F, Kleinert R, Offenbacher H, et al. The morphologic correlate of incidental punctate white matter hyperintensities on MR images. *AJNR Am J Neuroradiol* 1991; 12: 915-921.
11. Prins ND and Scheltens P. White matter hyperintensities, cognitive impairment and dementia: an update. *Nat Rev Neurol* 2015; 11: 157-165.
12. Griffanti L, Jenkinson M, Suri S, et al. Classification and characterization of periventricular and deep white matter hyperintensities on MRI: A study in older adults. *Neuroimage* 2018; 170: 174-181.
13. Conijn MM, Kloppenborg RP, Algra A, et al. Cerebral small vessel disease and risk of death, ischemic stroke, and cardiac complications in patients with atherosclerotic disease: the Second Manifestations of ARterial disease-Magnetic Resonance (SMART-MR) study. *Stroke* 2011; 42: 3105-3109.
14. DeBette S and Markus HS. The clinical importance of white matter hyperintensities on brain magnetic resonance imaging: systematic review and meta-analysis. *Bmj* 2010; 341: c3666.
15. Jokinen H, Gouw AA, Madureira S, et al. Incident lacunes influence cognitive decline: the LADIS study. *Neurology* 2011; 76: 1872-1878.
16. Benisty S, Gouw AA, Porcher R, et al. Location of lacunar infarcts correlates with cognition in a sample of non-disabled subjects with age-related white-matter changes: the LADIS study. *J Neurol Neurosurg Psychiatry* 2009; 80: 478-483.

17. Andersen SD, Skjoth F, Yavarian Y, Bach FW, Lip GY and Larsen TB. Multiple Silent Lacunes Are Associated with Recurrent Ischemic Stroke. *Cerebrovasc Dis* 2016; 42: 73-80.
18. de Bresser J, Kuijff HJ, Zaanen K, Viergever MA, Hendrikse J and Biessels GJ. White matter hyperintensity shape and location feature analysis on brain MRI; proof of principle study in patients with diabetes. *Sci Rep* 2018; 8: 1893.
19. Geerlings MI, Appelman AP, Vincken KL, et al. Brain volumes and cerebrovascular lesions on MRI in patients with atherosclerotic disease. The SMART-MR study. *Atherosclerosis* 2010; 210: 130-136.
20. Anbeek P, Vincken KL, van Bochove GS, van Osch MJ and van der Grond J. Probabilistic segmentation of brain tissue in MR imaging. *Neuroimage* 2005; 27: 795-804.
21. Kempton MJ, Underwood TS, Brunton S, et al. A comprehensive testing protocol for MRI neuroanatomical segmentation techniques: Evaluation of a novel lateral ventricle segmentation method. *Neuroimage* 2011; 58: 1051-1059.
22. Liu EJ, Cashman KV and Rust AC. Optimising shape analysis to quantify volcanic ash morphology. *GeoResJ* 2015; 8: 14-30.
23. Rost NS, Rahman RM, Biffi A, et al. White matter hyperintensity volume is increased in small vessel stroke subtypes. *Neurology* 2010; 75: 1670-1677.
24. Pantoni L. Cerebral small vessel disease: from pathogenesis and clinical characteristics to therapeutic challenges. *Lancet Neurol* 2010; 9: 689-701.
25. Potter GM, Doubal FN, Jackson CA, et al. Counting cavitating lacunes underestimates the burden of lacunar infarction. *Stroke* 2010; 41: 267-272.
26. Wardlaw JM. What is a lacune? *Stroke* 2008; 39: 2921-2922.
27. Wardlaw JM, Sandercock PA, Dennis MS and Starr J. Is breakdown of the blood-brain barrier responsible for lacunar stroke, leukoaraiosis, and dementia? *Stroke* 2003; 34: 806-812.
28. Ogata J, Yutani C, Otsubo R, et al. Heart and vessel pathology underlying brain infarction in 142 stroke patients. *Ann Neurol* 2008; 63: 770-781.
29. Ogata J, Yamanishi H and Ishibashi-Ueda H. Review: role of cerebral vessels in ischaemic injury of the brain. *Neuropathol Appl Neurobiol* 2011; 37: 40-55.
30. Eng JA, Frosch MP, Choi K, Rebeck GW and Greenberg SM. Clinical manifestations of cerebral amyloid angiopathy-related inflammation. *Ann Neurol* 2004; 55: 250-256.
31. Gouw AA, van der Flier WM, Pantoni L, et al. On the etiology of incident brain lacunes: longitudinal observations from the LADIS study. *Stroke* 2008; 39: 3083-3085.
32. Duering M, Csanadi E, Gesierich B, et al. Incident lacunes preferentially localize to the edge of white matter hyperintensities: insights into the pathophysiology of cerebral small vessel disease. *Brain* 2013; 136: 2717-2726.
33. Reijmer YD, Freeze WM, Leemans A and Biessels GJ. The effect of lacunar infarcts on white matter tract integrity. *Stroke* 2013; 44: 2019-2021.
34. Bezerra DC, Sharrett AR, Matsushita K, et al. Risk factors for lacune subtypes in the Atherosclerosis Risk in Communities (ARIC) Study. *Neurology* 2012; 78: 102-108.

35. Longstreth WT, Jr., Bernick C, Manolio TA, Bryan N, Jungreis CA and Price TR. Lacunar infarcts defined by magnetic resonance imaging of 3660 elderly people: the Cardiovascular Health Study. *Arch Neurol* 1998; 55: 1217-1225.
36. DeCarli C, Fletcher E, Ramey V, Harvey D and Jagust WJ. Anatomical mapping of white matter hyperintensities (WMH): exploring the relationships between periventricular WMH, deep WMH, and total WMH burden. *Stroke* 2005; 36: 50-55.
37. Jackson CA, Hutchison A, Dennis MS, et al. Differing risk factor profiles of ischemic stroke subtypes: evidence for a distinct lacunar arteriopathy? *Stroke* 2010; 41: 624-629.

Supplementary Material

WMH subtypes

Definitions of WMH subtype categories were based on two classification systems for WMH previously described in the literature¹⁻⁴. In the first classification system, WMH are divided into lesions adjacent to the margins of the lateral ventricles, and those that are separated from the margins of the lateral ventricles and are located in the deep white matter¹. In the second classification, WMH are labelled if they are located within or outside a user-defined distance from the lateral ventricular wall^{2,4}. By combining these two classification systems, we categorized patients into those with periventricular or confluent lesions, with or without deep WMH. Of the 215 patients with confluent WMH, however, only five patients did not show deep WMH. This finding can be explained by the natural course of progression of WMH, in which deep WMH coalesce with each other and eventually with periventricular WMH¹. Due to this process, periventricular WMH expand into the white matter and are more likely to be labelled as confluent lesions in our study. Hence, due to the relatively small number of patients with confluent WMH without deep lesions, we chose not to subdivide patients with confluent WMH into those with (n=210) and those without deep WMH (n=5).

WMH shape features

With regard to periventricular or confluent WMH, previous histopathological studies have shown that increased complexity of lesions is associated with more severe small vessel changes⁵⁻¹⁰. On the other hand, smooth periventricular WMH have been shown to correspond to only mild histopathological changes⁵⁻¹⁰. Thus, we hypothesized that presence of lacunes may be associated with a more complex shape of periventricular or confluent WMH. First, we performed a search of the literature to examine which shape features can be used to assess the complexity of periventricular or confluent WMH¹¹⁻¹⁷. Next, we rated shape features on the following criteria; volume dependence (the degree to which a shape feature is dependent on WMH volume), presence of a flooring effect (the minimum measured value is close to or similar to the smallest possible value of the shape descriptor), presence of a ceiling effect (the maximum measured value is close to or similar to the largest possible value of the shape feature), robustness (the degree to which positioning of WMH influences the shape feature), usability on 1.5T MRI resolution, and comprehensibility (the ability to link shape feature output to visual observations of WMH shape on MRI). Shape features that showed the most favorable combinations of criteria, i.e. limited volume dependence, limited flooring and/or ceiling effect, adequate robustness, usability on 1.5T MRI and comprehensibility, were selected for use in the current study and definitions of these shape features are given in Supplementary Table 1.

For deep WMH, we used shape features previously described in the literature to assess to the roundness¹³. In addition, we used a shape feature to assess the degree of complexity of deep WMH.

Examples of WMH that correspond to a low or a high value of a shape feature are given in Supplementary Table 2. For periventricular and confluent WMH, a lower convexity and a higher solidity, concavity index or fractal dimension correspond to a more irregularly shaped or more complex lesion. In deep WMH, a higher eccentricity corresponds to a more round lesion, while a lower eccentricity corresponds to a more elongated lesion. A higher fractal dimension of a deep WMH corresponds to a more complex lesion.

Supplementary Table 1. Definitions of WMH shape features.

Name	Formula
Convexity (C) ^a	$C = \frac{\text{Convex hull area}}{\text{Area}}$
Solidity (S) ^b	$S = \frac{\text{Volume}}{\text{Convex hull volume}}$
Concavity index (CI) ^c	$CI = \sqrt{(2 - C)^2 + (1 - S)^2}$
Fractal dimension (FD) ^d	$FD = \lim_{r \rightarrow x_{xyz}} \frac{\log(n_r)}{\log\left(\frac{1}{r}\right)}$
Eccentricity (E) ^e	$E = \frac{\text{Minor axis}}{\text{Major axis}}$

^aIn this definition, 'area' denotes the surface area of the WMH lesion and 'convex hull area' the surface area of the convex hull, which is the smallest convex object that contains the lesion shape^{11, 12}.







^bIn this definition, 'volume' denotes the volume of the WMH lesion and 'convex hull volume' the volume of the corresponding convex hull¹².

^cIn this definition, 'C' represents the convexity of the lesion and 'S' the solidity¹².

^dFractal dimension is calculated using the box count method, in which 'n' is the number of boxes, 'x_{xyz}' is the voxel size and 'r' is the box size^{13, 14, 16}.

^eIn this definition, 'major axis' denotes the largest diameter of the lesion in three dimensions and 'minor axis' the smallest diameter orthogonal to the major axis^{13, 15, 17}.

Supplementary Table 2. Examples of WMHs that correspond to a low or high value of a shape feature. Images represent schematic representations of WMHs as generated using our algorithm.

Shape feature	Low value (25 th percentile)	High value (75 th percentile)
Convexity periventricular or confluent WMH		
Solidity periventricular or confluent WMH		
Concavity index periventricular or confluent WMH		

Supplementary Table 2. continued

Shape feature	Low value (25 th percentile)	High value (75 th percentile)
Fractal dimension periventricular or confluent WMH		
Eccentricity deep WMH		
Fractal dimension deep WMH		

References

1. Fazekas F, Chawluk JB, Alavi A, Hurtig HI and Zimmerman RA. MR signal abnormalities at 1.5 T in Alzheimer's dementia and normal aging. *AJR Am J Roentgenol* 1987; 149: 351-356.
2. Wen W and Sachdev P. The topography of white matter hyperintensities on brain MRI in healthy 60- to 64-year-old individuals. *Neuroimage* 2004; 22: 144-154.
3. van der Lijn F, Verhaaren BF, Ikram MA, et al. Automated measurement of local white matter lesion volume. *Neuroimage* 2012; 59: 3901-3908.
4. DeCarli C, Fletcher E, Ramey V, Harvey D and Jagust WJ. Anatomical mapping of white matter hyperintensities (WMH): exploring the relationships between periventricular WMH, deep WMH, and total WMH burden. *Stroke* 2005; 36: 50-55.
5. Gouw AA, Seewann A, van der Flier WM, et al. Heterogeneity of small vessel disease: a systematic review of MRI and histopathology correlations. *J Neurol Neurosurg Psychiatry* 2011; 82: 126-135.
6. Kim KW, MacFall JR and Payne ME. Classification of White Matter Lesions on Magnetic Resonance Imaging in Elderly Persons. *Biological Psychiatry* 2008; 64: 273-280.
7. Fazekas F, Kleinert R, Offenbacher H, et al. The morphologic correlate of incidental punctate white matter hyperintensities on MR images. *AJNR Am J Neuroradiol* 1991; 12: 915-921.
8. Munoz DG, Hastak SM, Harper B, Lee D and Hachinski VC. Pathologic correlates of increased signals of the centrum ovale on magnetic resonance imaging. *Arch Neurol* 1993; 50: 492-497.
9. Scarpelli M, Salvolini U, Diamanti L, Montironi R, Chiaromoni L and Maricotti M. MRI and pathological examination of post-mortem brains: the problem of white matter high signal areas. *Neuroradiology* 1994; 36: 393-398.
10. Bronge L, Bogdanovic N and Wahlund LO. Postmortem MRI and histopathology of white matter changes in Alzheimer brains. A quantitative, comparative study. *Dement Geriatr Cogn Disord* 2002; 13: 205-212.
11. Zimmer Y, Tepper R and Akselrod S. An improved method to compute the convex hull of a shape in a binary image. *Pattern Recognition* 1997; 30: 397-402.
12. Liu EJ, Cashman KV and Rust AC. Optimising shape analysis to quantify volcanic ash morphology. *GeoResJ* 2015; 8: 14-30.
13. de Bresser J, Kuijff HJ, Zaanen K, Viergever MA, Hendrikse J and Biessels GJ. White matter hyperintensity shape and location feature analysis on brain MRI; proof of principle study in patients with diabetes. *Sci Rep* 2018; 8: 1893.
14. Esteban FJ, Sepulcre J, de Miras JR, et al. Fractal dimension analysis of grey matter in multiple sclerosis. *J Neurol Sci* 2009; 282: 67-71.
15. Murphy K, van Ginneken B, Schilham AM, de Hoop BJ, Gietema HA and Prokop M. A large-scale evaluation of automatic pulmonary nodule detection in chest CT using local image features and k-nearest-neighbour classification. *Med Image Anal* 2009; 13: 757-770.
16. Zhang L, Liu JZ, Dean D, Sahgal V and Yue GH. A three-dimensional fractal analysis method for quantifying white matter structure in human brain. *J Neurosci Methods* 2006; 150: 242-253.

17. Loizou CP, Petroudi S, Seimenis I, Pantziaris M and Pattichis CS. Quantitative texture analysis of brain white matter lesions derived from T2-weighted MR images in MS patients with clinically isolated syndrome. *J Neuroradiol* 2015; 42: 99-114.

3

CHAPTER 3

Association of white matter hyperintensity markers on MRI and long-term risk of mortality and ischemic stroke. The SMART-MR study

Rashid Ghaznawi ^{1,2}, Mirjam I. Geerlings ², Myriam G. Jaarsma-Coes ³, Jeroen Hendrikse ¹, Jeroen de Bresser ³; on behalf of the UCC-SMART Study Group

¹Department of Radiology, University Medical Center Utrecht, Netherlands;

²Julius Center for Health Sciences and Primary Care, University Medical Center Utrecht, Netherlands; ³Department of Radiology, Leiden University Medical Center, Netherlands

Objective

To determine whether white matter hyperintensity (WMH) markers on MRI are associated with long-term risk of mortality and ischemic stroke.

Methods

We included consecutive patients with manifest arterial disease enrolled in the SMART-MR study. We obtained WMH markers (volume, type and shape) from brain MRI scans performed at baseline using an automated algorithm. During follow-up, occurrence of death and ischemic stroke was recorded. Using Cox regression, we investigated associations of WMH markers with risk of mortality and ischemic stroke, adjusting for demographics, cardiovascular risk factors and cerebrovascular disease.

Results

We included 999 patients (59 ± 10 years; 79% male) with a median follow-up of 12.5 years (range 0.2-16.0 years). A greater periventricular or confluent WMH volume was independently associated with a greater risk of vascular death (hazard ratio (HR) 1.29, 95% CI 1.13-1.47 for a 1 unit increase in natural log-transformed WMH volume) and ischemic stroke (HR=1.53, 95% CI 1.26-1.86). A confluent WMH type was independently associated with a greater risk of vascular (HR=2.05, 95% CI 1.20-3.48) and nonvascular death (HR=1.65, 95% CI 1.01-2.73), and ischemic stroke (HR=4.01, 95% CI 1.72-9.35). A more irregular shape of periventricular or confluent WMH, as expressed by an increase in concavity index, was independently associated with a greater risk of vascular (HR=1.20, 95% CI 1.05-1.38 per standard deviation increase) and nonvascular death (HR=1.21, 95% CI 1.03-1.42), and ischemic stroke (HR=1.28, 95% CI 1.05-1.55).

Conclusions

WMH volume, type and shape are associated with long-term risk of mortality and ischemic stroke in patients with manifest arterial disease.

Introduction

White matter hyperintensities (WMH) of presumed vascular origin are frequently observed in older individuals on brain magnetic resonance imaging (MRI) and are an important cause of cognitive decline and dementia.¹⁻³ They are considered hallmark features of cerebral small vessel disease (CSVD).^{4,5}

WMH are heterogeneous lesions that correspond to different underlying brain parenchymal changes.⁶⁻⁸ Previous studies on CSVD mainly focused on WMH volume as a marker for CSVD severity.^{4,9-12} However, there is evidence to suggest that other markers of WMH may also provide clinically relevant information on severity and prognosis of CSVD.^{6,7,13-16} Specifically, histopathologic studies reported that smooth and periventricular WMH are associated with mild changes of the brain parenchyma, whereas irregular and confluent WMH are associated with more severe parenchymal changes, including loss of myelin and incomplete parenchymal destruction.^{6,13} We previously developed an automated MRI method to assess *in vivo* advanced WMH markers (volume, type and shape).¹⁴ Using this algorithm, we reported differences in advanced WMH markers such as shape in frail elderly patients, patients with diabetes mellitus and patients with lacunes on MRI.¹⁴⁻¹⁶ These findings suggest that advanced WMH MRI markers may provide clinically important information on CSVD severity.

The relationship between advanced WMH markers and long-term clinical outcomes, however, is not clear. Examining this relationship is of importance as WMH markers may aid in future patient selection for preventive treatment to ameliorate the risk of CSVD-related death and ischemic stroke. Therefore, in the present study, we aimed to assess whether WMH volume, type and shape were associated with greater risk of mortality (including vascular death) and ischemic stroke in patients with manifest arterial disease over 12 years of follow-up.

Methods

Study population

We used data from the Second Manifestations of ARterial disease-Magnetic Resonance (SMART-MR) study.¹⁷ The SMART-MR study is a prospective cohort study at the University Medical Center Utrecht with the aim of investigating risk factors and consequences of brain changes on MRI in patients with manifest arterial disease.¹⁷ One thousand three hundred nine middle-aged and older adult patients referred to our medical center for treatment of manifest arterial disease (cerebrovascular disease, manifest coronary artery disease, abdominal aortic aneurysm or peripheral arterial disease) were included for baseline measurements between 2001 and 2005.¹⁷ During a one day visit to the University Medical Center Utrecht, ultrasonography of the carotid arteries to measure the intima-media

thickness (mm), blood and urine samplings, a physical examination, neuropsychological assessment and a 1.5T brain MRI scan were performed.¹⁷ We used questionnaires for the assessment of demographics, medical history, risk factors, medication use and cognitive and physical functioning.¹⁷

Standard Protocol Approvals, Registration, and Patient Consents

The SMART-MR study was approved by the medical ethics committee of the University Medical Center Utrecht according to the guidelines of the Declaration of Helsinki of 1975. Written informed consent was obtained from all patients participating in the SMART-MR study.

Vascular risk factors

We assessed age, sex, smoking habits and alcohol intake at baseline using questionnaires. The body mass index (BMI) was calculated (kg/m^2) by measuring weight and height. We measured systolic blood pressure (mmHg) and diastolic blood pressure (mmHg) three times with a sphygmomanometer and the average of these measurements was calculated. Hypertension was defined as a mean systolic blood pressure of > 160 mmHg, a mean diastolic blood pressure of > 95 mmHg or the self-reported use of antihypertensive drugs.¹⁷ To determine glucose and lipid levels, an overnight fasting venous blood sample was taken. We defined diabetes mellitus as a fasting serum glucose levels of ≥ 7.0 mmol/l, and/or use of glucose-lowering medication, and/or a known history of diabetes.¹⁷ The degree of carotid artery stenosis at both sides was assessed with color Doppler-assisted duplex scanning using a 10MHz linear-array transducer (ATL Ultramark 9).¹⁸ Blood flow velocity patterns were used to evaluate the severity of carotid artery stenosis and the greatest stenosis observed on the left or right side of the common or internal carotid artery was taken to determine the severity of carotid artery disease.¹⁸ We defined a carotid artery stenosis $\geq 70\%$ as a peak systolic velocity > 210 cm/s.¹⁸

Brain MRI

MR imaging of the brain was performed on a 1.5T whole-body system (Gyrosan ACS-NT, Philips Medical Systems, Best, the Netherlands) using a standardized scan protocol.^{17, 19} Transversal fluid-attenuated inversion recovery (FLAIR) [repetition time (TR) = 6000 ms; echo time (TE) = 100 ms; inversion time (TI) = 2000 ms], T1-weighted [TR = 235 ms; TE = 2 ms], T1-weighted inversion recovery [TR = 2900 ms; TE = 22 ms; TI = 410 ms] and T2-weighted images [TR = 2200 ms; TE = 11 ms] were acquired with a voxel size of $1.0 \times 1.0 \times 4.0$ mm³ and contiguous slices.^{14, 19} A neuroradiologist blinded to patient characteristics visually rated brain infarcts on the T1-weighted, T2-weighted and FLAIR images of the MRI scans. We defined lacunes as focal lesions between 3 to 15 mm according to the STRIVE criteria.⁴ Non-lacunar lesions were categorized into large infarcts (i.e. cortical infarcts and

subcortical infarcts not involving the cerebral cortex) and those located in the brain stem or cerebellum.¹⁴

WMH volumes

WMH and brain volumes (intracranial volume and total brain volume) were obtained using the *k*-nearest neighbor (kNN) automated segmentation program on the T1-weighted, FLAIR, and T1-weighted inversion recovery sequences of the MRI scans.^{19, 20} WMH segmentations were visually assessed by an investigator (RG) using an image processing framework (MeVisLab 2.7.1., MeVis Medical Solutions AG, Bremen, Germany) to ensure that cerebral infarcts were correctly removed from the WMH segmentations.¹⁴ Next, we performed ventricle segmentation using the fully automated lateral ventricle delineation (ALVIN) algorithm in Statistical Parametric Mapping 8 (SPM8, Wellcome Trust Centre for Neuroimaging, University College London, London, UK) for Matlab (The MathWorks, Inc., Natick, MA, United States).¹⁴ The procedure is described in detail elsewhere.^{14, 21} We labeled WMH according to their continuity with the margins of the lateral ventricle and their extension from the lateral ventricle into the white matter.¹⁴ Periventricular WMH were defined as lesions contiguous with the margins of the lateral ventricles and extending up to 10 mm from the lateral ventricle into the white matter.¹⁴ We defined confluent WMH as lesions contiguous with the margins of the lateral ventricles and extending more than 10 mm from the lateral ventricles into the white matter.¹⁴ We defined deep WMH as lesions that were separated from the margins of the lateral ventricles.¹⁴ Examples of periventricular, confluent and deep WMH visualized in our algorithm are shown in Figure 1. Total WMH volume was calculated as the sum of deep WMH and periventricular or confluent WMH.

WMH types

We categorized patients into the following three WMH types: periventricular WMH type without deep WMH, periventricular WMH type with deep WMH and a confluent WMH type. We did not categorize the latter type according to presence or absence of deep WMH as the number of patients with a confluent WMH without deep WMH ($n = 5$) was insufficient to perform statistical analyses.¹⁴

WMH shape markers

We hypothesized that a more irregular shape of WMH may indicate more severe cerebral parenchymal damage based on previous histopathologic studies.^{6-8, 13, 22, 23} The degree to which deep WMH are punctiform or ellipsoidal may also provide information on CSVD severity.¹⁵

Irregularity of periventricular or confluent WMH was quantified using the concavity index and fractal dimension. In previous work, we established that the concavity index was a robust shape marker that showed a normal distribution in the study sample and

provided information on WMH shape irregularity based on volume and surface area.^{14,24} The concavity index was calculated by reconstructing convex hulls and calculating volume and surface area ratios of lesions, in which a higher concavity index value corresponds to a more irregular shape of periventricular or confluent WMH.¹⁴ Fractal dimension was calculated using the box counting method and was used to quantify irregularity of periventricular or confluent WMH and of deep WMH.^{14, 25, 26} A higher fractal dimension value indicated a more irregular WMH shape. As patients frequently show multiple deep WMH, a mean value for the fractal dimension was calculated across all deep WMH per patient.

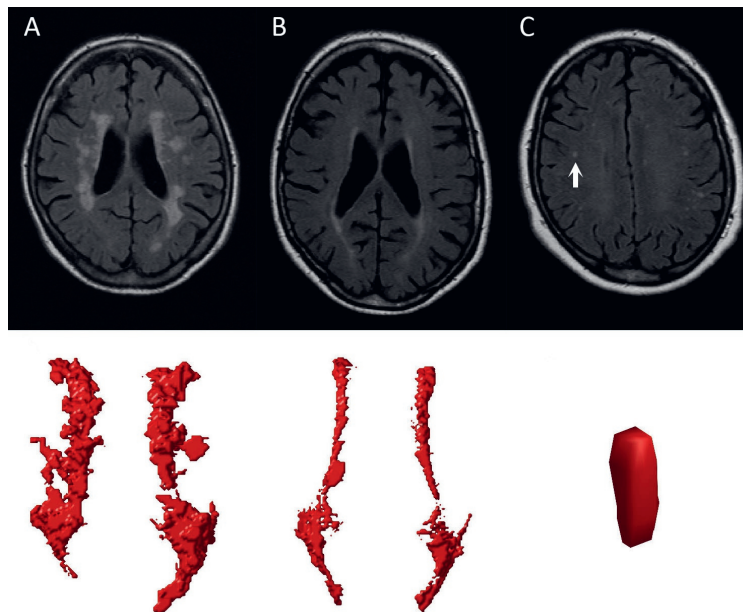


Figure 1. Examples of confluent (A), periventricular (B) and deep (C) WMH on FLAIR images with the corresponding visualizations in our algorithm shown below. The deep WMH lesion (arrow) is reconstructed in the coronal view, while the periventricular and confluent WMH are viewed from a transverse perspective. Note that the coronal reconstruction of the deep WMH lesion (C) may be influenced by the slice thickness and the lesion may be more punctiform. The confluent WMH lesion in A showed a volume of 11.57 mL with an accompanying deep WMH volume of 0.25 mL. The periventricular WMH lesion in B showed a volume of 4.98 mL without any accompanying deep WMH lesions. The deep WMH lesion in C showed a volume of 0.02 mL with an accompanying periventricular and deep WMH volume of 2.12 mL and 0.49 mL, respectively.

The degree to which deep WMH are punctiform or ellipsoidal was assessed using the eccentricity, which was calculated by dividing the minor axis of a deep WMH lesion by its major axis.^{14, 15} A high eccentricity value corresponded to a punctiform deep WMH

lesion, whereas a low value corresponded to an ellipsoidal lesion.^{27,28} A mean value for the eccentricity was calculated across all deep WMH per patient.

Clinical outcomes

Patients received a questionnaire every six months to provide information on outpatient clinic visits and hospitalization.¹⁸ If a fatal or nonfatal event was reported, original source documents were obtained and reviewed to determine the cause of the event. All possible events were audited independently by three physicians of the End Point Committee.¹⁸ Follow-up of patients was performed until death, refusal of further participation or loss to follow-up. Vascular-related death was defined as death caused by myocardial infarction, stroke, sudden death (unexpected cardiac death occurring within 1 hour after onset of symptoms, or within 24 hours given convincing circumstantial evidence), congestive heart failure or rupture of an abdominal aortic aneurysm.¹⁸ We defined non-vascular related death as death caused by cancer, infection, unnatural death, or death from another non-vascular cause.¹⁸ Ischemic stroke was defined as the occurrence of relevant clinical features that caused an increase in impairment of at least one grade on the modified Rankin scale, with or without a new relevant ischemic lesion on brain imaging.¹⁸

Study sample

Of the 1309 patients included, MRI data was irretrievable for 19 patients and 239 patients had missing data of one or more MRI sequences due to logistic reasons or motion artifacts. Forty-four of the remaining 1051 patients had unreliable brain volume data due to motion artifacts in all three MRI sequences. Four patients were excluded due to undersegmentation of WMH by the automated segmentation algorithm and another four patients were excluded because they did not have any WMH greater than five voxels. As a result, 999 patients were included in the current study.

Statistical analysis

Baseline characteristics of the study sample were reported as means or percentages where applicable.

Patients were followed from the date of the MRI until ischemic stroke, death, loss to follow-up, or end of follow-up (March 2017), whichever came first. Cox proportional hazard analysis was used to estimate hazard ratios (HR) for the occurrence of all-cause, vascular-related and nonvascular-related death and ischemic stroke associated with WMH volumes, type and shape markers. The proportional hazards assumption was checked by inspection of Schoenfeld residuals. We concluded that the proportional hazards assumption was met for all covariates.

To reduce the risk of bias due to complete case analysis, we performed chained equations imputation on missing covariates to generate 10 imputed datasets using SPSS

25.0 (Chicago, IL, USA).²⁹ The Cox regression analyses were performed on the imputed datasets and the pooled results were presented. We used SAS 9.4 (SAS Institute, Cary, NC, USA) and SPSS 25.0 (Chicago, IL, USA) to perform the statistical analyses.

WMH volumes and clinical outcomes

To assess whether WMH volumes were associated with clinical outcomes, we separately entered total, periventricular or confluent, and deep WMH volumes in a Cox regression model with age, sex and intracranial volume as covariates and all-cause death, vascular-related death, nonvascular-related death and ischemic stroke as outcomes. WMH volumes were natural log-transformed due to a non-normal distribution. In a second model, we additionally adjusted for large infarcts, lacunes, diastolic blood pressure, systolic blood pressure, diabetes mellitus, body mass index and smoking pack years at baseline. We also assessed the association between quartiles of WMH volumes (not natural log-transformed) and clinical outcomes, adjusted for all of the aforementioned covariates.

WMH types and clinical outcomes

To assess whether WMH types were associated with clinical outcomes, a categorical variable with the three WMH types as outcomes was entered in a Cox regression model with age and sex as covariates and all-cause death, vascular-related death, nonvascular-related death and ischemic stroke as outcomes. A periventricular WMH type without deep WMH was chosen as the reference category as this type represents the smallest WMH burden. In a second model, we additionally adjusted for the aforementioned covariates.

WMH shape markers and clinical outcomes

Z-scores of WMH shape markers were calculated to facilitate comparison and these were entered in a Cox regression model with age and sex as covariates and all-cause death, vascular-related death, nonvascular-related death and ischemic stroke as outcomes. In a second model, we additionally adjusted for the aforementioned covariates. If an association between a WMH shape marker and clinical outcome was observed, we additionally adjusted for total WMH volume to assess whether the association was independent of WMH volume.

Results

Baseline characteristics of the study sample (n = 999) are shown in Table 1. A total of 784 patients (78%) had periventricular WMH and 215 patients (22%) had confluent WMH. A periventricular with deep WMH type was present in 423 patients (42%) and a periventricular without deep WMH type was present in 361 patients (36%). In total, 274 patients died (149 vascular-related and 125 nonvascular-related) and 75 patients had an

ischemic stroke during a median follow-up of 12.5 years (range 0.2 to 16.0 years; total number of person-years follow-up 11 303).

Table 1. Baseline characteristics of the study sample (n = 999).

Age (years)	59 ± 10
Sex, % men	79.0
BMI (kg/m ²)	27 ± 4
Smoking, pack years ^a	18 (0, 50)
Alcohol intake, % current	74
Hypertension, %	51
Diabetes mellitus, %	20
Infarcts on MRI, %	
Large	12
Cerebellar	4
Brainstem	2
Lacunes	19
WMH volumes, mL ^a	
Total	0.9 (0.2, 6.4)
Periventricular or confluent	0.7 (0.1, 5.3)
Deep	0.1 (0.0, 0.8)
WMH types, %	
Periventricular	78
With deep	42
Without deep	36
Confluent	22
WMH shape markers	
Periventricular or confluent	
Concavity index	1.06 ± 0.11
Fractal dimension	1.24 ± 0.22
Deep	
Eccentricity	0.48 ± 0.14
Fractal dimension	1.45 ± 0.15

Characteristics are presented as mean ± SD or %.

^aMedian (10th percentile, 90th percentile).

BMI: body mass index; SD: standard deviation; WMH: white matter hyperintensities.

Associations between WMH volumes and long-term clinical outcomes

Greater total WMH volume was associated with all-cause death (HR = 1.32, 95% CI: 1.19 to 1.46 for a 1 unit increase in natural log-transformed total WMH volume), particularly vascular-related death (HR = 1.47, 95% CI: 1.29 to 1.68) and to a lesser extent with nonvascular-related death (HR = 1.15, 95% CI: 0.99 to 1.34), as well as with ischemic stroke (HR = 1.79, 95% CI: 1.48 to 2.16), adjusted for age, sex and total intracranial volume. These

associations persisted after adjusting for cardiovascular risk factors and cerebrovascular disease (Table 2).

Table 2. Results of Cox proportional hazard regression analyses with total, periventricular or confluent and deep WMH volumes (all natural log-transformed) as independent variables and all-cause, vascular-related and nonvascular-related death and ischemic stroke as dependent variables. Estimates represent hazard ratios with 95% CI for a 1 unit increase in natural log-transformed WMH volumes.

	No. of deaths or events	No. per 1000 person-years	Model 1 Estimate (95% CI)	Model 2 Estimate (95% CI)
Total WMH				
All-cause death	274	24.2	1.32 (1.19 to 1.46)	1.22 (1.10 to 1.36)
Vascular death	149	13.2	1.47 (1.29 to 1.68)	1.32 (1.14 to 1.51)
Nonvascular death	125	11.1	1.15 (0.99 to 1.34)	1.11 (0.95 to 1.30)
Ischemic stroke	75	6.8	1.79 (1.48 to 2.16)	1.58 (1.29 to 1.93)
Periventricular or confluent WMH				
All-cause death	274	24.2	1.29 (1.17 to 1.42)	1.20 (1.09 to 1.33)
Vascular death	149	13.2	1.43 (1.26 to 1.63)	1.29 (1.13 to 1.47)
Nonvascular death	125	11.1	1.14 (0.99 to 1.32)	1.10 (0.95 to 1.28)
Ischemic stroke	75	6.8	1.73 (1.45 to 2.08)	1.53 (1.26 to 1.86)
Deep WMH				
All-cause death	212	30.8	1.13 (1.04 to 1.24)	1.10 (1.01 to 1.21)
Vascular death	122	17.8	1.15 (1.03 to 1.30)	1.11 (0.98 to 1.25)
Nonvascular death	90	13.1	1.10 (0.96 to 1.26)	1.10 (0.96 to 1.26)
Ischemic stroke	62	9.4	1.24 (1.05 to 1.46)	1.18 (0.99 to 1.40)

Model 1: adjusted for age, sex and intracranial volume.

Model 2: model 1 additionally adjusted for large infarcts on MRI, lacunes on MRI, diastolic blood pressure, systolic blood pressure, diabetes mellitus, body mass index and smoking pack years at baseline.

CI: confidence interval, WMH: white matter hyperintensities.

Greater periventricular or confluent WMH volume was associated with all-cause death (HR = 1.29, 95% CI: 1.17 to 1.42), particularly vascular-related death (HR = 1.43, 95% CI: 1.26 to 1.63) and to a lesser extent with nonvascular-related death (HR = 1.14, 95% CI: 0.99 to 1.32), as well as with ischemic stroke (HR = 1.73, 95% CI: 1.45 to 2.08). These associations persisted after adjusting for cardiovascular risk factors and cerebrovascular disease (Table 2).

Greater deep WMH volume was associated with all-cause death (HR = 1.13, 95% CI: 1.04 to 1.24), vascular-related death (HR = 1.15, 95% CI: 1.03 to 1.30) and more strongly with ischemic stroke (HR = 1.24, 95% CI: 1.05 to 1.46). Risk estimates slightly attenuated

after adjusting for cardiovascular risk factors and cerebrovascular disease (Table 2). A non-significant association was observed between greater deep WMH volume and nonvascular death (HR = 1.10, 95% CI: 0.96 to 1.26), which did not change after adjusting for cardiovascular risk factors and cerebrovascular disease (Table 2).

Risk of vascular-related death and ischemic stroke increased per quartile of periventricular or confluent WMH volume (Figure 2). Similarly, risk of ischemic stroke increased per quartile of deep WMH volume (Figure 3).

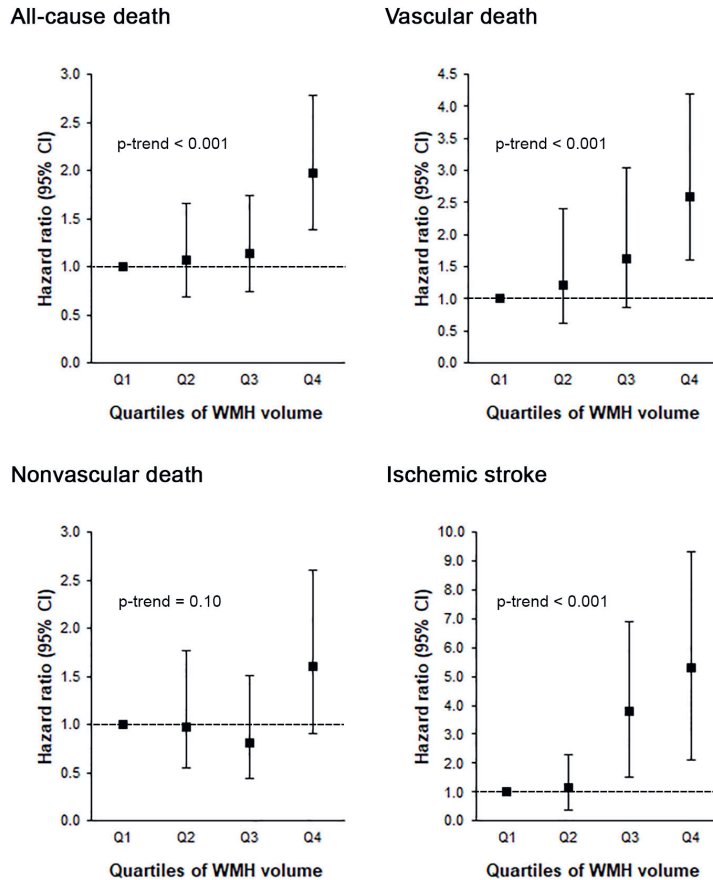


Figure 2. Associations between quartiles of periventricular or confluent WMH volume and risk of all-cause death, vascular death, nonvascular death and ischemic stroke. Results adjusted for age, sex, intracranial volume, large infarcts on MRI, lacunes on MRI, diastolic blood pressure, systolic blood pressure, diabetes mellitus, body mass index and smoking pack years at baseline. The lowest quartile (< 0.33 mL) was chosen as the reference category. Range second to fourth quartiles; 0.33 mL to 0.74 mL, 0.74 mL to 2.04 mL, ≥ 2.04 mL, respectively. Note that the scale of the y-axis may differ between outcomes. Examples of periventricular or confluent WMH from each quartile are shown in Supplemental Figure 1. CI indicates confidence interval.

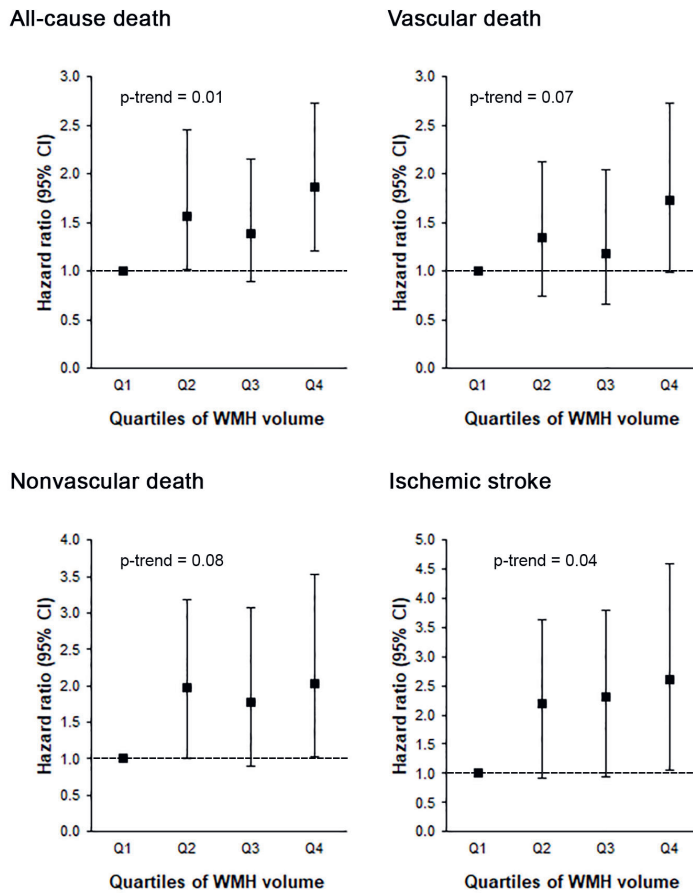


Figure 3. Associations between quartiles of deep WMH volume and risk of all-cause death, vascular death, nonvascular death and ischemic stroke. Results adjusted for age, sex, intracranial volume, large infarcts on MRI, lacunes on MRI, diastolic blood pressure, systolic blood pressure, diabetes mellitus, body mass index and smoking pack years at baseline. The lowest quartile (< 0.03 mL) was chosen as the reference category. Range second to fourth quartiles; 0.03 mL to 0.08 mL, 0.08 mL to 0.35 mL, \geq 0.35 mL, respectively. Note that the scale of the y-axis may differ between outcomes. CI indicates confidence interval.

Associations between WMH types and long-term clinical outcomes

Compared to a periventricular WMH type without deep WMH, a confluent WMH type was associated with a greater risk of all-cause death (HR = 2.29, 95% CI: 1.64 to 3.19), particularly vascular-related death (HR = 2.81, 95% CI: 1.75 to 4.49) and to a lesser extent nonvascular-related death (HR = 1.85, 95% CI: 1.15 to 2.98), as well as with ischemic stroke (HR = 4.36, 95% CI: 2.20 to 8.65). These associations persisted after adjusting for cardiovascular risk factors and cerebrovascular disease (Table 3). Non-significant associations were observed

between a periventricular WMH type with deep WMH and vascular-related death (HR = 1.53, 95% CI: 0.96 to 2.42) and ischemic stroke (HR = 1.75, 95% CI: 0.90 to 3.41), which attenuated after adjusting for cardiovascular risk factors and cerebrovascular disease (Table 3).

Table 3. Results of Cox proportional hazard regression analyses with WMH types as independent variables and all-cause, vascular-related and nonvascular-related death and ischemic stroke as dependent variables. Estimates represent hazard ratios with 95% CI for WMH types. A periventricular WMH type without deep WMH was the reference category.

	No. of deaths or events	No. per 1000 person-years	Model 1	Model 2
			Estimate (95% CI)	Estimate (95% CI)
Periventricular without deep WMH (n = 360)				
All-cause death	60	13.7	1 (reference)	1 (reference)
Vascular death	27	6.2	1 (reference)	1 (reference)
Nonvascular death	33	7.5	1 (reference)	1 (reference)
Ischemic stroke	13	3.0	1 (reference)	1 (reference)
Periventricular with deep WMH (n = 424)				
All-cause death	105	21.5	1.27 (0.92 to 1.75)	1.14 (0.82 to 1.58)
Vascular death	58	11.9	1.53 (0.96 to 2.42)	1.31 (0.82 to 2.09)
Nonvascular death	47	9.6	1.06 (0.68 to 1.67)	1.01 (0.64 to 1.59)
Ischemic stroke	28	5.9	1.75 (0.90 to 3.41)	1.48 (0.75 to 2.91)
Confluent WMH (n = 215)				
All-cause death	109	53.3	2.29 (1.64 to 3.19)	1.74 (1.23 to 2.47)
Vascular death	64	31.3	2.81 (1.75 to 4.49)	1.89 (1.15 to 3.11)
Nonvascular death	45	22.0	1.85 (1.15 to 2.98)	1.65 (1.01 to 2.73)
Ischemic stroke	34	17.8	4.36 (2.20 to 8.65)	2.83 (1.36 to 5.87)

Model 1: adjusted for age and sex.

Model 2: model 1 additionally adjusted for large infarcts on MRI, lacunes on MRI, diastolic blood pressure, systolic blood pressure, diabetes mellitus, body mass index and smoking pack years at baseline.

CI: confidence interval, WMH: white matter hyperintensities.

Associations between WMH shape markers and long-term clinical outcomes

A greater concavity index of periventricular or confluent WMH was associated with a greater risk of all-cause death (HR = 1.30, 95% CI: 1.18 to 1.43 per SD increase), particularly vascular-related death (HR = 1.34 (95% CI: 1.18 to 1.52) and to a lesser extent nonvascular-related death (HR = 1.25 (95% CI: 1.07 to 1.45), as well as with ischemic stroke (HR = 1.47, 95% CI: 1.23 to 1.76), adjusted for age and sex. These associations persisted after adjusting

for cardiovascular risk factors and cerebrovascular disease (Table 4). After additionally adjusting for total WMH volume, the association of concavity index with all-cause and nonvascular-related death persisted (HR = 1.21, 95% CI: 1.02 to 1.42; HR = 1.23, 95% CI: 1.02 to 1.49, respectively), whereas the association with vascular-related death and ischemic stroke attenuated (HR = 1.11, 95% CI: 0.89 to 1.39; HR = 1.23, 95% CI: 0.95 to 1.77, respectively).

Table 4. Results of Cox proportional hazard regression analyses with standardized WMH shape markers as independent variables and all-cause, vascular-related and nonvascular-related death and ischemic stroke as dependent variables.

	No. of deaths or events	No. per 1000 person-years	Model 1 Estimate (95% CI)	Model 2 Estimate (95% CI)
Periventricular or confluent WMH				
Concavity index				
All-cause death	274	24.2	1.30 (1.18 to 1.43)	1.21 (1.09 to 1.35)
Vascular death	149	13.2	1.34 (1.18 to 1.52)	1.20 (1.05 to 1.38)
Nonvascular death	125	11.1	1.25 (1.07 to 1.45)	1.21 (1.03 to 1.42)
Ischemic stroke	75	6.8	1.47 (1.23 to 1.76)	1.28 (1.05 to 1.55)
Fractal dimension				
All-cause death	274	24.2	1.33 (1.16 to 1.52)	1.19 (1.04 to 1.36)
Vascular death	149	13.2	1.52 (1.27 to 1.82)	1.29 (1.08 to 1.55)
Nonvascular death	125	11.1	1.13 (0.92 to 1.37)	1.06 (0.87 to 1.30)
Ischemic stroke	75	6.8	2.06 (1.60 to 2.65)	1.73 (1.33 to 2.25)
Deep WMH				
Fractal dimension				
All-cause death	212	30.8	1.03 (0.89 to 1.20)	1.07 (0.92 to 1.26)
Vascular death	122	17.8	1.06 (0.87 to 1.29)	1.11 (0.91 to 1.37)
Nonvascular death	90	13.1	1.00 (0.79 to 1.25)	1.02 (0.81 to 1.29)
Ischemic stroke	62	9.4	0.82 (0.63 to 1.06)	0.85 (0.65 to 1.12)
Eccentricity				
All-cause death	212	30.8	0.93 (0.81 to 1.07)	0.98 (0.85 to 1.14)
Vascular death	122	17.8	1.01 (0.84 to 1.21)	1.09 (0.90 to 1.33)
Nonvascular death	90	13.1	0.84 (0.68 to 1.04)	0.85 (0.68 to 1.07)
Ischemic stroke	62	9.4	0.99 (0.77 to 1.28)	1.14 (0.87 to 1.49)

Model 1: adjusted for age and sex.

Model 2: model 1 additionally adjusted for large infarcts on MRI, lacunes on MRI, diastolic blood pressure, systolic blood pressure, diabetes mellitus, body mass index and smoking pack years at baseline.

Estimates represent hazard ratios with 95% CI for one SD increase in the marker.

CI: confidence interval, SD: standard deviation, WMH: white matter hyperintensities.

A greater fractal dimension of periventricular or confluent WMH was associated with a greater risk of all-cause death (HR = 1.33, 95% CI: 1.16 to 1.52 per SD increase), vascular-related death (HR = 1.52, 95% CI: 1.27 to 1.82) and ischemic stroke (HR = 2.06, 95% CI: 1.60 to 2.65), adjusted for age and sex. These relationships persisted after adjusting for cardiovascular risk factors and cerebrovascular disease (Table 4). After additionally adjusting for total WMH volume, the association of fractal dimension with all-cause death, vascular-related death and ischemic stroke attenuated (HR = 1.10, 95% CI: 0.93 to 1.30; HR = 1.20, 95% CI: 0.95 to 1.51; HR = 1.09, 95% CI: 0.52 to 2.27, respectively). A greater fractal dimension of periventricular or confluent WMH was not associated with a greater risk of nonvascular-related death (HR = 1.13, 95% CI: 0.92 to 1.37).

No associations were observed between eccentricity and fractal dimension of deep WMH and long-term clinical outcomes (Table 4).

Discussion

In this cohort of patients with manifest arterial disease, we observed that WMH volume, type and shape were associated with long-term clinical outcomes. Specifically, we found that a greater volume and a more irregular shape of periventricular or confluent WMH were related to a higher risk of death and ischemic stroke. A confluent WMH type was also associated with a greater risk of death and ischemic stroke. These relationships were independent of demographics, cardiovascular risk factors and cerebrovascular disease at baseline.

Our finding that total WMH volume was related to risk of mortality and stroke is in line with previous studies.³⁰⁻³⁴ However, the associations of WMH volume sub-classifications and WMH types with clinical outcomes presented in this study are novel. We found that the risk of mortality and ischemic stroke was predominantly determined by the volume of periventricular or confluent WMH, rather than the volume of deep WMH. This was supported by the observation that risk estimates for mortality and ischemic stroke were higher for a confluent WMH type than a periventricular WMH type with deep WMH. A possible explanation for this finding may be that confluent WMH represent more severe parenchymal changes due to their relatively central location in the brain. Previous studies showed that pathological changes in the smaller vessels of the brain can induce secondary ischemia, which may be more profound in the white matter surrounding the lateral ventricles as these regions are furthest removed from collateral circulation.^{4,35} This notion may explain the relatively strong association between a confluent WMH type and occurrence of ischemic stroke in the present study.

To the best of our knowledge, no previous studies reported on the longitudinal association of WMH shape with clinical outcomes. In the present study, we observed that a more irregular shape of periventricular or confluent WMH was related to an increased

risk of mortality and ischemic stroke, which was only partly explained by WMH volume. An explanation for this finding may be that cerebral small vessel disease consists of a heterogeneous group of small vessel changes and a more irregular shape of WMH may indicate the presence of a more severe cerebral small vessel disease subtype.^{35,36} Support for this notion is provided by histopathologic studies that reported ischemic damage, loss of myelin and incomplete parenchymal destruction in more irregular shaped WMH, whereas smooth WMH correlated with more benign pathologic changes such as venous congestion.^{6,8,13} Furthermore, a previous study reported an association between a more irregular shape of WMH and frailty in elderly patients¹⁶ and in previous work we showed that presence of lacunes on MRI was related to a more irregular shape of WMH.¹⁴ These investigations and the results of the present study suggest that in addition to WMH volume, shape of WMH may represent a clinically relevant marker in patients with WMH on MRI.

We observed that a confluent WMH type and a more irregular shape of periventricular or confluent WMH were not only associated with a greater risk of vascular death, but also of nonvascular death. In previous work, we similarly reported that presence of lacunes on MRI was related to a greater risk of nonvascular death.³⁷ An explanation for these findings is that cerebral small vessel disease may be a marker of overall increased vulnerability to adverse outcomes, possibly through the concomitant presence of generalized microvascular disease.^{2,4,35} Further studies in different cohorts are needed to confirm this hypothesis, however the reported associations with vascular and nonvascular death suggest that WMH markers may be important in determining overall prognosis of patients with manifest arterial disease.

Key strengths of the present study are the large number of patients included, the longitudinal design, the relatively long follow-up period and the use of automated image processing techniques that enabled us to examine multiple and also novel features of WMH in relation to clinical outcomes. Furthermore, all MRI scans were visually checked and corrected if needed to ensure that WMH segmentation and subsequent analysis of WMH type and shape were accurate.

Limitations of this study include, first, the use of 1.5T MRI instead of 3.0T MRI, which is likely more sensitive in detecting small WMH lesions. It should be noted, however, that clinical 3.0T MRI scanners were not readily available during the inclusion period of our study starting in 2001. Second, we did not categorize deep WMH into lesions located directly under the cerebral cortex (i.e. infracortical) and those located more centrally in the subcortical white matter, which may differ in terms of etiology.³⁸ Third, MRI sequences were used with a relatively large slice thickness of 4 mm, which is likely less accurate in determining WMH shape markers than three-dimensional MR sequences. The impact of slice thickness, however, may be less profound on measurements of the concavity index as it is calculated by determining volume and surface area ratios of periventricular or confluent WMH, which are expected to remain relatively constant.¹⁴ On the other hand,

a more profound impact can be expected on measurements of the fractal dimension, which is directly dependent on voxel size.¹⁴ A larger slice thickness will therefore lead to reduced information in the z-axis. Similarly, shape determination of smaller deep WMH in the size range of several millimeters may also be impacted by a relatively large slice thickness. Despite this limitation, however, we were able to detect associations between WMH shape markers and clinical outcomes, suggesting that WMH shape may represent a clinically relevant marker for occurrence of ischemic stroke and death.

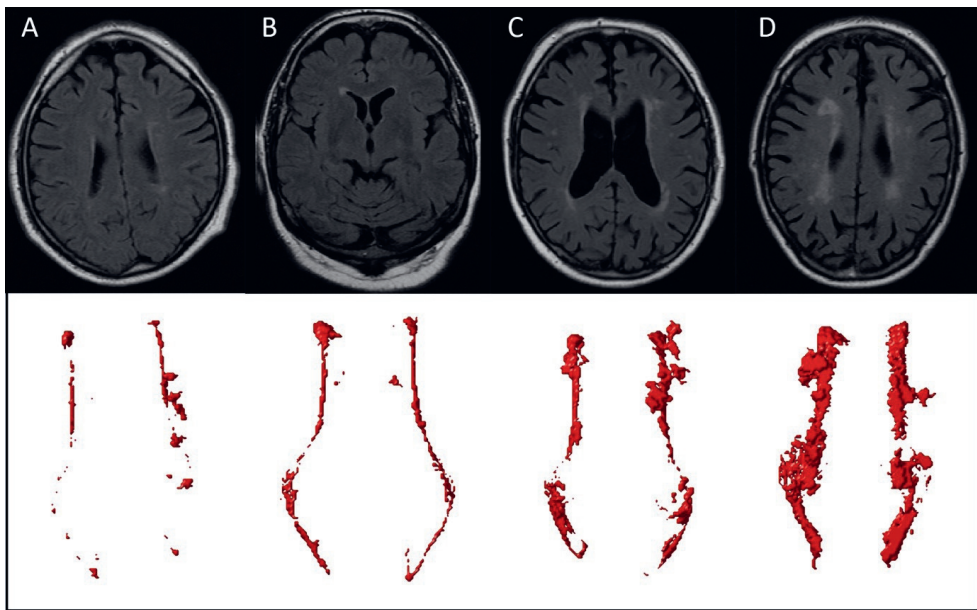
In conclusion, our findings demonstrate that WMH volume, type and shape are associated with long-term risk of mortality and ischemic stroke in patients with manifest arterial disease. These findings suggest that WMH markers on MRI may be useful in determining patient's prognosis and may aid in future patient selection for preventive treatment.

References

1. DeBette S and Markus HS. The clinical importance of white matter hyperintensities on brain magnetic resonance imaging: systematic review and meta-analysis. *Bmj* 2010; 341: c3666.
2. Wardlaw JM, Smith C and Dichgans M. Mechanisms of sporadic cerebral small vessel disease: insights from neuroimaging. *Lancet Neurol* 2013; 12: 483-497.
3. Prins ND and Scheltens P. White matter hyperintensities, cognitive impairment and dementia: an update. *Nat Rev Neurol* 2015; 11: 157-165.
4. Wardlaw JM, Smith EE, Biessels GJ, et al. Neuroimaging standards for research into small vessel disease and its contribution to ageing and neurodegeneration. *Lancet Neurol* 2013; 12: 822-838.
5. Ostergaard L, Engedal TS, Moreton F, et al. Cerebral small vessel disease: Capillary pathways to stroke and cognitive decline. *J Cereb Blood Flow Metab* 2016; 36: 302-325.
6. Gouw AA, Seewann A, van der Flier WM, et al. Heterogeneity of small vessel disease: a systematic review of MRI and histopathology correlations. *J Neurol Neurosurg Psychiatry* 2011; 82: 126-135.
7. Fazekas F, Kleinert R, Offenbacher H, et al. The morphologic correlate of incidental punctate white matter hyperintensities on MR images. *AJNR Am J Neuroradiol* 1991; 12: 915-921.
8. Fazekas F, Kleinert R, Offenbacher H, et al. Pathologic correlates of incidental MRI white matter signal hyperintensities. *Neurology* 1993; 43: 1683-1689.
9. Schmidt R, Fazekas F, Kleinert G, et al. Magnetic resonance imaging signal hyperintensities in the deep and subcortical white matter. A comparative study between stroke patients and normal volunteers. *Arch Neurol* 1992; 49: 825-827.
10. Gouw AA, van der Flier WM, Fazekas F, et al. Progression of white matter hyperintensities and incidence of new lacunes over a 3-year period: the Leukoaraiosis and Disability study. *Stroke* 2008; 39: 1414-1420.
11. van Dijk EJ, Prins ND, Vrooman HA, et al. Progression of cerebral small vessel disease in relation to risk factors and cognitive consequences: Rotterdam Scan study. *Stroke* 2008; 39: 2712-2719.
12. Kloppenborg RP, Nederkoorn PJ, Grool AM, et al. Cerebral small-vessel disease and progression of brain atrophy: the SMART-MR study. *Neurology* 2012; 79: 2029-2036.
13. Kim KW, MacFall JR and Payne ME. Classification of White Matter Lesions on Magnetic Resonance Imaging in Elderly Persons. *Biological Psychiatry* 2008; 64: 273-280.
14. Ghaznawi R, Geerlings MI, Jaarsma-Coes MG, et al. The association between lacunes and white matter hyperintensity features on MRI: The SMART-MR study. *J Cereb Blood Flow Metab* 2019; 39: 2486-2496.
15. de Bresser J, Kuijf HJ, Zaanen K, et al. White matter hyperintensity shape and location feature analysis on brain MRI; proof of principle study in patients with diabetes. *Sci Rep* 2018; 8: 1893.
16. Kant IMJ, Mutsaerts H, van Montfort SJJ, et al. The association between frailty and MRI features of cerebral small vessel disease. *Sci Rep* 2019; 9: 11343.
17. Geerlings MI, Appelman AP, Vincken KL, et al. Brain volumes and cerebrovascular lesions on MRI in patients with atherosclerotic disease. The SMART-MR study. *Atherosclerosis* 2010; 210: 130-136.

18. Goessens BM, Visseren FL, Kappelle LJ, et al. Asymptomatic carotid artery stenosis and the risk of new vascular events in patients with manifest arterial disease: the SMART study. *Stroke* 2007; 38: 1470-1475.
19. Ghaznawi R, Zwartbol MH, Zuithoff NP, et al. Reduced parenchymal cerebral blood flow is associated with greater progression of brain atrophy: The SMART-MR study. *J Cereb Blood Flow Metab* 2020: 271678x20948614.
20. Anbeek P, Vincken KL, van Bochove GS, et al. Probabilistic segmentation of brain tissue in MR imaging. *Neuroimage* 2005; 27: 795-804.
21. Kempton MJ, Underwood TS, Brunton S, et al. A comprehensive testing protocol for MRI neuroanatomical segmentation techniques: Evaluation of a novel lateral ventricle segmentation method. *Neuroimage* 2011; 58: 1051-1059.
22. Fazekas F, Chawluk JB, Alavi A, et al. MR signal abnormalities at 1.5 T in Alzheimer's dementia and normal aging. *AJR Am J Roentgenol* 1987; 149: 351-356.
23. Fazekas F, Barkhof F, Wahlund LO, et al. CT and MRI rating of white matter lesions. *Cerebrovasc Dis* 2002; 13 Suppl 2: 31-36.
24. Liu EJ, Cashman KV and Rust AC. Optimising shape analysis to quantify volcanic ash morphology. *GeoResJ* 2015; 8: 14-30.
25. Zhang L, Liu JZ, Dean D, et al. A three-dimensional fractal analysis method for quantifying white matter structure in human brain. *J Neurosci Methods* 2006; 150: 242-253.
26. Esteban FJ, Sepulcre J, de Miras JR, et al. Fractal dimension analysis of grey matter in multiple sclerosis. *J Neurol Sci* 2009; 282: 67-71.
27. Loizou CP, Petroudi S, Seimenis I, et al. Quantitative texture analysis of brain white matter lesions derived from T2-weighted MR images in MS patients with clinically isolated syndrome. *J Neuroradiol* 2015; 42: 99-114.
28. Murphy K, van Ginneken B, Schilham AM, et al. A large-scale evaluation of automatic pulmonary nodule detection in chest CT using local image features and k-nearest-neighbour classification. *Med Image Anal* 2009; 13: 757-770.
29. White IR, Royston P and Wood AM. Multiple imputation using chained equations: Issues and guidance for practice. *Stat Med* 2011; 30: 377-399.
30. Weinstein G, Wolf PA, Beiser AS, et al. Risk estimations, risk factors, and genetic variants associated with Alzheimer's disease in selected publications from the Framingham Heart Study. *J Alzheimers Dis* 2013; 33 Suppl 1: S439-445.
31. Lim JS, Hong KS, Kim GM, et al. Cerebral microbleeds and early recurrent stroke after transient ischemic attack: results from the Korean Transient Ischemic Attack Expression Registry. *JAMA Neurol* 2015; 72: 301-308.
32. Kuller LH, Arnold AM, Longstreth WT, Jr., et al. White matter grade and ventricular volume on brain MRI as markers of longevity in the cardiovascular health study. *Neurobiol Aging* 2007; 28: 1307-1315.
33. Henneman WJ, Sluimer JD, Cordonnier C, et al. MRI biomarkers of vascular damage and atrophy predicting mortality in a memory clinic population. *Stroke* 2009; 40: 492-498.

34. DeBette S, Beiser A, DeCarli C, et al. Association of MRI markers of vascular brain injury with incident stroke, mild cognitive impairment, dementia, and mortality: the Framingham Offspring Study. *Stroke* 2010; 41: 600-606.
35. Pantoni L. Cerebral small vessel disease: from pathogenesis and clinical characteristics to therapeutic challenges. *Lancet Neurol* 2010; 9: 689-701.
36. Rost NS, Rahman RM, Biffi A, et al. White matter hyperintensity volume is increased in small vessel stroke subtypes. *Neurology* 2010; 75: 1670-1677.
37. Conijn MM, Kloppenborg RP, Algra A, et al. Cerebral small vessel disease and risk of death, ischemic stroke, and cardiac complications in patients with atherosclerotic disease: the Second Manifestations of ARterial disease-Magnetic Resonance (SMART-MR) study. *Stroke* 2011; 42: 3105-3109.
38. Wiggins ME, Jones J, Tanner JJ, et al. Pilot Investigation: Older Adults With Atrial Fibrillation Demonstrate Greater Brain Leukoaraiosis in Infracortical and Deep Regions Relative to Non-Atrial Fibrillation Peers. *Front Aging Neurosci* 2020; 12.



Supplemental Figure 1. Examples of periventricular or confluent WMH according to quartiles of WMH volume (see also Figure 2). The FLAIR images (shown above) correspond with visualizations in our algorithm shown below. The periventricular WMH lesion in A showed a volume of 0.29 mL (first quartile) and was predominately located in the left centrum semiovale, as can be seen in the FLAIR image. The periventricular lesion in B showed a volume of 0.72 mL (second quartile) and the bulk of volume was located along the anterior horn of the right lateral ventricle, as can be seen in the FLAIR image. The confluent lesion in C showed a volume of 1.99 mL (third quartile) and the bulk of volume was located along the anterior and posterior horns of the lateral ventricles. The confluent lesion in D showed a volume of 6.19 mL (fourth quartile).

CHAPTER 4



MRI phenotypes of the brain are related to future stroke and mortality in patients with manifest arterial disease: the SMART-MR study

Myriam G. Jaarsma-Coes^{1,2,3}, Rashid Ghaznawi^{1,4}, Jeroen Hendrikse¹, Cornelis Slump², Theo D. Witkamp¹, Yolanda van der Graaf⁴, Mirjam I. Geerlings⁴, Jeroen de Bresser^{1,3}; on behalf of the Second Manifestations of ARterial disease (SMART) Study group

¹Department of Radiology, University Medical Center Utrecht, Netherlands;

²MIRA Institute for Biomedical Technology and Technical Medicine, University of Twente, Netherlands; ³Department of Radiology, Leiden University Medical Center, Netherlands; ⁴Julius Center for Health Sciences and Primary Care, University Medical Center Utrecht, Netherlands

Neurodegenerative and neurovascular diseases lead to heterogeneous brain abnormalities. A combined analysis of these abnormalities by phenotypes of the brain might give a more accurate representation of the underlying aetiology. We aimed to identify different MRI phenotypes of the brain and assessed the risk of future stroke and mortality within these subgroups. In 1003 patients (59±10 years) from the Second Manifestations of ARterial disease-Magnetic Resonance (SMART-MR) study, different quantitative 1.5T brain MRI markers were used in a hierarchical clustering analysis to identify 11 distinct subgroups with a different distribution in brain MRI markers and cardiovascular risk factors, and a different risk of stroke (Cox regression: from no increased risk compared to the reference group with relatively few brain abnormalities to HR=10.34; 95%-CI 3.80-28.12 for the multi burden subgroup) and mortality (from no increased risk compared to the reference group to HR=4.00; 95%-CI 2.50-6.40 for the multi burden subgroup). In conclusion, within a group of patients with manifest arterial disease we showed that different MRI phenotypes of the brain can be identified and that these were associated with different risks of future stroke and mortality. These MRI phenotypes can possibly classify individual patients and assess their risk of future stroke and mortality.

Introduction

Older patients with manifest arterial disease often also have neurodegenerative and neurovascular diseases. Neurodegenerative diseases frequently lead to brain abnormalities like cerebral atrophy¹. Neurovascular diseases are associated with cortical infarcts, lacunes and white matter hyperintensities (WMH)^{2,3}. Although these diseases lead to heterogeneous brain abnormalities, to date these are most commonly analysed as separate entities⁴⁻⁶. For example, presence of brain infarcts has been related to stroke⁵, WMH volume has been related to stroke and mortality^{5,7}, presence of lacunes has been associated with mortality⁸ and cerebral atrophy has been linked to stroke and mortality^{7,9}. However, a combined analysis of MRI phenotypes of the brain may show a better relation with underlying aetiology and could therefore lead to a better approximation of an individual patient's risk of future stroke or (vascular) mortality. Although the application of MRI phenotypes of the brain in neuroimaging is relatively novel, a comparable approach has recently been performed in cognitive impairment¹⁰ and in other research fields, including asthma^{11,12}, chronic obstructive pulmonary disease^{13,14} and breast cancer¹⁵.

In the present study our first aim was to identify different MRI phenotypes of the brain in middle-aged and older patients with manifest arterial disease and relate these to clinical characteristics. Our second aim was to estimate the risk of future ischemic stroke and mortality for each of these MRI phenotypes of the brain subgroups.

Material and methods

SMART-MR study

In the present study, patient data from the Second Manifestations of ARterial disease-Magnetic Resonance (SMART-MR) study were used¹⁶. The SMART-MR study is a prospective cohort study at the University Medical Center Utrecht aimed to examine risk factors and consequences of brain MRI abnormalities in patients with manifest arterial disease¹⁶. Patients newly referred to the University Medical Center Utrecht for treatment of manifest arterial disease (cerebrovascular disease, peripheral arterial disease, manifest coronary artery disease or an abdominal aortic aneurysm) were invited to participate between May 2001 and December 2005. In the present study follow-up data until March 2015 are used. During a one-day visit to the medical center, a physical examination, blood and urine samples, neuropsychological assessment, ultrasonography of the common carotid arteries, and a 1.5T brain MRI scan were performed. Questionnaires were used to assess cardiovascular risk factors, medical history, medication use and demographics. The SMART-MR study was approved by the medical ethics committee of our institution and written informed consent was obtained from all patients.

Study sample

Of the 1309 patients included, 19 patients had no MRI, 239 patients had one or more missing MRI sequences, and 48 patients had severe motion artefacts or other artefacts in their MRI scans. As a result, a total of 1003 patients were available for the present study.

Cardiovascular risk factors

Weight and height were measured and the body mass index was calculated (kg/m^2). Systolic and diastolic blood pressures (mmHg) were measured with a sphygmomanometer. These measurements were repeated twice and the average between the two measurements was calculated. Glucose and lipid levels were determined from an overnight fasting blood sample. Diabetes mellitus was defined as a glucose level of ≥ 7.0 mmol/L, a history of diabetes mellitus, reported in the questionnaire or use of oral antidiabetic drugs or insulin. Hyperlipidaemia was defined as a total cholesterol level of > 5.0 mmol/L, self-reported use of lipid-lowering drugs or a low-density lipoprotein cholesterol level of > 3.2 mmol/L. Hyperhomocysteinemia was defined as a homocysteine level of ≥ 16.2 $\mu\text{mol}/\text{L}$. Smoking (pack-years) and drinking habits (never, past and current) were assessed by questionnaires. Ultrasonography was performed to measure the intima-media thickness (IMT) in both common carotid arteries (in mm).

Brain MRI

MR imaging of the brain was performed on a 1.5T MRI system (Gyrosan ACS-NT, Philips Medical Systems, Best, The Netherlands) using a standardized scan protocol. Transversal T1-weighted (repetition time (TR) = 235 ms; echo time (TE) = 2 ms), T1-weighted inversion recovery (TR = 2900 ms; TE = 22 ms; TI = 410 ms), T2-weighted (TR = 2200 ms; TE = 11 ms) and FLAIR (TR = 6000 ms; TE = 100 ms; TI = 2000 ms) images were acquired with a voxel size of $0.9 \times 0.9 \times 4.0$ mm³ and 38 contiguous slices. Cerebral infarcts (cortical, subcortical and lacunes) were rated by a neuroradiologist according to the STRIVE criteria³. The location and affected flow territory were rated for every cerebral infarct¹⁷. The flow through both internal carotid arteries and the basilar artery were determined by phase contrast imaging and summed to calculate the total CBF (ml/min)¹⁷.

Brain MRI features

Segmentations of white matter, grey matter, peripheral cerebrospinal fluid (CSF outside the brain), lateral ventricles and WMH were obtained by a k-nearest neighbour-based automated probabilistic segmentation method, which was performed on the T1 inversion recovery and FLAIR MRI images¹⁸. Cerebral infarcts were manually segmented and WMH segmentations were manually corrected. Total brain volume was calculated by summing the volumes white matter, grey matter, WMH and cerebral infarcts. Intracranial volume (ICV) was calculated by summing all other brain volumes. Brain volume fractions (brain parenchymal fraction, white matter fraction, grey matter fraction, peripheral CSF fraction,

lateral ventricular fraction, and WMH fraction) were calculated by dividing the respective brain volumes by the intracranial volume and expressing these as a percentage of ICV.

The WMH segmentations were used in a different algorithm to automatically determine periventricular or confluent WMH (distanced ≤ 3 mm from the lateral ventricles) and deep WMH (distanced >3 mm from the lateral ventricles)^{19,20}. This classification of WMH into WMH subtypes was visually checked and corrected if necessary. The classification was used to calculate different WMH shape features per lesion (surface area, convexity, surface index and curvature, volume, solidity, complexity, eccentricity and fractal dimension²¹. For more details see Supplementary Table 1. The means over all WMH per shape feature were calculated for each patient.

Outcomes

Patients received a questionnaire every 6 months to provide the investigators information on hospitalization and outpatient clinic visits. All possible events were audited independently by 3 physicians of the End Point Committee. Patients were followed until death or refusal of further participation. The primary outcomes used in this study were overall mortality, vascular related mortality and ischemic stroke. Vascular related mortality was defined as death caused by a myocardial infarction, stroke, sudden death (unexpected cardiac death occurring within 1 hour after onset of symptoms, or within 24 hours given convincing circumstantial evidence), congestive heart failure, rupture of an abdominal aortic aneurysm or death from another vascular cause. Ischemic stroke was defined as relevant clinical features that caused an increase in impairment of at least one grade on the modified Rankin scale, with or without a new relevant ischemic lesion at brain imaging⁸. Patients were followed from the date of the MRI scan until death, loss to follow-up, or end of follow-up (March 2015).

Statistical analysis

Identification of subgroups with different MRI phenotypes of the brain

The brain MRI features used to determine the MRI phenotypes of the brain were brain volumes (brain parenchymal fraction, white matter fraction, grey matter fraction, peripheral CSF fraction, lateral ventricular fraction), WMH features (ventricular WMH fraction per lobe, deep WMH fraction per lobe, and the shape parameters fractal dimension, solidity, convexity, concavity index and eccentricity), cerebral infarcts (number of lacunes and cortical and subcortical infarcts, cortical infarcts and number of lacunes per lobe), and cerebral blood flow (as fraction of total brain volume). These brain MRI features were normalized as Z-scores for normal distributed continuous variables, or otherwise scaled between 0 and 2.

To obtain MRI phenotypes of the brain, hierarchical clustering with Ward's criteria was performed¹⁵ using R version 3.3.2 and packages: NbClust²², cIValid²³ and R.Matlab²⁴. Hierarchical clustering is an iterative algorithm that groups patients together based

on similarities in brain MRI features. A level is a new joining of groups. Therefore, at each increasing level, the number of groups decreases. These different levels of grouping from an individual patient to one large group can be visualized using a dendrogram (Figure 1). To obtain subgroups for identification of the MRI phenotypes of the brain, the dendrogram needs to be cut at a certain level. The optimal level for this cut was determined by assessment of the average silhouette width and the Dunn index (Supplementary Figure 1) and was also based on the heatmap (Figure 2).

Brain MRI features and cardiovascular risk factors were compared between subgroups with a different brain imaging phenotype using analysis of covariance (ANCOVA) for continuous variables and multinomial logistic regression for variables with discrete values, both corrected for age and sex. IMT and WMH were log transformed for these analyses due to a non-normal distribution. A Bonferroni correction was used to correct for multiple testing. A p -value of 0.05 or smaller was considered statistically significant.

Outcome assessment

Cox regression was used to estimate associations between MRI phenotypes of the brain and future ischemic stroke, mortality and vascular related mortality, adjusted for age and sex. The reference category consisted of subgroups 1, 2, 3 and 7, as these subgroups contained relatively few brain abnormalities. We used multiple subgroups as the reference category to achieve a sufficient number of events in the reference category. These groups form the entire left branch of the dendrogram ($n = 534$, see Figure 1). SPSS version 21 (Chicago, IL, USA) was used for the analyses.

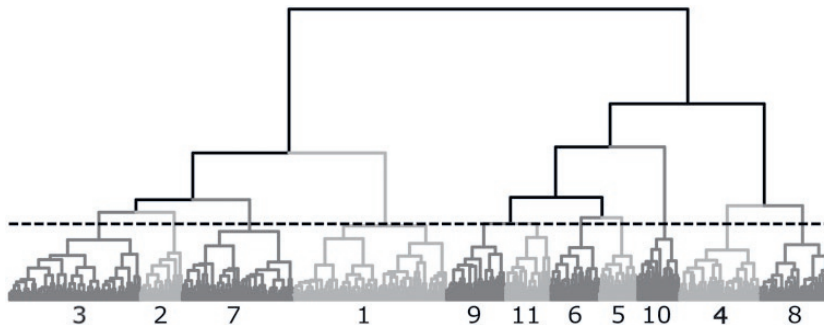


Figure 1. The dendrogram resulting from hierarchical clustering using Ward's criteria is visualized. The black dashed line indicates the level the dendrogram is cut to create the 11 subgroups.

Results

A hierarchical clustering algorithm was applied on the quantified brain MRI features (brain volumes, cerebral blood flow, different types of cerebral infarcts and WMH shape

features) of patients with manifest vascular disease (n=1003). The baseline characteristics of these patients are shown in Table 1. Based on the average silhouette width, Dunn index and clustering parameters in the heatmap, the optimal cut-off was considered to be at 11 subgroups, resulting in group sizes between 46 and 188 patients (Table 2 and Supplementary Results). Subgroups were significantly different in age ($p < 0.05$) and sex ($p < 0.05$). After Bonferroni correction differences between the age of most subgroup remained significant. See Table 2, Supplementary Table 2 and the Supplementary Results for a detailed description of between group differences.

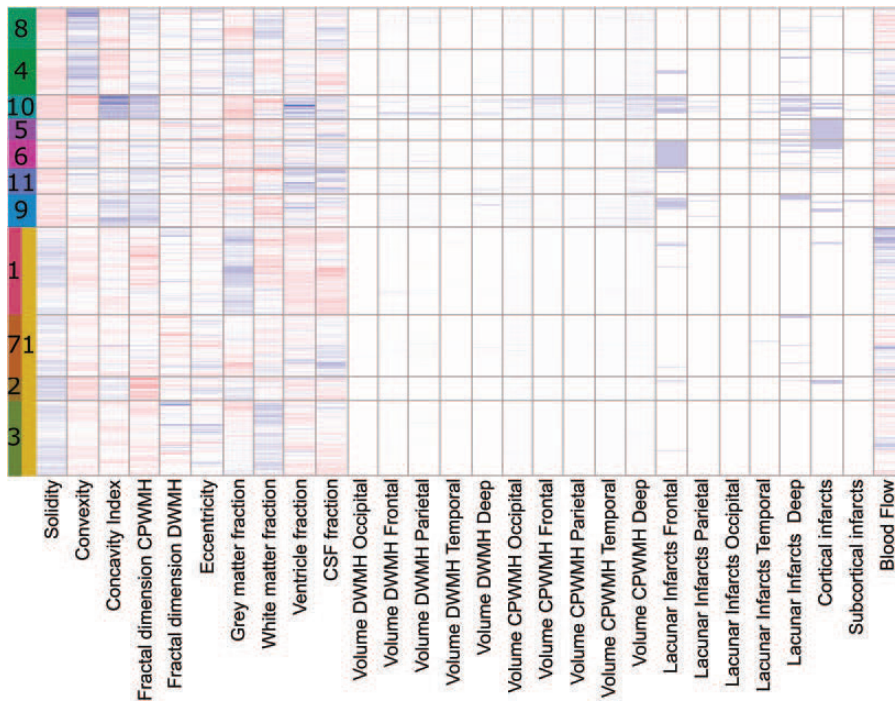


Figure 2. Heatmap of the hierarchical clustering results. The different colours and numbers in the first column represent the different subgroups. The subgroups are numbered based on average age (the first group is the youngest group). In the second column the four subgroups in the bottom branch were merged resulting in the reference subgroup used for Cox regression. Each row represent one patient and each column represents a brain MRI feature used for the hierarchical clustering. Parameter values in blue are relatively high values and parameter values in red are relatively low values. For example, the Z-score of solidity for the references group is mainly above 0 and for the other groups mainly below 0. Some between subgroup differences in brain MRI features are already visible; for example, subgroup 10 clearly has a higher concavity index, WMH volume and more cerebral atrophy, and especially subgroup 5 and 6 have a higher percentage of patients with cerebral infarcts compared to the other subgroups.

Table 1. Baseline characteristics of the study sample (n=1003).

Age (years)	59 ± 10
Gender, men (%)	79
Cardiovascular risk factors	
BMI (kg/m ²)	26.8 ± 3.8
Smoking (pack years)	18 (0, 50)
Alcohol intake, former (%)	26
Hypertension (%)	52
Hyperlipidaemia (%)	80
Hyperhomocysteinemia (%)	12
Diabetes mellitus (%)	12
IMT (mm)	0.88 (0.63, 1.25)
ApoE ε4 (%)	34
Arterial disease location, n (%)	
Peripheral arterial disease	22.3 (224)
Cerebrovascular disease	22.7 (228)
Coronary artery disease	57.7 (579)
Abdominal aortic aneurysm	9.2 (92)

Values represent means ± SD, percentages, and medians (10th, 90th percentile).

BMI: Body mass index, IMT: average intima-media thickness.

Range age: 25 to 82 years. Range BMI: 15.4 to 42.9 kg/m².

Percentage missing: BMI: 0.1%, Smoking: 0.5%, Alcohol intake: 0.6%, Hypertension: 0.8%, Hyperlipidaemia: 1.4%, Hyperhomocysteinemia: 0.4%, Diabetes mellitus: 1.7%, IMT: 2.0%, ApoE: 15.8%.

MRI phenotypes of the brain

Brain MRI features of the 11 subgroups are shown in Table 2. Significant between subgroup differences were found for all brain MRI features as these were based on the hierarchical clustering classification. The following subgroups showed typical brain MRI features: subgroup 5 included patients who had mainly cortical infarcts, with presence of cortical infarcts in 98% of the study sample; in subgroup 6 mainly lacunes were found, with presence of lacunes in 98%; subgroup 9 had prominent cerebral small vessel disease (CSVD) with a relatively large WMH volume of 0.38 ml and presence of lacunes in 37% of the patients; neurodegenerative changes were mostly observed in subgroup 11 with a relatively large amount of cerebral atrophy; and a multi burden subgroup 10 could be discerned with a relatively large amount of both cerebral atrophy and WMH volume, and presence of lacunes in 59% of the patients. The six remaining subgroups showed relatively mild brain abnormalities, characterized by few cerebral infarcts and a low CSVD burden. To illustrate the between group differences, the probability of WMH presence is visualized per subgroup in Figure 3.

The subgroups showed significant differences with respect to age, sex, smoking, alcohol intake, hypertension, hyperhomocysteinemia, diabetes mellitus and IMT ($p < 0.05$; see Supplementary Table 2). No between subgroup differences were found for BMI, hyperlipidaemia and number of ApoE ε4 carriers ($p > 0.05$).

Table 2. MRI features of the eleven subgroups with different MRI phenotypes of the brain.

Subgroup (n)	1 (n=186) Limited burden	2 (n=51) Limited burden	3 (n=160) Limited burden	4 (n=99) Limited burden	5 (n=46) Cortical infarcts	6 (n=60) Lacunar infarcts	7 (n=135) Limited burden	8 (n=86) Limited burden	9 (n=70) Mainly CSVD	10 (n=51) Multi burden	11 (n=55) Neurodegenerative	p value
Volume fractions (% ICV)												
BPF	81.8±1.9	80.5±2.3	80.1±1.7	80.3±1.9	77.6±2.4	77.4±2.4	77.3±2.1	77.9±2.1	78.2±1.8	75.5±2.3	74.6±2.8	<0.001
WM	41.5±1.6	42.4±1.4	44.4±1.3	42.1±1.5	42.3±1.7	42.4±2.0	42.3±1.4	43.9±1.4	41.1±1.8	41.3±2.4	41.6±2.7	<0.001
CGM	40.3±2.1	38.0±1.9	35.7±2.1	38.1±2.0	33.5±2.9	34.2±2.3	35.0±2.5	33.8±2.3	36.4±2.5	32.2±2.9	32.5±3.0	<0.001
Lateral ventricles	1.3±0.5	1.8±1.0	1.7±0.6	2.0±0.7	2.5±1.0	2.5±0.9	2.1±0.7	1.9±0.5	2.6±0.9	3.7±1.4	3.4±0.9	<0.001
Periphera CSF	16.8±1.8	17.8±2.0	18.2±1.6	17.6±1.8	19.9±2.3	20.1±2.0	20.6±1.8	20.2±2.0	19.2±2.0	20.8±2.2	22.0±2.8	<0.001
WMH	0.03 (0.01,0.11)	0.01 (0.00,0.02)	0.03 (0.01,0.07)	0.10 (0.05,0.28)	0.06 (0.03,0.18)	0.14 (0.05,0.34)	0.05 (0.02,0.13)	0.12 (0.05,0.29)	0.38 (0.17,0.85)	1.13 (0.62,3.01)	0.27 (0.07,0.60)	<0.001*
Cerebral blood flow (ml/min)	4.2±0.9	3.4±0.6	3.4±0.7	3.9±0.7	3.2±0.7	3.4±0.8	3.6±0.8	3.0±0.6	3.2±0.5	3.2±1.0	3.1±0.7	<0.001
WMH shape features												
Solidity	0.75±0.15	0.90±0.07	0.78±0.11	0.36±0.12	0.56±0.17	0.41±0.17	0.70±0.16	0.31±0.12	0.30±0.10	0.24±0.05	0.33±0.10	<0.001
Convexity	1.00±0.07	0.89±0.05	1.01±0.06	1.28±0.12	1.10±0.11	1.16±0.12	1.02±0.07	1.33±0.16	1.05±0.09	0.87±0.13	1.13±0.10	<0.001
Concavity Index	1.04±0.05	1.12±0.05	1.02±0.05	0.97±0.06	1.03±0.07	1.04±0.07	1.04±0.06	0.98±0.07	1.18±0.08	1.36±0.10	1.11±0.08	<0.001
Fractal dimension CPWMH	1.12±0.16	0.85±0.16	1.12±0.11	1.31±0.12	1.21±0.13	1.33±0.12	1.19±0.13	1.34±0.11	1.51±0.11	1.68±0.12	1.40±0.13	<0.001
Fractal dimension DWMH	1.50±0.17	1.38±0.19	1.5±0.27	1.45±0.11	1.45±0.14	1.46±0.12	1.36±0.14	1.48±0.11	1.46±0.07	1.44±0.06	1.47±0.12	<0.001
Eccentricity	0.45±0.14	0.50±0.24	0.52±0.18	0.51±0.13	0.50±0.17	0.45±0.14	0.49±0.16	0.55±0.13	0.44±0.08	0.44±0.07	0.46±0.12	<0.001
DWMH, % present	45%	35%	44%	70%	78%	78%	61%	74%	68%	100%	84%	
Infarcts, % present												
Cortical	2%	16%	0%	0%	98%	38%	0%	2%	15%	29%	9%	<0.001
Large subcortical	0%	0%	0%	1%	0%	2%	1%	0%	6%	2%	0%	0.031
Lacunar; WM	1%	6%	1%	7%	0%	98%	2%	0%	37%	59%	10%	<0.001
Lacunar; Deep GM	4%	2%	0%	7%	15%	18%	7%	2%	20%	55%	6%	<0.001

Values represent means ± SD, % (OR (95% CI)) or median (10th, 90th percentile). *Natural log transformed due to a non-normal distribution. For the between subgroup comparison, an ANCOVA was used for continuous data and multinomial logistic regression was used for discrete data, both with age as a covariate and Bonferroni correction to correct for multiple testing. A p-value < 0.05 was considered statistically significant.

Percentage missing: Solidity/Convexity/Concavity index/CPWMH: 0.4%, FD DWMH/Eccentricity: 38.5%, Blood flow: 6.4%.

FD: Fractal Dimension, CPWMH: Confluent or periventricular white matter hyperintensities, DWMH: Deep white matter hyperintensities, ICV: Intracranial volume, BPF: Brain parenchymal fraction, WM: White matter, CGM: Cortical grey matter.

The post-hoc using Bonferroni correction shows significant differences in the following groups: BPF: 1=all; 2=1,5-11; 3=1,5-11; 4=1,5-11; 5=1-4,10,11; 6=1-4,10,11; 7=1-4,10,11; 8=1-4,10,11; 9=1-4,10,11; 10=1-9; 11=1-9; WM: 1=2,3,7,8; 2=1,3,8-10; 3=1-7,9-11; 4=3,8,9; 5=3,8,9; 6=1,3,8-10; 7=1,3,8-10; 8=1,2,4-11; 9=2-8; 10=2,3,6-8; 11=3-8; CGM: 1=all; 2=1-3,5-11; 3=1-6,8,10,11; 4=1-4,9-11; 5=1-4,9-11; 6=1-4,9-11; 7=1,2,5,8-11; 8=1-4,7,9,10; 9=1,2,4-11; 10=1-4,6,7,9; lateral ventricles: 1=all; 2=1,5,9-11; 3=1,5,7,9-11; 4=1,5,6,9-11; 5=1-4,8,10,11; 6=1-4,7,8,10,11; 7=1,3,6,9-11; 8=1,5,6,9-11; 9=1-4,7-11; 10=1-9; 11=1-9; Peripheral CSF: 1=3-11; 2=5-11; 3=1,5-11; 4=1,5-11; 5=1-4,11; 6=1-4,11; 7=1-4,9,11; 8=1-4,11; 9=1-4,7,10,11; 10=1-4,9,11; 11=all; WMH: 1=2,4-11; 2=all; 3=2-11; 4=1-5,7,9-11; 5=1-6,8-11; 6=1-3,6,7,9-11; 7=1-4,6-11; 8=1-3,5,7-11; 9=1-10; 10=all; 11=1-8,10; blood flow: 1=1-3,5-11; 2=1,4; 3=1,4,8; 4=2-6,8-11; 5=1,4,7; 6=1,4,8; 7=1,5,8-11; 8=1,3,4,6,7; 9=1,4,7; 10=1,4,7; 11=1,4,7; solidity: 1=2,4,5,8-11; 2=all; 3=2-11; 4=1-3,5,7,10; 5=all; 6=1-3,5-11; 7=all; 8=1-3,5-7; 9=1-3,5-7; 10=1-7,11; 11=1-3,5-7,10; convexity: 1=2,4-6,8-11; 2=1-10; 3=2-6,8,10,11; 4=all; 5=1-8,10; 6=1-10; 7=2,4-8,10,11; 8=all; 9=1,2,4,6,8,10,11; 10=1,3-11; 11=1-4,7-11; concavity index: 1=2,4,8-11; 2=1-10; 3=2-11; 4=1-5,7,9-11; 5=2,4,8-11; 6=2,4,8-11; 7=2,4,8-11; 8=1-3,5-11; 9=all; 10=all; 11=1,3-10; FD CPWMH: 1=2,4-11; 2=all; 3=2-11; 4=1-5,7,9-11; 5=1-6,8-11; 6=1-3,5,7,9,10; 7=1-4,6-11; 8=1-3,5,7,9,10; 9=all; 10=all; 11=1-5,7,9,10; FD DWMH: 1=2,4-11; 2=all; 3=2-11; 4=1-5,7,9-11; 5=1-6,8-11; 6=1-3,5,7,9,10; 7=1-4,6-11; 8=1-3,5,7,9,10; 9=all; 10=all; 11=1-5,7,9-11 and eccentricity: 1=8; 3=9; 6=8; 8=1,6,9,10; 9=3,8; 10=8;

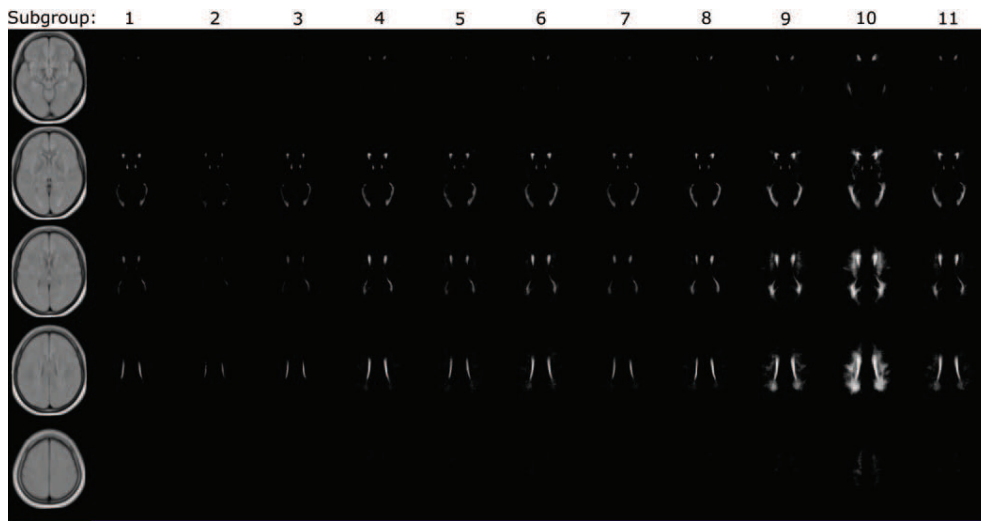


Figure 3. The likelihood of WMH presence per voxel is summarized for all patients in each subgroup and visualized for 5 different slices. For example, patients in subgroup 10 have the most WMH lesions, where patients in subgroup 2 have the least WMH.

Outcome assessment

After a mean follow-up of 15.3 years, 217 patients had died of whom 111 patients (51%) had vascular related mortality, and 67 patients had a new ischemic stroke.

The results of the Cox regression analyses (Figure 4 and Table 3) showed that, compared to the reference group with relatively few brain abnormalities (subgroups 1, 2, 3, and 7), the multi burden subgroup had the highest increased risk of overall mortality (HR 4.00; 95% CI 2.50 to 6.40; subgroup 10), followed by the subgroup with neurodegenerative changes (HR 2.70; 95% CI 1.66 to 4.39; subgroup 11), the subgroup with mainly lacunar infarcts (HR 2.58; 95% CI 1.59 to 4.20; subgroup 6), the subgroup with mainly cortical infarcts (HR 1.85; 95% CI 1.03 to 3.34; subgroup 5), the subgroup with mainly CSVD (HR 1.72; 95% CI 1.04 to 2.83; subgroup 9). The other two groups with a limited burden (subgroup 4 and 8) showed no increased risk of overall mortality compared to the reference group with relatively few brain abnormalities.

Compared to the reference group with relatively few brain abnormalities (subgroups 1, 2, 3, and 7), the multi burden subgroup had the highest increased risk of vascular related mortality (HR 8.00; 95% CI 4.20 to 15.21; subgroup 10), followed by the subgroup with neurodegenerative changes (HR 4.14; 95% CI 2.06 to 8.34; subgroup 11), the subgroup with mainly cortical infarcts (HR 4.00; 95% CI 1.92 to 8.32; subgroup 5), the subgroup with mainly lacunar infarcts (HR 3.45; 95% CI 1.66 to 7.16; subgroup 6), and the mainly CSVD subgroup (HR 2.31; 95% CI 1.10 to 4.88; subgroup 9). The other two groups with a limited burden (subgroup 4 and 8) showed no increased risk of vascular mortality compared to the reference group with relatively few brain abnormalities.

Compared to the reference group with relatively few brain abnormalities (subgroups 1, 2, 3, and 7), the multi burden subgroup had the highest increased risk of future ischemic stroke (HR 10.34; 95% CI 3.80 to 28.12; subgroup 10), followed by the subgroup with mainly CSVD (HR 8.54; 95% CI 3.50 to 20.83; subgroup 9), the subgroup with mainly lacunar infarcts (HR 7.22; 95% CI 2.89 to 18.03; subgroup 6), the subgroup with neurodegenerative changes (HR 7.17; 95% CI 2.42 to 21.21; subgroup 11), and the subgroup with mainly cortical infarcts (HR 4.19; 95% CI 1.33 to 13.15; subgroup 5). The other two groups with a limited burden (subgroup 4 and 8) showed no increased risk of ischemic stroke compared to the reference group with relatively few brain abnormalities.

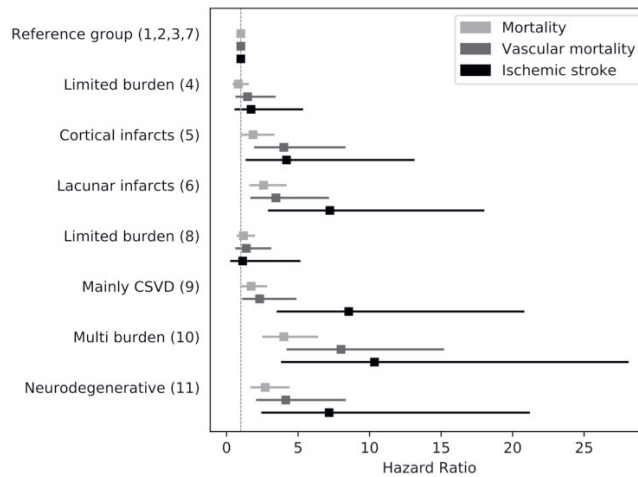


Figure 4. The likelihood of WMH presence per voxel is summarized for all patients in each subgroup and visualized for 5 different slices. For example, patients in subgroup 10 have the most WMH lesions, where patients in subgroup 2 have the least WMH.

Table 3. Relationship between MRI phenotypes of the brain and outcome in patients with manifest arterial disease (n=1003).

	Mortality			Vascular related mortality			Ischemic stroke		
	No. of cases	No. per 1000 Person-years	Hazard ratio	No. of cases	No. per 1000 Person-years	Hazard ratio	No. of cases	No. per 1000 Person-years	Hazard ratio
Reference subgroup with limited burden subgroups 1, 2, 3, 7; n=534	66	11.7	1 (reference)	24	4.2	1 (reference)	12	2.2	1 (reference)
Limited burden subgroup 4; n=99	11	10.5	0.82 (0.43-1.55)	7	6.7	1.47 (0.63-3.43)	4	3.9	1.71 (0.55-5.35)
Cortical infarcts subgroup 5; n=46	14	30.4	1.85 (1.03-3.34)*	11	23.9	4.00 (1.92-8.32)*	4	9.1	4.19 (1.33-13.15)*
Lacunar infarcts subgroup 6; n=60	23	41.2	2.58 (1.59-4.20)*	11	19.7	3.45 (1.66-7.16)*	8	15.9	7.22 (2.89-18.03)*
Limited burden subgroup 8; n=87	19	21.5	1.18 (0.70-1.99)	8	9.1	1.38 (0.61-3.12)	2	2.3	1.13 (0.25-5.17)
Mainly CSVD subgroup 9; n=71	23	34.6	1.72 (1.04-2.83)*	11	16.6	2.31 (1.10-4.88)*	11	17.9	8.54 (3.50-20.83)*
Multi burden subgroup 10; n=51	32	88.4	4.00 (2.50-6.40)*	23	63.5	8.00 (4.20-15.21)*	8	23.0	10.34 (3.80-28.12)*
Neurodegenerative subgroup 11; n=55	29	65.3	2.70 (1.66-4.39)*	16	36.1	4.14 (2.06-8.34)*	6	15.0	7.17 (2.42-21.21)*

Differences in outcome of the different subgroups was compared to the combined reference group. Cox regression was used with correction for age and sex. In the table the results are shown by giving the hazard ratio with the 95% confidence interval.

* p -value < 0.05

Vascular related mortality is defined as: Death caused by myocardial infarction, stroke, sudden death (unexpected cardiac death occurring within 1 hour after onset of symptoms, or within 24 hours given convincing circumstantial evidence), congestive heart failure, rupture of abdominal aortic aneurysm or death from another vascular cause.

Ischemic stroke is defined as: Relevant clinical features that caused an increase in impairment of at least one grade on the modified Rankin scale, with or without a new relevant ischemic lesion at brain imaging.

Discussion

In this study in middle-aged and older patients with manifest arterial disease, we identified different MRI phenotypes of the brain with hierarchical clustering of brain MRI features. We showed that these different MRI phenotypes of the brain were associated with a difference in risk of ischemic stroke, vascular related mortality and overall mortality.

Multiple neurodegenerative and neurovascular diseases are often present within one patient. As a single disease frequently leads to multiple brain abnormalities and brain abnormalities show overlap between diseases, it is difficult to discriminate all underlying brain diseases in one patient²⁵. Previous approaches have mainly focused on assessing single to a few brain MRI features for identification of different neurodegenerative and neurovascular diseases⁴⁻⁶. Indeed, some diseases can be discriminated based on a single or a combination of brain MRI features. An example of this is cerebral amyloid angiopathy, which is characterized by lobar microbleeds and superficial siderosis²⁶. However, most other neurodegenerative and neurovascular diseases are often difficult to discriminate solely based on single brain MRI features. As most brain diseases lead to a specific pattern of brain abnormalities, MRI phenotypes of the brain might be used to identify previously unknown brain diseases or combinations of brain diseases by their specific pattern of brain abnormalities. This is possibly a completely new field of research.

This concept of identifying imaging phenotypes has already been performed to identify phenotypes in other types of diseases, including clinical asthma phenotypes^{11,12} and subphenotypes of COPD^{13,14} or differences in DNA methylation and gene expression in breast cancer¹⁵. Two previous studies also assessed brain MRI phenotypes^{10,27}. Artero et al²⁷ studied the distribution of white matter lesions in the aging brain and found that their distribution was associated with age and presence of clinical symptoms. Nettiksimmons et al¹⁰ studied the distribution of MRI, cerebrospinal fluid and serum biomarkers across ADNI subjects diagnosed with amnesic mild cognitive impairment (MCI). They found substantial heterogeneity in biomarkers in clinically similar MCI.

To the best of our knowledge, our study is the first to identify different MRI phenotypes of the brain by assessing different vascular and non-vascular quantitative brain MRI markers in patients with manifest arterial disease. With our elaborate approach using multiple brain imaging features in patients with manifest arterial disease, we found several MRI phenotypes of the brain that were associated with a different risks of future stroke and (vascular) mortality. MRI phenotypes of the brain might in the future be used to identify individual patients that could benefit from personalized medicine approaches to prevent adverse outcome. To pave the way for clinical use, a future prediction study would be useful to confirm our results and validation studies in other populations would have to confirm the external validity of our study. Furthermore, software (fully automated and robust image processing software with MRI phenotype of the brain identification) needs to be developed, tested and implemented in hospitals. Currently more and more vendors

are bringing image processing closer to clinical practice which helps in future integration of bringing brain imaging phenotype identification.

The strengths of our study are the approach where we combine different brain MRI features to assess MRI phenotypes of the brain and the use of this approach in a large cohort of patients with manifest arterial disease with a long follow-up duration (15 years). A strength of our technical approach includes the use of automatic brain MRI features by segmentation of brain volumes, including WMH, which also enabled us to include novel WMH shape features²¹. Furthermore, our approach of assessing MRI phenotypes of the brain is robust, as it allows different MRI features to be used within the same method.

A limitation of our study could be the limited number of events in some subgroups, especially in the subgroups with few brain abnormalities, even with a mean follow-up of 15.3 years. To meet this limitation, we decided to combine subgroups with few brain abnormalities as a reference group. A potential technical limitation of our study is that patients were scanned on a 1.5T MRI scanner that included a 2D FLAIR sequence with a slice thickness of 4 mm. This influenced the results of the WMH shape features, especially for small WMH lesions, which could have led to an underestimation of group differences. On the other hand, a larger slice thickness increases contrast in bigger lesions and is more clinically relevant. The 1.5T MRI scanners are nowadays more and more replaced by 3T MRI scanners, because of the potential of higher resolution images and improved visualization and sensitivity for ischemic lesions. However, our study started with the baseline MRI scans over 17 years ago when 3T MRI was less widely available. Another technical limitation could be that, although hierarchical clustering is a machine learning method that is not biased by assumptions, some choices such as the number of subgroups need to be made that may be arbitrary. To limit this subjectivity, we used quantitative evaluation measures such as the average silhouette width and Dunn index to determine the most appropriate number of subgroups (see Supplementary materials).

In conclusion, within a group of middle-aged and older patients with manifest arterial disease, we identified subgroups with different MRI phenotypes of the brain and showed that there was a difference in risk of future stroke and mortality between these subgroups. These MRI phenotypes of the brain can possibly be used to classify individual patients and assess their risk of future stroke and mortality.

Supplementary Table 1. WMH shape features for the subgroup analysis.

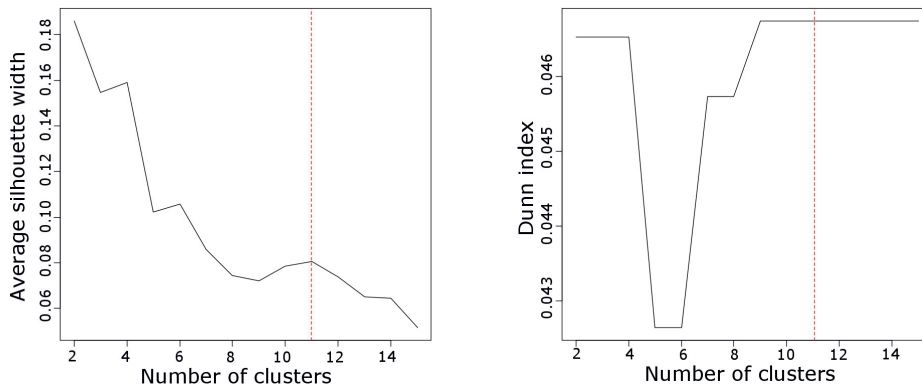
Name	Description	Formula
Convexity (C) (1)	Describes the extent to which the shape is convex or concave. A fully convex shape has a convexity and solidity of 1. The solidity will decrease and the convexity increase as the shape becomes more concave.	$C = \frac{\text{Convex hull area}}{\text{Area}}$
Solidity (S) (1)		$S = \frac{\text{Volume}}{\text{Convex hull volume}}$
Concavity index (CI) (1)	The concavity index is a measure of roughness and can be used to differentiate between dens and irregular or elongated and curved WMH.	$CI = \sqrt{(2 - C)^2 + (1 - S)^2}$
Fractal dimension (FD) (2,3)	The Minkowski-Bouligand dimension (box-counting dimension) is a measure for textural roughness.	$FD = \lim_{r \rightarrow 1} \frac{\log(n_r)}{\log(\frac{1}{r})}$ <p>With n as the number of boxes and r the box size.</p>
Eccentricity (E) (4,5)	Eccentricity describes the deviation from a circle. The eccentricity of a circle is one and the eccentricity of a line is zero. The major axis denotes the largest diameter of the lesions in 3D and minor axis the smallest diameter orthogonal to the major axis.	$E = \frac{\text{Minor axis}}{\text{Major axis}}$

This table describes the definitions of the used shape features and shortly describes interpretation of the shape feature values.

Supplementary Table 2. Demographics and clinical characteristics of the eleven subgroups with different MRI phenotypes of the brain.

Subgroup (n)	1 (n=186)	2 (n=51)	3 (n=160)	4 (n=99)	5 (n=46)	6 (n=60)	7 (n=135)	8 (n=86)	9 (n=70)	10 (n=51)	11 (n=55)	p value
Group name	Limited burden	Limited burden	Limited burden	Limited burden	Cortical infarcts	Lacunar infarcts	Limited burden	Limited burden	Mainly CSVD	Multi burden	Neurodegenerative	
Age (years)	51±9	52±9	54±8	57±10	60±10	61±8	62±8	63±7	65±7	69±6	70±7	<0.001
Sex, % men	68%	92%	81%	63%	80%	77%	88%	89%	83%	80%	89%	<0.001
BMI (kg/m ²)	27±4	27±4	27±4	27±4	27±4	27±3	27±4	27±4	26±4	26±3	27±4	0.292
Smoking (pack years)	14 (0, 43)	17 (0, 57)	19 (0, 49)	13 (0, 42)	26 (1, 72)	20 (0, 63)	24 (0, 60)	24 (0, 49)	25 (0, 53)	15 (0, 67)	13 (0, 70)	0.004
Alcohol intake, never/former	29%	14%	25%	30%	15%	28%	20%	31%	23%	20%	42%	0.030
Hypertension	42%	51%	41%	54%	57%	65%	50%	54%	59%	69%	67%	0.006
Hyperlipidaemia	81%	82%	75%	75%	73%	83%	84%	83%	84%	78%	73%	0.385
Hyperhomocysteinemia	10%	2%	5%	9%	9%	12%	11%	9%	16%	36%	37%	0.002
Diabetes mellitus	12%	8%	12%	20%	22%	27%	27%	32%	13%	34%	38%	0.002
IMT (mm)	0.80 (0.62, 1.11)	0.87 (0.55, 1.27)	0.80 (0.62, 1.12)	0.85 (0.63, 1.20)	0.98 (0.64, 1.38)	0.89 (0.68, 1.58)	0.92 (0.72, 1.26)	0.98 (0.65, 1.46)	0.98 (0.88, 1.35)	1.02 (0.78, 1.47)	1.00 (0.74, 1.34)	0.001*
ApoE E4	33%	52%	29%	37%	36%	35%	37%	26%	36%	31%	28%	0.392

Values represent means ± SD, percentages, medians (10th, 90th percentile). BMI: Body mass index, IMT: average intima-media thickness. For the between subgroup comparison, an ANCOVA was used for continuous data and multinomial logistic regression was used for discrete data, both with age and sex as a covariate and Bonferroni correction to correct for multiple testing. A p-value < 0.05 was considered statistically significant. The post-hoc analysis using Bonferroni correction shows significant differences in the following groups: age: 1≠4-11; 2≠4-11; 3≠5-11; 4≠1,2,7-11; 5≠1-3,9-11; 6≠1-3,10,11; 7≠1-4,10,11; 8≠1-4,10,11; 9≠1-5; 10≠1-8, 11≠1-8; smoking: 1≠7 and IMT: 1≠5-11; 2≠8-11; 3≠5-11; 4≠8-11; 5≠1,3; 6≠1,3; 7≠1,3; 8≠1-4; 9≠1-4; 10≠1-4; 11≠1-4



Supplementary Figure 1. On the left the average silhouette width for 2 - 15 subgroups is plotted. The silhouette width is the average of the silhouette values of all the subgroups. The silhouette value measures the degree of confidence in the clustering assignment of a particular observation. A well clustered observation has a value near 1 and poorly clustered observations have values near -1. The average silhouette width (ASW) should be maximized. Peaks are observed at 2, 4, 6 and 11 subgroups. However, the average silhouette width values will get lower with more clusters. On the right the Dunn Index for 2 - 15 subgroups is plotted. The Dunn Index is a ratio of the smallest distance between observations of different subgroups and the largest distance within the subgroup. The Dunn Index ranges between 0 and infinity and should be maximized. Between 9 and 15 subgroups, the Dunn Index is the highest.

Supplementary Results

Subgroup 1 (n=186; mean age= 51±9 years) and 3 (n=160; mean age=54±8 years) have few brain abnormalities. These subgroups have a low WMH burden (0.03 ml (0.02, 0.06) and 0.03 ml (0.02, 0.05); medians (10th, 90th percentile)) with several small, solid and smooth WMH lesions around the lateral ventricles (convexity: 1.00±0.07 and 1.01±0.06; solidity: 0.75±0.15 and 0.78±0.11). These subgroups are characterized by only minor brain atrophy (BPF: 81.8±1.9 and 80.1±1.7 %) and a low number of cerebral infarcts (lacunar infarcts: 5% and 1%; cortical infarcts: 2% and 0%). The main differences between both subgroups are found in eccentricity (0.45±0.05 and 0.52±0.18), white matter fraction (41.5±1.6 and 44.4±1.3 %), cortical grey matter fraction (40.3±2.1 and 35.7±2.1 %) and blood flow (4.2±0.9 and 3.4±0.7 ml/min). These two subgroups with relatively few brain abnormalities are relatively young (age: 51±9 and 54±8 years) with a relative low IMT (0.80 mm (0.68, 0.93) and 0.80 mm (0.67,0.97)) and have a relatively low prevalence of hypertension (42% and 41%).

Subgroup 2 (n=51; mean age=52±9 years) also has few brain abnormalities, with the lowest burden of WMH (0.01 ml (0.00, 0.01)) with only small, solid and smooth WMH lesions around the lateral ventricles (convexity: 0.89±0.05 and solidity: 0.90±0.07). This subgroup is characterized by minor brain atrophy (BPF: 80.5±2.3 %) and few cerebral infarcts (lacunar infarcts: 6% and cortical infarcts 16%). This subgroup with relatively few brain abnormalities is relatively young (age: 52±9 years), has a cardiovascular risk factor profile comparable to subgroup 1 and 3. However, a relatively large number of patients in this subgroup consume alcohol (86%) and are ApoE ε4 carriers (52%).

Subgroup 4 (n=99; mean age= 57±10 years) has moderate brain abnormalities with an intermediate WMH burden (0.10 ml (0.06, 0.16)), consisting of PVWMH lesions that are elongated and smooth (solidity: 0.36±0.12 and convexity: 1.28±0.12). In contrast to the small, solid and smooth WMH lesions of subgroup 1, 2 and 3. This subgroup is characterized by only minor brain atrophy (BPF: 80.3±1.9 %), a low number of cerebral infarcts (lacunar infarcts 13% and cortical infarcts 0%) and relatively high cerebral blood flow (3.9±0.7 ml/min). This subgroup has relatively few brain abnormalities, is of intermediate age (57±10 years) and has a cardiovascular risk factor profile that is comparable to subgroup 1 and 3.

Subgroup 5 (n=46; mean age= 60±10 years) is characterized by a high number of cortical infarcts (98%), a low number of lacunar infarcts (15%) and intermediate brain atrophy (BPF: 77.6±2.4 %). This subgroup has a low WMH burden (0.06 ml (0.04, 0.09)) consisting of relative elongated PVWMH lesions (solidity: 0.56±0.17, convexity: 1.10±0.11).

This subgroup showed predominantly cortical infarcts, is of intermediate age (60±10 years) and has a relatively large IMT (0.98 mm (0.75,1.25)).

Subgroup 6 (n=60; mean age=61±8 years) is characterized by a high number of lacunar infarcts (98%), an intermediate number of cortical infarcts (38%) and intermediate brain atrophy (BPF: 77.4±2.4 %). This subgroup has moderate brain abnormalities with

an intermediate WMH burden (0.14 % (0.07, 0.23)) consisting of relative elongated WMH (solidity: 0.41 ± 0.17) with an increased roughness of PVWMH lesions compared to subgroup 4 (convexity: 1.16 ± 0.12). This subgroup showed predominantly lacunar infarct, is of intermediate age (61 ± 8 years), has a relatively high number of patients with hypertension (65%) and diabetes mellitus (27%), and has an intermediate IMT thickness (0.89 mm (0.77, 1.13)).

Subgroup 7 (n=135; mean age= 62 ± 8 years) has few brain abnormalities with a low WMH burden (0.05 % (0.03, 0.08)) with relatively solid (0.70 ± 0.16) and smooth (1.02 ± 0.07) PVWMH lesions. This subgroup is characterized by intermediate brain atrophy (BPF: 77.3 ± 2.1 %) and a low number of cerebral infarcts (lacunar infarcts: 9%, cortical infarcts: 0%). This subgroup has relatively few brain abnormalities, is of intermediate age (62 ± 8 years), has the heaviest smokers (26 ± 22) and has a relatively high number of patients with diabetes mellitus (27%).

Subgroup 8 (n=134; mean age= 63 ± 7 years) has moderate brain abnormalities with an intermediate WMH burden (0.12 % (0.07, 0.19)) consisting of elongated and smooth PVWMH lesions (solidity: 0.31 ± 0.12 ; convexity: 1.33 ± 0.16). This subgroup is characterized by intermediate brain atrophy (BPF: 77.9 ± 2.1 %) and a low number of cerebral infarcts (lacunar infarcts: 2%, cortical infarcts: 2%). This subgroup has relatively few brain abnormalities, is of intermediate age (63 ± 7 years), has a relatively large IMT (0.98 mm (0.85, 1.18) and a large number of patients with diabetes mellitus (32%).

Subgroup 9 (n=70; mean age= 65 ± 7 years) has more severe brain abnormalities, with an intermediate WMH burden (0.38 % (0.22, 0.59)) with large PVWMH lesions with increased roughness (solidity: 0.30 ± 0.10 and convexity: 1.05 ± 0.09). This subgroup is characterized by intermediate brain atrophy (BPF: 78.2 ± 1.8 %) and a high number of patients with lacunar infarcts (44%) and relatively more patients with cortical infarcts (15%). This subgroup with predominantly features of cerebral small vessel disease, has a relatively old age (65 ± 7 years), a large IMT (0.98 mm (0.85, 1.12)) and a large number of patients with hypertension (59%).

Subgroup 10 (n=51; mean age= 69 ± 6 years) has severe brain abnormalities with a high WMH burden (1.13 % (0.91, 2.03)) with large PVWMH lesions with increased roughness (solidity: 0.24 ± 0.05 and convexity: 0.87 ± 0.13). This subgroup is characterized by more severe brain atrophy (BPF: 75.5 ± 2.3 %) and a high number of patients with cerebral infarcts (lacunar infarcts: 78% and cortical infarcts 29%). This subgroup with predominantly multi burden, is relatively old (69 ± 6 years), has a large IMT (1.02 mm (0.93, 1.16)), a large number of patients with hypertension (69%), hyperhomocysteinemia (36%) and diabetes mellitus (34%).

Subgroup 11 (n=55; mean age= 70 ± 7 years), has severe brain abnormalities characterized by more severe brain atrophy (BPF: 74.6 ± 2.8 %) and a relatively low number of patients with cerebral infarcts (lacunar infarcts: 13% and cortical infarcts: 9%). This subgroup has an intermediate WMH burden (0.27 % (0.12, 0.37)) with large PVWMH lesions

with only slightly increased roughness (solidity: 0.33 ± 0.10 and convexity: 1.13 ± 0.10). This subgroup with predominantly neurodegenerative features, is relatively old (70 ± 7 years), has a large IMT (1.00 mm (0.85, 1.15), a large number of patients with hypertension (67%), hyperhomocysteinemia (37%) and diabetes mellitus (38%).

References

1. Liu EJ, Cashman K V., Rust AC. Optimising shape analysis to quantify volcanic ash morphology. *GeoResJ*. 2015;8:14–30.
2. Zhang L, Liu JZ, Dean D, Sahgal V, Yue GH. A three-dimensional fractal analysis method for quantifying white matter structure in human brain. *J Neurosci Methods*. 2006;150(2):242–53.
3. Esteban FJ, Sepulcre J, de Miras JR, Navas J, de Mendizábal NV, Goñi J, et al. Fractal dimension analysis of grey matter in multiple sclerosis. *J Neurol Sci*. 2009;282(1):67–71.
4. Murphy K, van Ginneken B, Schilham AMR, De Hoop BJ, Gietema HA, Prokop M. A large-scale evaluation of automatic pulmonary nodule detection in chest CT using local image features and k-nearest-neighbour classification. *Med Image Anal*. 2009;13(5):757–70.
5. Loizou CP, Pattichis CS, Seimenis I, Pantziaris M. Quantitative analysis of brain white matter lesions in multiple sclerosis subjects. In: *Information Technology and Applications in Biomedicine, 2009 ITAB 2009 9th International Conference on*. IEEE; 2009. p. 1–4.

PART II



Microinfarcts in the deep gray matter on MRI

CHAPTER 5

5

Detection and characterization of small infarcts in the caudate nucleus on 7 Tesla MRI: The SMART-MR study

Rashid Ghaznawi ^{1,2}, Jeroen de Bresser ¹, Yolanda van der Graaf ², Maarten HT Zwartbol ¹, Theo D Witkamp ¹, Mirjam I. Geerlings ², Jeroen Hendrikse ¹; on behalf of the SMART Study Group

¹Department of Radiology, University Medical Center Utrecht, Netherlands; ²Julius Center for Health Sciences and Primary Care, University Medical Center Utrecht, Netherlands

Small infarcts are among the key imaging features of cerebral small vessel disease (CSVD), but remain largely undetected on conventional MRI. We aimed to evaluate 1) imaging criteria for the detection of small infarcts in the caudate nucleus on 7T MRI, 2) intra- and inter-rater agreement, 3) frequency and 4) detection rate on 7T versus 1.5T MRI. In 90 patients (68 ± 8 years) with a history of vascular disease from the SMART-MR study we defined 7T imaging criteria for cavitated and non-cavitated small infarcts in the caudate nucleus. In a separate set of 23 patients from the SMART study intra-rater and inter-rater agreement were excellent for presence, number, and individual locations (Kappa's, ICCs, and Dice similarity coefficients ranged from 0.85 to 1.00). In the 90 patients, 21 infarcts (20 cavitated) in 12 patients were detected on 7T (13%) compared to 7 infarcts in 6 patients on 1.5T (7%). In conclusion, we established reproducible imaging criteria for the detection of small infarcts in the caudate nucleus on 7T MRI and showed that 7T MRI allows for a higher detection rate than conventional 1.5T MRI. These imaging criteria can be used in future studies to provide new insights into the pathophysiology of CSVD.

Introduction

Cerebral small vessel disease (CSVD) is associated with cognitive decline and is considered a risk factor for dementia¹⁻³. The main brain MRI features of CSVD are white matter hyperintensities and lacunar infarcts of presumed vascular origin⁴⁻⁶. Brain autopsy studies showed the presence of cerebral small infarcts that can range from 50 μm to 15 mm in size and which are also considered a feature of CSVD⁷⁻⁹. In autopsy studies, these small infarcts can occur in up to 43% of non-demented older individuals in cortical and subcortical areas of the brain⁷. Despite this high prevalence, these small infarcts are largely undetected on conventional 1.5T MRI due to their small size⁹.

Recently, it was shown that small infarcts in the cerebral cortex can be detected *in vivo* on 7T MRI¹⁰. Although the presence and imaging characteristics of small infarcts in the cortical gray matter on high field MRI have been studied¹¹⁻¹⁵, small infarcts in the subcortical gray matter on high field MRI have not been studied. To determine the total CSVD burden more accurately, it is necessary to assess not only cortical, but also subcortical gray matter in greater detail. The caudate nucleus has advantages over other subcortical gray matter structures when assessing small infarcts. The caudate nucleus has a paraventricular location and is better demarcated from surrounding tissues compared to the rest of the subcortical gray matter, thus allowing for a more accurate determination of the frequency of small infarcts in this subcortical structure¹⁶.

The aim of the present study was first, to establish imaging criteria for the detection of small infarcts in the caudate nucleus on 7T MRI; second, to determine the intra- and inter-rater agreement for detection of these small infarcts on 7T MRI; third, to estimate the frequency and explore possible determinants of these small infarcts in patients with a history of symptomatic atherosclerotic disease; and fourth, to assess differences in detection rate of these small infarcts between 7T MRI and 1.5T MRI.

Material and methods

Study populations

We used cross-sectional data from the SMART study and the SMART-MR study^{17, 18}. The Second Manifestations of ARterial disease (SMART) study is a prospective cohort study at the University Medical Center Utrecht designed to establish the prevalence of concomitant arterial diseases and risk factors for atherosclerosis in a high-risk population¹⁷. The SMART-MR study is a sub-study of the SMART study, with the aim to investigate risk factors and consequences of brain changes on MRI in patients with symptomatic atherosclerotic disease¹⁸. The SMART-MR study is an ongoing prospective cohort study in 1309 middle-aged and older adult patients newly referred to the University Medical Center Utrecht for treatment of symptomatic atherosclerotic disease (manifest coronary artery disease,

cerebrovascular disease, peripheral arterial disease or abdominal aortic aneurysm) enrolled between May 2001 and December 2005 for baseline measurements, and of whom 754 patients had follow-up measurements four years later between January 2006 and May 2009. During a one day visit to our medical center, a physical examination, ultrasonography of the carotid arteries, blood and urine samplings, neuropsychological assessment, and a 1.5T brain MRI scan were performed. Questionnaires were used for assessing demographics, risk factors and medical history, medication use, and functioning. Since November 2013, all patients alive are invited for a second follow-up, including a 7T brain MRI. For objectives 1, 3 and 4, we included 90 patients who had second follow-up measurements between December 2013 and May 2016 and who had a 7T MRI scan.

For objective 2 we used a random selection of 23 patients with asymptomatic (e.g. hypertension) or symptomatic (e.g. coronary artery disease) atherosclerotic disease from the SMART study, who had a 7T MRI of the brain between September 2012 and September 2013. There was no overlap between the group of 23 patients used for objective 2 and the group of 90 patients used for objectives 1, 3 and 4.

To assess the frequency of small infarcts in the caudate nucleus in primary care patients not selected on disease status, we included 48 participants with a 7T brain MRI from the PREDICT-MR study¹⁹. In this study, adult patients aged 18 years or older were included from the waiting room of the general practitioner, irrespective of their reasons for consulting their general practitioner. Participants were considered eligible for the PREDICT-MR study if they were not demented or severely ill. A 1.5T and 7T brain MRI was performed on the same day between June 2010 and January 2012 as part of follow-up measurements¹⁹.

All studies were approved by the medical ethics committee of the University Medical Center Utrecht according to the guidelines of the Declaration of Helsinki of 1975 and written informed consent was obtained from all participants.

Magnetic resonance imaging protocol

Conventional MR imaging of the brain was performed on a 1.5T whole-body system (Gyrosan ACS-NT, Philips Medical Systems, Best, The Netherlands) using a standardized scan protocol. Transversal T1-weighted [repetition time (TR) = 235 ms; echo time (TE) = 2 ms], T2-weighted [TR = 2200 ms; TE = 11 ms], fluid-attenuated inversion recovery (FLAIR) [TR = 6000 m; TE = 100 ms; inversion time (TI) = 2000 ms] and T1-weighted inversion recovery images [TR = 2900 ms; TE = 22 ms; TI = 410 ms] were acquired with a voxel size of 1.0x1.0x4.0 mm³ and contiguous slices. Infarcts on 1.5T MRI scans were rated on all MRI sequences (T1, T2 and FLAIR) by a rater with 5 years of experience in brain MRI (MHTZ). Ratings were performed blinded to patient characteristics.

High-field imaging of the brain was performed on a whole-body 7T MR system (Philips Healthcare, Cleveland, OH, USA) with a volume transmit and 32-channel receive head coil (Nova Medical, Wilmington, MA, USA). The standardized scan protocol consisted of volumetric (3D) T1-weighted [voxel size = 0.66x0.66x0.50 mm³; TR = 4.8 ms; TE = 2.2

ms; flip angle 8°), 3D T2-weighted turbo-spin echo [voxel size = 0.35x0.35x0.35 mm³, TR = 3158 ms, TE = 301 ms] and 3D magnetization prepared FLAIR images [voxel size = 0.49x0.49x0.49 mm³, TR = 8000 ms, TE = 300 ms]^{10, 19, 20}.

Cardiovascular risk factors

Smoking habits and alcohol intake were assessed with questionnaires, and were categorized as never, former or current. Height and weight were measured, and the body mass index (BMI) was calculated (kg/m²). Systolic blood pressure (SBP; mmHg) and diastolic blood pressure (DBP; mmHg) were measured three times with a sphygmomanometer, and the average of these measures was calculated. Hypertension was defined as a mean SBP of ≥160 mmHg, or a mean DBP of ≥95 mmHg, or self-reported use of antihypertensive drugs, or a known history of hypertension at inclusion. An overnight fasting venous blood sample was taken to determine glucose and lipid levels. Diabetes mellitus was defined as use of glucose-lowering agents, or a known history of diabetes mellitus, or a fasting plasma glucose level of >11.1 mmol/l. Hyperlipidemia was defined as a total cholesterol of >5.0 mmol/l, or a low-density lipoprotein cholesterol of >3.2 mmol/l, or use of lipid-lowering drugs, or a known history of hyperlipidemia. Ultrasonography was performed with a 10MHz linear-array transducer (ATL Ultramark 9) by an ultrasound technician. Mean carotid intima-media thickness (in mm) was calculated for the left and right common carotid arteries based on 6 far-wall measurements.

MRI analysis

All ratings were performed blinded to patient characteristics. For the first objective, to establish imaging criteria for the detection of small infarcts in the caudate nucleus on 7T MRI, the 7T MRI scans of patients with symptomatic atherosclerotic disease (SMART-MR study; n=90) were examined by one rater (RG) for possible lesions in the caudate nucleus. Subsequently, a meeting was held with two raters with 30 and 15 years of experience in brain MRI imaging (TW and JH; senior neuroradiologists) and a rater with 9 years of experience in brain MRI imaging (JdB) to define and characterize lesions.

For the second objective, intra- and inter-rater agreement for the detection of small infarct on 7T MRI were determined. The 7T MRI scans of patients with atherosclerotic disease (SMART study; n=23) were rated twice by one rater (TW) and rated once by two raters (JdB and JH) using all 7T MRI sequences (T1, T2 and FLAIR) in three orthogonal viewing directions (sagittal, coronal, and transversal). Intra-observer agreement was calculated for presence (Cohen's kappa), number (intra-class correlation coefficient (ICC)) and overlap in individual locations (Dice similarity coefficient²¹) of small infarcts in the caudate nucleus. Inter-observer agreement between the three raters was calculated for presence (Fleiss' kappa), number (ICC) and overlap in individual locations (Dice similarity coefficient).

For the third objective, the scans of patients with symptomatic atherosclerotic disease (SMART-MR study; n=90) and of primary care patients not selected on disease status

(PREDICT-MR study; n=48) were randomly mixed and rated for presence of small infarcts in the caudate nucleus by one rater (TW) blinded to patient status. Uncertain lesions were discussed during a consensus meeting (TW, JH and JdB) to reach agreement. The side (left, right), location (head, body or tail of the caudate nucleus) and maximal diameter of all small infarcts were determined on the FLAIR sequence in three orthogonal directions (sagittal, coronal or transversal). Baseline characteristics were compared between the patients with versus without small infarcts in the caudate nucleus by Chi square tests or t-tests. A Chi square test was performed to assess differences in frequency of small infarcts between patients with atherosclerotic disease (n=90) and the primary care patients not selected on disease status (n=48).

For the fourth objective, presence and individual locations of small infarcts identified on 7T MRI were compared to those on 1.5T MRI in patients with symptomatic atherosclerotic disease (SMART-MR study; n=90).

Results

7T MRI imaging criteria of small infarcts in the caudate nucleus

Based on our assessment of infarct types in the caudate nucleus on 7T MRI, we identified two distinct morphologies. First, cavitated small infarcts were identified as lesions that were hypointense on T1-weighted images, hyperintense on T2-weighted images and hypointense with a hyperintense rim on FLAIR images (Table 1). Second, non-cavitated small infarcts were identified as hypointense on T1-weighted images and hyperintense on T2-weighted and FLAIR images (Table 1). Tissue loss with a surrounding hyperintense rim on FLAIR images was characterized as a cavitated small infarct. Lesions with a maximum diameter of 15 mm were considered small infarcts in the caudate nucleus²², while we did not define a minimum size criterion for small infarcts. Examples of cavitated and non-cavitated small infarcts in the caudate nucleus can be seen in Figures 1 and 2.

Table 1. Proposed imaging criteria for small infarcts in the caudate nucleus on 7T MRI.

Type	T1	T2	FLAIR
Cavitated	●	●	●
Non-cavitated	●	●	●

We defined cavitated small infarcts in the caudate nucleus as lesions that were hypointense on T1-weighted images, hyperintense on T2-weighted images and hypointense with a hyperintense rim on FLAIR images. We defined non-cavitated small infarcts as hypointense on T1-weighted images and hyperintense on T2-weighted and FLAIR images.

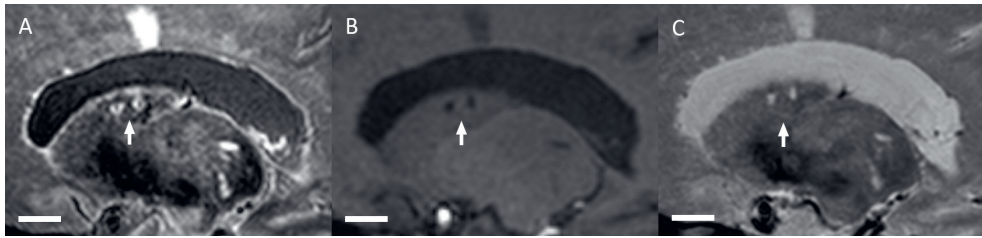


Figure 1. Two cavitated small infarcts (arrow) in the body of the left caudate nucleus in a 67-year old female shown on sagittal FLAIR (A), T1-weighted (B) and T2-weighted images (C) of the 7T MRI scan. These lesions are hypointense with a hyperintense rim on the FLAIR image, hypointense on the T1-weighted image and hyperintense on the T2-weighted image. Scale bar indicates 10 mm.

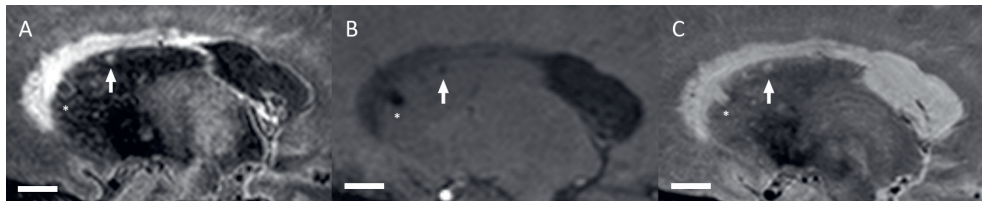


Figure 2. A non-cavitated small infarct (arrow) in the body of the right caudate nucleus in a 69-year old male shown on sagittal FLAIR (A), T1-weighted (B) and T2-weighted images (C) of the 7T MRI scan. This lesion is hyperintense on the FLAIR image, hypointense on the T1-weighted image and hyperintense on the T2-weighted image. Note the presence of a cavitated small infarct (*) in the head of the caudate nucleus. Scale bar indicates 10 mm.

Intra- and inter-rater agreement of small infarcts in the caudate nucleus

In the MRI scans of the 23 patients (mean age 61 ± 11 years; 65% male) used to measure intra- and inter-rater agreement, the first rater identified a total number of 13 cavitated small infarcts in five patients (22%) during the first rating. During the second rating, the first rater identified a total number of 12 cavitated small infarcts in the same five patients (22%). The first rater identified no non-cavitated infarcts (Supplementary Table 1). The second rater identified a total number of 12 small infarcts in four patients (17%), of which ten were rated as cavitated and two as non-cavitated. The third rater identified a total number of 14 small infarcts in five patients (22%), of which 12 were rated as cavitated and two as non-cavitated (Supplementary Table 1). The intra-rater agreement for the first rater was excellent for presence (Cohen's kappa: 1.00), number (ICC: 0.99 (95% CI 0.98 to 1.00)) and individual locations (Dice similarity coefficient: 0.96) of small infarcts in the caudate nucleus. The inter-rater agreement for all three raters was very good to excellent for presence (Fleiss' kappa: 0.91), number (ICC: 0.99 (95% CI 0.98 to 1.00)) and individual locations (Dice similarity coefficient between rater 1 and 2/rater 1 and 3/rater 2 and 3, respectively: 0.88/0.89/0.85) of small infarcts in the caudate nucleus.

Patients with versus without small infarcts in the caudate nucleus

The baseline characteristics for the 90 patients with symptomatic atherosclerotic disease (SMART-MR study; mean age 68 ± 8 years; 80% male) are shown in Table 2. A total number of 21 small infarcts were identified in the caudate nucleus (20 cavitated; 1 non-cavitated) in 12 patients (13%). A maximum of 5 small infarcts was identified in one patient. The mean size of small infarcts in the caudate nucleus was 5.2 mm (range: 2.1 to 8.6 mm). Most small infarcts were located in the caudate head (11 infarcts), followed by the body (6 infarcts) and tail (4 infarcts) (Table 3). In two patients (2%) a cavitated small infarct was identified that consisted of tissue loss with a surrounding hyperintense rim on the FLAIR image (Figure 3). Three patients (3%) showed a large infarct in the flow territory of the middle cerebral artery, which included infarcted tissue in a large part of the caudate nucleus in one hemisphere.

Table 2 . Baseline characteristics of the study population (n=90).

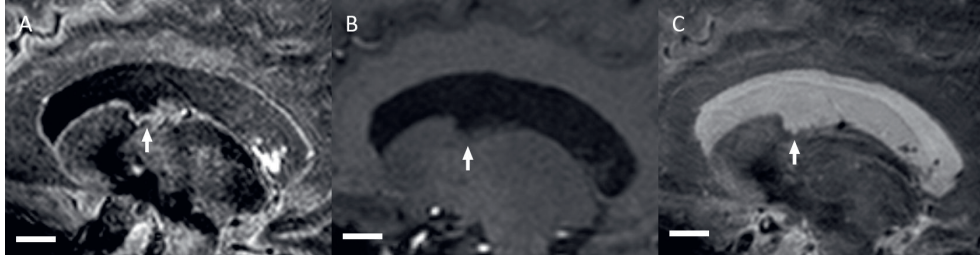
Age (years)	68 ± 8
Sex, n (%) men	73 (81)
Vascular disease location, n (%)	
Coronary artery disease	60 (67)
Cerebrovascular disease	28 (31)
Peripheral arterial disease	9 (10)
Abdominal aortic aneurysm	2 (2)
Multiple vascular diseases	13 (14)
Cardiovascular risk factors	
BMI (kg/m^2)	27 ± 4
Smoking, % current	17 (19)
Alcohol intake, % current	82 (91)
Hypertension, n (%)	73 (81)
Hyperlipidemia, n (%)	76 (84)
Diabetes mellitus, n (%)	16 (18)
IMT (mm)	0.9 ± 0.2
Infarcts on 1.5T MRI, n (%)	
Any infarct	26 (29)
Cortical	12 (13)
Large subcortical	0 (0)
Lacunar	17 (19)
Other ^a	7 (8)

Characteristics are presented as mean \pm SD or n (%).

^a Cerebellum and brain stem.

Table 3 . Characteristics of the 21 small infarcts found in the caudate nucleus in 12 patients (13%) with symptomatic atherosclerotic disease (n=90).

	n	Mean size \pm SD (mm)	Left side; n (%)	Location; n (%)		
				Head	Body	Tail
Cavitated	20	5.2 \pm 1.6	9 (45%)	11 (55%)	5 (25%)	4 (20%)
Non-cavitated	1	5.4	0	0	1	0

**Figure 3 .** An area of tissue loss with a hyperintense rim on FLAIR (arrow) in the body of the left caudate nucleus in a 80-year old male shown on sagittal FLAIR (A), T1-weighted (B) and T2-weighted images (C) of the 7T MRI scan. We defined this type of infarct as a cavitated small infarct. Scale bar indicates 10 mm.

In the 48 primary care patients not selected on disease status (PREDICT-MR study; mean age 60 ± 10 years; 38% male), we identified one cavitated small infarct in the head of the caudate nucleus in one patient (2%). More small infarcts were detected in the caudate nucleus in the 90 patients with symptomatic atherosclerotic disease compared to the 48 primary care patients not selected on disease status ($p=0.031$).

In the 90 patients with symptomatic atherosclerotic disease, patients with small infarcts ($n=12$) in the caudate nucleus were older (mean difference of 6.9 years; 95% CI 2.1 to 11.6) than patients without small infarcts ($n=78$). Furthermore, patients with small infarcts in the caudate nucleus showed a higher number of cerebral infarcts in the entire brain on 1.5T MRI (58% versus 24%; $p=0.017$), specifically of lacunar infarcts (58% versus 13%; $p<0.001$), compared to patients without small infarcts. No differences in sex, vascular disease location or cardiovascular risk factors were found between the patients with and without small infarcts in the caudate nucleus (Table 4).

Detection rate of small infarcts in the caudate nucleus on 7T MRI versus 1.5T MRI

In the 90 patients with symptomatic atherosclerotic disease, the median duration between the 1.5T and 7T MRI scans was 0 months (10th-90th percentile: 0-28 months). The majority of patients received both MRI scans on the same day (50 patients; 56%). A total number of 21 small infarcts were identified on 7T MRI compared to 7 small infarcts on 1.5T MRI scans.

On 7T MRI scans (n=12; 13%) twice the number of patients had small infarcts compared to 1.5T MRI scans (n=6; 7%). A similar difference between detection of small infarcts on 7T MRI and 1.5T MRI scans was seen in patients who did not receive both MRI scans on the same day. All small infarcts detected on 1.5T MRI scans were also rated on the 7T MRI scans (Supplementary Table 2). An example of a small infarct in the caudate nucleus that was rated on both 1.5T and 7T MRI and one that was only rated on 7T MRI can be seen in Supplementary Figures 1 and 2, respectively.

Table 4. Characteristics of patients with versus without small infarcts in the caudate nucleus.

	With small infarcts (n=12)	Without small infarcts (n=78)	p-value
Age (years)	73.8 ± 7.3	66.9 ± 7.6	0.005
Sex, n (%) men	11 (92)	61 (78)	0.32
Vascular disease location, n (%)			
Coronary artery disease	8 (67)	52 (67)	1.00
Cerebrovascular disease	3 (25)	25 (32)	0.62
Peripheral arterial disease	3 (25)	6 (8)	0.06
Abdominal aortic aneurysm	0	2 (3)	0.58
Multiple vascular diseases	2 (17)	11 (14)	0.81
Cardiovascular risk factors			
BMI (kg/m ²)	28.1 ± 4.3	26.9 ± 3.8	0.34
Smoking, % current	0 (0)	17 (22)	0.07
Alcohol intake, % current	12 (100)	70 (90)	0.25
Hypertension, n (%)	10 (83)	63 (82)	0.90
Hyperlipidemia, n (%)	10 (83)	66 (87)	0.74
Diabetes mellitus, n (%)	2 (17)	14 (18)	0.91
IMT (mm) ^b	0.9 ± 0.1	0.9 ± 0.2	0.17
Infarcts on 1.5T MRI, n (%)			
Any infarct	7 (58)	19 (24)	0.016
Cortical	3 (25)	9 (12)	0.20
Large subcortical	0 (0)	0 (0)	-
Lacunar	7 (58)	10 (13)	<0.001
Other ^a	2 (17)	5 (6)	0.22

Characteristics are presented as mean ± SD or n (%).

^a Cerebellum and brain stem.

^b Natural log-transformed for the between group analysis due to a non-normal distribution.

Discussion

We established imaging criteria for the detection of small infarcts in the caudate nucleus on 7T MRI that differentiate between cavitated and non-cavitated small infarcts. The intra-

and inter-rater agreement for detection of these small infarcts was very good to excellent. We observed that small infarcts in the caudate nucleus were a relatively common finding on 7T MRI in patients with symptomatic atherosclerotic disease. Furthermore, they were associated with older age and presence of other cerebral infarcts on 1.5T MRI. More small infarcts were detected on 7T MRI compared to 1.5T MRI.

To our knowledge, this is the first study that used 7T MRI to evaluate the deep gray matter for the presence of small infarcts, both in terms of characterizing lesions and assessing intra- and inter-rater agreement for detection. We showed that on 7T MRI the MRI signal intensity characteristics of small infarcts in the caudate nucleus are similar to those described in the STRIVE criteria²². The STRIVE criteria, which were originally formulated for use on 1.5T or 3T MRI, characterize small infarcts as lesions between 3 mm and 15 mm in diameter. Contrary to the STRIVE criteria, we did not define a minimum size criterion for small infarcts in the caudate nucleus, because smaller infarcts can be detected on 7T MRI compared to 1.5T or 3T MRI. This increased detection can be explained by the enhanced resolution of 7T MRI and the higher image quality due to a higher signal-to-noise and contrast-to-noise ratio. Hence, we believe that the STRIVE criteria should be extended by a lower minimum size criterion for small infarcts on 7T MRI images.

The prevalence of small infarcts in the caudate nucleus (13%) in patients with symptomatic atherosclerotic disease in our subset of the SMART-MR study (n=90; mean age 68 ± 8 years) is higher than reported in studies using low field MRI. Only few studies reported small infarcts in the caudate nucleus separately. In a study including patients with CSVD (n=633; mean age 74 ± 5 years), the prevalence of small infarcts in the caudate nucleus on 1.5T MRI was 7.7%²³. Although our findings cannot be directly compared, we will provide prevalences of small infarcts in the basal ganglia and brain as a frame of reference. In a study in community dwelling older individuals (n=477; mean age 63 ± 2 years), small infarcts in the basal ganglia on 1.5T MRI were observed in 4.6%²⁴. In other studies in community dwelling individuals, the combined prevalence of small infarcts in the entire brain on 1.5T MRI was 15.4% (range: 5.8 to 23.0%; mean age range: 49 to 72 years)²⁵⁻³⁰. The higher prevalence of small infarcts in the caudate nucleus found in our study may be explained by the higher detection rate on 7T MRI, which is caused by a combination of an increased signal-to-noise ratio, an increased contrast-to-noise ratio and a higher resolution compared to conventional 1.5T MRI scans³¹.

In previous studies using 7T or 3T MRI to detect small infarcts in the cortical gray matter, lesions smaller than 5 mm were sometimes defined as microinfarcts^{10, 32-35}. If we apply this size criterion to our study, 9 of 21 small infarcts (43%) are smaller than 5 mm and could thus be defined as microinfarcts. However, we would like to emphasize that the etiological significance of the term "microinfarct" in the context of the caudate nucleus remains questionable and its use is not in concordance with current consensus reporting standards. This lack of consistency does not only apply to microinfarcts, but also to other manifestations of CSVD. Definitions and terminology for imaging features of CSVD vary

widely in the literature, as was highlighted in the Position Paper for the STRIVE criteria²². Our use of the consensus term small infarct is in concordance with the STRIVE reporting standards, in which small infarcts are defined as cavitated lesions (e.g. lacunes of presumed vascular origin) or in some cases non-cavitated lesions without a fluid cavity on FLAIR images²². Use of standardized neuroimaging criteria for CSVD will facilitate across-study comparisons of findings, thereby possibly accelerating the translation of new findings into clinical practice^{22, 36, 37}.

The strengths of our study are the use of high quality 7T MRI data that enabled us to accurately detect and characterize small infarcts in the caudate nucleus. Our study made it possible to detect small infarcts that would have remained undetected on conventional 1.5T MRI scans. Also, compared to other 7T MRI studies, we had a large cohort of patients. A limitation of our study may be the lack of histopathological validation of the observed small infarcts. However, we applied strict MRI imaging criteria aimed at identifying lesions with a high probability of being small infarcts. This approach could also have resulted in an underrating of small infarcts in the caudate nucleus. For example, we found one potential lesion that did not conform to our imaging criteria. This lesion was hypointense with a hyperintense rim on FLAIR and hyperintense on T2, however on T1 this lesion appeared isointense to the surrounding tissue. It is possible that this lesion was a small infarct. Infarcts in the caudate nucleus of around 1 mm in diameter are at the detection limit of 7T MRI, thus the true burden of small infarcts might be underestimated. Another limitation might be that although the sample size of our study is among the largest for 7T MRI studies, a larger sample is needed to examine determinants of small infarcts in the caudate nucleus in more detail. Lastly, a limitation may be that the intra- and inter-rater agreement was performed by three raters with extensive experience in neuroradiology. Performing ratings by less experienced raters could result in a lower intra- and inter-rater agreement.

The increased detection rate of small infarcts at 7T MRI is most likely not limited to the caudate nucleus. We started with the caudate nucleus due to its paraventricular location. This paraventricular location allowed for a better demarcation from surrounding tissues compared to other structures of the subcortical gray matter, thus enabling a more accurate determination of the frequency of small infarcts in the caudate nucleus. Expanding the research of small infarcts to other structures of the subcortical gray matter will most likely lead to other challenges. For example, compared to the caudate nucleus, the lentiform nucleus and thalamus are less well-demarcated from surrounding tissues on MRI scans. This can lead to challenges in the localization of small infarcts in these structures in some cases.

In conclusion, we established reproducible imaging criteria for the detection of small infarcts in the caudate nucleus on 7T MRI and showed that 7T MRI allows for a higher detection rate than conventional 1.5T MRI. These imaging criteria can be used in future studies to provide new insights into the pathophysiology of CSVD.

References

1. Pantoni L, Poggesi A and Inzitari D. Cognitive decline and dementia related to cerebrovascular diseases: some evidence and concepts. *Cerebrovasc Dis* 2009; 27 Suppl 1: 191-196.
2. Makin SD, Turpin S, Dennis MS and Wardlaw JM. Cognitive impairment after lacunar stroke: systematic review and meta-analysis of incidence, prevalence and comparison with other stroke subtypes. *J Neurol Neurosurg Psychiatry* 2013; 84: 893-900.
3. Ostergaard L, Engedal TS, Moreton F, et al. Cerebral small vessel disease: Capillary pathways to stroke and cognitive decline. *J Cereb Blood Flow Metab* 2016; 36: 302-325.
4. Wardlaw JM, Smith C and Dichgans M. Mechanisms of sporadic cerebral small vessel disease: insights from neuroimaging. *Lancet Neurol* 2013; 12: 483-497.
5. Gouw AA, Seewann A, van der Flier WM, et al. Heterogeneity of small vessel disease: a systematic review of MRI and histopathology correlations. *J Neurol Neurosurg Psychiatry* 2011; 82: 126-135.
6. De Guio F, Jouvent E, Biessels GJ, et al. Reproducibility and variability of quantitative magnetic resonance imaging markers in cerebral small vessel disease. *J Cereb Blood Flow Metab* 2016; 36: 1319-1337.
7. Brundel M, de Bresser J, van Dillen JJ, Kappelle LJ and Biessels GJ. Cerebral microinfarcts: a systematic review of neuropathological studies. *J Cereb Blood Flow Metab* 2012; 32: 425-436.
8. Kalaria RN, Kenny RA, Ballard CG, Perry R, Ince P and Polvikoski T. Towards defining the neuropathological substrates of vascular dementia. *J Neurol Sci* 2004; 226: 75-80.
9. Smith EE, Schneider JA, Wardlaw JM and Greenberg SM. Cerebral microinfarcts: the invisible lesions. *Lancet Neurol* 2012; 11: 272-282.
10. van Veluw SJ, Zwanenburg JJ, Engelen-Lee J, et al. In vivo detection of cerebral cortical microinfarcts with high-resolution 7T MRI. *J Cereb Blood Flow Metab* 2013; 33: 322-329.
11. van Veluw SJ, Zwanenburg JJ, Rozemuller AJ, Luijten PR, Spliet WG and Biessels GJ. The spectrum of MR detectable cortical microinfarcts: a classification study with 7-tesla postmortem MRI and histopathology. *J Cereb Blood Flow Metab* 2015; 35: 676-683.
12. Brundel M, Reijmer YD, van Veluw SJ, et al. Cerebral microvascular lesions on high-resolution 7-Tesla MRI in patients with type 2 diabetes. *Diabetes* 2014; 63: 3523-3529.
13. De Reuck J, Deramecourt V, Auger F, et al. Post-mortem 7.0-tesla magnetic resonance study of cortical microinfarcts in neurodegenerative diseases and vascular dementia with neuropathological correlates. *J Neurol Sci* 2014; 346: 85-89.
14. De Reuck JL, Deramecourt V, Auger F, et al. The significance of cortical cerebellar microbleeds and microinfarcts in neurodegenerative and cerebrovascular diseases. A post-mortem 7.0-tesla magnetic resonance study with neuropathological correlates. *Cerebrovasc Dis* 2015; 39: 138-143.
15. de Rotte AA, Koning W, den Hartog AG, et al. 7.0 T MRI detection of cerebral microinfarcts in patients with a symptomatic high-grade carotid artery stenosis. *J Cereb Blood Flow Metab* 2014; 34: 1715-1719.
16. Pellizzaro Venti M, Paciaroni M and Caso V. Caudate infarcts and hemorrhages. *Front Neurol Neurosci* 2012; 30: 137-140.

17. Simons PC, Algra A, van de Laak MF, Grobbee DE and van der Graaf Y. Second manifestations of ARterial disease (SMART) study: rationale and design. *Eur J Epidemiol* 1999; 15: 773-781.
18. Geerlings MI, Appelman AP, Vincken KL, et al. Brain volumes and cerebrovascular lesions on MRI in patients with atherosclerotic disease. The SMART-MR study. *Atherosclerosis* 2010; 210: 130-136.
19. Wisse LE, Biessels GJ, Stegenga BT, et al. Major depressive episodes over the course of 7 years and hippocampal subfield volumes at 7 tesla MRI: the PREDICT-MR study. *J Affect Disord* 2015; 175: 1-7.
20. Visser F, Zwanenburg JJ, Hoogduin JM and Luijten PR. High-resolution magnetization-prepared 3D-FLAIR imaging at 7.0 Tesla. *Magn Reson Med* 2010; 64: 194-202.
21. Kuijf HJ, van Veluw SJ, Viergever MA, Vincken KL and Biessels GJ. How to assess the reliability of cerebral microbleed rating? *Front Aging Neurosci* 2013; 5: 57.
22. Wardlaw JM, Smith EE, Biessels GJ, et al. Neuroimaging standards for research into small vessel disease and its contribution to ageing and neurodegeneration. *Lancet Neurol* 2013; 12: 822-838.
23. Benisty S, Gouw AA, Porcher R, et al. Location of lacunar infarcts correlates with cognition in a sample of non-disabled subjects with age-related white-matter changes: the LADIS study. *J Neurol Neurosurg Psychiatry* 2009; 80: 478-483.
24. Chen X, Wen W, Anstey KJ and Sachdev PS. Prevalence, incidence, and risk factors of lacunar infarcts in a community sample. *Neurology* 2009; 73: 266-272.
25. Das RR, Seshadri S, Beiser AS, et al. Prevalence and correlates of silent cerebral infarcts in the Framingham offspring study. *Stroke* 2008; 39: 2929-2935.
26. Kohara K, Fujisawa M, Ando F, et al. MTHFR gene polymorphism as a risk factor for silent brain infarcts and white matter lesions in the Japanese general population: The NILS-LSA Study. *Stroke* 2003; 34: 1130-1135.
27. Lee SC, Park SJ, Ki HK, et al. Prevalence and risk factors of silent cerebral infarction in apparently normal adults. *Hypertension* 2000; 36: 73-77.
28. Longstreth WT, Jr., Bernick C, Manolio TA, Bryan N, Jungreis CA and Price TR. Lacunar infarcts defined by magnetic resonance imaging of 3660 elderly people: the Cardiovascular Health Study. *Arch Neurol* 1998; 55: 1217-1225.
29. Schmidt R, Schmidt H, Pichler M, et al. C-reactive protein, carotid atherosclerosis, and cerebral small-vessel disease: results of the Austrian Stroke Prevention Study. *Stroke* 2006; 37: 2910-2916.
30. van Dijk EJ, Prins ND, Vermeer SE, et al. C-reactive protein and cerebral small-vessel disease: the Rotterdam Scan Study. *Circulation* 2005; 112: 900-905.
31. Madai VI, von Samson-Himmelstjerna FC, Bauer M, et al. Ultrahigh-field MRI in human ischemic stroke--a 7 tesla study. *PLoS One* 2012; 7: e37631.
32. van Veluw SJ, Hilal S, Kuijf HJ, et al. Cortical microinfarcts on 3T MRI: Clinical correlates in memory-clinic patients. *Alzheimers Dement* 2015; 11: 1500-1509.
33. Hilal S, Sikking E, Shaik MA, et al. Cortical cerebral microinfarcts on 3T MRI: A novel marker of cerebrovascular disease. *Neurology* 2016; 87: 1583-1590.
34. Wang Z, van Veluw SJ, Wong A, et al. Risk Factors and Cognitive Relevance of Cortical Cerebral Microinfarcts in Patients With Ischemic Stroke or Transient Ischemic Attack. *Stroke* 2016; 47: 2450-2455.

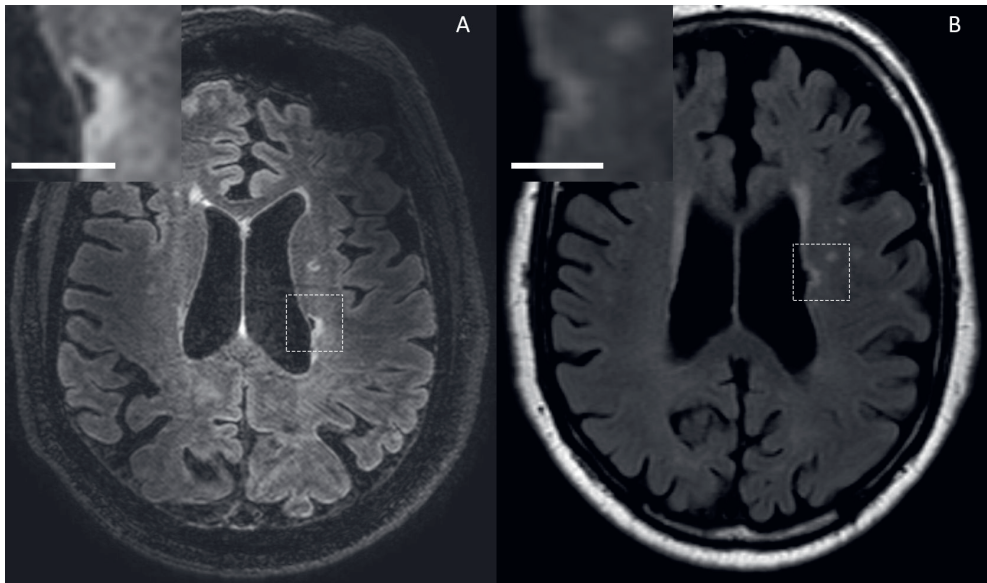
35. van Dalen JW, Scuric EE, van Veluw SJ, et al. Cortical microinfarcts detected in vivo on 3 Tesla MRI: clinical and radiological correlates. *Stroke* 2015; 46: 255-257.
36. Dichgans M, Wardlaw J, Smith E, et al. METACOHORTS for the study of vascular disease and its contribution to cognitive decline and neurodegeneration: An initiative of the Joint Programme for Neurodegenerative Disease Research. *Alzheimers Dement* 2016.
37. Rosenberg GA, Wallin A, Wardlaw JM, et al. Consensus statement for diagnosis of subcortical small vessel disease. *J Cereb Blood Flow Metab* 2016; 36: 6-25.

Supplementary Table 1. Frequency of small infarcts in the caudate nucleus per patient found by rater one (TW), rater two (JdB) and rater three (JH) on the 7T MRI scans.

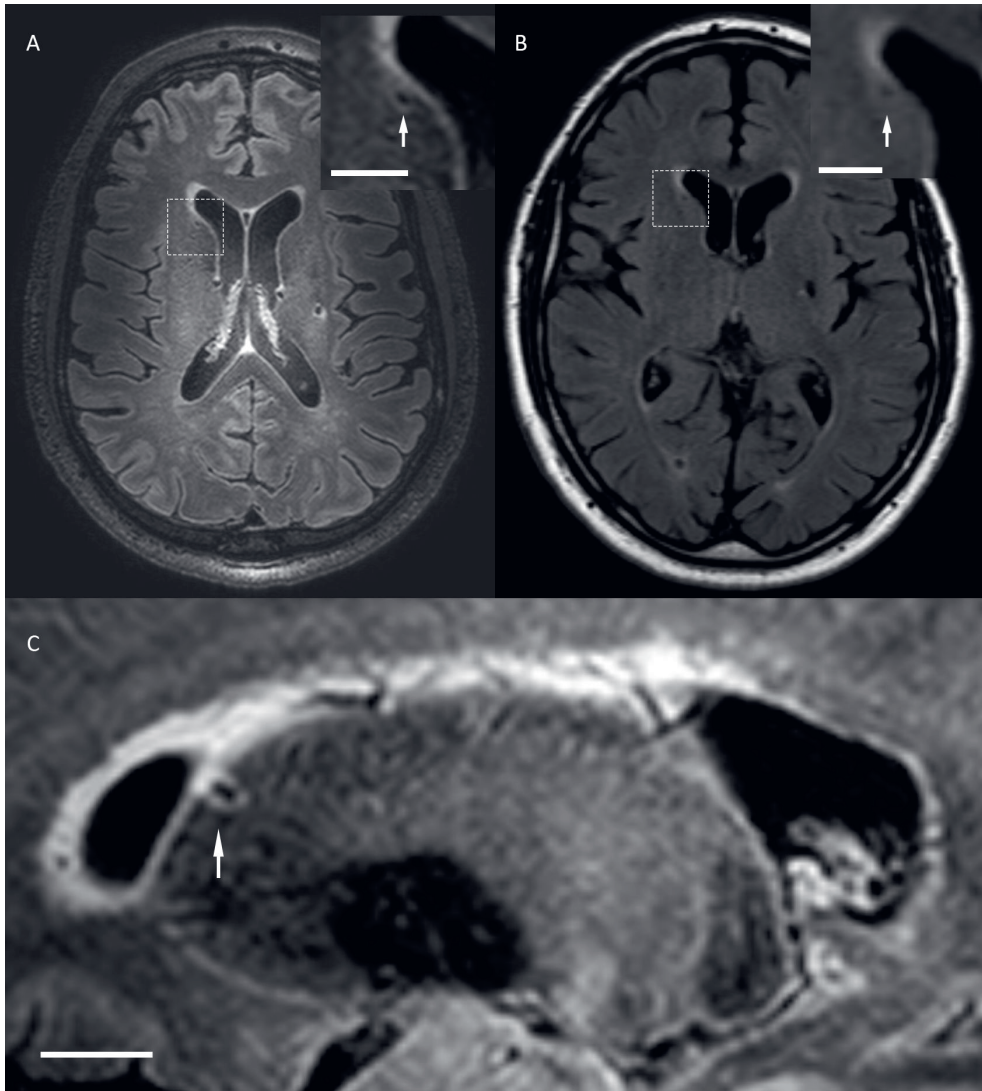
Patient	Frequency per patient			
	Rater one 1 st rating	Rater one 2 nd rating	Rater two	Rater three
1	3	2	2	2
2	1	1	1	1
3	7	7	8	8
4	1	1	1	1
5	1	1	0	2
6	0	0	0	0
7	0	0	0	0
8	0	0	0	0
9	0	0	0	0
10	0	0	0	0
11	0	0	0	0
12	0	0	0	0
13	0	0	0	0
14	0	0	0	0
15	0	0	0	0
16	0	0	0	0
17	0	0	0	0
18	0	0	0	0
19	0	0	0	0
20	0	0	0	0
21	0	0	0	0
22	0	0	0	0
23	0	0	0	0
Total	13	12	12	14

Supplementary Table 2. Contingency table of the frequency of patients with small infarcts in the caudate nucleus on 7T MRI versus 1.5T MRI.

		Small infarct on 1.5T MRI		Total
		Yes	No	
Small infarct on 7T MRI	Yes	6	6	12
	No	0	78	78
	Total	6	84	90



Supplementary Figure 1. A cavitated small infarct (arrow) in the tail of the left caudate nucleus in a 75-year old male is shown on a transverse FLAIR image (A) of the 7T MRI scan. This lesion was also rated on the corresponding transverse FLAIR image (B) of the 1.5T MRI scan. Scale bar indicates 10 mm.



Supplementary Figure 2. A cavitated small infarct (arrow) in the head of the right caudate nucleus in a 84-year old male is shown on a transverse FLAIR image (A) of the 7T MRI scan. Although abnormalities can be seen in the corresponding area on the transverse FLAIR image (B) of the 1.5T MRI scan, this lesion was not rated as a small infarct on the 1.5T MRI scan. This was due to the fact that on the 1.5T MRI scan the contrast-to-noise ratio and the resolution were insufficient to reliably characterize this abnormality as a small infarct. The small infarct (arrow) can be characterized more clearly on the sagittal 7T FLAIR image (C). Scale bar indicates 10 mm.

CHAPTER 6



Microinfarcts in the deep gray matter on 7 tesla MRI: Risk factors, MRI correlates and relation to cognitive functioning. The SMART-MR study

Rashid Ghaznawi ^{1,2}, Maarten H.T. Zwartbol ¹, Jeroen de Bresser ³, Hugo J. Kuijf ⁴, Koen L. Vincken ⁴, Ina Rissanen ², Mirjam I. Geerlings ², Jeroen Hendrikse ¹, on behalf of the UCC-SMART Study Group

¹Department of Radiology, University Medical Center Utrecht, Netherlands;

²Julius Center for Health Sciences and Primary Care, University Medical Center Utrecht, Netherlands; ³Department of Radiology, Leiden University Medical

Center, Netherlands; ⁴Image Sciences Institute, University Medical Center Utrecht, Netherlands

Background and purpose

The clinical relevance of cortical microinfarcts has recently been established, however studies on microinfarcts in the deep gray matter are lacking. We examined the risk factors and MRI correlates of microinfarcts in the deep gray matter on 7T MRI and their relation to cognitive functioning.

Materials and Methods

Within the SMART-MR study, 213 patients (68 ± 8 years) had risk factor assessment, a 7T and 1.5T brain MRI, and cognitive examination. Microinfarcts on 7T MRI were defined as lesions <5 mm. Regression models were used to examine the age-adjusted associations between risk factors, MRI markers and microinfarcts. Cognitive function was summarized as composite and domain-specific z-scores.

Results

A total of 47 microinfarcts were found in 28 patients (13%), most commonly in the thalamus. Older age, history of stroke, hypertension and intima-media thickness were associated with microinfarcts. On 1.5T MRI, cerebellar infarcts (RR=2.75, 95% CI:1.4-5.33), lacunes in the white (RR=3.28, 95% CI:3.28-6.04) and deep gray matter (RR=3.06, 95% CI:1.75-5.35) were associated with microinfarcts, and on 7T MRI cortical microinfarcts (RR=2.33, 95% CI:1.32-4.13). Microinfarcts were also associated with poorer global cognitive functioning (mean difference in global z-score between patients with multiple microinfarcts vs. none = -0.97, 95% CI: -1.66 to -0.28, $p=0.006$) and across all cognitive domains.

Conclusion

Microinfarcts in the deep gray matter on 7T MRI were associated with worse cognitive functioning and risk factors and MRI markers of small vessel and large vessel disease. Our findings suggest that microinfarcts in the deep gray matter may represent a novel imaging marker of vascular brain injury.

Introduction

Cerebral microinfarcts are a common neuropathological finding in older individuals.¹⁻³ Conventionally, they are defined as small ischemic lesions that are not visible to the naked eye on gross pathology and can range from 100 μm to a few mm in size.² Although small, microinfarcts often occur in large numbers and their effect is thought to extend well beyond their lesion boundaries.^{2,4} Associations with cognitive impairment and dementia have been reported, and microinfarcts may play an important role in silent cerebrovascular disease.⁴

Recently, cortical microinfarcts have been identified *in vivo* using 7T MRI.² Subsequent neuroimaging studies reported that the causes of cortical microinfarcts are heterogeneous, and their occurrence has been associated with both small vessel and large vessel disease, microemboli and hypoperfusion.⁵⁻⁸ The clinical importance of cortical microinfarcts has been demonstrated by their association with worse cognitive functioning.⁹ *In vivo* data on the prevalence and risk factors of microinfarcts in the deep gray matter, however, is lacking. Moreover, it is not known to what extent microinfarcts in the deep gray matter are related to cognitive functioning. Previous histopathologic studies reported that microinfarcts as well as lacunes in the deep gray matter were associated with worse antemortem cognitive performance.¹⁰⁻¹² Identifying the risk factors and MRI markers associated with microinfarcts in the deep gray matter is of importance as these may provide clues to their underlying etiology and may provide potential targets for intervention. Examining the association with cognitive functioning is important as it will provide evidence whether microinfarcts in the deep gray matter are structural correlates of impaired cognitive performance.

In the current study, we examined the frequency and distribution of microinfarcts in the caudate nucleus, lentiform nucleus and thalamus on 7T MRI in a large sample of older persons with a history of arterial disease. In addition, we examined whether microinfarcts in the deep gray matter were associated with risk factors, MRI markers of cerebrovascular disease and cognitive functioning.

Methods

Study population

Data were used from the Second Manifestations of ARterial disease-Magnetic Resonance (SMART-MR) study, a prospective cohort study at the University Medical Center Utrecht with the aim to investigate risk factors and consequences of brain changes on MRI in patients with symptomatic atherosclerotic disease.¹³ In brief, between 2001 and 2005, 1309 middle-aged and older adult persons newly referred to the University Medical Center Utrecht for treatment of symptomatic atherosclerotic disease (coronary artery disease, cerebrovascular disease, peripheral arterial disease or abdominal aortic aneurysm) were

included for baseline measurements. During a one-day visit to our medical center, a physical examination, ultrasonography of the carotid arteries to measure the intima-media thickness (mm), blood and urine samplings, neuropsychological assessment and a 1.5T brain MRI scan were performed. The height and weight were measured, and the body mass index (kg/m²) was calculated. Questionnaires were used for the assessment of demographics, risk factors, medical history, medication use and cognitive and physical functioning.

Of the 1309 persons included, 754 had follow-up measurements after an average of four years between January 2006 and May 2009. From November 2013, all patients alive were invited for a second follow-up, including a 7T brain MRI. Of the 329 persons included between November 2013 and October 2017, 213 had a 7T MRI scan and these patients formed the current study sample. A participation flowchart of the SMART-MR study is shown in Supplementary Figure 1.

In the present study, we used the 1.5T brain MRI, cognitive functioning and vascular risk factor data obtained during follow-up. Due to logistic reasons, however, the 1.5T brain MRI and cognitive function measurements were obtained prior to the 7T brain MRI in 97 patients (median 1.5 years; range 0.6-2.7 years), whereas in 116 patients these examinations were obtained on the same day. Also, vascular risk factor assessment was performed prior to the 7T brain MRI in 163 patients (median 2.3 years; range 0.6-9.4 years), whereas in 50 patients vascular risk factors were obtained concurrently with the 7T brain MRI.

The SMART-MR study was approved by the medical ethics committee of the University Medical Center Utrecht according to the guidelines of the Declaration of Helsinki of 1975 and written informed consent was obtained from all patients.

Vascular risk factors

Methods of measuring vascular risk factors are described in the Supplementary Material.

MRI protocol

High-field imaging of the brain was performed on a whole-body 7T MR system (Philips Healthcare, Cleveland, OH, USA) with a volume transmit and 32-channel receive head coil (Nova Medical, Wilmington, MA, USA). Conventional MR imaging of the brain was performed on a 1.5T whole-body system (Gyrosan ACS-NT, Philips Medical Systems, Best, the Netherlands). The 7T and 1.5T scan protocols are described in the Supplementary Material.

Assessment of MRI markers of cerebrovascular disease

Brain infarcts (cortical, cerebellar or brain stem), lacunes of presumed vascular origin, and white matter hyperintensity (WMH) and brain volumes were determined using 1.5T MRI data. Cortical microinfarcts and cerebral microbleeds were rated on 7T MRI data due to the enhanced conspicuity of these lesions at higher field strengths.^{14, 15} All ratings were performed blinded to patient characteristics.

Brain infarcts (cortical, cerebellar or brainstem) and lacunes were visually rated by an experienced rater (MHTZ) with 6 years of experience in neuroradiology on the T1-weighted, T2-weighted and FLAIR images of the 1.5T MRI scans. Lacunes were rated according to the STRIVE criteria as round or ovoid, subcortical, fluid-filled cavities (signal similar to cerebrospinal fluid) of 3-15mm in diameter, in the territory of one perforating arteriole.¹⁶ Uncertain lesions were discussed during a consensus meeting (MHTZ) to reach agreement.

WMH and brain volumes were obtained using an automated segmentation program on the T1-weighted, FLAIR, and T1-weighted inversion recovery sequences of the 1.5T MR scans. A probabilistic segmentation technique was performed with *k*-nearest neighbor classification distinguishing gray matter, white matter, cerebrospinal fluid and lesions.¹⁷ Brain infarcts, including lacunes and their hyperintense rim, were manually segmented. All WMH segmentations were visually checked by an investigator (RG) using an image processing framework (MeVisLab 2.7.1., MeVis Medical Solutions AG, Bremen, Germany) to ensure that brain infarcts were correctly removed from the WMH segmentations.

Periventricular WMH were defined as adjacent to or within 1 cm of the lateral ventricles and deep WMH were defined as located in the deep white matter tracts that may or may not have adjoined periventricular WMH. Total brain volume was calculated by summing the volumes of gray matter, white matter, total WMH and, if present, the volumes of brain infarcts. Total intracranial volume (ICV) was calculated by summing the cerebrospinal fluid volume and total brain volume.

Phase-contrast MR angiography was used to measure total cerebral blood flow, as this method has been demonstrated to be a fast, reproducible, and noninvasive method to measure total cerebral blood flow in large cohorts.¹⁸ Previous studies established that phase-contrast MR angiography correlates well with arterial spin-labeled perfusion MRI, although estimates tend to be somewhat higher and more variable than arterial spin-labeled perfusion MRI.¹⁹ Post-processing of the cerebral blood flow measurements was performed by one investigator (MHTZ). The flow through the basilar artery and the left and right internal carotid arteries was summed to calculate the total cerebral blood flow (ml/min). Total cerebral blood flow was expressed per 100 ml brain parenchymal volume to obtain parenchymal cerebral blood flow (pCBF).

Cortical microinfarcts were visually rated by a rater (MHTZ) on the 3D T1-weighted, 3D T2-weighted and 3D FLAIR sequences of the 7T MRI scans according to criteria previously described.² Cerebral microbleeds were rated by a rater (MHTZ) using the minimum intensity projection images and source images of the 7T SWI sequence. Microbleeds were labeled as lobar or deep using the Microbleed Anatomical Rating Scale.²⁰

We considered cortical, cerebellar and brain stem infarcts rated on 1.5T MRI as markers of large vessel disease²¹, whereas lacunes of presumed vascular origin, white matter hyperintensities and microbleeds were considered markers of small vessel disease, consistent with the STRIVE criteria.¹⁶

Assessment of cognitive functioning

All patients underwent neuropsychological assessment for memory, executive functioning, information processing speed and working memory. The tests used to assess each of these cognitive domains are described in the Supplementary Material. Domain-specific z scores were calculated by converting raw test scores to standardized z scores and averaging these for each domain prior to the final z transformation. A global cognitive functioning composite z score was calculated by standardizing the averaged domain-specific z scores.

Assessment of microinfarcts in the deep gray matter

First, all available 7T MRI scans were screened by an experienced neuroradiologist. All lesions hypointense on T1-weighted images, hyperintense on T2-weighted images, and either hyperintense or hypointense with a hyperintense rim on FLAIR images consistent with the imaging criteria set forth in our previous work¹⁴ were rated as possible microinfarcts. The lesions were restricted to the caudate nucleus, lentiform nucleus or thalamus and not appearing as a perivascular space, artery, vein or microbleed on the SWI sequence. In addition, the lesion had to be detectable in the axial, coronal, and sagittal views. Uncertain lesions were discussed during a consensus meeting to reach agreement. Next, all identified possible microinfarcts were inspected by an investigator (RG) using MR imaging software and the largest diameter of each lesion was determined on the FLAIR sequence. Lesions <5mm in their largest diameter were accepted as microinfarcts as this value has been suggested by previous studies on cortical microinfarcts.^{6,22-26} Presence and number of lesions ≥ 5 mm in the deep gray matter were also recorded as these may act as potential confounders in the relation between microinfarcts and cognitive functioning.

Statistical analysis

First, vascular risk factors and MRI markers of cerebrovascular disease were calculated of patients with and without microinfarcts in the deep gray matter on 7T MRI, and of the entire study sample. Second, relative risks for presence of microinfarcts in the deep gray matter were estimated for vascular risk factors and MRI markers of cerebrovascular disease using log-binomial regression, adjusted for age. For continuous variables, a relative risk for presence of microinfarcts was estimated for one standard deviation increase. For dichotomous variables, a relative risk for microinfarcts was calculated for presence of a vascular risk factor or MRI marker. Third, to examine the association between microinfarcts in the deep gray matter and cognitive functioning, analysis of covariance (ANCOVA) was used to estimate age and education level adjusted cognitive functioning z scores for patients without microinfarcts, with a single microinfarct and with multiple microinfarcts. Age and education level were entered as covariates as these represent the most important potential confounders in the relation between microinfarcts and cognitive functioning.

We repeated the abovementioned analyses with additional adjustment for number of infarcts $\geq 5\text{mm}$ in the deep gray matter on 7T MRI. Statistical significance was set at a p value of <0.05 .

Results

A total of 47 deep gray matter microinfarcts (caudate nucleus; $n=17$, lentiform nucleus; $n=9$, thalamus; $n=21$) were identified in 28 patients on 7T MRI (range 1-6 microinfarcts). A single microinfarct was seen in 19 patients (68%), while multiple microinfarcts were seen in 9 patients (32%). Size of microinfarcts ranged from 2.1 to 4.8mm (caudate nucleus; 2.1 to 4.7mm, lentiform nucleus; 2.7 to 4.1mm, thalamus; 2.4 to 4.8mm). Of patients with microinfarcts ($n=28$), twelve patients (42%) also showed infarcts $\geq 5\text{mm}$ in the deep gray matter on 7T MRI (Table 1). Examples of deep gray matter microinfarcts are shown in Figure 1. Twenty-six patients showed a total of 33 infarcts $\geq 5\text{mm}$ in the deep gray matter on 7T MRI, ranging from 6.7 to 15.7mm in size (Table 1). Of these 33 lesions, 18 (55%) were rated as lacunes in the deep gray matter on the corresponding 1.5T MRI scans.

Baseline characteristics and MRI markers of patients with microinfarcts in the deep gray matter ($n=28$), those without microinfarcts ($n=185$) and in the total study sample ($n=213$) are shown in Tables 2 and 3, respectively.

Compared to baseline (2001-2005) characteristics of patients without a 7T brain MRI, patients in the study sample with a 7T brain MRI were younger, had more often current alcohol intake, less often diabetes mellitus, and showed a slightly lower intima-media thickness and a slightly higher ankle brachial index (Supplementary Table 1).

Table 1. Frequency of patients with microinfarcts and with infarcts $\geq 5\text{mm}$ in the deep gray matter on 7T MRI.

Microinfarct ($<5\text{mm}$)	Infarct $\geq 5\text{mm}$		Total
	No	Yes	
No	171	14	185
Yes	16	12	28
Total	187	26	213

Vascular risk factors

Higher age was associated with presence of microinfarcts in the deep gray matter (RR per year increase = 1.05, 95%CI: 1.02 to 1.08, $p=0.001$). In addition, after adjusting for age, a history of stroke (RR=2.88, 95%CI: 1.24 to 6.67, $p=0.01$), hypertension (RR=3.16, 95%CI: 1.30 to 7.65, $p=0.01$) and a higher intima-media thickness (RR per 1 SD increase = 1.29, 95%CI: 1.04 to 1.61, $p=0.02$) were associated with microinfarcts. Number of smoking pack years (RR per SD increase = 1.11, 95%CI: 0.87 to 1.42, $p=0.40$), carotid artery stenosis

≥50% (RR=1.39, 95%CI: 0.70 to 2.75, $p=0.34$) and presence of metabolic syndrome (RR=1.47, 95%CI: 0.74 to 2.91, $p=0.27$) were not significantly associated with presence of microinfarcts in the deep gray matter after adjusting for age (Table 2).

Table 2. Association of vascular risk factors and presence of microinfarcts in the deep gray matter on 7T MRI.

	Patients with microinfarcts in the deep gray matter (n=28)	Patients without microinfarcts in the deep gray matter (n=185)	All patients (n=213)	Microinfarct (presence vs. absence) RR (95% CI) ^a
Age (years)	70 ± 7	64 ± 9	64 ± 9	1.05 (1.02 to 1.08) ^{b*}
Sex, % men	85.7	82.2	82.6	0.78 (0.30 to 2.02) ^c
History of stroke, %	50.0	23.2	26.8	2.88 (1.24 to 6.67) [*]
BMI (kg/m ²)	28 ± 4	27 ± 4	27 ± 4	1.20 (0.87 to 1.65)
Smoking, packyears ^d	27 (0, 56)	20 (0, 47)	22 (0, 49)	1.11 (0.87 to 1.42)
Alcohol intake				
No or <1 unit/week, %	22.2	26.5	25.9	1 (reference)
1–10 units/week, %	59.3	41.1	43.4	1.55 (0.67 to 3.61)
≥11 units/week, %	18.5	32.4	30.7	0.65 (0.22 to 1.98)
Hypertension, %	96.4	72.4	75.6	3.16 (1.30 to 7.65) [*]
Diabetes mellitus, %	14.3	16.2	16.0	0.85 (0.32 to 2.21)
Carotid stenosis ≥50%, %	17.9	7.6	8.9	1.39 (0.70 to 2.75)
Hypercholesterolemia, %	77.8	86.4	85.3	1.33 (0.86 to 2.05)
IMT (mm)	1.0 ± 0.3	0.8 ± 0.2	0.9 ± 0.2	1.29 (1.04 to 1.61) [*]
ABI	1.1 ± 0.2	1.1 ± 0.1	1.1 ± 0.2	0.86 (0.67 to 1.11)
Homocysteine (μmol/l)	13.0 ± 5.2	12.5 ± 4.3	12.5 ± 4.4	1.07 (0.40 to 2.82)
Apo-B (g/l)	0.8 ± 0.2	0.8 ± 0.2	0.8 ± 0.2	0.84 (0.58 to 1.23)
Metabolic syndrome, %	60.7	51.4	52.6	1.47 (0.74 to 2.91)
≥1 Apo-E ε4 allele, %	35.7	28.1	29.1	1.58 (0.79 to 3.20)

Characteristics are presented as mean ± SD or %. RR represents the relative risk for microinfarcts in the presence of a risk factor (in case of a dichotomous variable) or for 1 SD increase in the risk factor (in case of a continuous variable).

^a Log-binomial regression with adjustment for age.

^b Per year increase.

^c Men vs. women.

^d Median (10th percentile, 90th percentile). Natural log-transformed due to a non-normal distribution in the analysis.

* $p<0.05$

BMI: body mass index; LDL: low density lipoprotein; HDL: high density lipoprotein; IMT: intima-media thickness; ABI: ankle brachial index; Apo-B: apolipoprotein B; Apo-E: apolipoprotein E; SD: standard deviation; CI: confidence interval.

After additionally adjusting for number of infarcts ≥ 5 mm in the deep gray matter on 7T MRI, higher age (RR per year increase = 1.04, 95%CI: 1.01 to 1.07, $p=0.01$) and hypertension (RR=5.25, 95%CI: 1.43 to 19.28, $p=0.01$) remained associated with microinfarcts, whereas a history of stroke (RR=2.37, 95%CI: 0.94 to 5.79, $p=0.07$) and a higher intima-media thickness (RR per 1 SD increase = 1.25, 95%CI: 0.98 to 1.57, $p=0.07$) lost statistical significance.

MRI markers of cerebrovascular disease

For cerebrovascular markers on 1.5T MRI, cerebellar infarcts (RR=2.18, 95%CI: 1.23 to 3.87, $p=0.008$), lacunes in the white matter (RR=3.28, 95%CI: 1.79 to 6.04, $p<0.0001$) and lacunes in the deep gray matter (RR=3.93, 95%CI: 1.99 to 7.78, $p<0.0001$) were associated with presence of microinfarcts in the deep gray matter, after adjusting for age. For cerebrovascular markers on 7T MRI, cortical microinfarcts (RR=2.33, 95%CI: 1.32 to 4.13, $p=0.004$) were associated with microinfarcts in the deep gray matter after adjusting for age. Although the RR was increased, cortical infarcts (RR=1.64, 95%CI: 0.76 to 3.51, $p=0.21$), brainstem infarcts (RR=3.37, 95%CI: 0.95 to 12.0, $p=0.07$) and periventricular WMH volume (RR per SD increase = 1.14, 95%CI: 0.95 to 1.37, $p=0.16$) on 1.5T MRI were not significantly associated with presence of microinfarcts in the deep gray matter after adjusting for age. Deep microbleeds (RR=1.60, 95%CI: 0.70 to 3.68, $p=0.27$) and lobar microbleeds (RR=1.27, 95%CI: 0.59 to 2.72, $p=0.54$) on 7T MRI were also not significantly associated with microinfarcts in the deep gray matter after adjusting for age (Table 3).

After additionally adjusting for number of infarcts ≥ 5 mm in the deep gray matter on 7T MRI, lacunes in the white matter on 1.5T MRI (RR=2.76, 95%CI: 1.45 to 5.27, $p=0.002$), cerebellar infarcts on 1.5T MRI (RR=2.05, 95%CI: 1.13 to 3.73, $p=0.02$) and cortical microinfarcts on 7T MRI (RR=2.16, 95%CI: 1.20 to 3.90, $p=0.01$) remained associated with microinfarcts.

Cognitive functioning

Global cognitive functioning z scores differed significantly between patients without ($n = 185$), with a single ($n=19$) and with multiple microinfarcts ($n=9$) in the deep gray matter (ANCOVA $p=0.007$), adjusted for age and education level. Specifically, presence of multiple microinfarcts in the deep gray matter was associated with worse global cognitive functioning compared to absence of microinfarcts or presence of a single microinfarct (mean difference in z-score = -0.92, 95%CI: -1.53 to -0.31, $p=0.003$; -1.10, 95%CI: -1.81 to -0.39, $p=0.002$, respectively). This pattern was observed for each cognitive domain. The mean estimates of domain-specific z-scores were lower for patients with multiple microinfarcts compared to patients with none or a single microinfarct for memory, executive functioning, information processing speed and working memory (Figure 2).

Table 3. Association of MRI markers of cerebrovascular disease and presence of microinfarcts in the deep gray matter on 7T MRI.

	Patients with microinfarcts in the deep gray matter (n=28)	Patients without microinfarcts in the deep gray matter (n=185)	All patients (n=213)	Microinfarct (presence vs. absence) RR (95% CI) ^a
Infarcts on 1.5T MRI, %				
Cortical	21	11	12	1.64 (0.76 to 3.51)
Cerebellar	32	9	12	2.18 (1.23 to 3.87)*
Brainstem	7	1	2	3.37 (0.95 to 12.0)
Lacunae in the white matter on 1.5T MRI, %	32	6	9	3.28 (1.79 to 6.04)*
Lacunae in the deep gray matter on 1.5T MRI, %	43	8	12	3.93 (1.99 to 7.78)*
WMH volumes on 1.5T MRI, ml ^b				
Total	3.3 (0.9, 32.5)	2.0 (0.3, 9.3)	2.0 (0.4, 10.0)	1.13 (0.93 to 1.38) ^c
Periventricular	2.9 (0.7, 31.7)	1.4 (0.2, 8.3)	1.4 (0.3, 9.0)	1.14 (0.95 to 1.37) ^c
Deep	0.2 (0.1, 0.9)	0.3 (0.0, 1.5)	0.2 (0.0, 1.4)	0.67 (0.38 to 1.16) ^c
Total brain volume, ml	1104.9 ± 116.5	1125.3 ± 104.3	1122.7 ± 105.9	0.84 (0.56 to 2.72) ^d
Total intracranial volume, ml	1449.2 ± 114.7	1452.6 ± 126.4	1452.16 ± 128.5	1.21 (0.85 to 1.73)
Parenchymal CBF, ml/min per 100 ml brain volume	50.5 ± 16.8	48.2 ± 12.0	48.5 ± 12.7	1.13 (0.93 to 1.38)
Cortical microinfarcts on 7T MRI, %	32	9	12	2.33 (1.32 to 4.13)*
Deep microbleeds on 7T MRI, %	21	10	12	1.60 (0.70 to 3.68)
Lobar microbleeds on 7T MRI, %	36	26	27	1.27 (0.59 to 2.72)

Characteristics are presented as mean ± SD or %. RR represents the relative risk for microinfarcts in the presence of a MRI marker (in case of a dichotomous variable) or for 1 SD increase in the MRI marker (in case of a continuous variable).

^a Log-binomial regression with adjustment for age.

^b Median (10th percentile, 90th percentile).

^c Natural log-transformed due to a non-normal distribution and normalized for total intracranial volume.

^d Adjusted for age and total intracranial volume.

**p* < 0.05

WMH: white matter hyperintensity; CBF: cerebral blood flow; SD: standard deviation; CI: confidence interval

After additionally adjusting for number of infarcts $\geq 5\text{mm}$ in the deep gray matter on 7T MRI, the association between microinfarcts and global cognitive functioning persisted (ANCOVA $p=0.01$; mean difference in z-score between patients with multiple microinfarcts versus none = -0.97 , 95%CI: -1.66 to -0.28 , $p=0.006$; versus a single microinfarct = -1.13 , 95%CI: -1.88 to -0.39 , $p=0.003$).

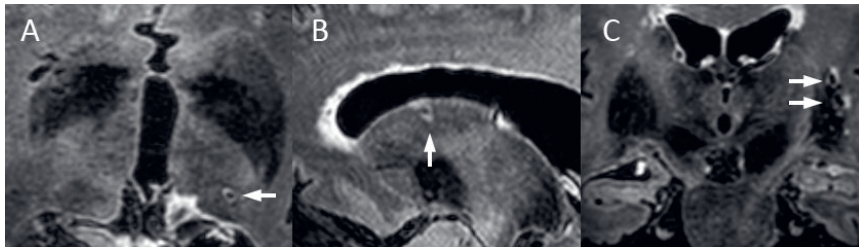


Figure 1. Examples of microinfarcts in the deep gray matter on 7T MRI. A: Microinfarct with a diameter of 2.3 mm (arrow) in the left thalamus of a 73-year old female on transversal 7T FLAIR. B: Microinfarct with a diameter of 2.9 mm (arrow) in the left caudate nucleus of a 64-year old male on sagittal 7T FLAIR. C: Two microinfarcts with diameters of 3.0 mm and 3.2 mm (arrows) in the left putamen of a 65-year old male on coronal 7T FLAIR. Note that the gliotic rim extends into the adjacent external capsule.

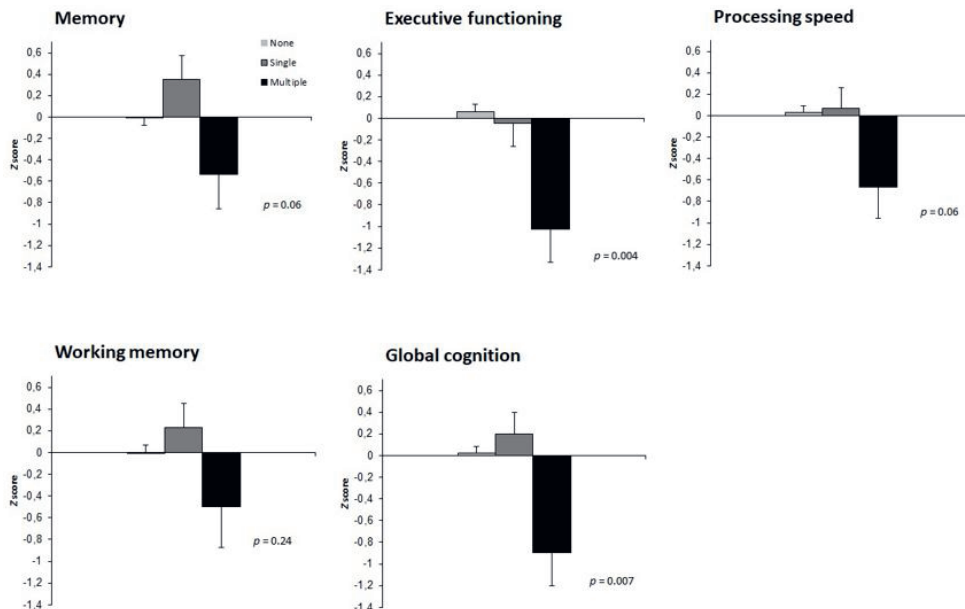


Figure 2. Association between microinfarcts in the deep gray matter and global and domain-specific cognitive functioning z-scores. Values are mean \pm standard error z scores, adjusted for age and educational level. Memory: none; -0.01 ± 0.07 , single; 0.35 ± 0.22 , multiple; -0.54 ± 0.32 . Executive

functioning: none; 0.05 ± 0.07 , single; -0.05 ± 0.21 , multiple; -1.02 ± 0.31 . Processing speed: none; 0.02 ± 0.06 , single; 0.07 ± 0.20 , multiple; -0.67 ± 0.29 . Working memory: none; -0.01 ± 0.07 , single; 0.22 ± 0.22 , multiple; -0.50 ± 0.37 . Global cognition: none; 0.02 ± 0.06 , single; 0.20 ± 0.20 , multiple; -0.90 ± 0.30 .

Discussion

In this cohort of patients with a history of arterial disease, microinfarcts in the deep gray matter on 7T MRI were detected in 13% of patients. These lesions were associated with older age, a history of stroke, hypertension and a higher intima-media thickness. With regard to MRI markers, they were associated with lacunes and cerebellar infarcts on 1.5T MRI, and with cortical microinfarcts on 7T MRI. Presence of multiple microinfarcts in the deep gray matter was associated with worse global cognitive functioning independent of age, education level and number of infarcts ≥ 5 mm.

We previously reported that small infarcts in the caudate nucleus on 7T MRI can be detected with excellent intra-rater and inter-rater agreement, and that the imaging characteristics of these lesions are similar to those in the cerebral cortex.¹⁴ The present study extends our previous findings and emphasizes the potential clinical importance of these lesions, which is in accordance with autopsy studies that reported associations between microinfarcts in the deep gray matter and ante-mortem cognitive impairment.^{10, 12} In addition, we found that the majority of patients with microinfarcts in the deep gray matter did not show larger infarcts in the deep gray matter on 7T MRI and, importantly, that the relationship between microinfarcts and worse global cognitive functioning was independent of infarcts ≥ 5 mm. These findings suggest that microinfarcts in the deep gray matter are structural correlates of impaired cognitive functioning that are largely undetected on conventional MRI.¹

The association between microinfarcts and worse cognitive functioning may be explained by the important role that the basal ganglia play in cognition through receiving and processing cortical information in the caudate and lentiform nuclei and sending information back to the cerebral cortex through the thalamus.^{27, 28} Damage to this neuronal network may compromise cognition.²⁹ However, we did not find significant differences in cognition between patients without microinfarcts and patients with a single microinfarct, suggesting that the impact of a single microinfarct on cognition may be weak, contrary to the presence of multiple lesions. A possible explanation is that the damage associated with a single microinfarct is insufficient to affect neural network integrity and therefore result in lower cognitive performance, whereas this may be the case for multiple microinfarcts. Alternatively, it may be that patients with multiple microinfarcts are also more likely to have smaller lesions that are not discernible on 7T MRI.³⁰

The associations of microinfarcts in the deep gray matter with older age, hypertension, a higher intima-media thickness, lacunes and cerebellar infarcts suggest that small vessel

and large vessel disease may be involved in the pathogenesis of these lesions. Support for this notion is provided by a large postmortem study in which atherosclerosis and arteriolosclerosis were associated with subcortical microinfarcts.³¹ However, as the *in vivo* associations presented in this study are novel, further studies in different populations are needed to identify risk factors of microinfarcts that may pose potential targets for intervention.

Strengths of our study include the large sample size for a 7T MRI study and the detailed information available on vascular risk factors, MRI markers of cerebrovascular disease and cognitive functioning that enabled us to examine these relationships within one study. A limitation of this study is that microinfarcts in the deep gray matter, cortical microinfarcts and microbleeds were rated on 7T MRI data whereas other MRI markers were evaluated on 1.5T MRI data. Several remarks have to be made with respect to this matter. First, we obtained brain volumes from 1.5T MRI data due to a lack of robust and validated brain segmentation software for 7T MRI data. Second, cerebral blood flow measurements were obtained from 1.5T MRI data because our standardized 7T MRI protocol did not contain phase contrast sequences. Third, it should be noted that the greatest added value of ultra-high field 7T MRI lies in its ability to visualize the smallest cerebrovascular lesions (i.e., microinfarcts and microbleeds) due to the higher signal-to-noise ratio compared to conventional 1.5T MRI. Although it would be preferable to determine all cerebrovascular lesions on the 7T MRI scans for consistency, it is unlikely that 7T MRI yields a greater detection rate for larger lesions such as cortical infarcts. Another limitation is the potential overlap that may occur between microinfarcts and lacunes of presumed vascular origin in the deep gray matter. According to the STRIVE criteria, lacunes of presumed vascular origin are defined as small subcortical infarcts ranging from 3 to 15mm in size.¹⁶ As microinfarcts were previously defined as lesions <5mm, it is possible that larger microinfarcts in the range of 4mm may have been classified as lacunes on 1.5T MRI. The potential overlap however was limited as the majority of patients with microinfarcts did not show lacunes in the deep gray matter on 1.5T MRI. In addition, we controlled for the effects of infarcts ≥ 5 mm in the analyses. Another possible limitation of this study is that the sample consisted of patients who completed two follow-up measurements and these patients represent a slightly healthier subset. This may have led to an underestimation of the association of microinfarcts with vascular risk factors, MRI markers of cerebrovascular disease and cognitive functioning. A further limitation of this study is that in some patients the 7T brain MRI did not coincide with the 1.5T brain MRI, cognitive function measurements and vascular risk factor assessment. Especially for the vascular risk factor assessment the interval was quite large in some patients. Due to logistical reasons, we were not able to repeat the measurement of vascular risk factors at the time of the brain MRI and cognitive assessment in these patients, which may have under- or overestimated the associations. However, in a previous analysis³² we did not see major changes in the

relationship with 7T MRI outcomes when adjusting for the time interval between vascular risk factor assessment and 7T brain MRI.

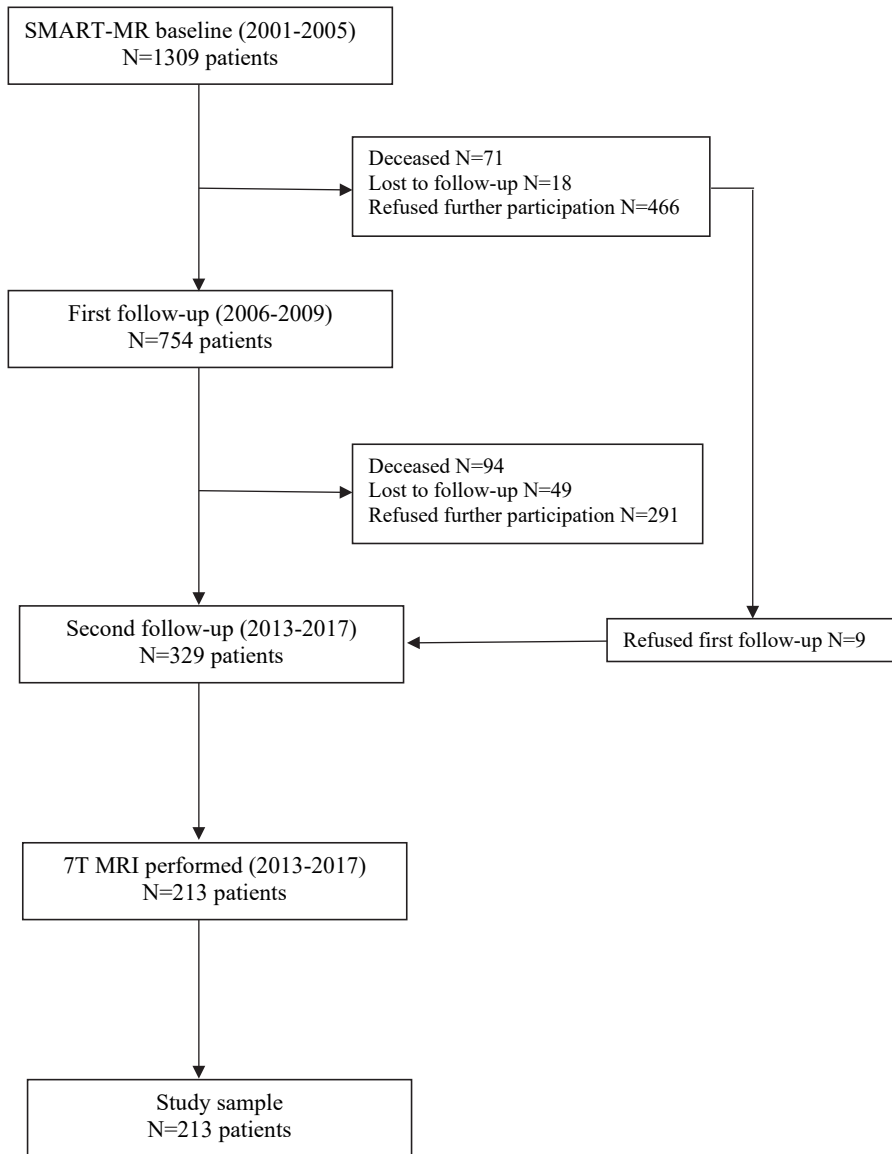
Conclusions

Our findings demonstrate that microinfarcts in the deep gray matter on 7T MRI are associated with worse cognitive functioning and vascular risk factors and MRI markers of small vessel and large vessel disease in patients with a history of arterial disease. These results suggest that microinfarcts in the deep gray matter may be relevant imaging markers of vascular brain injury that, together with cortical microinfarcts, could be a potential target for future prevention strategies of vascular cognitive impairment.

References

1. Smith EE, Schneider JA, Wardlaw JM, et al. Cerebral microinfarcts: the invisible lesions. *Lancet Neurol* 2012; 11: 272-282.
2. van Veluw SJ, Shih AY, Smith EE, et al. Detection, risk factors, and functional consequences of cerebral microinfarcts. *Lancet Neurol* 2017; 16: 730-740.
3. Brundel M, de Bresser J, van Dillen JJ, et al. Cerebral microinfarcts: a systematic review of neuropathological studies. *J Cereb Blood Flow Metab* 2012; 32: 425-436.
4. Summers PM, Hartmann DA, Hui ES, et al. Functional deficits induced by cortical microinfarcts. *J Cereb Blood Flow Metab* 2017; 37: 3599-3614.
5. Wang Z, van Veluw SJ, Wong A, et al. Risk Factors and Cognitive Relevance of Cortical Cerebral Microinfarcts in Patients With Ischemic Stroke or Transient Ischemic Attack. *Stroke* 2016; 47: 2450-2455.
6. van Dalen JW, Scuric EE, van Veluw SJ, et al. Cortical microinfarcts detected in vivo on 3 Tesla MRI: clinical and radiological correlates. *Stroke* 2015; 46: 255-257.
7. van Veluw SJ, Hilal S, Kuijf HJ, et al. Cortical microinfarcts on 3T MRI: Clinical correlates in memory-clinic patients. *Alzheimers Dement* 2015; 11: 1500-1509.
8. Hilal S, Chai YL, van Veluw S, et al. Association Between Subclinical Cardiac Biomarkers and Clinically Manifest Cardiac Diseases With Cortical Cerebral Microinfarcts. *JAMA Neurol* 2017; 74: 403-410.
9. Hilal S, Sikking E, Shaik MA, et al. Cortical cerebral microinfarcts on 3T MRI: A novel marker of cerebrovascular disease. *Neurology* 2016; 87: 1583-1590.
10. Troncoso JC, Zonderman AB, Resnick SM, et al. Effect of infarcts on dementia in the Baltimore longitudinal study of aging. *Ann Neurol* 2008; 64: 168-176.
11. Gold G, Kovari E, Herrmann FR, et al. Cognitive consequences of thalamic, basal ganglia, and deep white matter lacunes in brain aging and dementia. *Stroke* 2005; 36: 1184-1188.
12. White L, Petrovitch H, Hardman J, et al. Cerebrovascular pathology and dementia in autopsied Honolulu-Asia Aging Study participants. *Ann NY Acad Sci* 2002; 977: 9-23.
13. Geerlings MI, Appelman AP, Vincken KL, et al. Brain volumes and cerebrovascular lesions on MRI in patients with atherosclerotic disease. The SMART-MR study. *Atherosclerosis* 2010; 210: 130-136.
14. Ghaznawi R, de Bresser J, van der Graaf Y, et al. Detection and characterization of small infarcts in the caudate nucleus on 7 Tesla MRI: The SMART-MR study. *J Cereb Blood Flow Metab* 2018; 38: 1609-1617.
15. Conijn MM, Geerlings MI, Biessels GJ, et al. Cerebral microbleeds on MR imaging: comparison between 1.5 and 7T. *AJNR Am J Neuroradiol* 2011; 32: 1043-1049.
16. Wardlaw JM, Smith EE, Biessels GJ, et al. Neuroimaging standards for research into small vessel disease and its contribution to ageing and neurodegeneration. *Lancet Neurol* 2013; 12: 822-838.
17. Anbeek P, Vincken KL, van Bochove GS, et al. Probabilistic segmentation of brain tissue in MR imaging. *Neuroimage* 2005; 27: 795-804.

18. Spilt A, Box FM, van der Geest RJ, et al. Reproducibility of total cerebral blood flow measurements using phase contrast magnetic resonance imaging. *J Magn Reson Imaging* 2002; 16: 1-5.
19. Dolui S, Wang Z, Wang DJJ, et al. Comparison of non-invasive MRI measurements of cerebral blood flow in a large multisite cohort. *J Cereb Blood Flow Metab* 2016; 36: 1244-1256.
20. Gregoire SM, Chaudhary UJ, Brown MM, et al. The Microbleed Anatomical Rating Scale (MARS): reliability of a tool to map brain microbleeds. *Neurology* 2009; 73: 1759-1766.
21. De Cocker LJ, Kloppenborg RP, van der Graaf Y, et al. Cerebellar Cortical Infarct Cavities: Correlation With Risk Factors and MRI Markers of Cerebrovascular Disease. *Stroke* 2015; 46: 3154-3160.
22. Takasugi J, Miwa K, Watanabe Y, et al. Cortical Cerebral Microinfarcts on 3T Magnetic Resonance Imaging in Patients With Carotid Artery Stenosis. *Stroke* 2019; 50: 639-644.
23. Sagnier S, Okubo G, Catheline G, et al. Chronic Cortical Cerebral Microinfarcts Slow Down Cognitive Recovery After Acute Ischemic Stroke. *Stroke* 2019; 50: 1430-1436.
24. li Y, Maeda M, Ishikawa H, et al. Cortical microinfarcts in patients with multiple lobar microbleeds on 3 T MRI. *J Neurol* 2019; 266: 1887-1896.
25. Fu R, Wang Y, Wang Y, et al. The Development of Cortical Microinfarcts Is Associated with Intracranial Atherosclerosis: Data from the Chinese Intracranial Atherosclerosis Study. *J Stroke Cerebrovasc Dis* 2015; 24: 2447-2454.
26. van Rooden S, Goos JD, van Opstal AM, et al. Increased number of microinfarcts in Alzheimer disease at 7-T MR imaging. *Radiology* 2014; 270: 205-211.
27. Alexander GE. Basal ganglia-thalamocortical circuits: their role in control of movements. *J Clin Neurophysiol* 1994; 11: 420-431.
28. Alexander GE and Crutcher MD. Functional architecture of basal ganglia circuits: neural substrates of parallel processing. *Trends Neurosci* 1990; 13: 266-271.
29. Leh SE, Petrides M and Strafella AP. The neural circuitry of executive functions in healthy subjects and Parkinson's disease. *Neuropsychopharmacology : official publication of the American College of Neuropsychopharmacology* 2010; 35: 70-85.
30. Auriel E, Westover MB, Bianchi MT, et al. Estimating Total Cerebral Microinfarct Burden From Diffusion-Weighted Imaging. *Stroke* 2015; 46: 2129-2135.
31. Arvanitakis Z, Capuano AW, Leurgans SE, et al. The Relationship of Cerebral Vessel Pathology to Brain Microinfarcts. *Brain Pathol* 2017; 27: 77-85.
32. Zwartbol MHT, van der Kolk AG, Ghaznawi R, et al. Intracranial Vessel Wall Lesions on 7T MRI (Magnetic Resonance Imaging). *Stroke* 2019; 50: 88-94.



Supplementary Figure 1. Participation flowchart of the SMART-MR study.

Supplementary Table 1. Baseline vascular risk factors of the study population (n=1309) according to presence or absence of 7T brain MRI data.

	Patients with a 7T brain MRI scan (n=213)	Patients without a 7T brain MRI scan (n=1096)	<i>p</i> value
Age (years)	55 ± 8	59 ± 10	<0.001
Sex, % men	82.6	79.1	0.242
History of stroke, %	24.4	22.8	0.611
BMI (kg/m ²)	27 ± 3	27 ± 4	0.628
Smoking, pack years ^a	21 (0, 47)	23 (0, 52)	0.772 ^b
Alcohol use, % current	85	73	<0.001
Hypertension, %	51.2	52.0	0.823
Diabetes mellitus, %	11.5	22.7	<0.001
Carotid artery stenosis ≥70%, %	7.4	11.9	0.06
IMT (mm)	0.9 ± 0.2	1.0 ± 0.3	<0.001
ABI	1.2 ± 0.2	1.1 ± 0.2	<0.001

Characteristics are presented as mean ± SD or %.

BMI: body mass index; SD: standard deviation; IMT: intima-media thickness; ABI: ankle brachial index.

^a Median (10th percentile, 90th percentile).

^b Natural log-transformed due to a non-normal distribution in the statistical analysis.

SUPPLEMENTARY MATERIAL

Vascular risk factors

Baseline smoking habits and alcohol intake were assessed with questionnaires. Packyears of smoking was calculated and alcohol intake was categorized as 'no or <1 unit per week', '1-10 units per week', and '≥11 units per week'. Height and weight were measured, and the body mass index (BMI) was calculated (kg/m^2). Systolic blood pressure (SBP) (mmHg) and diastolic blood pressure (DBP) (mmHg) were measured three times with a sphygmomanometer, and the average of these measures was calculated. Hypertension was defined as a mean SBP of > 140 mmHg, a mean DBP of > 90 mmHg or self-reported use of antihypertensive drugs. An overnight fasting venous blood sample was taken to determine glucose, lipids, total homocysteine and apolipoprotein-B levels. Diabetes mellitus was defined as fasting serum glucose levels of ≥ 7.0 mmol/l, and/or use of glucose-lowering medication, and/or a known history of diabetes. Hyperlipidemia was considered if the serum cholesterol was ≥ 5.0 mmol/l, a low-density lipoprotein cholesterol of > 3.2 mmol/l, or if the patient was using lipid lowering medication. History of stroke was based on a composite scoring made of neurologist-verified self-reported symptoms of previous stroke, previous history of carotid artery operation, or a physician diagnosis at study inclusion of the following conditions: transient ischemic attack, brain infarct, ischemic stroke, cerebral ischemia, amaurosis fugax or retinal infarction. Mean carotid intima-media thickness (in mm) was calculated for the left and right common carotid arteries based on six far-wall measurements on ultrasound. Ankle brachial index measurements were made using a Vasoguard Doppler probe (8 MHz) and measurement techniques have been described in detail elsewhere.¹ Metabolic syndrome was determined by the National Cholesterol Education Program Adult Treatment Panel III criteria.² Genotyping for apolipoprotein-E (Apo-E) was performed on coded DNA specimens and has been described in detail elsewhere.³

MRI protocol

High-field imaging of the brain was performed on a whole-body 7T MR system (Philips Healthcare, Cleveland, OH, USA) with a volume transmit and 32-channel receive head coil (Nova Medical, Wilmington, MA, USA). The standardized scan protocol is described in detail in previous publications.^{4,5}

Conventional MR imaging of the brain was performed on a 1.5T whole-body system (Gyrosan ACS-NT, Philips Medical Systems, Best, the Netherlands) using a standardized scan protocol described in detail in previous work.^{6,7}

Assessment of cognitive functioning

Memory was assessed with the 15 Word Learning Test using a composite score of the immediate and delayed recall based on five trials, and the Rey-Osterrieth Complex figure

test.^{8,9} Executive functioning was assessed with the Verbal Fluency test using animals as categories (2 minutes) and the letter A (1 minute); the Visual Elevator test (10 trials), and the Brixton Spatial Anticipation test.¹⁰⁻¹² Working memory was assessed with the combined longest span scores and total span scores of the Forward Digit Span and Backward Digit Span.¹³ Processing speed was assessed with the Digit Symbol Substitution Test (120 seconds).¹⁴

References

1. Hendriks EJ, Westerink J, de Jong PA, et al. Association of High Ankle Brachial Index With Incident Cardiovascular Disease and Mortality in a High-Risk Population. *Arterioscler Thromb Vasc Biol* 2016; 36: 412-417.
2. Third Report of the National Cholesterol Education Program (NCEP) Expert Panel on Detection, Evaluation, and Treatment of High Blood Cholesterol in Adults (Adult Treatment Panel III) final report. *Circulation* 2002; 106: 3143-3421.
3. Jochemsen HM, Muller M, van der Graaf Y, et al. APOE epsilon4 differentially influences change in memory performance depending on age. The SMART-MR study. *Neurobiol Aging* 2012; 33: 832.e815-822.
4. Visser F, Zwanenburg JJ, Hoogduin JM, et al. High-resolution magnetization-prepared 3D-FLAIR imaging at 7.0 Tesla. *Magn Reson Med* 2010; 64: 194-202.
5. Ghaznawi R, de Bresser J, van der Graaf Y, et al. Detection and characterization of small infarcts in the caudate nucleus on 7 Tesla MRI: The SMART-MR study. *J Cereb Blood Flow Metab* 2018; 38: 1609-1617.
6. Geerlings MI, Appelman AP, Vincken KL, et al. Brain volumes and cerebrovascular lesions on MRI in patients with atherosclerotic disease. The SMART-MR study. *Atherosclerosis* 2010; 210: 130-136.
7. Ghaznawi R, Geerlings MI, Jaarsma-Coes MG, et al. The association between lacunes and white matter hyperintensity features on MRI: The SMART-MR study. *J Cereb Blood Flow Metab* 2019; 39: 2486-2496.
8. Lu PH, Boone KB, Cozolino L, et al. Effectiveness of the Rey-Osterrieth Complex Figure Test and the Meyers and Meyers recognition trial in the detection of suspect effort. *Clin Neuropsychol* 2003; 17: 426-440.
9. Brand N and Jolles J. Learning and retrieval rate of words presented auditorily and visually. *J Gen Psychol* 1985; 112: 201-210.
10. Wilkins AJ, Shallice T and McCarthy R. Frontal lesions and sustained attention. *Neuropsychologia* 1987; 25: 359-365.
11. Robertson IH, Ward T, Ridgeway V, et al. The structure of normal human attention: The Test of Everyday Attention. *J Int Neuropsychol Soc* 1996; 2: 525-534.
12. Burgess PW and Shallice T. Bizarre responses, rule detection and frontal lobe lesions. *Cortex* 1996; 32: 241-259.
13. Wechsler D, Psychological C and Pearson Education I. WAIS-IV : Wechsler adult intelligence scale. 2008.
14. Lezak MD and Lezak MD. *Neuropsychological assessment*. Oxford; New York: Oxford University Press, 2004.



PART III

Determinants of brain atrophy progression on MRI

CHAPTER 7



Low-grade carotid artery stenosis is associated with progression of brain atrophy and cognitive decline. The SMART-MR study

Rashid Ghaznawi ^{1,2}, Jet M.J. Vonk ², Maarten H.T. Zwartbol ¹, Jeroen de Bresser ³, Ina Rissanen ², Jeroen Hendrikse ¹ and Mirjam I. Geerlings ²; on behalf of the UCC-SMART Study Group

¹Department of Radiology, University Medical Center Utrecht, Netherlands;

²Julius Center for Health Sciences and Primary Care, University Medical Center

Utrecht, Netherlands; ³Department of Radiology, Leiden University Medical Center, Netherlands

Asymptomatic low-grade carotid artery stenosis (LGCS) is a common finding in patients with manifest arterial disease, however its relationship with brain MRI changes and cognitive decline is unclear. We included 902 patients (58 ± 10 years; 81% male) enrolled in the Second Manifestations of Arterial Disease – Magnetic Resonance (SMART-MR) study without a history of cerebrovascular disease. LGCS was defined as 1-49% stenosis on baseline carotid ultrasound, whereas no LGCS (reference category) was defined as absence of carotid plaque. Brain and white matter hyperintensity (WMH) volumes and cognitive function were measured at baseline and after 4 ($n=480$) and 12 years ($n=222$) of follow-up. Using linear mixed-effects models, we investigated associations of LGCS with progression of brain atrophy, WMH, and cognitive decline. LGCS was associated with greater progression of global brain atrophy (estimate -0.03; 95%CI, -0.06 to -0.01; $p=0.002$), and a greater decline in executive functioning (estimate -0.02; 95%CI, -0.031 to -0.01; $p<0.001$) and memory (estimate -0.012; 95%CI, -0.02 to -0.001; $p=0.032$), independent of demographics, cardiovascular risk factors, and incident brain infarcts on MRI. No association was observed between LGCS and progression of WMH. Our results indicate that LGCS may represent an early marker of greater future brain atrophy and cognitive decline.

Introduction

Carotid artery stenosis refers to the buildup of atherosclerotic plaque along the lining of the carotid arteries and represents a well-recognized cause of atheroembolic stroke.¹ At the highest levels of stenosis, carotid atheroma may also lead to hemodynamic stroke through flow restriction and cerebral ischemic injury.²

Mild carotid atheroma resulting in low-grade (1-49%) carotid artery stenosis (LGCS) is associated with a relatively low risk of atheroembolic stroke compared to moderate or severe stenosis^{3, 4}, but is a common finding in older individuals and patients with atherosclerotic disease.⁵⁻⁸ In clinical practice, LGCS is frequently identified incidentally in asymptomatic patients on imaging studies.⁹ Results from recent cross-sectional studies suggest that asymptomatic LGCS may be of clinical importance as a risk factor for smaller brain volumes and worse cognitive performance.¹⁰ The cross-sectional design of these studies, however, precludes establishing a cause-effect relationship. To the best of our knowledge, no previous studies examined the longitudinal relationship of LGCS with brain MRI changes and cognitive decline in patients without a history of cerebrovascular disease.

Here, we tested the hypothesis that asymptomatic LGCS may represent a risk factor for greater progression of brain atrophy, WMH and cognitive decline. Using data from the Second Manifestations of ARterial disease-Magnetic Resonance (SMART-MR) study, we compared trajectories of brain volumes, WMH volumes, and cognitive domains between patients with asymptomatic LGCS and patients without LGCS over 12 years of follow-up, adjusting for demographics and cardiovascular risk factors.

Methods

Study population

We used data from the SMART-MR study, a prospective cohort study at the University Medical Center Utrecht to investigate risk factors and consequences of brain changes on MRI in patients with manifest arterial disease.^{11, 12} A total of 1,309 adult patients newly referred to the University Medical Center Utrecht for treatment of atherosclerotic disease (manifest coronary artery disease, cerebrovascular disease, peripheral arterial disease or abdominal aortic aneurysm) between 2001 and 2005 were included for baseline measurements, including a 1.5T brain MRI.^{11, 12} During a 1-day visit to the University Medical Center Utrecht, a physical examination, ultrasonography of the carotid arteries, blood and urine samplings, and a 1.5T brain MRI scan were performed.^{11, 12} Neuropsychological assessment was added to the research protocol from 2003 onwards. We used questionnaires to assess demographics, risk factors, medical history, medication use, and cognitive and physical functioning.^{11, 12} Of the 1,309 patients included, 754 patients had follow-up measurements

four years later between January 2006 and May 2009. Between November 2013 and October 2017, all patients alive were invited for a second follow-up, including a 1.5T brain MRI. Second follow-up measurements were obtained from 329 patients.

The SMART-MR study was approved by the medical ethics committee of the University Medical Center Utrecht according to the guidelines of the Declaration of Helsinki of 1975. Written informed consent was obtained from all patients participating in the SMART-MR study.

Study sample

Of the 1,309 patients included in the SMART-MR study, carotid ultrasound data were irretrievable or incomplete in 56 patients and 181 patients were categorized as having moderate (50-69%) or severe (>70%) carotid stenosis. These patients were excluded from the present analyses. In addition, we excluded 170 patients with a history of cerebrovascular disease (defined as transient ischemic attack, stroke, cerebral ischemia, amaurosis fugax, or retinal infarction)¹³ as these may include patients with a symptomatic LGCS, resulting in a study sample of 902 patients (LGCS n=713; no LGCS n=189). Flow diagrams of patients with available neuroimaging and cognition data at each visit are shown in Figure 1 and Figure 2 of the Supplemental Material, respectively.

Carotid stenosis

At baseline, ultrasonography consisting of color Doppler-assisted duplex scanning was performed with a 10 MHz linear-array transducer (ATL Ultramark 9) by experienced ultrasound technicians to determine the presence and degree of carotid stenosis. The severity of carotid stenosis was evaluated based on blood flow velocity patterns and presence of plaque, and was recorded on a categorical scale.^{14, 15} The greatest stenosis observed on the right or the left side of the common or internal carotid artery was taken to determine the severity of carotid artery disease. Carotid stenosis 1-29% and 30-49% were defined as presence of plaque with a peak systolic velocity (PSV) ≤ 100 cm/s and > 100 to ≤ 150 cm/s, respectively. In the present study, we defined LGCS as 1-49% stenosis, in accordance with the North American Symptomatic Carotid Endarterectomy Trial criteria.¹ No LGCS (reference category) was defined as absence of carotid plaque.

MRI protocol

MR imaging of the brain was performed on a 1.5T whole-body system (Gyrosan ACS-NT, Philips Medical Systems, Best, the Netherlands) using a standardized scan protocol.¹ Transversal T1-weighted [repetition time (TR) = 235 ms; echo time (TE) = 2 ms], T2-weighted [TR = 2200 ms; TE = 11 ms], fluid-attenuated inversion recovery (FLAIR) [TR = 6000 ms; TE = 100 ms; inversion time (TI) = 2000 ms] and T1-weighted inversion recovery images [TR = 2900 ms; TE = 22 ms; TI = 410 ms] were acquired with a voxel size of 1.0 x 1.0 x 4.0 mm³ and contiguous slices.²

Brain infarcts

Although we excluded patients with a history of symptomatic cerebrovascular disease, patients in the study sample may show clinically non-manifest brain infarcts on MRI (i.e., silent cerebrovascular disease), which may confound the relationship between LGCS and change in neuroimaging and cognitive outcomes. We therefore accounted for brain infarcts on MRI in our analyses. Brain infarcts were visually rated by a neuroradiologist blinded to patient characteristics on the T1-weighted, T2-weighted, and FLAIR images of the MRI scans. Lacunes were defined as focal lesions between 3 to 15 mm according to the STRIVE criteria¹⁶, whereas non-lacunar lesions were categorized in large infarcts (i.e., cortical infarcts and subcortical infarcts not involving the cerebral cortex) and infarcts located in the cerebellum or brain stem.

Brain volume measurements

White matter hyperintensity (WMH) volumes and brain volumes were obtained using the *k*-nearest neighbor (kNN) automated segmentation program on the T1-weighted, FLAIR, and T1-weighted inversion recovery sequences of the MRI scans.¹⁷ The kNN segmentation method has been shown to be suitable for detecting longitudinal brain volume changes.^{11, 18} All WMH segmentations were visually checked by an investigator (RG) using an image processing framework (MeVisLab 2.7.1., MeVis Medical Solutions AG, Bremen, Germany). Incorrectly segmented voxels were added to the correct segmentation volumes using the image processing framework.

Total brain volume (including the volume of the cerebellum) was calculated by summing the volumes of gray matter, white matter, WMH and, if present, the volumes of brain infarcts. Total intracranial volume (ICV) was calculated by summing the total brain volume and the volume of cerebrospinal fluid. Total brain volume, sulcal cerebrospinal fluid volume and ventricular volume were normalized for ICV and expressed as brain parenchymal fraction (BPF), sulcal cerebrospinal fluid fraction (CSFF) and ventricular fraction (VF), and were used as indicators of global, cortical, and subcortical atrophy, respectively. Similarly, WMH volume was normalized for ICV. Natural log transformation was performed on WMH volumes due to a non-normal distribution.

Cognitive functioning

Cognitive functioning was measured at baseline, and first and second follow-up visits with a set of standard neuropsychological tests covering the domains of memory and executive functioning. Memory was assessed with the 15 Word Learning test (immediate recall based on five trials and delayed recall) and with the delayed recall of the Rey-Osterrieth Complex Figure test.^{19, 20} Executive functioning was assessed by the Visual Elevator test (10 trials), the Brixton Spatial Anticipation test, and the Verbal Fluency test (letter A with a time span of 60 seconds).²¹⁻²³ Visual Elevator test scores were natural log-transformed due to a non-normal distribution and multiplied by minus one so that higher

scores represented better performance. Similarly, Brixton test scores were multiplied by minus one so that higher scores represented better performance.

To assess change in cognitive functioning, we converted test scores from each visit to z-scores based on the baseline population mean and standard deviation (SD). These z-scores were averaged to create domain-specific z-scores for memory and executive functioning, which were subsequently standardized to the baseline domain-specific z-score mean and SD for all patients.

Covariates

At baseline, age, sex, smoking habits, alcohol intake and highest level of education were assessed using questionnaires. Height and weight were measured, and the body mass index (BMI) was calculated (kg/m^2). Systolic blood pressure (SBP) (mmHg) and diastolic blood pressure (DBP) (mmHg) were measured three times with a sphygmomanometer, and the average of these measures was calculated. Hypertension was defined as a mean SBP of >160 mmHg, a mean DBP of >95 mmHg, or self-reported use of antihypertensive drugs. Threshold values of SBP and DBP for hypertension were determined according to criteria established in 2001. An overnight fasting venous blood sample was taken to determine glucose and lipids. Diabetes mellitus was defined as fasting serum glucose levels of ≥ 7.0 mmol/l, and/or use of glucose-lowering medication, and/or known history of diabetes.

Education level was categorized into three categories based on the Dutch education system and ranged from no education/primary school to university education. Low level education included no education or primary school only (comparable to up to six years of education), whereas high level education included higher professional education and university education (comparable to ≥ 15 years of education). All other educational levels were defined as intermediate (comparable to around 7-14 years of education).

Statistical analysis

Baseline characteristics of the total study sample, and stratified by presence and absence of LGCS were reported with descriptive statistics.

Linear mixed-effects models

We used linear mixed-effects models with random effects to assess changes in neuroimaging outcomes and cognitive functioning over time.²⁴ The age of patients at each visit was chosen as the time variable, which was centered at 58 years (the mean value at the first visit) and hereinafter referred to as 'time'. LGCS was represented by a dichotomous variable with absence of LGCS as the reference category.

Models were run in two steps. In the first model, time, LGCS, and an interaction term between LGCS and time (our primary coefficient of interest) were entered, together with sex, large infarcts on MRI, lacunes on MRI, hypertension, diabetes mellitus, body mass index, smoking pack years and alcohol use at baseline as covariates. Models that estimated

cognitive change in addition included education level and a practice effect, which was modeled using an indicator fixed at the square root of the number of prior visits.²⁵

Incident brain infarcts and lacunes may act as a confounder on the relationship between LGCS and change in neuroimaging and cognitive outcomes. Therefore, in a second model, the covariates indicating large infarcts and lacunes on baseline MRI were replaced with time-varying covariates indicating the presence of large infarcts and lacunes at both baseline and follow-up MRI.

Adequacy of the linear mixed-effects models was determined by examining the residuals for approximate normality and homoscedasticity. We concluded that model assumptions were adequately met.

Missing covariates

To reduce the risk of bias due to complete case analysis, we performed chained equations imputation on missing baseline covariates to generate 10 imputed datasets using SPSS 25.0 (Chicago, IL, USA). The linear mixed-effects models were performed on the imputed datasets and the pooled results were presented. Statistical significance was set at $p \leq 0.05$.

Sensitivity analysis

The substantial attrition during follow-up in the present study may lead to informative dropout. To determine whether this was the case in the study sample, we used joint models that allow for controlling the results of the linear mixed models for dropout (including due to death) using correlated survival data.²⁶ Joint models consist of a longitudinal and a survival submodel.²⁶ The longitudinal submodel consisted of the linear mixed-effects models used in the primary analyses with adjustment for demographics, cardiovascular risk factors and brain infarcts on MRI at baseline. The survival submodel consisted of a Cox proportional hazards regression model with baseline age, sex and LGCS (with absence of LGCS as the reference category) as predictors. Follow-up data for the survival submodel were obtained from questionnaires that patients received biannually and are described in detail in previous work.¹² We defined dropout (i.e., the “event” in the survival submodel) as having a missing outcome for the second follow-up measurement, either due to death or any other reason.

We compared joint models using different baseline hazard functions and we selected the baseline hazard function that yielded the lowest Akaike information criterion. The Weibull baseline hazard function was chosen for models that estimated change in brain volumes, whereas the piecewise baseline hazard function was chosen for models that estimated change in cognitive functioning. The JM package for R version 4.0.5 (R Core Team, 2021) was used for the joint model analysis.²⁶

Results

Baseline characteristics of the study sample ($n = 902$; mean age 58 ± 10 years; 81% male) are shown in Table 1. LGCS was present in 713 patients (79%) at baseline, whereas 189 patients (21%) did not show any carotid stenosis.

Patients with LGCS were older, had a less favorable cardiovascular profile, showed more often lacunes on baseline MRI, and had lower executive functioning and memory z-scores compared to the reference group (Table 1).

Table 1. Baseline characteristics of patients with low-grade carotid stenosis, patients without stenosis and the total study sample.

	Low-grade carotid stenosis ($n = 713$)	No carotid stenosis ($n = 189$)	All patients ($n = 902$)
Age (years)	59 ± 9	51 ± 10	58 ± 10
Sex, % men	81.5	78.3	80.8
BMI (kg/m^2)	27 ± 4	26 ± 4	27 ± 4
Smoking, pack years ^a	20 (0, 52)	14 (0, 42)	19 (0, 49)
Alcohol use, %			
Current	75	74	75
Former	10	9	10
Abstinent	15	17	15
Hypertension, %	48.8	37.6	46.5
Diabetes mellitus, %	20.9	10.1	18.6
Education level, % ^b			
Low	13.0	8.4	11.9
Intermediate	67.5	63.5	66.6
High	19.5	28.1	21.5
Infarcts on MRI, %			
Large	3.5	1.1	3.0
Cerebellar	2.7	2.7	2.5
Brainstem	1.4	0.5	1.2
Lacunes on MRI, %	10.9	3.2	9.3
pCBF, ml/min per 100 ml brain volume	52.2 ± 10.3	53.2 ± 9.0	52.4 ± 10.1
BPF, % ICV	79.0 ± 2.8	80.7 ± 2.5	79.3 ± 2.8
CSFF, % ICV	18.9 ± 2.3	17.5 ± 2.0	18.6 ± 2.3
VF, % ICV	2.1 ± 1.1	1.8 ± 1.0	2.0 ± 1.0
WMH volume on MRI, ml ^a	0.9 (0.2, 5.6)	0.5 (0.1, 2.2)	0.8 (0.2, 4.9)
Executive functioning, z-score	-0.02 ± 0.96	0.23 ± 0.98	0.05 ± 0.97
Memory, z-score	-0.10 ± 0.97	0.27 ± 0.96	0.00 ± 0.98

Characteristics are presented as mean \pm SD or %.

BMI: body mass index; SD: standard deviation; WMH: white matter hyperintensity; pCBF: parenchymal cerebral blood flow; BPF: brain parenchymal fraction; ICV: total intracranial volume; CSFF: sulcal

cerebrospinal fluid fraction; VF: ventricular fraction.

^a Median (10th percentile, 90th percentile).

Mean time between baseline and first follow-up measurements was 3.9 ± 0.4 years (range 2.9 – 5.8 years), whereas there were 12.0 ± 0.4 years (range 11.1 – 13.5 years) between baseline and the second follow-up measurements.

Associations between LGCS and brain MRI changes

Mean decrease in BPF per year for the study sample was 0.25% ICV (95% CI, -0.28 to -0.22), whereas CSFF and VF were estimated to increase at 0.19% ICV (95% CI, 0.16 to 0.22) and 0.06% ICV (95% CI, 0.05 to 0.06) per year, respectively (Table 2). Mean increase in WMH per year was 0.08 natural log-transformed ml (95% CI, 0.07 to 0.10).

At age 58 (i.e., intercept), no main effects were observed of LGCS on BPF (estimate 0.07; 95% CI, -0.30 to 0.40; $p=0.717$), CSFF (estimate 0.07; 95% CI, -0.23 to 0.37; $p=0.661$), VF (estimate -0.10.15; 95% CI, -0.24 to 0.03; $p=0.134$), or WMH volume (estimate 0.00; 95% CI, -0.18 to 0.17; $p=0.978$).

LGCS, compared with no LGCS, was however associated with greater change in BPF (estimate -0.03; 95% CI, -0.06 to -0.01; $p=0.002$), CSFF (estimate 0.03; 95% CI, 0.01 to 0.05; $p=0.011$) and VF (estimate 0.01; 95% CI, 0.002 to 0.02; $p=0.019$), and these results did not substantially change after adjusting for incident large brain infarcts or lacunes (Table 2). LGCS was not associated with greater change in WMH volume over time (estimate 0.01; 95% CI, -0.03 to 0.02; $p=0.162$).

In the joint model analysis, parameter estimates for the time effect were slightly smaller for BPF, CSFF, VF and WMH compared with the primary analysis (Table 1 in the Supplementary Material). Controlling for death/dropout, LGCS versus no LGCS remained significantly associated with a greater decline in BPF (estimate -0.036; 95% CI, -0.06 to -0.01; $p=0.001$), and a greater increase in CSFF (estimate 0.03; 95% CI, 0.01 to 0.05; $p=0.006$) and VF (estimate 0.01; 95% CI, 0.002 to 0.017; $p=0.013$). Consistent with the primary analysis, LGCS was not related to a greater change in WMH volume (estimate 0.007; 95% CI, -0.003 to 0.017; $p=0.179$). Estimates of association parameters were significant for CSFF (estimate 0.0485; $p=0.036$) and VF (estimate 0.143; $p=0.002$), thereby indicating that death/dropout impacted average change in CSFF and VF over time, whereas this was not the case for BPF (estimate -0.037; $p=0.063$) and WMH volume (estimate -0.012; $p=0.722$) (Table 1 in the Supplementary Material).

Table 2. Output of the linear mixed-effects models with age of patients at each visit as the time variable, neuroimaging outcomes as dependent variables and low-grade carotid stenosis as independent variable.

	BPF		CSFF		VF		WMH ^b	
	Estimate (95% CI)	p value	Estimate (95% CI)	p value	Estimate (95% CI)	p value	Estimate (95% CI)	p value
Intercept								
Model 1	79.6 (78.5 to 80.8)	<0.001	18.4 (17.5 to 19.5)	<0.001	1.99 (1.54 to 2.43)	<0.001	-3.34 (-3.94 to -2.74)	<0.001
Model 2	79.5 (78.3 to 80.6)	<0.001	18.6 (17.5 to 19.6)	<0.001	2.08 (1.64 to 2.52)	<0.001	-3.21 (-3.81 to -2.61)	<0.001
Time								
Model 1	-0.25 (-0.28 to -0.22)	<0.001	0.19 (0.16 to 0.22)	<0.001	0.06 (0.05 to 0.07)	<0.001	0.08 (0.07 to 0.10)	<0.001
Model 2	-0.24 (-0.27 to -0.21)	<0.001	0.19 (0.16 to 0.21)	<0.001	0.06 (0.05 to 0.07)	<0.001	0.08 (0.07 to 0.10)	<0.001
LGCS ^a								
Model 1	0.07 (-0.30 to 0.40)	0.717	0.07 (-0.23 to 0.37)	0.661	-0.10 (-0.24 to 0.03)	0.134	0.00 (-0.18 to 0.17)	0.987
Model 2	0.04 (-0.31 to 0.37)	0.858	0.09 (-0.22 to 0.38)	0.591	-0.09 (-0.22 to 0.05)	0.200	0.03 (-0.15 to 0.20)	0.763
LGCS x Time								
Model 1	-0.03 (-0.06 to -0.01)	0.002	0.03 (0.01 to 0.05)	0.011	0.01 (0.002 to 0.02)	0.019	0.01 (-0.03 to 0.02)	0.162
Model 2	-0.03 (-0.05 to -0.01)	0.004	0.02 (0.01 to 0.04)	0.014	0.01 (0.001 to 0.02)	0.026	0.01 (-0.03 to 0.02)	0.156

Model 1: adjusted for sex, large infarcts on MRI, lacunes on MRI, hypertension, diabetes mellitus, body mass index, smoking pack years and alcohol use at baseline.

Model 2: model 1 with time-varying covariates for large infarcts and lacunes on MRI.

^aNo LGCS as the reference category.

^bNatural log-transformed and standardized for total intracranial volume.

CI: confidence interval, LGCS: low-grade carotid stenosis, BPF: brain parenchymal fraction, CSFF: sulcal cerebrospinal fluid fraction, VF: ventricular fraction, WMH: white matter hyperintensity volume.

Associations between LGCS and cognitive domain changes

Executive functioning was estimated to decrease by 0.06 z-score units (95% CI, -0.08 to -0.05; $p < 0.001$) on average per year. For memory, mean decrease was estimated at 0.06 z-score units (95% CI, -0.04 to -0.08; $p < 0.001$) per year for the study sample (Table 3).

Table 3. Output of the linear mixed-effects models with age of patients at each visit as the time variable, cognition domain-specific z-scores as dependent variables and low-grade carotid stenosis as independent variable.

	Executive functioning		Memory	
	Estimate (95% CI)	<i>p</i> value	Estimate (95% CI)	<i>p</i> value
Intercept				
Model 1	-0.84 (-1.37 to -0.32)	0.002	-0.29 (-0.84 to 0.27)	0.311
Model 2	-0.78 (-1.31 to -0.25)	0.004	-0.30 (-0.86 to 0.26)	0.293
Time				
Model 1	-0.06 (-0.08 to -0.05)	<0.001	-0.06 (-0.04 to -0.08)	<0.001
Model 2	-0.06 (-0.07 to -0.04)	<0.001	-0.06 (-0.04 to -0.07)	<0.001
LGCS^a				
Model 1	-0.06 (-0.20 to 0.09)	0.403	0.05 (-0.10 to 0.20)	0.496
Model 2	-0.04 (-0.18 to 0.10)	0.577	0.04 (-0.11 to 0.19)	0.586
LGCS x Time				
Model 1	-0.020 (-0.031 to -0.01)	<0.001	-0.012 (-0.02 to -0.001)	0.032
Model 2	-0.017 (-0.028 to -0.006)	0.003	-0.010 (-0.02 to 0.001)	0.082

Model 1: adjusted for sex, education level, practice effect, large infarcts on MRI, lacunes on MRI, hypertension, diabetes mellitus, body mass index, smoking pack years and alcohol use at baseline. Model 2: model 1 with time-varying covariates for large infarcts and lacunes on MRI.

^aNo LGCS as the reference category.

CI: confidence interval, LGCS: low-grade carotid stenosis.

At age 58 (i.e., intercept), LGCS versus no LGCS was not associated with a lower z-score in executive functioning (estimate -0.06; 95% CI, -0.20 to 0.09; $p = 0.403$) or memory (estimate 0.05; 95% CI, -0.10 to 0.20; $p = 0.496$), and these estimates did not substantially change after accounting for incident large brain infarcts or lacunes (Table 3).

LGCS, compared with no LGCS, was however associated with a greater decline in executive functioning by 0.02 z-score units (95% CI, -0.031 to -0.01; $p < 0.001$; Figure 1) per year. The association between LGCS and change in executive functioning persisted after controlling for incident large brain infarcts and lacunes (Table 3). For memory, LGCS versus no LGCS was associated with a greater decline by 0.012 z-score units (95% CI, -0.02 to -0.001; $p = 0.032$; Figure 2) per year. The association between LGCS and change in memory slightly attenuated after controlling for incident large brain infarcts and lacunes (Table 3).

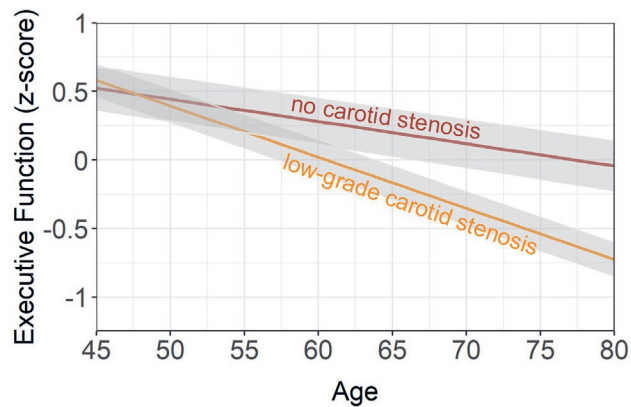


Figure 1. Longitudinal relationship between executive functioning (z-score), low-grade carotid stenosis, and no stenosis. Age of patients at each visit was chosen as the time variable. The shaded grey area represents the 95% confidence interval. Results adjusted for sex, education level, large infarcts on MRI, lacunes on MRI, hypertension, diabetes mellitus, body mass index, smoking pack years, alcohol use and practice effect.

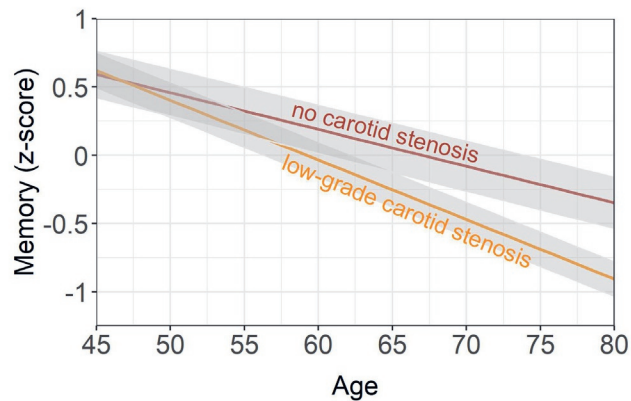


Figure 2. Longitudinal relationship between memory (z-score), low-grade carotid stenosis, and no stenosis. Age of patients at each visit was chosen as the time variable. The shaded grey area represents the 95% confidence interval. Results adjusted for sex, education level, large infarcts on MRI, lacunes on MRI, hypertension, diabetes mellitus, body mass index, smoking pack years, alcohol use and practice effect.

In the joint model analysis, parameter estimates for the time effect were comparable with the primary analyses (Table 1 in the Supplementary Material). Controlling for death/dropout, LGCS remained associated with a greater decline in executive functioning (estimate -0.017 ; 95% CI, -0.026 to -0.01 ; $p < 0.001$) and memory (estimate -0.011 ; 95% CI, -0.017 to -0.004 ; $p = 0.002$). Estimates of association parameters were significant for both

executive functioning (estimate -1.34; $p < 0.001$) and memory (estimate -0.546; $p < 0.001$), indicating that death/dropout impacted average change in executive functioning and memory over time.

Discussion

In this cohort of patients with manifest arterial disease, we observed that asymptomatic low-grade carotid artery stenosis (LGCS) was associated with greater progression of global, cortical and subcortical brain atrophy, but not with white matter hyperintensities (WMH) compared with absence of stenosis. LGCS was also associated with a greater decline in executive functioning and memory throughout the follow-up period of 12 years. These relationships were independent of demographics, cardiovascular risk factors and brain infarcts on MRI.

In clinical practice, emphasis is on the detection of carotid stenosis due to the associated risk of atheroembolic stroke. The risk of atheroembolic stroke is relatively low in LGCS but increases substantially in moderate and severe stenosis.^{3,4} The findings of this long-term follow-up study, however, suggest that asymptomatic LGCS may be of clinical importance as a marker of greater future brain atrophy and cognitive decline. Our results are consistent with a recent cross-sectional study in which mild carotid atheroma was related to cortical thinning and worse fluid intelligence.¹⁰

It is noteworthy that we detected associations between LGCS, progression of brain atrophy and cognitive decline in a study population consisting entirely of patients with manifest arterial disease. This observation suggests that presence of atherosclerotic disease alone may not explain the abovementioned relationships. Cerebral hypoperfusion secondary to LGCS is also less likely an explanation as carotid artery stenosis $< 50\%$ is usually considered hemodynamically insignificant. Likewise, symptomatic or silent brain infarcts and lacunes are also less likely to explain the observed relationships because we included only asymptomatic patients with LGCS, and we adjusted the analyses for prevalent and incident silent brain infarcts on MRI. A more likely explanation for our findings may be that LGCS represents an early marker of more profound atherosclerotic vascular changes within the cerebrum, which may gradually negatively impact brain health over time.¹⁰ These detrimental effects, however, may not become fully apparent until late-life, and may not be fully captured by measurable cardiovascular risk factors. We observed that at age 58 (the mean baseline age of the study sample), LGCS was not associated with worse cognitive functioning or smaller brain volumes, however from age 58 onwards we did observe significant differences in trajectories of cognitive domains and brain volumes. We also observed that, while patients with LGCS showed a less favorable cardiovascular profile at baseline, measurable cardiovascular risk factors, such as smoking or diabetes mellitus, did not explain the greater cognitive decline and progression of brain atrophy

associated with LGCS. It is therefore possible that the impact of LGCS on brain health is indirect as a marker for the cumulative effects of both measurable and non-measurable vascular risk factors.¹⁰

To the best of our knowledge, no previous studies compared trajectories of brain MRI changes and cognitive functioning between asymptomatic patients with LGCS and those without. Studies examining the impact of carotid plaque (irrespective of degree of stenosis) on cognitive functioning have reported conflicting findings. In the Northern Manhattan Study, carotid plaque was not related to greater cognitive decline throughout the follow-up period of 5 years. In the Tromsø Study, however, presence of carotid plaque at baseline was associated with lower cognitive test scores measured 7 years later.²⁷ With respect to WMH, our findings are in line with a prospective analysis of the Rotterdam Scan Study in which increasing carotid plaque severity was not associated with progression of WMH over 3 years of follow-up.²⁸

Limitations of this study include, first, the substantial attrition during follow-up. However, we addressed this issue by performing sensitivity analyses using joint models and we observed that the relations between LGCS, progression of brain atrophy and cognitive decline held after controlling for death/dropout. Second, although executive functioning and memory likely represent the most important cognitive domains in clinical practice²⁹, cognitive testing in this analysis was limited to only two cognitive domains. Third, the volumetric MRI technique used in our study did not allow us to measure region-specific brain volume changes. Results from a recent cross-sectional analysis in the Lothian Birth Cohort 1936 indicate that carotid atheroma was predominantly associated with smaller volumes in specific anterior and posterior cortical regions, whereas regions of the primary motor and sensory cortex were spared.¹⁰ Fourth, volumetry in this study was performed on MRI sequences with a slice thickness of 4 mm instead of 1 mm, which is likely more sensitive in detecting brain volume changes.

Strengths of this study are the large number of patients included, the long follow-up period and the multiple brain MRI and cognitive functioning measurements recorded over time. In addition, we accounted for silent cerebrovascular disease on baseline MRI in the analyses. Also, we used prospective MRI data to adjust the analyses for incident brain infarcts and lacunes during follow-up. Lastly, we also accounted for a potential practice effect in the analyses concerning cognitive functioning due to the relatively short interval between the baseline and first follow-up measurement of 4 years.

Overall, our findings demonstrate that asymptomatic LGCS is associated with greater cognitive decline and greater progression of global, cortical, and subcortical brain atrophy over 12 years of follow-up, independent of demographics, cardiovascular risk factors, or brain infarcts on MRI. These results indicate that LGCS, a common finding in older individuals and patients with manifest arterial disease, may be a clinical marker of greater future brain atrophy and cognitive decline.

References

1. Barnett HJM, Taylor DW, Haynes RB, et al. Beneficial effect of carotid endarterectomy in symptomatic patients with high-grade carotid stenosis. *N Engl J Med* 1991; 325: 445-453.
2. Derdeyn CP, Grubb RL, Jr. and Powers WJ. Cerebral hemodynamic impairment: methods of measurement and association with stroke risk. *Neurology* 1999; 53: 251-259.
3. Singh N, Marko M, Ospel JM, et al. The Risk of Stroke and TIA in Nonstenotic Carotid Plaques: A Systematic Review and Meta-Analysis. *AJNR Am J Neuroradiol* 2020; 41: 1453-1459.
4. Howard DPJ, Gaziano L and Rothwell PM. Risk of stroke in relation to degree of asymptomatic carotid stenosis: a population-based cohort study, systematic review, and meta-analysis. *The Lancet Neurology* 2021; 20: 193-202.
5. O'Leary DH, Polak JF, Kronmal RA, et al. Distribution and correlates of sonographically detected carotid artery disease in the Cardiovascular Health Study. The CHS Collaborative Research Group. *Stroke* 1992; 23: 1752-1760.
6. Song P, Fang Z, Wang H, et al. Global and regional prevalence, burden, and risk factors for carotid atherosclerosis: a systematic review, meta-analysis, and modelling study. *The Lancet Global Health* 2020; 8: e721-e729.
7. Sturlaugsdottir R, Aspelund T, Bjornsdottir G, et al. Prevalence and determinants of carotid plaque in the cross-sectional REFINE-Reykjavik study. *BMJ Open* 2016; 6: e012457.
8. Ihle-Hansen H, Vigen T, Ihle-Hansen H, et al. Prevalence of Carotid Plaque in a 63- to 65-Year-Old Norwegian Cohort From the General Population: The ACE (Akershus Cardiac Examination) 1950 Study. *J Am Heart Assoc* 2018; 7.
9. Wasserman BA, Wityk RJ, Trout HH, et al. Low-Grade Carotid Stenosis. *Stroke* 2005; 36: 2504-2513.
10. Alhusaini S, Karama S, Nguyen TV, et al. Association between carotid atheroma and cerebral cortex structure at age 73 years. *Ann Neurol* 2018; 84: 576-587.
11. Geerlings MI, Appelman AP, Vincken KL, et al. Brain volumes and cerebrovascular lesions on MRI in patients with atherosclerotic disease. The SMART-MR study. *Atherosclerosis* 2010; 210: 130-136.
12. Ghaznawi R, Geerlings MI, Jaarsma-Coes M, et al. Association of White Matter Hyperintensity Markers on MRI and Long-term Risk of Mortality and Ischemic Stroke: The SMART-MR Study. *Neurology* 2021; 96: e2172-e2183.
13. den Hartog AG, Achterberg S, Moll FL, et al. Asymptomatic carotid artery stenosis and the risk of ischemic stroke according to subtype in patients with clinical manifest arterial disease. *Stroke* 2013; 44: 1002-1007.
14. Elgersma OE, van Leersum M, Buijs PC, et al. Changes over time in optimal duplex threshold for the identification of patients eligible for carotid endarterectomy. *Stroke* 1998; 29: 2352-2356.
15. Goessens BM, Visseren FL, Kappelle LJ, et al. Asymptomatic carotid artery stenosis and the risk of new vascular events in patients with manifest arterial disease: the SMART study. *Stroke* 2007; 38: 1470-1475.
16. Wardlaw JM, Smith EE, Biessels GJ, et al. Neuroimaging standards for research into small vessel disease and its contribution to ageing and neurodegeneration. *Lancet Neurol* 2013; 12: 822-838.

17. Anbeek P, Vincken KL, van Bochove GS, et al. Probabilistic segmentation of brain tissue in MR imaging. *Neuroimage* 2005; 27: 795-804.
18. de Bresser J, Portegies MP, Leemans A, et al. A comparison of MR based segmentation methods for measuring brain atrophy progression. *Neuroimage* 2011; 54: 760-768.
19. Brand N and Jolles J. Learning and retrieval rate of words presented auditorily and visually. *J Gen Psychol* 1985; 112: 201-210.
20. Lu PH, Boone KB, Cozolino L, et al. Effectiveness of the Rey-Osterrieth Complex Figure Test and the Meyers and Meyers recognition trial in the detection of suspect effort. *Clin Neuropsychol* 2003; 17: 426-440.
21. Robertson IH, Ward T, Ridgeway V, et al. The structure of normal human attention: The Test of Everyday Attention. *J Int Neuropsychol Soc* 1996; 2: 525-534.
22. Burgess PW and Shallice T. Bizarre responses, rule detection and frontal lobe lesions. *Cortex* 1996; 32: 241-259.
23. Wilkins AJ, Shallice T and McCarthy R. Frontal lesions and sustained attention. *Neuropsychologia* 1987; 25: 359-365.
24. Benedictus MR, Leeuwis AE, Binnewijzend MA, et al. Lower cerebral blood flow is associated with faster cognitive decline in Alzheimer's disease. *Eur Radiol* 2017; 27: 1169-1175.
25. Vivot A, Power MC, Glymour MM, et al. Jump, Hop, or Skip: Modeling Practice Effects in Studies of Determinants of Cognitive Change in Older Adults. *Am J Epidemiol* 2016; 183: 302-314.
26. Rizopoulos D. JM: An R Package for the Joint Modelling of Longitudinal and Time-to-Event Data. *Journal of Statistical Software*; Vol 1, Issue 9 (2010) 2010.
27. Arntzen KA, Schirmer H, Johnsen SH, et al. Carotid atherosclerosis predicts lower cognitive test results: a 7-year follow-up study of 4,371 stroke-free subjects - the Tromso study. *Cerebrovasc Dis* 2012; 33: 159-165.
28. van Dijk EJ, Prins ND, Vrooman HA, et al. Progression of cerebral small vessel disease in relation to risk factors and cognitive consequences: Rotterdam Scan study. *Stroke* 2008; 39: 2712-2719.
29. Harvey PD. Domains of cognition and their assessment. *Dialogues Clin Neurosci* 2019; 21: 227-237.

Supplementary Material

Table 1. Joint Model Analysis with brain volumes and cognitive domains as dependent variables

	Joint Models		Association parameter	
	Estimate (SE)	p values	Estimate	p values
BPF				
Intercept	92.7 (0.46)	<0.001	-0.0374	0.0631
Time	-0.21 (0.006)	<0.001		
LGCS ^a	2.18 (0.66)	0.001		
LGCS x Time	-0.036 (0.01)	0.0013		
CSFF				
Intercept	8.52 (0.41)	<0.001	0.0485	0.0356
Time	0.16 (0.006)	<0.001		
LGCS ^a	-1.55 (0.59)	0.0081		
LGCS x Time	0.0278 (0.01)	0.0057		
VF				
Intercept	-1.02 (0.16)	<0.001	0.1428	0.0021
Time	0.05 (0.002)	<0.001		
LGCS ^a	-0.67 (0.21)	0.0013		
LGCS x Time	0.0097 (0.004)	0.0124		
WMH				
Intercept	-7.60 (0.23)	<0.001	-0.0117	0.772
Time	0.076 (0.003)	<0.001		
LGCS ^a	-0.42 (0.31)	0.1727		
LGCS x Time	0.0073 (0.005)	0.1786		
Executive functioning				
Intercept	2.69 (0.22)	<0.001	-1.340	<0.001
Time	-0.06 (0.003)	<0.001		
LGCS ^a	1.04 (0.256)	<0.001		
LGCS x Time	-0.0174 (0.005)	<0.001		
Memory				
Intercept	2.59 (0.14)	<0.001	-0.546	<0.001
Time	-0.06 (0.002)	<0.001		
LGCS ^a	0.68 (0.20)	<0.001		
LGCS x Time	-0.011 (0.003)	0.002		

The longitudinal submodel was adjusted for sex, large infarcts on MRI, lacunes on MRI, hypertension, diabetes mellitus, body mass index, smoking pack years and alcohol use at baseline. Models that estimated cognitive change in addition included education level and practice effect as covariates. The survival submodel included LGCS, baseline age and sex as predictors.

Note that the time variable (i.e., age of patients at each visit) was not centered as negative values for the time variable are not compatible with the JM package.

^aNo LGCS as the reference category.

SE: standard error, LGCS: low-grade carotid stenosis, BPF: brain parenchymal fraction, CSFF: sulcal

cerebrospinal fluid fraction, VF: ventricular fraction, WMH: white matter hyperintensity volume.

The estimates of the association parameters in the joint models for CSFF, VF, executive functioning and memory were statistically significant, indicating that death/dropout impacted change in CSFF, VF, executive functioning and memory throughout the follow-up period. This was not however the case for BPF and WMH.

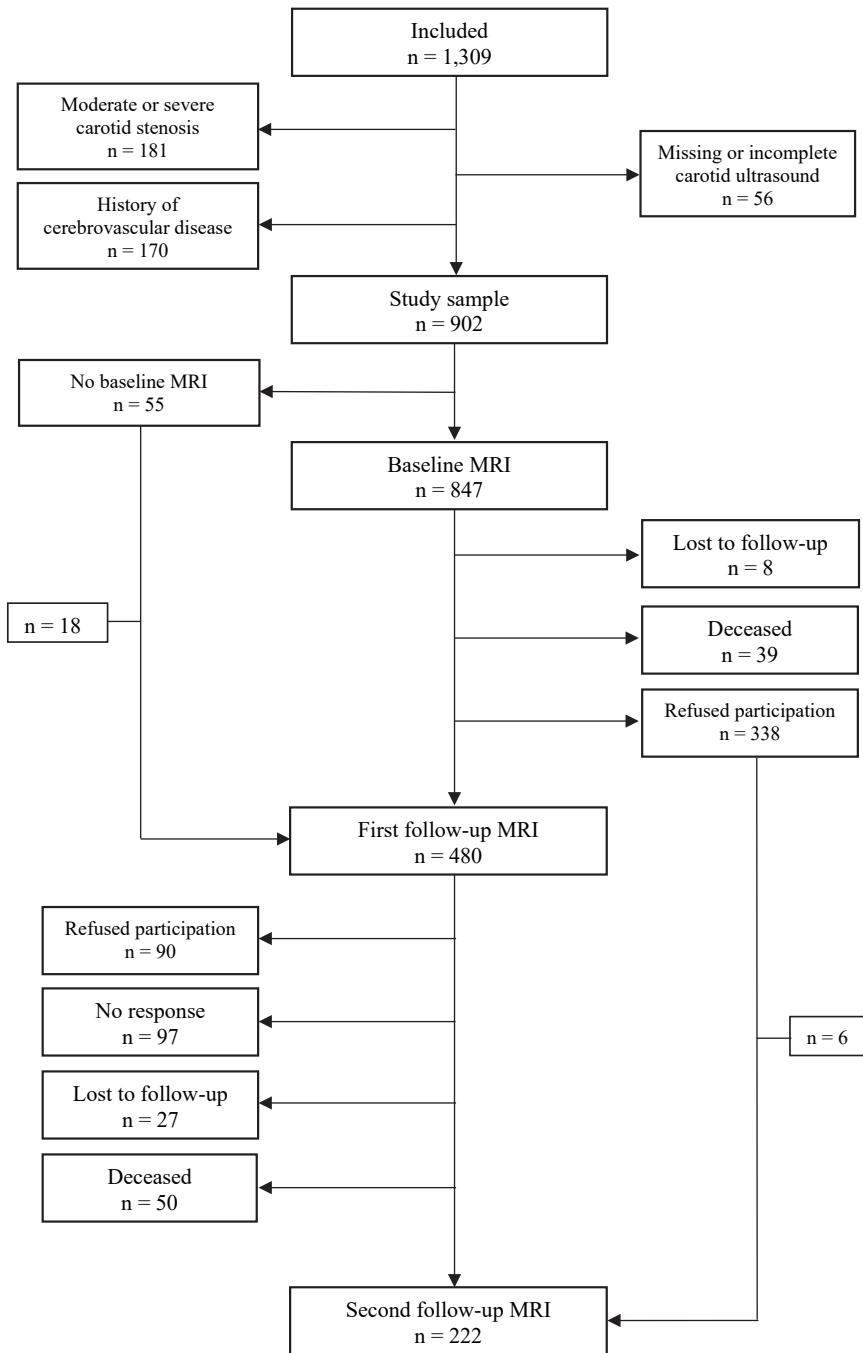


Figure 1. Participation flow diagram of the 902 patients included in this study for neuroimaging analysis. The neuroimaging analysis included patients with consecutive and non-consecutive MRI measurements.

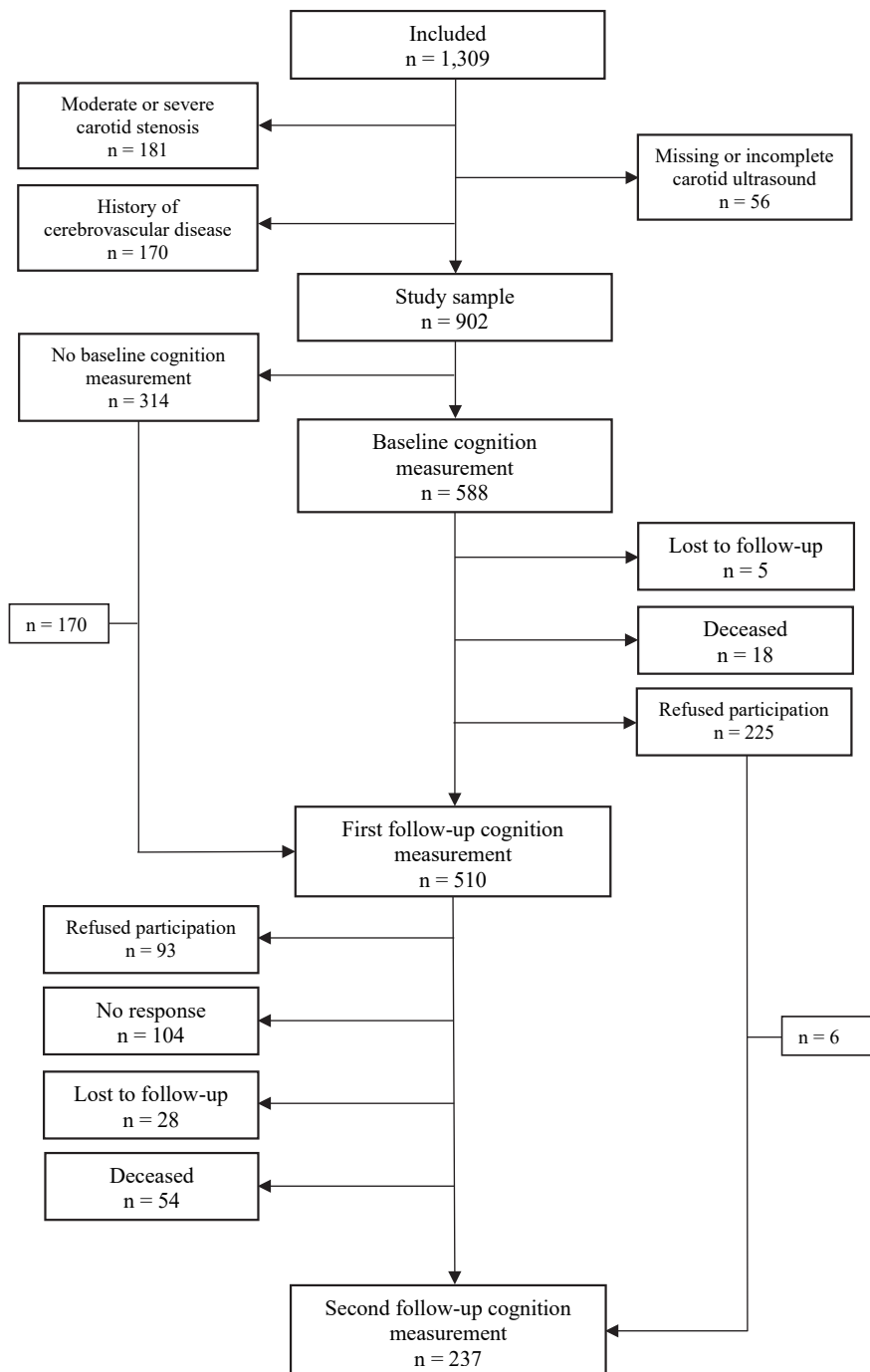


Figure 2. Participation flow diagram of the 902 patients included in this study for cognitive analysis. The cognitive analysis included patients with consecutive and non-consecutive cognitive functioning assessment.

CHAPTER 8



Carotid artery stenosis and progression of hemispheric brain atrophy. The SMART-MR study

Rashid Ghaznawi ^{1,2}, Ina Rissanen ², Jeroen de Bresser ³, Hugo J. Kuijf ⁴, Nicolaas P.A. Zuithoff ², Jeroen Hendrikse ¹, Mirjam I. Geerlings ²; on behalf of the UCC-SMART Study Group

¹Department of Radiology, University Medical Center Utrecht, Netherlands; ²Julius Center for Health Sciences and Primary Care, University Medical Center Utrecht, Netherlands; ³Department of Radiology, Leiden University Medical Center, Netherlands; ⁴Image Sciences Institute, University Medical Center Utrecht, Netherlands

Introduction

It has been hypothesized that carotid artery stenosis (CAS) may lead to greater atrophy of subserved brain regions, however prospective studies on the impact of CAS on progression of hemispheric brain atrophy are lacking. We examined the association between CAS and progression of hemispheric brain atrophy.

Methods

We included 654 patients (57 ± 9 years) of the SMART-MR study, a prospective cohort study of patients with manifest arterial disease. Patients had baseline CAS duplex measurements and a 1.5T brain MRI at baseline and after 4 years of follow-up. Mean change in hemispheric brain volumes (% of intracranial volume (ICV)) was estimated between baseline and follow-up for left-sided and right-sided CAS across three degrees of stenosis (mild ($\leq 29\%$), moderate (30 to 69%) and severe ($\geq 70\%$)), adjusting for demographics, cerebrovascular risk factors, and brain infarcts.

Results

Mean decrease in left and right hemispheric brain volumes was 1.15 % ICV and 0.82 % ICV, respectively, over 4 years of follow-up. Severe right-sided CAS, compared to mild CAS, was associated with a greater decrease in volume of the left hemisphere ($B = -0.49\%$ ICV, 95% CI -0.86 to -0.13), and more profoundly of the right hemisphere ($B = -0.90\%$ ICV, 95% CI -1.27 to -0.54). This pattern was independent of cerebrovascular risk factors, brain infarcts and white matter hyperintensities on MRI, and was also observed when accounting for presence of severe bilateral CAS. Increasing degrees of left-sided CAS, however, was not associated with greater volume loss of the left or right hemisphere.

Conclusions

Our data indicate that severe ($\geq 70\%$) CAS could represent a risk factor for greater ipsilateral brain volume loss, independent of cerebrovascular risk factors, brain infarcts or white matter hyperintensities on MRI. Further longitudinal studies in other cohorts are warranted to confirm this novel finding.

Introduction

Brain atrophy is an important hallmark of dementia and is commonly seen in patients with atherosclerotic disease[1, 2]. Although brain volume loss occurs with normal ageing, accelerated brain atrophy has been shown to represent an important risk factor for cognitive impairment and dementia[3-5]. The underlying causes that lead to progression of brain atrophy remain largely unknown, however previous studies suggest that cerebrovascular disease, male sex and reduced cerebral blood flow may represent potential risk factors[6, 7].

Carotid artery stenosis (CAS) may also represent a risk factor for accelerated brain atrophy and development of dementia[8, 9]. Several hypotheses linking CAS to accelerated brain atrophy have been formulated. First, CAS can lead to atheroembolic stroke, which is a risk factor for accelerated brain atrophy[10]. Second, CAS may represent a proxy marker for cerebrovascular risk factors, which may negatively impact brain health through greater brain tissue loss over time[9]. Third, high-grade CAS may lead to compromised blood flow through the affected carotid artery that, if not adequately compensated for by collateral circulation, may result in brain tissue loss[11]. Several aspects of the association between CAS and progression of brain atrophy, however, are unclear. For example, it is not known whether CAS represents a risk factor for greater atrophy of the ipsilateral cerebral hemisphere, the contralateral cerebral hemisphere, or both. The limited number of studies on this relationship reported smaller brain volumes ipsilateral to the side of the stenosis[12-15]. The cross-sectional design of these studies, however, precludes establishing a cause-effect relationship and, to our knowledge, no previous longitudinal studies examined the effects of CAS on hemispheric brain volume changes.

Here, we hypothesized that CAS was associated with greater ipsilateral hemispheric brain atrophy. Using data from the Second Manifestations of ARterial disease - Magnetic Resonance (SMART-MR) study, we examined the longitudinal association of CAS with changes in hemispheric and total brain volumes over 4 years of follow-up, adjusting for demographics, cerebrovascular disease, and its risk factors.

Material and methods

Study population

Data were used from the SMART-MR study, a prospective cohort study at the University Medical Center Utrecht with the aim to investigate risk factors and consequences of brain changes on magnetic resonance imaging (MRI) in patients with manifest arterial disease. In brief, between 2001 and 2005, 1309 middle-aged and older patients newly referred to the University Medical Center Utrecht for treatment of manifest arterial disease (manifest coronary artery disease (59%), cerebrovascular disease (23%), peripheral arterial disease

(22%) or abdominal aortic aneurysm (9%)) were included for baseline measurements. During a one-day visit to our medical center, a physical examination, ultrasonography of the carotid arteries, blood and urine samplings, neuropsychological assessment and a 1.5T brain MRI scan were performed. Questionnaires were used to assess demographics, risk factors, medical history, and medication use. Between 2006 and 2009, follow-up measurements took place, including a 1.5T MRI of the brain. In total, 754 patients of the surviving cohort gave written informed consent and participated in the follow-up.

The SMART-MR study was approved by the medical ethics committee of the University Medical Center Utrecht according to the guidelines of the Declaration of Helsinki of 1975 and written informed consent was obtained from all patients.

Assessment of carotid artery stenosis

Presence of CAS was assessed at baseline with ultrasonography consisting of color Doppler-assisted duplex. Measurements were performed with a 10MHz linear-array transducer (ATL Ultramark 9) by ultrasound technicians. The severity of CAS was evaluated on the basis of blood flow velocity patterns [16]. The greatest stenosis observed on the right or the left side of the common or internal carotid artery was taken to determine the severity of CAS. CAS was classified into groups of mild ($\leq 29\%$; peak systolic velocity (PSV) ≤ 100 cm/s), moderate (30% to 69%; PSV > 100 to ≤ 210 cm/s) and severe ($\geq 70\%$; PSV > 210 cm/s) for each side. In addition, to examine the effects of unilateral CAS on brain volumes in the presence of bilateral stenosis, we classified patients into i) mild to moderate CAS at both sides, ii) severe unilateral left-sided CAS, iii) severe unilateral right-sided CAS, and iv) severe bilateral CAS.

MRI protocol

MR imaging of the brain was performed on a 1.5T whole-body system (Gyrosan ACS-NT, Philips Medical Systems, Best, The Netherlands) using a standardized scan protocol. Transversal T1-weighted [repetition time (TR) = 235 ms; echo time (TE) = 2 ms], T2-weighted [TR = 2200 ms; TE = 11 ms], fluid-attenuated inversion recovery (FLAIR) [TR = 6000 ms; TE = 100 ms; inversion time (TI) = 2000 ms] and T1-weighted inversion recovery images [TR = 2900 ms; TE = 22 ms; TI = 410 ms] were acquired with a voxel size of $1.0 \times 1.0 \times 4.0$ mm³ and contiguous slices.

Brain infarcts

Brain infarcts were visually rated by a neuroradiologist blinded to patient characteristics on the T1-weighted, T2-weighted and FLAIR images. Lacunes were defined as focal lesions between 3 to 15 mm according to the STRIVE criteria [17], whereas non-lacunar lesions were categorized in large infarcts (i.e., cortical infarcts and subcortical infarcts not involving the cerebral cortex) and infarcts located in the cerebellum or brain stem.

Brain volume measurements

The T1-weighted, the T1-weighted inversion recovery and FLAIR sequence were used for automated brain segmentation. A probabilistic brain segmentation method consisting of k-nearest neighbor classification was performed to segment cortical gray matter, white matter and deep gray matter, sulcal and ventricular cerebrospinal fluid, and white matter hyperintensities (WMH)[18]. The kNN segmentation method has been shown to be suitable for detecting longitudinal brain volume changes[19]. Brain infarcts were manually segmented, and the other segmentations were corrected for presence of infarcts. All WMH segmentations were visually checked by an investigator (RG) using an image processing framework (MeVisLab 2.7.1., MeVis Medical Solutions AG, Bremen, Germany) to ensure that brain infarcts were correctly removed from the WMH segmentations[20].

Total brain volume was calculated by summing the volumes of cortical gray matter, white matter, WMH, and, if present, the volume of brain infarcts. Total intracranial volume (ICV) was calculated by summing the total brain volume and the volume of cerebrospinal fluid. Hemispheric brain volumes were obtained using an automated method based on extraction of the midsagittal surface[21]. An illustration of the midsagittal surface is shown in Figure 1. Infratentorial volumes were automatically subtracted from the volumes to obtain hemispheric cerebral volumes that were used in analyses.

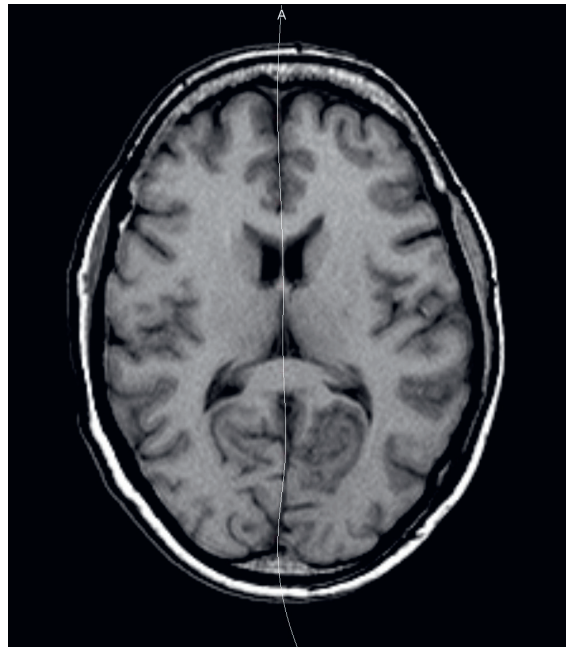


Figure 1. Illustration of the midsagittal surface (white line) separating the cerebral hemispheres on an axial T1-weighted MR image of a 52 year-old male patient. Note that the midsagittal surface also accounts for the presence of left-right asymmetry of the occipital lobes (i.e., “brain torque”) in this patient.

Cerebrovascular risk factors

At baseline, age, sex, smoking habits, and alcohol intake were assessed using questionnaires. Height and weight were measured, and the body mass index (BMI) was calculated (kg/m²). Systolic blood pressure (mm Hg) and diastolic blood pressure (mm Hg) were measured twice with a sphygmomanometer and the average of these measures was calculated. Hypertension was defined as a mean systolic blood pressure of >160 mm Hg, a mean diastolic blood pressure of >95 mm Hg, self-reported use of antihypertensive drugs, or a known history of hypertension at inclusion. An overnight fasting venous blood sample was taken to determine glucose and lipid levels. Diabetes mellitus was defined as the use of glucose-lowering drugs, a known history of diabetes mellitus, or a fasting plasma glucose level of ≥ 7.0 mmol/l. Hyperlipidemia was defined as a total cholesterol of >5.0 mmol/l, a low-density lipoprotein cholesterol of >3.2 mmol/l, use of lipid-lowering drugs, or a known history of hyperlipidemia.

Study sample

Of the 1309 patients included, 15 had no MRI and 12 had no FLAIR sequence. Furthermore, brain volume data were missing due to motion or artifacts in 39 patients. Of the remaining 1243 patients, 695 patients underwent a follow-up MRI. Of these, 16 patients had missing brain volume data due to motion or artifacts and CAS measurements were missing in 25 patients at one or both sides. As a result, the analyses were performed in 654 patients.

Statistical analysis

To examine the relationship of sidedness of CAS with total and hemispheric brain volume changes at follow-up, we chose a mixed model approach using the MIXED procedure of SAS (SAS Institute, Cary, NC, USA). We used this statistical approach because mixed models can estimate the effects of CAS on hemispheric brain volumes while taking into account the effects on the contralateral cerebral hemisphere. Degrees of left-sided and right-sided CAS at baseline were entered as independent variables, whereas total brain volume and hemispheric brain volumes at follow-up were entered as dependent variables.

Next, to examine the effects of severe unilateral CAS on brain volumes in the presence of severe bilateral CAS, we entered a categorical variable with mild to moderate CAS at both sides, severe unilateral left-sided CAS, severe unilateral right-sided CAS and severe bilateral CAS as outcomes as the independent variable. Mild to moderate CAS at both sides was chosen as the reference category. Total and hemispheric brain volumes at follow-up were entered as the dependent variables.

All of the abovementioned models were run in two steps. In the first model, we adjusted for age, sex, and baseline brain volumes. In the second model, we added covariates indicating hypertension, diabetes mellitus, body mass index, smoking pack years, alcohol use, and number of infarcts (including lacunes) and WMH volume on baseline and follow-up MRI.

As a supplementary analysis, we used analysis of covariance (ANCOVA) to estimate changes in hemispheric brain volumes for degrees of left-sided and right-sided CAS. Age, sex and the abovementioned cerebrovascular risk factors were added as covariates in addition to the number of infarcts and WMH volume on baseline and follow-up MRI in the cerebral hemisphere ipsilateral to the side of stenosis. This supplementary analysis allowed us to estimate changes in hemispheric brain volumes while specifically taking into account cerebrovascular lesions on the side of the stenosis. We excluded patients with a severe bilateral CAS from these analyses.

Estimates were considered statistically significant when their 95% confidence intervals (CI) excluded zero.

Results

Baseline characteristic of the study sample ($n = 654$, 57 ± 10 years, 81% male) and stratified according to the highest degree of CAS are shown in Table 1. At baseline, mean total brain volume of the study sample was 79.4 ± 2.6 % ICV. Mean right hemispheric volume was 79.9 ± 2.6 % ICV, whereas mean left hemispheric volume was 78.8 ± 2.7 % ICV. Severe CAS was present in 64 patients (left-sided: 37 (6%), right-sided: 43 (7%)) (Table 1). Patients with moderate or severe CAS were on average older, had a worse cardiovascular profile, and showed more infarcts and a greater WMH volume on MRI compared to patients with mild CAS (Table 1).

Mean decrease of total brain volume was 0.97 % ICV, of left hemispheric brain volume 1.15 % ICV and of right hemispheric brain volume 0.82 % ICV over 3.9 years of follow-up for the study sample.

Sidedness of CAS and brain volume changes

Compared to mild right-sided CAS, moderate right-sided CAS was associated with a greater decrease in total brain volume ($B = -0.20$ % ICV, 95% CI -0.55 to -0.14), left hemispheric volume ($B = -0.20$ % ICV, 95% CI -0.58 to 0.18) and, more strongly, in right hemispheric volume ($B = -0.37$ % ICV, 95% CI -0.76 to 0.02), although these estimates did not reach statistical significance (Table 2). Stronger associations, but in a similar pattern, were observed for severe right-sided CAS in relation to change in total brain volume ($B = -0.69$ % ICV, 95% CI -1.02 to -0.37), left hemispheric volume ($B = -0.49$ % ICV, 95% CI -0.86 to -0.13) and right hemispheric volume ($B = -0.90$ % ICV, 95% CI -1.27 to -0.54). Estimates slightly attenuated after adjusting for cerebrovascular risk factors, and number of infarcts and WMH volume on baseline and follow-up MRI (Table 2).

Table 1. Baseline characteristics of the study sample and stratified according to the highest degree of CAS.

	Total sample (n = 654)	Mild CAS (n = 541)	Moderate CAS (n = 49)	Severe CAS (n = 64)
Age (years)	57 ± 10	57 ± 10	61 ± 7	60 ± 8
Sex, % men	81	82	74	84
History of stroke, %	22	16	28.6	70.3
BMI (kg/m ²)	27 ± 3	27 ± 4	26 ± 3	27 ± 3
Smoking, pack years ^a	22 (0, 49)	20 (0, 48)	12 (0, 72)	26 (0, 54)
Alcohol intake, % current	77	78	79	78
Hypertension, %	46.8	43.4	55.1	68.8
Diabetes mellitus, %	15	13.5	22.4	26.6
Large infarcts on MRI, %	10	6.1	6.1	20.8
Lacunae on MRI, %	17	14.2	12.2	46.9
Number of infarcts on MRI ^b				
Total	0.6 ± 1.3	0.4 ± 1.1	0.6 ± 1.2	2.0 ± 2.1
Left hemisphere	0.2 ± 0.7	0.2 ± 0.6	0.2 ± 0.6	0.8 ± 1.4
Right hemisphere	0.3 ± 0.8	0.2 ± 0.6	0.2 ± 0.7	1.1 ± 1.7
WMH volume on MRI, ml				
Total	2.2 ± 5.1	2.2 ± 5.3	2.3 ± 3.2	2.5 ± 3.4
Left hemisphere	1.1 ± 2.6	1.1 ± 2.6	1.2 ± 1.8	1.4 ± 2.5
Right hemisphere	1.1 ± 2.6	1.1 ± 2.7	1.1 ± 1.6	1.1 ± 1.5
Brain volumes, % ICV				
Total	79.4 ± 2.6	79.6 ± 2.5	78.7 ± 2.4	78.1 ± 2.7
Left hemisphere	78.8 ± 2.7	79.0 ± 2.6	78.1 ± 2.5	77.6 ± 2.9
Right hemisphere	79.9 ± 2.6	80.1 ± 2.6	79.1 ± 2.2	78.6 ± 2.7
CAS, n (%)				
Left-sided CAS				
Mild (≤29%)	580 (88)	-	-	-
Moderate (30% to 69%)	37 (6)	-	-	-
Severe (≥70%)	37 (6)	-	-	-
Right-sided CAS				
Mild (≤29%)	576 (88)	-	-	-
Moderate (30% to 69%)	35 (5)	-	-	-
Severe (≥70%)	43 (7)	-	-	-

Characteristics are presented as mean ± SD, n (%) or %.

ICV = intracranial volume; WMH = white matter hyperintensity; CAS = carotid artery stenosis

^a Median (10th percentile, 90th percentile).

^b Including large infarcts, lacunae, cerebellar infarcts, and brain stem infarct

For left-sided CAS, a severe stenosis was associated with a greater decrease in volume of the left hemisphere (B = -0.32 % ICV, 95% CI -0.71 to 0.06), however this estimate did not reach statistical significance and attenuated after additionally adjusting for the

abovementioned covariates (Table 2). No associations were observed between degrees of left-sided CAS and change in total or right-hemispheric volumes (Table 2).

Table 2. Associations between degrees of carotid artery stenosis according to sidedness and changes in total and hemispheric brain volumes after a median of 3.9 years of follow-up compared to mild ($\leq 29\%$) stenosis on the same side.

	Change in total brain volume (% ICV)		Change in brain volume left hemisphere (% ICV)		Change in brain volume right hemisphere (% ICV)	
	B	95% CI	B	95% CI	B	95% CI
Left-sided CAS						
Moderate (30% to 69%)						
Model 1	0.22	-0.11 to 0.55	0.32	-0.06 to 0.69	0.21	-0.16 to 0.59
Model 2	0.27	-0.07 to 0.61	0.32	-0.05 to 0.70	0.22	-0.16 to 0.60
Severe ($\geq 70\%$)						
Model 1	-0.14	-0.50 to 0.22	-0.32	-0.71 to 0.06	0.09	-0.30 to 0.49
Model 2	0.03	-0.33 to 0.40	-0.16	-0.55 to 0.23	0.27	-0.13 to 0.67
Right-sided CAS						
Moderate (30% to 69%)						
Model 1	-0.20	-0.55 to 0.14	-0.20	-0.58 to 0.18	-0.37	-0.76 to 0.02
Model 2	-0.30	-0.65 to 0.05	-0.22	-0.60 to 0.16	-0.38	-0.77 to 0.01
Severe ($\geq 70\%$)						
Model 1	-0.69	-1.02 to -0.37*	-0.49	-0.86 to -0.13*	-0.90	-1.27 to -0.54*
Model 2	-0.59	-0.93 to -0.25*	-0.36	-0.72 to 0.00	-0.78	-1.15 to -0.41*

Model 1: Adjusted for age, sex and baseline brain volumes. Model 2: model 1 with adjustment for hypertension, diabetes mellitus, body mass index, smoking pack years, alcohol use, number of infarcts on baseline and follow-up MRI, and white matter hyperintensity volume on baseline and follow-up MRI. ICV: intracranial volume; CI: confidence interval. CAS: carotid artery stenosis.

* $p < 0.05$

Repeating the analyses after exclusion of patients with large infarcts showed a similar pattern (Supplementary Table 1), with severe right-sided CAS being significantly associated with a greater decrease in brain volumes compared to mild right-sided CAS, most profoundly of the right hemispheric volume ($B = -1.19\%$ ICV, 95% CI -1.68 to -0.69).

Unilateral and bilateral severe CAS and brain volume changes

Consistent with the previous analysis, a severe unilateral right-sided CAS was associated with a greater decrease in total brain volume ($B = -0.72\%$ ICV, 95% CI -1.09 to -0.35) and more profoundly in the right hemispheric volume ($B = -0.97\%$ ICV, 95% CI -1.39 to -0.55), compared to mild to moderate CAS at both sides. These estimates attenuated but remained significant after adjusting for cerebrovascular risk factors, number of infarcts and WMH volume on baseline and follow-up MRI (Table 3). A severe unilateral right-sided

CAS was also associated with a greater decrease in left hemispheric volume, however this relationship lost significance after adjusting for the abovementioned covariates ($B = -0.27\%$ ICV, 95% CI -0.69 to 0.15; Table 3).

Compared to mild to moderate CAS at both sides, a severe unilateral left-sided CAS was associated with a greater decrease in volume of the left hemisphere ($B = -0.41\%$ ICV, 95% CI -0.88 to 0.04), however this relationship did not reach statistical significance and attenuated after adjusting for the abovementioned covariates (Table 3). No significant associations were observed between a severe unilateral left-sided CAS and decrease in total and right hemispheric brain volumes (Table 3).

Table 3. Associations between sidedness of $\geq 70\%$ carotid artery stenosis and changes in total and hemispheric brain volumes after a median of 3.9 years of follow-up compared to $< 70\%$ stenosis at both sides.

	Change in total brain volume (% ICV)		Change in brain volume left hemisphere (% ICV)		Change in brain volume right hemisphere (% ICV)	
	B	95% CI	B	95% CI	B	95% CI
Severe ($\geq 70\%$) unilateral left-sided CAS						
Model 1	-0.31	-0.73 to 0.11	-0.41	-0.88 to 0.04	-0.18	-0.64 to 0.29
Model 2	-0.10	-0.53 to 0.32	-0.20	-0.66 to 0.26	0.05	-0.42 to 0.52
Severe ($\geq 70\%$) unilateral right-sided CAS						
Model 1	-0.72	-1.09 to -0.35*	-0.45	-0.86 to -0.04*	-0.97	-1.39 to -0.55*
Model 2	-0.56	-0.95 to -0.17*	-0.27	-0.69 to 0.15	-0.80	-1.22 to -0.37*
Severe ($\geq 70\%$) bilateral CAS						
Model 1	-0.72	-1.20 to -0.25*	-0.81	-1.34 to -0.28*	-0.64	-1.17 to -0.10*
Model 2	-0.54	-1.04 to -0.05*	-0.60	-1.13 to -0.07*	-0.42	-0.96 to 0.12

Model 1: Adjusted for age, sex and baseline brain volumes. Model 2: model 1 with adjustment for hypertension, diabetes mellitus, body mass index, smoking pack years, alcohol use, number of infarcts on baseline and follow-up MRI, and white matter hyperintensity volume on baseline and follow-up MRI.

ICV: intracranial volume; CI: confidence interval. CAS: carotid artery stenosis.

Number of patients with $< 70\%$ CAS at both sides (reference): 590 (91%), $\geq 70\%$ unilateral left-sided CAS: 21 (3%), $\geq 70\%$ unilateral right-sided CAS: 27 (4%), $\geq 70\%$ bilateral CAS: 16 (2%).

* $p < 0.05$

Severe bilateral CAS, compared to mild to moderate CAS at both sides, was significantly associated with a greater decrease in total brain volume ($B = -0.72\%$ ICV, 95% CI -1.20 to -0.25), right hemispheric volume ($B = -0.64\%$ ICV, 95% CI -1.17 to -0.10), and more profoundly in left hemispheric volume ($B = -0.81\%$ ICV, 95% CI -1.34 to -0.28).

These estimates slightly attenuated after additionally adjusting for the abovementioned covariates (Table 3).

Supplementary analysis

Change in right hemispheric brain volume differed significantly among degrees of right-sided CAS (ANCOVA $p=0.002$). Consistent with the primary analysis, moderate and severe right-sided CAS were associated with a greater decrease in right hemispheric volume (mean difference -0.29% ICV, 95% CI -0.66 to 0.08 ; -0.74% ICV, 95% CI -1.18 to -0.30 , respectively) compared to mild right-sided CAS, adjusting for demographics, cerebrovascular risk factors, and number of infarcts and WMH volume in the right hemisphere on baseline and follow MRI (Supplemental Table 2).

Change in left hemispheric brain volume did not differ significantly among degrees of left-sided CAS (ANCOVA $p=0.36$). Similarly, change in left hemispheric brain volume did not differ between degrees of right-sided CAS (ANCOVA $p=0.19$), and change in right hemispheric brain volume did not differ significantly between degrees of left-sided CAS (ANCOVA $p=0.88$).

Discussion

In this cohort of patients with manifest arterial disease, we found that severe right-sided carotid artery stenosis (CAS) was associated with a greater decrease in right hemispheric brain volume over 4 years of follow-up. This relationship was independent of age, sex, cerebrovascular risk factors, brain infarcts and WMH on baseline and follow-up MRI. A severe left-sided CAS, however, was not associated with a greater decrease of left hemispheric volume.

As noted in the introductory section, several hypotheses have been formulated that may explain the relation between CAS and progression of brain atrophy. First, brain infarcts may mediate the association between carotid atherosclerosis and brain atrophy[22]. Second, it has been hypothesized that carotid atherosclerosis may represent a proxy marker for cerebrovascular risk factors that result in both carotid atheroma formation and progression of brain atrophy[9]. Third, CAS may lead to reduced cerebral blood flow that, if not adequately compensated for by collateral circulation, may result in greater brain atrophy [11]. Until now, however, no previous studies to our knowledge reported on the association of CAS with progression of ipsilateral and contralateral brain atrophy. The findings of the present study suggest that severe CAS could represent a risk factor for greater tissue loss of the ipsilateral cerebral hemisphere. Our observation that this relationship was largely independent of brain infarcts and WMH on MRI suggests that mechanisms other than ischemic cerebrovascular disease may underlie the relation between CAS and brain atrophy. Given the novelty of our findings, however, further

longitudinal studies in other cohorts are needed to replicate the present association and to further investigate the exact underlying mechanisms.

As noted previously, a limited number of cross-sectional studies examined the association between CAS and hemispheric brain volumes[12-15]. A study in patients with $\geq 70\%$ unilateral CAS reported smaller hemispheric brain volumes ipsilateral to the side of CAS but only in patients with moderate or severe WMH[13]. In our study, however, we observed that the association between severe right-sided CAS and right hemispheric atrophy was independent of WMH volume on baseline and follow-up MRI. In two studies comparing regional brain volumes between patients with $\geq 70\%$ unilateral CAS and healthy controls, it was found that patients with $\geq 70\%$ CAS showed smaller cortical gray matter volumes ipsilateral to the side of stenosis[14, 15]. Similarly, a study comparing cortical thickness in patients with $\geq 80\%$ unilateral CAS reported smaller cortical gray matter volumes on the side of stenosis[12].

Our study has several limitations. First, we observed that some estimates, in particular those reflecting change between mild and moderate left-sided CAS, were positive (i.e., suggesting an increase in brain volume over time). Although none of these estimates were statistically significant, an underlying technical measurement error cannot be excluded. Second, the present study had a relatively short follow-up period and a relatively small number of patients with a severe CAS, which may have led to reduced statistical power to detect small differences in brain volume change. Third, we did not adjust the analyses for multiple comparisons. Fourth, the volumetric technique that we used did not allow us to measure region-specific brain volume changes. We therefore could not determine whether brain atrophy was due to volume loss of the gray matter, white matter or both.

Strengths of our study are the longitudinal design, the use of a large cohort of patients with varying degrees of CAS and volumetric assessment of total and hemispheric brain volumes. In addition, the data on cardiovascular risk factors and cerebrovascular lesions allowed us to determine whether the association between CAS and ipsilateral hemispheric brain atrophy was independent of potential confounders.

In conclusion, our findings indicate that severe ($\geq 70\%$) CAS could represent a risk factor for greater ipsilateral brain volume loss in patients with manifest arterial disease, independent of cerebrovascular risk factors, brain infarcts or WMH on MRI. Further longitudinal studies in other cohorts are needed to confirm this novel finding.

References

1. Resnick SM, Pham DL, Kraut MA, et al. Longitudinal magnetic resonance imaging studies of older adults: a shrinking brain. *J Neurosci* 2003; 23: 3295-3301.
2. Geerlings MI, Appelman AP, Vincken KL, et al. Brain volumes and cerebrovascular lesions on MRI in patients with atherosclerotic disease. The SMART-MR study. *Atherosclerosis* 2010; 210: 130-136.
3. Kramer JH, Mungas D, Reed BR, et al. Longitudinal MRI and cognitive change in healthy elderly. *Neuropsychology* 2007; 21: 412-418.
4. Jack CR, Jr., Shiung MM, Weigand SD, et al. Brain atrophy rates predict subsequent clinical conversion in normal elderly and amnesic MCI. *Neurology* 2005; 65: 1227-1231.
5. Jack CR, Jr., Shiung MM, Gunter JL, et al. Comparison of different MRI brain atrophy rate measures with clinical disease progression in AD. *Neurology* 2004; 62: 591-600.
6. van der Veen PH, Muller M, Vincken KL, et al. Longitudinal changes in brain volumes and cerebrovascular lesions on MRI in patients with manifest arterial disease: the SMART-MR study. *J Neurol Sci* 2014; 337: 112-118.
7. Ghaznawi R, Zwartbol MH, Zuithoff NP, et al. Reduced parenchymal cerebral blood flow is associated with greater progression of brain atrophy: The SMART-MR study. *J Cereb Blood Flow Metab* 2020: 271678x20948614.
8. Muller M, van der Graaf Y, Algra A, et al. Carotid atherosclerosis and progression of brain atrophy: the SMART-MR study. *Ann Neurol* 2011; 70: 237-244.
9. Alhusaini S, Karama S, Nguyen TV, et al. Association between carotid atheroma and cerebral cortex structure at age 73 years. *Ann Neurol* 2018; 84: 576-587.
10. Walters RJ, Fox NC, Schott JM, et al. Transient ischaemic attacks are associated with increased rates of global cerebral atrophy. *J Neurol Neurosurg Psychiatry* 2003; 74: 213-216.
11. Alosco ML, Gunstad J, Jerskey BA, et al. The adverse effects of reduced cerebral perfusion on cognition and brain structure in older adults with cardiovascular disease. *Brain Behav* 2013; 3: 626-636.
12. Marshall RS, Asllani I, Pavol MA, et al. Altered cerebral hemodynamics and cortical thinning in asymptomatic carotid artery stenosis. *PLoS One* 2017; 12: e0189727.
13. Enzinger C, Ropele S, Gatttringer T, et al. High-grade internal carotid artery stenosis and chronic brain damage: a volumetric magnetic resonance imaging study. *Cerebrovasc Dis* 2010; 30: 540-546.
14. Asllani I, Slattery P, Fafard A, et al. Measurement of cortical thickness asymmetry in carotid occlusive disease. *Neuroimage Clin* 2016; 12: 640-644.
15. Avelar WM, D'Abreu A, Coan AC, et al. Asymptomatic carotid stenosis is associated with gray and white matter damage. *Int J Stroke* 2015; 10: 1197-1203.
16. Goessens BM, Visseren FL, Kappelle LJ, et al. Asymptomatic carotid artery stenosis and the risk of new vascular events in patients with manifest arterial disease: the SMART study. *Stroke* 2007; 38: 1470-1475.

17. Wardlaw JM, Smith EE, Biessels GJ, et al. Neuroimaging standards for research into small vessel disease and its contribution to ageing and neurodegeneration. *Lancet Neurol* 2013; 12: 822-838.
18. Anbeek P, Vincken KL, van Bochove GS, et al. Probabilistic segmentation of brain tissue in MR imaging. *Neuroimage* 2005; 27: 795-804.
19. de Boer R, Vrooman HA, Ikram MA, et al. Accuracy and reproducibility study of automatic MRI brain tissue segmentation methods. *Neuroimage* 2010; 51: 1047-1056.
20. Ghaznawi R, Geerlings MI, Jaarsma-Coes M, et al. Association of White Matter Hyperintensity Markers on MRI and Long-term Risk of Mortality and Ischemic Stroke: The SMART-MR Study. *Neurology* 2021; 96: e2172-e2183.
21. Kuijf HJ, van Veluw SJ, Geerlings MI, et al. Automatic extraction of the midsagittal surface from brain MR Images using the Kullback-Leibler measure. *Neuroinformatics* 2014; 12: 395-403.
22. Manolio TA, Burke GL, O'Leary DH, et al. Relationships of cerebral MRI findings to ultrasonographic carotid atherosclerosis in older adults : the Cardiovascular Health Study. CHS Collaborative Research Group. *Arterioscler Thromb Vasc Biol* 1999; 19: 356-365.

Supplemental Table 1. Associations between degrees of carotid artery stenosis according to sidedness and changes in total and hemispheric brain volumes after a median of 3.9 years of follow-up compared to mild $\leq 29\%$ stenosis on the same side in patients without large brain infarcts (n = 572).

	Change in total brain volume (% ICV)		Change in brain volume left hemisphere (% ICV)		Change in brain volume right hemisphere (% ICV)	
	B ^a	95% CI	B ^a	95% CI	B ^a	95% CI
Left-sided CAS						
Moderate (30% to 69%)	0.12	-0.05 to 0.41	0.22	-0.07 to 0.37	0.13	-0.29 to 0.54
Severe ($\geq 70\%$)	0.17	-0.22 to 0.54	0.07	-0.47 to 0.59	0.19	-0.33 to 0.62
Right-sided CAS						
Moderate (30% to 69%)	-0.31	-0.68 to 0.05	-0.21	-0.61 to 0.19	-0.41	-0.81 to -0.01*
Severe ($\geq 70\%$)	-1.01	-1.47 to -0.56*	-0.81	-1.30 to -0.31*	-1.19	-1.68 to -0.69*

^a Adjusted for baseline brain volumes, age, sex, hypertension, diabetes mellitus, body mass index, smoking pack years, alcohol use, number of infarcts (lacunar, cerebellum and brainstem) on baseline and follow-up MRI, and white matter hyperintensity volume on baseline and follow-up MRI.

Number of patients with mild $\leq 29\%$ left-sided CAS: 524 (91%), moderate (30% to 69%) left-sided CAS: 26 (5%), severe ($\geq 70\%$) left-sided CAS: 25 (4%), mild $\leq 29\%$ right-sided CAS: 524 (91%), moderate (30% to 69%) right-sided CAS: 30 (5%), severe ($\geq 70\%$) right-sided CAS: 35 (6%).

ICV: intracranial volume; CI: confidence interval. CAS: carotid artery stenosis.

* $p < 0.05$

Supplemental Table 2. Association between degrees of carotid artery stenosis according to sidedness and change in hemispheric brain volumes after a median of 3.9 years of follow-up compared to mild ($\leq 29\%$) stenosis on the same side. Patients with severe ($\geq 70\%$) bilateral stenosis ($n=16$) were excluded from the analyses.

	Change in brain volume left hemisphere (% ICV)		Change in brain volume right hemisphere (% ICV)	
	B ^a	95% CI	B ^a	95% CI
Left-sided CAS				
Moderate (30% to 69%)	0.26	-0.10 to 0.62	0.04	-0.54 to 0.62
Severe ($\geq 70\%$)	-0.01	-0.48 to 0.46	-0.00	-0.48 to 0.47
Right-sided CAS				
Moderate (30% to 69%)	-0.19	-0.55 to 0.18	-0.29	-0.66 to 0.08
Severe ($\geq 70\%$)	-0.33	-0.74 to 0.08	-0.74	-1.18 to -0.30*

^a Adjusted for age, sex, baseline brain volumes, hypertension, diabetes mellitus, body mass index, smoking pack years, alcohol use, and number of infarcts and white matter hyperintensity volume on baseline and follow-up MRI in the cerebral hemisphere ipsilateral to the side of stenosis. ICV: intracranial volume; CI: confidence interval. CAS: carotid artery stenosis.

* $p < 0.05$

CHAPTER 9



Reduced parenchymal cerebral blood flow is associated with greater progression of brain atrophy. The SMART-MR study

Rashid Ghaznawi ^{1,2}, Maarten H.T. Zwartbol ¹, Nicolaas P.A. Zuithoff ², Jeroen de Bresser ³, Jeroen Hendrikse ¹, Mirjam I. Geerlings ²; on behalf of the UCC-SMART Study Group

¹Department of Radiology, University Medical Center Utrecht, Netherlands;

²Julius Center for Health Sciences and Primary Care, University Medical Center Utrecht, Netherlands; ³Department of Radiology, Leiden University Medical Center, Netherlands

Global cerebral hypoperfusion may be involved in the etiology of brain atrophy, however long-term longitudinal studies on this relationship are lacking. We examined whether reduced cerebral blood flow was associated with greater progression of brain atrophy. Data was used of 1165 patients (61 ± 10 years) from the SMART-MR study, a prospective cohort study of patients with arterial disease, of whom 689 participated after 4 years and 297 again after 12 years. Attrition was substantial. Total brain volume and total cerebral blood flow were obtained from MRI scans and expressed as brain parenchymal fraction (BPF) and parenchymal cerebral blood flow (pCBF). Mean decrease in BPF per year was 0.22 % total intracranial volume (95% CI: -0.23 to -0.21). Mean decrease in pCBF per year was 0.24 ml/min per 100 ml brain volume (95% CI: -0.29 to -0.20). Using linear mixed models, lower pCBF at baseline was associated with a greater decrease in BPF over time ($p=0.01$). Lower baseline BPF, however, was not associated with a greater decrease in pCBF ($p=0.43$). These findings indicate that reduced cerebral blood flow is associated with greater progression of brain atrophy and provide further support for a role of cerebral blood flow in the process of neurodegeneration.

Introduction

Brain atrophy is a common finding on magnetic resonance imaging (MRI) in older individuals and individuals with manifest arterial disease.¹⁻³ Although brain atrophy occurs with normal ageing, previous studies have demonstrated that accelerated brain atrophy is associated with cognitive decline and dementia.⁴⁻⁸ The underlying causes that can lead to progression of brain atrophy, however, remain largely unknown.⁹

Reduced cerebral blood flow has been postulated as a possible risk factor for brain tissue loss.^{2, 10-13} In physiological conditions, cerebral blood flow is regulated by the cerebral vasculature in order to maintain an adequate delivery of oxygen and nutrients to the brain.¹⁴ Failure of these mechanisms can lead to a reduced cerebral blood flow, which has been associated with mortality and an increased risk of dementia in large cohort studies.^{15, 16} Whether these relationships are mediated by progression of brain atrophy is not known as few studies have reported on the relationship between cerebral blood flow and brain atrophy.^{2, 10-12} In addition, there is some evidence to suggest that the relationship between cerebral blood flow and brain atrophy may be bidirectional, such that smaller brain volumes are a risk factor for greater decline in cerebral blood flow.¹¹ Examining the long-term longitudinal relationship between cerebral blood flow and brain atrophy is of importance as cerebral blood flow can be modified and may pose a potential target for future prevention strategies of brain atrophy and dementia.¹⁷⁻¹⁹

In the current study, we examined the longitudinal relationship between cerebral blood flow and brain atrophy in a large cohort of patients with manifest arterial disease over 12 years of follow-up.

Methods

Study population

Data were used from the Second Manifestations of ARterial disease-Magnetic Resonance (SMART-MR) study, a prospective cohort study at the University Medical Center Utrecht with the aim to investigate risk factors and consequences of brain changes on MRI in patients with symptomatic arterial disease.²⁰ Between 2001 and 2005, 1309 middle-aged and older adult individuals newly referred to the University Medical Center Utrecht for treatment of symptomatic atherosclerotic disease (manifest coronary artery disease (59%), cerebrovascular disease (23%), peripheral arterial disease (22%) or abdominal aortic aneurysm (9%)) were included for baseline measurements, including a 1.5T brain MRI. Presence of neurodegenerative disease was not considered an exclusion criterion. Of these, 754 persons had follow-up measurements four years later between January 2006 and May 2009. During a one day visit to our medical center, a physical examination, ultrasonography of the carotid arteries to measure the intima-media thickness (mm),

blood and urine samplings, neuropsychological assessment and a 1.5T brain MRI scan were performed. The height and weight were measured, and the body mass index (kg/m^2) was calculated. Questionnaires were used for the assessment of demographics, risk factors, medical history, medication use and cognitive and physical functioning. Since November 2013, all patients alive were invited for a second follow-up, including a 1.5T brain MRI, of which 329 persons had second follow-up measurements between November 2013 and October 2017. A flowchart of the SMART-MR study is shown in Figure 1.

The SMART-MR study was approved by the medical ethics committee of the University Medical Center Utrecht according to the guidelines of the Declaration of Helsinki of 1975 and written informed consent was obtained from all patients.

Vascular risk factors

At baseline, age, sex, smoking habits and alcohol intake were assessed with questionnaires. Height and weight were measured, and the body mass index (BMI) was calculated (kg/m^2). Systolic blood pressure (SBP) (mmHg) and diastolic blood pressure (DBP) (mmHg) were measured three times with a sphygmomanometer, and the average of these measures was calculated. Hypertension was defined as a mean SBP of >160 mmHg, a mean DBP of >95 mmHg or self-reported use of antihypertensive drugs. An overnight fasting venous blood sample was taken to determine glucose and lipids. Diabetes mellitus was defined as fasting serum glucose levels of ≥ 7.0 mmol/l, and/or use of glucose-lowering medication, and/or a known history of diabetes. Ultrasonography was performed with a 10MHz linear-array transducer (ATL Ultramark 9) and the degree of the carotid artery stenosis at both sides was assessed with color Doppler-assisted duplex scanning. The severity of carotid artery stenosis was evaluated on the basis of blood flow velocity patterns and the greatest stenosis observed on the right or the left side of the common or internal carotid artery was taken to determine the severity of carotid artery disease. Carotid artery stenosis $\geq 70\%$ was defined as peak systolic velocity >210 cm/s.²¹

MRI protocol

MR imaging of the brain was performed on a 1.5T whole-body system (Gyrosan ACS-NT, Philips Medical Systems, Best, the Netherlands) using a standardized scan protocol.²⁰ Transversal T1-weighted [repetition time (TR) = 235 ms; echo time (TE) = 2 ms], T2-weighted [TR = 2200 ms; TE = 11 ms], fluid-attenuated inversion recovery (FLAIR) [TR = 6000 ms; TE = 100 ms; inversion time (TI) = 2000 ms] and T1-weighted inversion recovery images [TR = 2900 ms; TE = 22 ms; TI = 410 ms] were acquired with a voxel size of $1.0 \times 1.0 \times 4.0$ mm³ and contiguous slices. For cerebral blood flow measurements, a 2-dimensional phase-contrast section was positioned at the level of the skull base to measure the volume flow in the basilar artery and in the internal carotid arteries on the basis of a localizer MR angiographic slab in the sagittal plane.²² The 2-dimensional phase-contrast section

was positioned through the basilar artery and the internal carotid arteries (TR/TE, 16/9 milliseconds; flip angle 7.5°; FOV 250 x 250 mm; matrix size 256 x 256; slice thickness 5.0 mm; 8 acquired signals; velocity sensitivity 100 cm/s).

Cerebral blood flow measurements

Phase-contrast MR angiography was used to measure total cerebral blood flow, as this method has been demonstrated to be a fast, reproducible, and noninvasive method to measure total cerebral blood flow in large cohorts.^{23,24} Previous studies established that phase-contrast MR angiography correlates well with arterial spin-labeled perfusion MRI, although estimates tend to be somewhat higher and more variable than arterial spin-labeled perfusion MRI.²⁵ Post processing of the flow measurements was performed by investigators blinded to patient characteristics. The flow through the basilar and internal carotid arteries was summed to calculate the total cerebral blood flow. Total cerebral blood flow was expressed per 100 ml brain parenchymal volume to obtain parenchymal cerebral blood flow (pCBF).¹⁶ Parenchymal CBF was measured at baseline, and at the first and second follow-up visits.

Brain volume measurements

White matter hyperintensity (WMH) volumes and brain volumes were obtained using the *k*-nearest neighbor (kNN) automated segmentation program on the T1-weighted, FLAIR, and T1-weighted inversion recovery sequences of the MRI scans.²⁶ The kNN segmentation method has been shown to be suitable for detecting longitudinal brain volume changes.^{20,27} All WMH segmentations were visually checked by an investigator (RG) using an image processing framework (MeVisLab 2.7.1., MeVis Medical Solutions AG, Bremen, Germany) to ensure that brain infarcts were correctly removed from the WMH segmentations. Incorrectly segmented voxels were added to the correct segmentation volumes using the image processing framework. Periventricular WMH were defined as lesions ≤ 1 cm of the lateral ventricles and deep WMH were defined as lesions that were located >1 cm of the lateral ventricles. Total brain volume was calculated by summing the volumes of gray matter, white matter, total WMH and, if present, the volumes of brain infarcts. Total intracranial volume (ICV) was calculated by summing the total brain volume and the volume of the cerebrospinal fluid. Total brain volume was normalized for ICV and expressed as brain parenchymal fraction (BPF). Brain volumes were measured at baseline, and at the first and second follow-up visits.

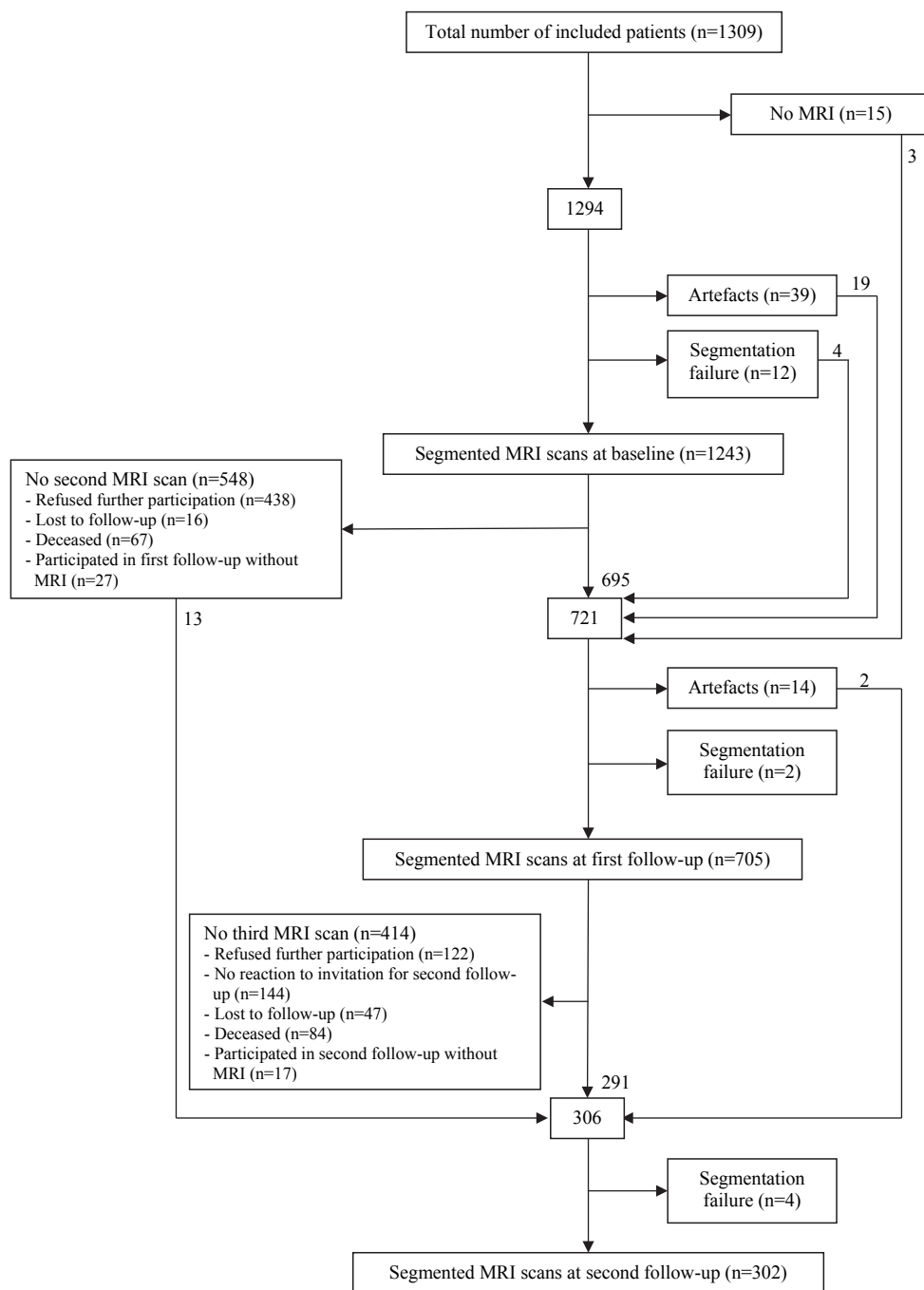


Figure 1. MRI participation flowchart of the SMART-MR study. Numbers in the boxes represent the numbers of patients who underwent a 1.5T MRI at each time point.

Brain infarcts

Brain infarcts were visually rated by a neuroradiologist blinded to patient characteristics on the T1-weighted, T2-weighted and FLAIR images of the MRI scans. Lacunes were defined as focal lesions between 3 to 15 mm according to the STRIVE criteria²⁸, whereas non-lacunar lesions were divided into large infarcts (i.e. cortical infarcts and subcortical infarcts not involving the cerebral cortex) and those located in the cerebellum or brain stem.

Study sample

At baseline, 1165 patients had both pCBF and BPF measurements, whereas this was the case for 689 and 297 patients at the first and second follow-up, respectively. The study sample included patients with consecutive and non-consecutive pCBF and/or BPF measurements.

Statistical analysis

Baseline characteristics of patients with BPF and pCBF measurements at baseline ($n = 1165$) were reported as means or percentages where applicable. Baseline characteristics of patients with follow-up measurements and those without were compared using an independent samples t -test and Chi square test for continuous and dichotomous variables, respectively.

Linear mixed models were used to analyze change in BPF and change in pCBF over time.^{29, 30} As the time intervals between MRI measurements differed between patients, the age of patients at the MRI measurements was chosen as the time variable. Age was centered on 61 years, the mean value at which the first MRI measurement was performed. BPF and pCBF were analyzed per standard deviation decrease. To minimize the risk of bias due to complete case analysis, chained equations imputation was performed on missing covariates to generate 10 imputed datasets using SPSS 25.0 (Chicago, IL, USA).³¹ The statistical analyses were performed on these datasets and pooled results were presented. In chained equations imputation, linear and logistic regression is used to impute continuous and categorical covariates, respectively, using other covariates as predictors.³¹

First, we modeled longitudinal measurements of BPF (dependent variable) with pCBF as time-varying predictor, with age at time of MRI as the time-scale and adjusted for baseline age and sex. In a second model, we additionally adjusted for large infarcts, lacunes and WMH volume on MRI, diastolic blood pressure, hypertension, carotid stenosis $\geq 70\%$, body mass index and smoking pack years at baseline. To determine whether baseline pCBF was a risk factor for subsequent BPF decline, we modeled change in BPF with baseline pCBF. Baseline pCBF, time, baseline age, sex and the interaction between baseline pCBF and time were entered in a model. Next, we additionally adjusted for large infarcts, lacunes and WMH volume on MRI, hypertension, diabetes mellitus, carotid stenosis $\geq 70\%$, body mass index and smoking pack years at baseline.

Second, we modeled longitudinal measurements of pCBF (dependent variable) with BPF as time-varying predictor with age at time of MRI as the time-scale and adjusted for baseline age and sex. In a second model, we additionally adjusted for large infarcts, lacunes and WMH volume on MRI, hypertension, diabetes mellitus, carotid stenosis $\geq 70\%$, body mass index and smoking pack years at baseline. To determine whether baseline BPF was a risk factor for subsequent pCBF decline, we modeled change in pCBF with baseline BPF. Next, we additionally adjusted for large infarcts, lacunes and WMH volume on MRI, hypertension, diabetes mellitus, carotid stenosis $\geq 70\%$, body mass index and smoking pack years at baseline.

In all models, a random intercept and random slope with time was assumed, meaning that the models accounted for individual variation in the starting level of BPF or pCBF (intercept) and in change of BPF or pCBF over time (slope), respectively. Adequacy of all models was determined by examining the residuals for homoscedasticity and normality.³² We concluded that model assumptions were adequately met. Statistical significance was set at $p \leq 0.05$. Due to the exploratory nature of the analyses, no adjustment of p values was made for multiple comparison. SAS 9.4 (SAS Institute, Cary, NC, USA) and SPSS 25.0 (Chicago, IL, USA) were used to perform the statistical analyses.

As sensitivity analyses, we assumed a fixed slope with time and repeated the analyses with baseline pCBF as predictor and change in BPF as outcome, and with baseline BPF as predictor and change in pCBF as outcome. In addition, to examine whether multiple imputation affected the results, we repeated the analyses in patients without missing data (i.e. complete case analysis). Lastly, to examine the effect of attrition on the results of the longitudinal analyses, we hypothesized that dropout due to death may represent a form of informative dropout. We examined the effect of dropout due to death on the results of the linear mixed models using a joint modelling approach that includes a time-to-event submodel.³³ For the time-to-event submodel, data on occurrence of death and survival times was obtained from questionnaires that patients received biannually. Acquisition of data relating to occurrence of death and survival times is described in detail elsewhere.³⁴ The JM package for R version 3.6.3 (R Core Team, 2019) was used to perform the joint model analysis.³³

Results

Baseline characteristics of the study sample ($n = 1165$) are shown in Table 1. The mean age at baseline was 61 ± 10 years and 80% was male. Mean pCBF was 51.4 ± 10.6 ml/min per 100 ml brain volume.

Mean time between baseline and first follow-up measurements for patients with available pCBF and BPF data ($n = 689$) was 3.9 ± 0.4 years (range 2.9 – 5.8 years). Mean time between the first follow-up and second follow-up measurements for patients with

available pCBF and BPF data ($n = 297$) was 8.2 ± 0.4 years (range 7.3 – 9.5 years). Mean time between baseline and the second follow-up measurements was 12.0 ± 0.4 years (range 11.1 – 13.5 years) for patients with available pCBF and BPF data on the second follow-up ($n = 297$). Mean decrease in BPF per year for the study sample was 0.22 % ICV (95% CI: -0.23 to -0.21). Mean decrease in pCBF per year was 0.24 ml/min per 100 ml brain volume (95% CI: -0.29 to -0.20).

Table 1. Characteristics of the study population with available pCBF and BPF data at baseline ($n = 1165$).

Age (years)	61 ± 10
Sex, % men	80.3
History of stroke, %	23.3
BMI (kg/m ²)	27 ± 4
Smoking, pack years ^a	19 (0, 50)
Alcohol use, %	
Current	75.0
Former	8.7
Never	16.3
Hypertension, %	50.9
Diabetes mellitus, %	20.6
Carotid artery stenosis ≥70%, %	10.6
Infarcts on MRI, %	
Large	12.2
Cerebellar	4.0
Brainstem	2.9
Lacunae on MRI, %	18.5
WMH volumes on MRI, ml ^a	
Total	0.9 (0.2, 6.5)
Periventricular	0.6 (0.1, 4.2)
Deep	0.3 (0.0, 2.5)
BPF, % ICV	79.0 ± 2.9
pCBF, ml/min per 100 ml brain volume	51.4 ± 10.6

Characteristics are presented as mean ± SD or %.

BMI: body mass index; SD: standard deviation;

WMH: white matter hyperintensity; BPF: brain parenchymal fraction;

ICV: total intracranial volume; pCBF: parenchymal cerebral blood flow.

^a Median (10th percentile, 90th percentile).

Patients with follow-up measurements ($n = 754$) were younger ($p < 0.001$), more often male ($p = 0.011$), had more often current alcohol use ($p = 0.001$), had less often hypertension ($p = 0.001$), diabetes mellitus ($p < 0.001$) and carotid artery stenosis ≥70% ($p = 0.04$), and had a greater BPF ($p < 0.001$) and smaller WMH volumes on MRI ($p < 0.001$) compared to patients without follow-up measurements ($n = 555$) (Table 2).

Time-varying pCBF as a predictor of time-varying BPF

Lower pCBF was associated with lower BPF at baseline and follow-up, adjusted for age and sex. Specifically, each standard deviation decrease in pCBF at a given time point was associated with an additional 0.10 % ICV lower BPF at that given time point (95% CI: -0.17 to -0.04, $p = 0.001$). This relationship remained statistically significant after adjusting for large infarcts, lacunes and WMH volume on MRI, hypertension, diabetes mellitus, carotid stenosis $\geq 70\%$, body mass index, alcohol use and smoking pack years at baseline ($B = -0.09$ % ICV, 95% CI: -0.15 to -0.03, $p = 0.005$).

Table 2. Baseline characteristics of the study population ($n = 1309$) according to participation in follow-up visits.

	Patients with one or two follow-up visits ($n = 754$)	Patients without follow-up visits ($n = 555$)	p value
Age (years)	58 ± 9	60 ± 11	<0.001
Sex, % men	82.1	76.4	0.011
History of stroke, %	23.7	22.2	0.503
BMI (kg/m^2)	27 ± 4	27 ± 4	0.568
Smoking, pack years ^a	20 (0, 49)	17 (0, 53)	0.253 ^b
Alcohol use, % current	79	70	0.001
Hypertension, %	47.9	57.3	0.001
Diabetes mellitus, %	16.3	27.1	<0.001
Carotid artery stenosis $\geq 70\%$, %	9.6	13.3	0.04
Infarcts on MRI, %			
Large	11.3	14.0	0.152
Cerebellar	3.8	4.5	0.528
Brainstem	2.7	3.2	0.490
Lacunes on MRI, %	17.3	20.7	0.117
WMH volumes on MRI, ml ^a			
Total	0.8 (0.2, 4.8)	1.1 (0.3, 8.8)	<0.001 ^b
Periventricular	0.5 (0.1, 3.0)	0.8 (0.1, 5.7)	<0.001 ^b
Deep	0.2 (0.0, 2.1)	0.3 (0.0, 3.6)	<0.001 ^b
BPF, % ICV	79.3 ± 2.6	78.5 ± 3.2	<0.001
pCBF, ml/min per 100 ml brain volume	51.6 ± 10.4	51.0 ± 10.9	0.336

Characteristics are presented as mean \pm SD or %.

BMI: body mass index; SD: standard deviation; WMH: white matter hyperintensity; BPF: brain parenchymal fraction; ICV: total intracranial volume; pCBF: parenchymal cerebral blood flow.

^aMedian (10th percentile, 90th percentile).

^bNatural log-transformed due to a non-normal distribution in the statistical analysis.

Baseline pCBF as a predictor of longitudinal BPF

Adjusted for age and sex, lower baseline pCBF was associated with greater subsequent decreases in BPF. Specifically, each standard deviation decrease in baseline pCBF was

associated with an additional 0.01 % ICV decrease per year in BPF (95% CI: -0.02 to -0.004, $p = 0.004$) (Table 3). This relationship remained statistically significant after adjusting for large infarcts, lacunes and WMH volume on MRI, hypertension, diabetes mellitus, carotid stenosis $\geq 70\%$, body mass index, alcohol use and smoking pack years at baseline ($B = -0.01$ % ICV, 95% CI: -0.02 to -0.003, $p = 0.010$).

Table 3. Results of the linear mixed model with BPF as dependent variable and baseline pCBF as independent variable. Estimates represent fixed effects of the linear mixed model with their 95% confidence intervals for a 1 unit increase of a continuous variable or presence of a dichotomous variable unless stated otherwise.

	Model 1		Model 2	
	Estimate (95% CI)	<i>p</i> value	Estimate (95% CI)	<i>p</i> value
Intercept	78.50 (78.35 to 78.64)	<0.001	78.61 (77.71 to 79.51)	<0.001
Baseline pCBF ^a	-0.19 (-0.32 to -0.07)	0.002	-0.12 (-0.24 to 0.00)	0.051
Rate of change				
Time ^b	-0.24 (-0.25 to -0.22)	<0.001	-0.23 (-0.25 to -0.22)	<0.001
Time x baseline pCBF	-0.01 (-0.02 to -0.004)	0.004	-0.01 (-0.02 to -0.003)	0.010
Age ^b	-0.04 (-0.06 to -0.03)	<0.001	-0.05 (-0.07 to -0.04)	<0.001
Sex ^c	0.90 (0.59 to 1.21)	<0.001	0.86 (0.55 to 1.17)	<0.001
Large infarcts on MRI	-		-0.61 (-1.00 to -0.20)	0.003
Lacunes on MRI	-		-0.60 (-0.94 to -0.26)	<0.001
WMH volume on MRI ^d	-		-0.01 (-0.11 to 0.09)	0.836
Hypertension	-		-0.19 (-0.43 to 0.05)	0.117
Diabetes mellitus	-		-1.05 (-1.35 to -0.74)	<0.001
Carotid stenosis $\geq 70\%$	-		-0.17 (-0.61 to 0.27)	0.460
Body mass index	-		0.03 (-0.01 to 0.06)	0.109
Smoking pack years	-		-0.01 (-0.02 to -0.01)	<0.001
Alcohol use				
Current	-		0 (reference)	-
Former	-		-0.41 (-0.84 to 0.01)	0.056
Never	-		0.06 (-0.28 to 0.40)	0.728

Model 1: adjusted for age and sex.

Model 2: additionally adjusted for large infarcts on MRI, lacunes on MRI, WMH volume on MRI, hypertension, diabetes mellitus, carotid stenosis $\geq 70\%$, body mass index, alcohol use and smoking pack years at baseline.

ICC model 1: 0.87. ICC model 2: 0.86. Marginal R² Model 1: 0.48. Conditional R² Model 1: 0.94. Marginal R² Model 2: 0.53. Conditional R² Model 2: 0.94.

^a Per standard deviation decrease.

^b Per year increase.

^c Females vs. males.

^d Natural log-transformed due to a non-normal distribution and normalized for total intracranial volume. BPF: brain parenchymal fraction, pCBF: parenchymal cerebral blood flow, CI: confidence interval, WMH: white matter hyperintensity.

Table 4. Results of the linear mixed model with pCBF as dependent variable and baseline BPF as independent variable. Estimates represent fixed effects of the linear mixed model with their 95% confidence intervals for a 1 unit increase of a continuous variable or presence of a dichotomous variable unless stated otherwise.

	Model 1		Model 2	
	Estimate (95% CI)	<i>p</i> value	Estimate (95% CI)	<i>p</i> value
Intercept	50.31 (49.57 to 51.06)	<0.001	51.56 (47.46 to 55.67)	<0.001
Baseline BPF ^a	-0.48 (-1.20 to 0.37)	0.185	-0.06 (-0.80 to 0.67)	0.868
Rate of change				
Time ^b	-0.35 (-0.45 to -0.26)	<0.001	-0.36 (-0.45 to -0.27)	<0.001
Time x baseline BPF	0.02 (-0.03 to 0.07)	0.439	0.02 (-0.03 to 0.07)	0.429
Age ^b	-0.18 (-0.30 to -0.07)	<0.001	-0.22 (-0.34 to -0.11)	<0.001
Sex ^c	3.56 (2.22 to 4.89)	<0.001	4.17 (2.78 to 5.55)	<0.001
Large infarcts on MRI	-		-1.40 (-3.17 to 0.37)	0.121
Lacunae on MRI	-		0.68 (-0.81 to 2.17)	0.371
WMH volume on MRI ^d	-		-0.50 (-0.97 to -0.04)	0.034
Hypertension	-		-1.32 (-2.39 to -0.24)	0.016
Diabetes mellitus	-		-0.36 (-1.74 to 1.02)	0.609
Carotid stenosis ≥70%	-		-4.98 (-6.88 to -3.08)	<0.001
Body mass index	-		-0.06 (-0.21 to 0.08)	0.410
Smoking pack years	-		0.02 (-0.01 to 0.04)	0.184
Alcohol use				
Current	-		0 (reference)	
Former	-		-1.28 (-3.21 to 0.64)	0.191
Never	-		0.45 (-1.05 to 1.96)	0.556

Model 1: adjusted for age and sex.

Model 2: additionally adjusted for large infarcts on MRI, lacunae on MRI, WMH volume on MRI, hypertension, diabetes mellitus, carotid stenosis ≥70%, body mass index, alcohol use and smoking pack years at baseline.

ICC model 1: 0.54. ICC model 2: 0.52. Marginal R² Model 1: 0.27. Conditional R² Model 1: 0.65. Marginal R² Model 2: 0.33. Conditional R² Model 2: 0.65.

^a Per standard deviation decrease.

^b Per year increase.

^c Females vs. males.

^d Natural log-transformed due to a non-normal distribution and normalized for total intracranial volume.

pCBF: parenchymal cerebral blood flow, BPF: brain parenchymal fraction, CI: confidence interval, WMH: white matter hyperintensity.

Time-varying BPF as a predictor of time-varying pCBF

Lower BPF was associated with lower pCBF at baseline and follow-up, adjusted for age and sex. Each standard deviation decrease in BPF at a given time point was associated with

an additional 0.90 ml/min per 100 ml brain volume lower pCBF at that given time point (95% CI: -1.57 to -0.24, $p = 0.008$). The estimate attenuated and lost statistical significance after adjusting for large infarcts, lacunes and WMH volume on MRI, hypertension, diabetes mellitus, carotid stenosis $\geq 70\%$, body mass index, alcohol use and smoking pack years at baseline ($B = -0.58$ ml/min per 100 ml brain volume, 95% CI: -1.28 to 0.12, $p = 0.104$).

Baseline BPF as a predictor of longitudinal pCBF

Adjusted for age and sex, lower baseline BPF was not associated with greater subsequent decreases in pCBF ($B = 0.02$ ml/min per 100 ml brain volume, 95% CI: -0.03 to 0.07, $p = 0.439$) (Table 4). This relationship did not change after adjusting for large infarcts, lacunes and WMH volume on MRI, hypertension, diabetes mellitus, carotid stenosis $\geq 70\%$, body mass index, alcohol use and smoking pack years at baseline ($B = 0.02$ ml/min per 100 ml brain volume, 95% CI: -0.03 to 0.07, $p = 0.429$).

Sensitivity analyses

Lower baseline pCBF was associated with a greater subsequent decrease in BPF when assuming a fixed slope with time or when performing the analysis only in patients without missing data, adjusted for age, sex, large infarcts, lacunes and WMH volume on MRI, hypertension, diabetes mellitus, carotid stenosis $\geq 70\%$, body mass index, alcohol use and smoking pack years at baseline (Supplementary Table 1 and Supplementary Table 2, respectively). Baseline BPF was not associated with change in pCBF over time when assuming a fixed slope with time or when performing the analysis only in patients without missing data.

A total of 167 patients (14%) died during the study. Accounting for dropout due to death, lower baseline pCBF was associated with a greater subsequent decline in BPF ($B = -0.02$, 95% CI: -0.03 to -0.002, $p = 0.009$) in a joint model that included age, sex, large infarcts, lacunes, WMH volume, hypertension, diabetes mellitus, carotid stenosis $\geq 70\%$, body mass index, alcohol use and smoking pack years at baseline as covariates in the linear mixed and time-to-event submodels.

Discussion

In this cohort of patients with manifest arterial disease, we observed that a reduced pCBF was associated with smaller total brain volumes, and that smaller total brain volumes were associated with reduced pCBF throughout the follow-up period of 12 years. Reduced pCBF at baseline was associated with a greater subsequent decline in BPF in a model that controlled for sex, cardiovascular risk factors, brain infarcts and small vessel disease. However, reduced BPF at baseline was not associated with a greater decline in pCBF.

Our finding that lower pCBF was associated with lower BPF at baseline and at follow-up is in line with previous cross-sectional studies that reported smaller total brain volumes in patients with reduced cerebral blood flow.^{12, 13, 35} A study in patients with a history of arterial disease found a significant correlation between total cerebral blood flow measured using phase-contrast MR angiography and total brain volume.¹³ Similarly, a smaller population-based study revealed that decreased total brain perfusion measured using arterial spin labeling MRI was associated with smaller total brain volumes.¹² A study comparing patients with Alzheimer's disease with age-matched controls showed that reduced total cerebral blood flow was associated with smaller total brain volumes only in patients with Alzheimer's disease, whereas this relation was not found in the control group.³⁵ To our knowledge, only one previous study reported on the longitudinal relationship between cerebral blood flow and total brain volume.¹¹ In this population-based cohort study, reduced total cerebral blood flow was associated with greater progression of brain atrophy only in older patients, whereas a smaller brain volume at baseline was associated with a steeper decrease in total cerebral blood flow in the whole population.¹¹ Direct comparison with the findings of the present study, however, is only possible to a limited extent due to the shorter follow-up period and the use of total cerebral blood flow instead of pCBF.

We found that reduced baseline pCBF was significantly associated with greater decline in BPF, however the effect size was modest when taking into account the estimated mean annual decline in BPF. A number of remarks should be made with respect to this finding. First, the volumetric technique used in our study did not allow us to measure region-specific brain volume changes. Recent cross-sectional studies using arterial spin labeling and dynamic-susceptibility contrast MRI reported regional effects of reduced cerebral blood flow on specific brain volumes, predominantly the temporal lobes.^{12, 35, 36} Similarly, the use of phase-contrast MR angiography did not allow us to measure region-specific cerebral blood flow. It is therefore possible that the association between pCBF and progression of brain atrophy in the present study reflects regional effects of cerebral blood flow on specific brain regions. Second, the longitudinal analysis included patients with multiple BPF measurements and these patients may represent a healthier group, which may have led to an underestimation of the association of pCBF with progression of brain atrophy. Nonetheless, the significant longitudinal relationship between pCBF and BPF in the present study supports a role of cerebral blood flow in the process of neurodegeneration and, from a clinical perspective, strengthens the notion that cerebral blood flow could be a potential target for future prevention strategies of brain atrophy.¹⁷⁻¹⁹

In the present study, we chose a bidirectional modelling approach between pCBF and BPF for the following reasons. First, although experimental studies using animal models suggest that reduced cerebral blood flow may be a risk factor for brain tissue loss³⁷, some studies hypothesized that smaller brain volumes may lead to reduced metabolic demand, which in turn may lead to a greater decrease in cerebral blood flow over time.³⁸ Second, a previous longitudinal study with a shorter follow-up period reported that smaller brain

volumes at baseline were associated with a greater decline in cerebral blood flow.¹¹ The results of the present study, however, provide support for the notion that reduced pCBF is a risk factor for greater subsequent brain atrophy.

Strengths of the present study are the longitudinal design with pCBF and BPF measurements at three time points, the large sample size and the relatively long follow-up period. In addition, the detailed information on cardiovascular risk factors and cerebrovascular lesions allowed us to adjust for these possible confounders in the association between pCBF and BPF over time. Also, we used a statistical modelling approach that allowed patients to have a variable number of measurements and accounted for differences in time intervals between measurements.

Limitations are, first, that cerebral autoregulatory mechanisms to maintain adequate cerebral blood flow and cardiac output were not considered in this study, which is a major limitation. Second, as mentioned above, the volumetric technique used in our study did not allow us to measure region-specific brain volume changes and phase-contrast MR angiography did not allow region-specific assessment of blood flow, which is likely more sensitive in detecting associations with brain atrophy. Third, volumetry was performed on MRI sequences with a slice thickness of 4 mm instead of 1 mm, which is more sensitive in detecting brain volume changes. Fourth, our study sample consisted of mostly males with a relatively young age and a history of arterial disease, which may limit the generalizability of our results. Lastly, although the MRI scan protocol did not change throughout the study, each patient was not necessarily scanned using the exact same MRI scanner over time and scanner stability was not determined.

In conclusion, our findings demonstrate that reduced parenchymal cerebral blood flow is independently associated with greater progression of brain atrophy in patients with manifest arterial disease. These findings provide further support for a role of cerebral blood flow in the process of neurodegeneration.

References

1. Resnick SM, Pham DL, Kraut MA, et al. Longitudinal magnetic resonance imaging studies of older adults: a shrinking brain. *J Neurosci* 2003; 23: 3295-3301.
2. Appelman AP, van der Graaf Y, Vincken KL, et al. Total cerebral blood flow, white matter lesions and brain atrophy: the SMART-MR study. *J Cereb Blood Flow Metab* 2008; 28: 633-639.
3. Enzinger C, Fazekas F, Matthews PM, et al. Risk factors for progression of brain atrophy in aging: six-year follow-up of normal subjects. *Neurology* 2005; 64: 1704-1711.
4. Jack CR, Jr, Shiung MM, Gunter JL, et al. Comparison of different MRI brain atrophy rate measures with clinical disease progression in AD. *Neurology* 2004; 62: 591-600.
5. Jack CR, Jr., Shiung MM, Weigand SD, et al. Brain atrophy rates predict subsequent clinical conversion in normal elderly and amnesic MCI. *Neurology* 2005; 65: 1227-1231.
6. Kramer JH, Mungas D, Reed BR, et al. Longitudinal MRI and cognitive change in healthy elderly. *Neuropsychology* 2007; 21: 412-418.
7. Silbert LC, Quinn JF, Moore MM, et al. Changes in premorbid brain volume predict Alzheimer's disease pathology. *Neurology* 2003; 61: 487-492.
8. Fox NC, Scahill RI, Crum WR, et al. Correlation between rates of brain atrophy and cognitive decline in AD. *Neurology* 1999; 52: 1687-1689.
9. Raz N and Kennedy K. A systems approach to age-related change: Neuroanatomical changes, their modifiers, and cognitive correlates. 2009, pp.43-70.
10. Kitagawa Y, Meyer JS, Tanahashi N, et al. Cerebral blood flow and brain atrophy correlated by xenon contrast CT scanning. *Comput Radiol* 1985; 9: 331-340.
11. Zonneveld HI, Loehrer EA, Hofman A, et al. The bidirectional association between reduced cerebral blood flow and brain atrophy in the general population. *J Cereb Blood Flow Metab* 2015; 35: 1882-1887.
12. Alosco ML, Gunstad J, Jerskey BA, et al. The adverse effects of reduced cerebral perfusion on cognition and brain structure in older adults with cardiovascular disease. *Brain Behav* 2013; 3: 626-636.
13. van Es AC, van der Grond J, ten Dam VH, et al. Associations between total cerebral blood flow and age related changes of the brain. *PLoS One* 2010; 5: e9825.
14. van Beek AH, Claassen JA, Rikkert MG, et al. Cerebral autoregulation: an overview of current concepts and methodology with special focus on the elderly. *J Cereb Blood Flow Metab* 2008; 28: 1071-1085.
15. Sabayan B, van der Grond J, Westendorp RG, et al. Total cerebral blood flow and mortality in old age: a 12-year follow-up study. *Neurology* 2013; 81: 1922-1929.
16. Wolters FJ, Zonneveld HI, Hofman A, et al. Cerebral Perfusion and the Risk of Dementia: A Population-Based Study. *Circulation* 2017; 136: 719-728.
17. Espeland MA, Luchsinger JA, Neiberg RH, et al. Long Term Effect of Intensive Lifestyle Intervention on Cerebral Blood Flow. *J Am Geriatr Soc* 2018; 66: 120-126.
18. Muller M, van der Graaf Y, Visseren FL, et al. Hypertension and longitudinal changes in cerebral blood flow: the SMART-MR study. *Ann Neurol* 2012; 71: 825-833.

19. de la Torre JC. Cerebral Perfusion Enhancing Interventions: A New Strategy for the Prevention of Alzheimer Dementia. *Brain Pathol* 2016; 26: 618-631.
20. Geerlings MI, Appelman AP, Vincken KL, et al. Brain volumes and cerebrovascular lesions on MRI in patients with atherosclerotic disease. The SMART-MR study. *Atherosclerosis* 2010; 210: 130-136.
21. Muller M, van der Graaf Y, Algra A, et al. Carotid atherosclerosis and progression of brain atrophy: the SMART-MR study. *Ann Neurol* 2011; 70: 237-244.
22. Bakker CJ, Kouwenhoven M, Hartkamp MJ, et al. Accuracy and precision of time-averaged flow as measured by nontriggered 2D phase-contrast MR angiography, a phantom evaluation. *Magn Reson Imaging* 1995; 13: 959-965.
23. Vernooij MW, van der Lugt A, Ikram MA, et al. Total cerebral blood flow and total brain perfusion in the general population: the Rotterdam Scan Study. *J Cereb Blood Flow Metab* 2008; 28: 412-419.
24. Spilt A, Box FM, van der Geest RJ, et al. Reproducibility of total cerebral blood flow measurements using phase contrast magnetic resonance imaging. *J Magn Reson Imaging* 2002; 16: 1-5.
25. Dolui S, Wang Z, Wang DJJ, et al. Comparison of non-invasive MRI measurements of cerebral blood flow in a large multisite cohort. *J Cereb Blood Flow Metab* 2016; 36: 1244-1256.
26. Anbeek P, Vincken KL, van Bochove GS, et al. Probabilistic segmentation of brain tissue in MR imaging. *Neuroimage* 2005; 27: 795-804.
27. de Boer R, Vrooman HA, Ikram MA, et al. Accuracy and reproducibility study of automatic MRI brain tissue segmentation methods. *Neuroimage* 2010; 51: 1047-1056.
28. Wardlaw JM, Smith EE, Biessels GJ, et al. Neuroimaging standards for research into small vessel disease and its contribution to ageing and neurodegeneration. *Lancet Neurol* 2013; 12: 822-838.
29. Carmichael O, Schwarz C, Drucker D, et al. Longitudinal changes in white matter disease and cognition in the first year of the Alzheimer disease neuroimaging initiative. *Arch Neurol* 2010; 67: 1370-1378.
30. Benedictus MR, Leeuwis AE, Binnewijzend MA, et al. Lower cerebral blood flow is associated with faster cognitive decline in Alzheimer's disease. *Eur Radiol* 2017; 27: 1169-1175.
31. White IR, Royston P and Wood AM. Multiple imputation using chained equations: Issues and guidance for practice. *Stat Med* 2011; 30: 377-399.
32. Singer JD and Willett JB. *Applied longitudinal data analysis : modeling change and event occurrence*. Oxford: Oxford University Press, 2003.
33. Rizopoulos D. JM: An R Package for the Joint Modelling of Longitudinal and Time-to-Event Data. *Journal of Statistical Software; Vol 1, Issue 9 (2010)* 2010.
34. Goessens BM, Visseren FL, Kappelle LJ, et al. Asymptomatic carotid artery stenosis and the risk of new vascular events in patients with manifest arterial disease: the SMART study. *Stroke* 2007; 38: 1470-1475.
35. Benedictus MR, Binnewijzend MAA, Kuijper JPA, et al. Brain volume and white matter hyperintensities as determinants of cerebral blood flow in Alzheimer's disease. *Neurobiol Aging* 2014; 35: 2665-2670.

36. Wirth M, Pichet Binette A, Brunecker P, et al. Divergent regional patterns of cerebral hypoperfusion and gray matter atrophy in mild cognitive impairment patients. *J Cereb Blood Flow Metab* 2017; 37: 814-824.
37. Washida K, Hattori Y and Ihara M. Animal Models of Chronic Cerebral Hypoperfusion: From Mouse to Primate. *Int J Mol Sci* 2019; 20.
38. Shaw TG, Mortel KF, Meyer JS, et al. Cerebral blood flow changes in benign aging and cerebrovascular disease. *Neurology* 1984; 34: 855-862.

Supplementary Table 1. Results of the linear mixed model with BPF as dependent variable and baseline pCBF as independent variable assuming a fixed slope with time. Estimates represent fixed effects of the linear mixed model with their 95% confidence intervals for a 1 unit increase of a continuous variable or presence of a dichotomous variable unless stated otherwise.

	Estimate (95% CI)	<i>p</i> value
Intercept	78.40 (77.50 to 79.30)	<0.001
Baseline pCBF ^a	-0.10 (-0.22 to 0.02)	0.096
Rate of change		
Time ^b	-0.23 (-0.24 to -0.22)	<0.001
Time x baseline pCBF	-0.01 (-0.02 to -0.003)	0.007
Age ^b	-0.05 (-0.07 to -0.03)	<0.001
Sex ^c	0.84 (0.53 to 1.15)	<0.001
Large infarcts on MRI	-0.64 (-1.04 to -0.25)	0.001
Lacunae on MRI	-0.54 (-0.87 to -0.21)	0.001
WMH volume on MRI ^d	-0.02 (-0.12 to 0.09)	0.748
Hypertension	-0.21 (-0.45 to 0.03)	0.087
Diabetes mellitus	-1.04 (-1.34 to -0.74)	<0.001
Carotid stenosis ≥70%	-0.16 (-0.59 to 0.27)	0.465
Body mass index	0.03 (-0.00 to 0.06)	0.082
Smoking pack years	-0.01 (-0.02 to -0.01)	<0.001
Alcohol use		
Current	0 (reference)	-
Former	-0.44 (-0.86 to -0.01)	0.043
Never	0.11 (-0.22 to 0.44)	0.522

^a Per standard deviation decrease.

^b Per year increase.

^c Females vs. males.

^d Natural log-transformed due to a non-normal distribution and normalized for total intracranial volume.

BPF: brain parenchymal fraction, pCBF: parenchymal cerebral blood flow, CI: confidence interval, WMH: white matter hyperintensity.

Supplementary Table 2. Results of the linear mixed model with BPF as dependent variable and baseline pCBF as independent variable in patients without missing data. Estimates represent fixed effects of the linear mixed model with their 95% confidence intervals for a 1 unit increase of a continuous variable or presence of a dichotomous variable unless stated otherwise.

	Estimate (95% CI)	<i>p</i> value
Intercept	78.69 (77.75 to 79.62)	<0.001
Baseline pCBF ^a	-0.12 (-0.25 to 0.00)	0.053
Rate of change		
Time ^b	-0.24 (-0.25 to -0.22)	<0.001
Time x baseline pCBF	-0.01 (-0.02 to -0.003)	0.011
Age ^b	-0.05 (-0.07 to -0.03)	<0.001
Sex ^c	0.75 (0.43 to 1.08)	<0.001
Large infarcts on MRI	-0.65 (-1.07 to -0.22)	0.003
Lacunae on MRI	-0.56 (-0.91 to -0.21)	0.002
WMH volume on MRI ^d	-0.01 (-0.11 to 0.10)	0.907
Hypertension	-0.17 (-0.42 to 0.08)	0.171
Diabetes mellitus	-1.09 (-1.40 to -0.77)	<0.001
Carotid stenosis $\geq 70\%$	-0.15 (-0.60 to 0.30)	0.509
Body mass index	0.02 (-0.01 to 0.06)	0.150
Smoking pack years	-0.01 (-0.02 to -0.01)	<0.001
Alcohol use		
Current	0 (reference)	-
Former	-0.44 (-0.86 to 0.01)	0.054
Never	0.09 (-0.25 to 0.44)	0.596

^a Per standard deviation decrease.

^b Per year increase.

^c Females vs. males.

^d Natural log-transformed due to a non-normal distribution and normalized for total intracranial volume.

BPF: brain parenchymal fraction, pCBF: parenchymal cerebral blood flow, CI: confidence interval, WMH: white matter hyperintensity.

CHAPTER 10

10

General discussion

The present thesis fills several gaps in the current body of literature with respect to pathologic brain parenchymal changes on magnetic resonance imaging (MRI). Specifically, in the present thesis we focused on white matter hyperintensities of presumed vascular origin, cerebral microinfarcts in the deep gray matter and brain atrophy.

Quantitative MRI markers in cerebrovascular diseases

In the first part of this thesis, we examined the detection and quantification of advanced white matter hyperintensity (WMH) markers on MRI and their relation to lacunes and clinical outcomes. As noted in the introductory section of this thesis, WMH of presumed vascular origin constitute a hallmark feature of cerebral small vessel disease (CSVD).¹ The severity of WMH on MRI is conventionally rated using semi-qualitative scales such as the Fazekas scale². However, with the advent of MRI segmentation techniques it is now possible to accurately determine the volume of WMH in each patient.³ Several studies demonstrated that increasing WMH volume on MRI was associated with a greater risk of stroke and mortality.^{4, 5} Recent histopathologic studies, however, suggest that other features of WMH such as shape and location may also provide clinically relevant information on severity of CSVD.^{6, 7} To test this hypothesis, we developed an automated algorithm to obtain WMH volume, type and shape from 1.5T brain MRI scans. In **Chapter 2**, we first applied this automated algorithm to brain MRI scans of 999 patients participating in the SMART-MR study. After successfully obtaining information on WMH markers, we then performed cross-sectional analyses to determine the relationship between WMH markers and presence of lacunes on MRI. Lacunes and WMH both represent hallmark features of CSVD⁸, however how the two are related is not clear. We found that presence of lacunes was associated with greater WMH volumes, an increased risk of a confluent WMH type, and a more irregular shape of WMH, all characteristics that correspond to more severe small vessel changes in histopathologic studies.^{6, 9}

After establishing that we can obtain quantitative WMH markers from brain MRI scans using our automated algorithm, we then investigated whether quantitative WMH markers on MRI are related to risk of mortality and ischemic stroke in **Chapter 3**. In the same group of 999 patients, we found that a greater volume and a more irregular shape of periventricular and confluent WMH were associated with a higher risk of death and ischemic stroke over a median follow-up period of 12.5 years. These results indicate that several features of WMH may provide information on CSVD severity and prognosis.

After we obtained quantitative advanced WMH markers, we took a step further by performing a combined analysis of brain parenchymal changes on MRI in relation to detrimental clinical outcomes in 1003 patients participating in the SMART-MR study. This study sample consisted of the 999 patients in which we determined the WMH markers using our automated algorithm, together with four patients that did not show any WMH

on their 1.5T brain MRI. The reasoning for a combined analysis is that neurodegenerative and cerebrovascular diseases can lead to heterogeneous brain parenchymal changes on MRI.¹⁰ Often, several types of brain parenchymal changes on MRI are present in one patient, making it difficult to determine the clinical and prognostic relevance of these changes. Therefore, in **Chapter 4**, we used hierarchical clustering (a machine learning method based on artificial intelligence) to identify 11 distinct MRI phenotypes. After correlating these MRI phenotypes with follow-up data, we observed that the risk of mortality and ischemic stroke differed considerably between the 11 MRI phenotypes. Specifically, we observed that patients in the subgroup with brain atrophy, WMH and lacunes showed an almost fourfold risk of mortality compared to subgroups with limited brain parenchymal changes on MRI.

Microinfarcts in the deep gray matter on MRI

In the second part of this thesis, we examined microinfarcts in the deep gray matter on 7T brain MRI. The term “cerebral microinfarct” originates from the field of neuropathology and refers to small ischemic lesions that are not visible to the naked eye on gross pathology, but can be seen on microscopy.¹¹ Although small, it is believed that the effects of cerebral microinfarct on neural network integrity extends well beyond their lesion boundaries.¹² Neuropathological studies showed that cerebral microinfarcts can occur in the white matter, deep gray matter and in the cerebral cortex.¹³ The seminal work of van Veluw et al. showed for the first time that microinfarcts in the cerebral cortex can be detected *in vivo* using ultra-high field 7T brain MR imaging.¹⁴ The ability to detect microinfarcts in the cerebral cortex *in vivo* has led to a considerably greater understanding of their pathogenesis and impact on cognitive functioning.¹⁵ Subsequent studies demonstrated that cortical cerebral microinfarcts are associated with cognitive impairment and dementia, independent of cardiovascular risk factors.¹⁶

Although the clinical relevance of cortical cerebral microinfarcts has been established, studies on *subcortical* microinfarcts, and in particular those located in the deep gray matter, are lacking. Data from neuropathological studies indicate that microinfarcts in the deep gray matter were associated with worse ante mortem cognitive functioning, suggesting that these lesions could be a potential target for future prevention strategies of vascular cognitive impairment.¹⁷⁻¹⁹ Therefore, in the present thesis we investigated whether these lesions can be detected on 7T brain MR imaging, and if so, their risk factors and relation to cognitive functioning. First, in **Chapter 5**, we examined whether small ischemic lesions in the caudate nucleus can be detected on 7T brain MR imaging. We found that the imaging criteria for small infarcts in the caudate nucleus is similar to that of cortical cerebral microinfarcts on the T1-weighted, T2-weighted and FLAIR MRI sequences. Importantly, we also observed that the intra-observer and inter-observer agreement for presence,

number and individual locations of these lesions was excellent. With the ability to reliably detect microinfarcts in the caudate nucleus on 7T MRI, we expanded our work by also examining microinfarcts in the thalamus and lentiform nucleus in **Chapter 6**. Using our previously established imaging criteria, we observed that in a large group of 213 patients from the SMART-MR study, most microinfarcts were located in the thalamus. When we examined the cardiovascular risk factors and MRI correlates of microinfarcts in the deep gray matter, we noted that these lesions were associated with markers of both large vessel and small vessel disease. Another important finding was that microinfarcts in the deep gray matter were associated with cortical microinfarcts, suggesting that these lesions may have a common pathogenesis. We also examined the relation between microinfarcts and cognitive functioning, and found that presence of multiple microinfarcts in the deep gray matter was associated with poorer global cognitive functioning and across all cognitive domains.

Our findings presented in **Chapter 5** and **Chapter 6** of this thesis have several implications. First, we demonstrated the feasibility of ultra-high field 7T MRI to reliably detect microinfarcts in the deep gray matter *in vivo*. Second, our data indicate that microinfarcts in the deep gray matter may be manifestations of both small vessel and large vessel disease, suggesting that their pathogenesis is diverse, similar to cortical microinfarcts¹⁵. Third, microinfarcts in the deep gray matter may be clinically relevant lesions due to their association with worse cognitive performance.

Determinants of brain atrophy progression on MRI

In the third part of this thesis, we examined potential determinants of brain atrophy progression on MRI. In older individuals and patients with manifest atherosclerotic disease, brain atrophy is a common finding on MRI.²⁰ Brain atrophy occurs with normal ageing, however there is increasing evidence to suggest that accelerated brain atrophy is a risk factor for cognitive decline and dementia.²¹⁻²³ In addition, in patients with manifest atherosclerotic disease, smaller brain volumes were shown to be associated with an increased risk of mortality and ischemic stroke.²⁴ As noted in the introductory section of this thesis, the determinants of brain atrophy progression are not entirely clear, however increasing age, male sex, diabetes mellitus and CSVD have been suggested as potential risk factors in previous longitudinal studies.²⁵

Carotid artery stenosis (CAS) may also represent a risk factor for brain atrophy progression.^{26, 27} There are however several gaps in the current body of literature with respect to this relationship. First, only severe CAS has been linked in longitudinal studies to greater progression of brain atrophy.²⁶ Recent cross-sectional analyses, however, indicate that even low-grade (i.e., mild) CAS may relate to smaller brain volumes.²⁸ The cross-sectional design of these studies, however, precludes establishing a potential

cause-effect relationship, and longitudinal studies examining the impact of low-grade CAS on progression of brain atrophy are lacking. Second, it remains to be determined whether the impact of CAS is on both cerebral hemispheres, or primarily on one cerebral hemisphere. Examining this topic may aid future research in elucidating the exact mechanisms underlying CAS and brain atrophy. Therefore, in **Chapter 7**, we investigated whether asymptomatic (i.e., in patients without a history of cerebrovascular disease) low-grade CAS at baseline (measured on ultrasound) was associated with change in several MRI indices of brain atrophy. We also examined whether low-grade CAS at baseline was associated with change in executive functioning and memory throughout the 12 year follow-up period. Interestingly, compared to patients without CAS, low-grade CAS was related to greater brain atrophy progression and cognitive decline, but not to change in WMH volume. These results suggest that low-grade CAS, a common finding in the general population and in patients with manifest atherosclerotic disease, may represent a novel marker for greater neurodegenerative changes in the future, independent of traditional cardiovascular risk factors. In **Chapter 8**, we found evidence to support the hypothesis that CAS leads to greater brain atrophy of the cerebral hemisphere ipsilateral to the side of stenosis. Specifically, in 654 patients who had a follow-up brain MRI after 4 years, we observed that increasing degrees of right-sided CAS on baseline ultrasound was associated with greater progression of atrophy of the right cerebral hemisphere. Importantly, this relationship was independent of brain infarcts and WMH on baseline and follow-up MRI, suggesting that mechanisms other than ischemic cerebrovascular disease may underlie the relation between CAS and brain atrophy.

In **Chapter 9**, we examined whether reduced parenchymal cerebral blood flow (pCBF) was a risk factor for greater progression of brain atrophy and vice versa. Both pCBF and total brain volumes were measured on 1.5T brain MRI scans. We used data of 1 165 patients participating in the SMART-MR study of whom 689 participated after 4 years and 297 again after 12 years. Both total brain volume and pCBF declined over time in the study sample. We observed that a reduced pCBF was associated with smaller total brain volumes at each measurement, and that a reduced pCBF at baseline was associated with a greater subsequent decline in total brain volume throughout the 12 years follow-up period. Conversely, reduced total brain volumes at baseline were not associated with a greater decline in pCBF. Our findings are an important addition to the current body of literature on the relation between cerebral blood flow and brain atrophy for several reasons. First, they indicate that global cerebral hypoperfusion may be involved in the aetiology of brain atrophy. Second, they provide support for the notion that cerebral blood flow, which can be modified by lifestyle modifications and pharmacological interventions^{29, 30}, may pose a potential target for future prevention strategies of brain atrophy.

Future prospects for research

The automated algorithm used in this thesis to quantify volume, shape and type of WMH of presumed vascular origin represents a considerable step forward in the *in vivo* analysis of WMH. Future studies are needed to determine whether the observed associations between advanced WMH markers and detrimental clinical outcomes in **Chapter 3** are also present in population based cohorts as an external validation. In addition, it should be noted that WMH are heterogeneous lesions that are not only of presumed vascular origin but can also be related to auto-immune diseases such as multiple sclerosis.^{31, 32} Quantitative WMH analysis using our automated algorithm may also be applied to brain MRI scans of patients with auto-immune diseases to determine whether WMH markers may provide clinically relevant information on disease severity and prognosis.³³

With respect to cerebral microinfarcts in the deep gray matter, future studies are warranted to examine several aspects of these lesions. First, the prevalence of microinfarcts in the deep gray matter needs to be determined in population based cohorts. In the SMART-MR study, we observed that 13% of patients showed one or more microinfarct in the deep gray matter (**Chapter 6**), however our study sample consisted entirely of patients with manifest atherosclerotic disease and these lesions may be less prevalent in the general population. Second, studies are needed to determine whether microinfarcts in the deep gray matter are also discernible on 3T MRI due to the limited availability of 7T MRI.¹⁶ Third, although our cross-sectional analyses showed that presence of microinfarcts in the deep gray matter was associated with worse cognitive performance, longitudinal studies are needed to establish an etiologic link between these lesions and cognitive impairment.

A key strength of the SMART-MR study is the relatively large number of patients included and the long follow-up period of 12 years with two follow-up brain MRI scans. These characteristics of the study provided us with valuable data on progression of brain atrophy. Although we found evidence that low-grade CAS and reduced pCBF at baseline may lead to greater progression of brain atrophy and cognitive decline (**Chapter 7** and **Chapter 9**), several questions remain unanswered. Low-grade CAS may be a marker for the cumulative effects of both measurable and non-measurable vascular risk factors on the brain.²⁸ Alternatively, low-grade CAS may lead to cerebral micro-emboli that negatively impact brain health.³⁴ To determine whether this is the case, future longitudinal studies should also take into account carotid plaque characteristics on ultrasound or MRI.³⁵ Furthermore, low-grade CAS on ultrasound should be correlated with presence and occurrence of cerebral microinfarcts on MRI (as a possible manifestation of micro-emboli), preferably in the cerebral hemisphere ipsilateral to the side of the carotid plaque. With respect to reduced pCBF as a potential risk factor for brain atrophy progression, we were not able to measure regional brain volumes or region-specific cerebral blood flow.³⁶ To determine an etiologic link between cerebral blood flow and brain atrophy, longitudinal

studies using advanced MR techniques such as arterial spin labelling in large study samples are warranted to investigate regional effects of cerebral blood flow on brain regions.

Translation into clinical practice

In the first part of this thesis, we presented several novel findings with respect to quantitative imaging markers of cerebrovascular disease and their relation to clinical outcomes. Specifically, we showed that several markers of WMH of presumed vascular origin (volume, type and shape) and several MRI phenotypes obtained using hierarchical clustering were related to an increased risk of ischemic stroke and death. Although these findings provide valuable insights into the influence of brain parenchymal abnormalities on health outcomes, a key question remains as to how these results may eventually benefit the patient. In the context of WMH of presumed vascular origin (**Chapter 3**), one such way would be to apply quantitative MRI techniques in the clinical radiological setting to efficiently and rapidly extract information on WMH markers from brain MRI scans using our automated algorithm. The quantitative neuroradiology initiative (QNI) can potentially be used as model framework for this purpose.³⁷ Quantitative WMH analysis in the clinical setting may provide several key advantages. First, such an algorithm may identify patients with excessive or irregular WMH and predict the associated risk of vascular-related death or ischemic stroke. In our study, for example, we determined that patients with as little as 2 mL of WMH had a considerably increased risk of ischemic stroke compared to patients with little or no WMH. Secondary analyses of randomized clinical trials suggest that these patients may benefit from interventions such as blood pressure lowering to ameliorate the risk of stroke.³⁸ A second advantage of quantitative MRI techniques is that WMH characteristics of an individual patient can be compared to age- and sex-matched normative data from the population to differentiate between normal (i.e., age-related) and excessive WMH. For patients with manifest atherosclerotic disease, curves depicting the distribution of WMH volume per age can be determined from our data. A third advantage is that the use of quantitative WMH analysis in the clinical setting will likely reduce the intra- and inter-observer variability of neuroradiologists in determining WMH severity. Lastly, quantitative analysis may also support the clinician in their discussion with patients regarding the potential significance and implications of WMH encountered on their brain MRI.³⁹

Several challenges however need to be overcome prior to implementation of WMH quantification into clinical neuroradiology practice. First, large normative datasets from the general population are needed to allow comparison of a patient's WMH characteristics to a range of normal values in order to contextualize the findings. Second, technical validation of the quantitative WMH tool is necessary to assess reproducibility and the impact of image artefacts. Third, quantitative WMH data obtained using automated

algorithms require integration into a radiology report in a clinically meaningful and structured manner.³⁷

Key findings of this thesis

- Both quantitative white matter hyperintensity markers on MRI as well as MRI phenotypes are associated with risk of mortality and ischemic stroke in patients with manifest arterial disease.
- Lacunes on MRI are associated with quantitative white matter hyperintensity markers that correspond to more severe small vessel changes.
- Microinfarcts in the deep gray matter can be reliably detected on 7T brain MRI, are associated with markers of both large vessel and small vessel disease, and may represent structural correlates of impaired cognitive performance.
- Reduced cerebral blood flow and low-grade carotid artery stenosis are associated with greater progression of brain atrophy in patients with manifest arterial disease.

References

1. Wardlaw JM, Smith C and Dichgans M. Mechanisms of sporadic cerebral small vessel disease: insights from neuroimaging. *Lancet Neurol* 2013; 12: 483-497.
2. Fazekas F, Barkhof F, Wahlund LO, et al. CT and MRI rating of white matter lesions. *Cerebrovasc Dis* 2002; 13 Suppl 2: 31-36.
3. Kuijf HJ, Biesbroek JM, De Bresser J, et al. Standardized Assessment of Automatic Segmentation of White Matter Hyperintensities and Results of the WMH Segmentation Challenge. *IEEE Trans Med Imaging* 2019; 38: 2556-2568.
4. Debette S and Markus HS. The clinical importance of white matter hyperintensities on brain magnetic resonance imaging: systematic review and meta-analysis. *Bmj* 2010; 341: c3666.
5. Conijn MM, Kloppenborg RP, Algra A, et al. Cerebral small vessel disease and risk of death, ischemic stroke, and cardiac complications in patients with atherosclerotic disease: the Second Manifestations of ARterial disease-Magnetic Resonance (SMART-MR) study. *Stroke* 2011; 42: 3105-3109.
6. Kim KW, MacFall JR and Payne ME. Classification of White Matter Lesions on Magnetic Resonance Imaging in Elderly Persons. *Biological Psychiatry* 2008; 64: 273-280.
7. Gouw AA, Seewann A, van der Flier WM, et al. Heterogeneity of small vessel disease: a systematic review of MRI and histopathology correlations. *J Neurol Neurosurg Psychiatry* 2011; 82: 126-135.
8. Wardlaw JM, Smith EE, Biessels GJ, et al. Neuroimaging standards for research into small vessel disease and its contribution to ageing and neurodegeneration. *Lancet Neurol* 2013; 12: 822-838.
9. Fazekas F, Kleinert R, Offenbacher H, et al. Pathologic correlates of incidental MRI white matter signal hyperintensities. *Neurology* 1993; 43: 1683-1689.
10. Doyle FH, Gore JC, Pennock JM, et al. Imaging of the brain by nuclear magnetic resonance. *Lancet* 1981; 2: 53-57.
11. Smith EE, Schneider JA, Wardlaw JM, et al. Cerebral microinfarcts: the invisible lesions. *Lancet Neurol* 2012; 11: 272-282.
12. Summers PM, Hartmann DA, Hui ES, et al. Functional deficits induced by cortical microinfarcts. *J Cereb Blood Flow Metab* 2017; 37: 3599-3614.
13. Brundel M, de Bresser J, van Dillen JJ, et al. Cerebral microinfarcts: a systematic review of neuropathological studies. *J Cereb Blood Flow Metab* 2012; 32: 425-436.
14. van Veluw SJ, Zwanenburg JJ, Engelen-Lee J, et al. In vivo detection of cerebral cortical microinfarcts with high-resolution 7T MRI. *J Cereb Blood Flow Metab* 2013; 33: 322-329.
15. van Veluw SJ, Shih AY, Smith EE, et al. Detection, risk factors, and functional consequences of cerebral microinfarcts. *Lancet Neurol* 2017; 16: 730-740.
16. Hilal S, Sikking E, Shaik MA, et al. Cortical cerebral microinfarcts on 3T MRI: A novel marker of cerebrovascular disease. *Neurology* 2016; 87: 1583-1590.
17. Troncoso JC, Zonderman AB, Resnick SM, et al. Effect of infarcts on dementia in the Baltimore longitudinal study of aging. *Ann Neurol* 2008; 64: 168-176.

18. Gold G, Kovari E, Herrmann FR, et al. Cognitive consequences of thalamic, basal ganglia, and deep white matter lacunes in brain aging and dementia. *Stroke* 2005; 36: 1184-1188.
19. White L, Petrovitch H, Hardman J, et al. Cerebrovascular pathology and dementia in autopsied Honolulu-Asia Aging Study participants. *Ann NY Acad Sci* 2002; 977: 9-23.
20. Resnick SM, Pham DL, Kraut MA, et al. Longitudinal magnetic resonance imaging studies of older adults: a shrinking brain. *J Neurosci* 2003; 23: 3295-3301.
21. Fox NC, Scahill RI, Crum WR, et al. Correlation between rates of brain atrophy and cognitive decline in AD. *Neurology* 1999; 52: 1687-1689.
22. Jack CR, Jr., Shiung MM, Gunter JL, et al. Comparison of different MRI brain atrophy rate measures with clinical disease progression in AD. *Neurology* 2004; 62: 591-600.
23. Jack CR, Jr., Shiung MM, Weigand SD, et al. Brain atrophy rates predict subsequent clinical conversion in normal elderly and amnesic MCI. *Neurology* 2005; 65: 1227-1231.
24. van der Veen PH, Muller M, Vincken KL, et al. Brain volumes and risk of cardiovascular events and mortality. The SMART-MR study. *Neurobiol Aging* 2014; 35: 1624-1631.
25. Enzinger C, Fazekas F, Matthews PM, et al. Risk factors for progression of brain atrophy in aging: six-year follow-up of normal subjects. *Neurology* 2005; 64: 1704-1711.
26. Muller M, van der Graaf Y, Algra A, et al. Carotid atherosclerosis and progression of brain atrophy: the SMART-MR study. *Ann Neurol* 2011; 70: 237-244.
27. Romero JR, Beiser A, Seshadri S, et al. Carotid artery atherosclerosis, MRI indices of brain ischemia, aging, and cognitive impairment: the Framingham study. *Stroke* 2009; 40: 1590-1596.
28. Alhusaini S, Karama S, Nguyen TV, et al. Association between carotid atheroma and cerebral cortex structure at age 73 years. *Ann Neurol* 2018; 84: 576-587.
29. Espeland MA, Luchsinger JA, Neiberg RH, et al. Long Term Effect of Intensive Lifestyle Intervention on Cerebral Blood Flow. *J Am Geriatr Soc* 2018; 66: 120-126.
30. de la Torre JC. Cerebral Perfusion Enhancing Interventions: A New Strategy for the Prevention of Alzheimer Dementia. *Brain Pathol* 2016; 26: 618-631.
31. Cannerfelt B, Nystedt J, Jönsen A, et al. White matter lesions and brain atrophy in systemic lupus erythematosus patients: correlation to cognitive dysfunction in a cohort of systemic lupus erythematosus patients using different definition models for neuropsychiatric systemic lupus erythematosus. *Lupus* 2018; 27: 1140-1149.
32. Aradi M, Schwarcz A, Perlaki G, et al. Quantitative MRI studies of chronic brain white matter hyperintensities in migraine patients. *Headache* 2013; 53: 752-763.
33. Inglese F, Jaarsma-Coes MG, Steup-Beekman GM, et al. Neuropsychiatric systemic lupus erythematosus is associated with a distinct type and shape of cerebral white matter hyperintensities. *Rheumatology (Oxford)* 2022; 61: 2663-2671.
34. Spence JD. Transcranial Doppler monitoring for microemboli: a marker of a high-risk carotid plaque. *Semin Vasc Surg* 2017; 30: 62-66.
35. Casadei A, Floreani M, Catalini R, et al. Sonographic characteristics of carotid artery plaques: Implications for follow-up planning? *J Ultrasound* 2012; 15: 151-157.

36. Wirth M, Pichet Binette A, Brunecker P, et al. Divergent regional patterns of cerebral hypoperfusion and gray matter atrophy in mild cognitive impairment patients. *J Cereb Blood Flow Metab* 2017; 37: 814-824.
37. Goodkin O, Pemberton H, Vos SB, et al. The quantitative neuroradiology initiative framework: application to dementia. *Br J Radiol* 2019; 92: 20190365.
38. Ikeme JC, Pergola PE, Scherzer R, et al. Cerebral White Matter Hyperintensities, Kidney Function Decline, and Recurrent Stroke After Intensive Blood Pressure Lowering: Results From the Secondary Prevention of Small Subcortical Strokes (SPS 3) Trial. *J Am Heart Assoc* 2019; 8: e010091.
39. Yassi N and Campbell BCV. White Matter Hyperintensities: How Much (and What Shape) Is Too Much? *Neurology* 2021; 96: 781-782.

APPENDICES

A

Appendices

Dutch summary (Nederlandse samenvatting)
Acknowledgements (Dankwoord)
Curriculum Vitae
List of publications

Dutch summary (Nederlandse samenvatting)

Cerebrovasculaire ziekten zijn aandoeningen waarbij pathologische veranderingen optreden in de bloedvaten van de hersenen. Deze veranderingen kunnen leiden tot afwijkingen in het hersenparenchym die middels beeldvorming of histologie gedetecteerd kunnen worden. Cerebral small vessel disease (CSVD) en large vessel disease (LVD) zijn veelvoorkomende cerebrovasculaire ziekten waarbij pathologische veranderingen optreden in respectievelijk de kleine en grote bloedvaten van de hersenen.

Het gebruik van magnetische resonantie beeldvorming (MRI) heeft geleid tot een aanzienlijke toename in kennis omtrent veranderingen in het hersenparenchym bij cerebrovasculaire ziekten. Desalniettemin is er een tekort aan kennis over een aantal belangrijke onderwerpen. Zo is recent aangetoond dat microinfarcten in de hersenschors middels ultrahoog veld 7 tesla MRI gevisualiseerd kunnen worden, maar kennis over microinfarcten in de diepe grijze stof ten aanzien van detectie, risicofactoren en relatie tot cognitief functioneren ontbreekt. Van witte stofafwijkingen van vasculaire origine, een belangrijke manifestatie van CSVD, is reeds bekend dat een grote volume op MRI geassocieerd is met mortaliteit, cognitieve achteruitgang en het optreden van dementie. Histologisch onderzoek suggereert echter dat ook andere kenmerken van witte stofafwijkingen zoals vorm en type informatie over de ernst van CSVD kunnen verschaffen. *In vivo* onderzoek middels MRI over de relatie tussen deze kenmerken van witte stofafwijkingen en klinische uitkomsten ontbreekt echter. Hersenatrofie op MRI kan een teken zijn van versnelde cognitieve achteruitgang en is geassocieerd met mortaliteit, maar er is weinig bekend over de determinanten van hersenatrofie. Recente studies suggereren dat een verlaagde cerebrale bloedflow en laaggradige carotisstenose risicofactoren kunnen vormen voor progressie van hersenatrofie. Deze onderzoeken zijn echter gebaseerd op cross-sectionele analyses, terwijl longitudinale studies (die doorgaans beter in staat zijn om een oorzaak-gevolg relatie aan te tonen) ontbreken.

Het doel van dit proefschrift is om de detectie, determinanten en relatie tot klinische uitkomsten van een aantal hersenparenchymafwijkingen op MRI te onderzoeken. Deze afwijkingen omvatten witte stofafwijkingen van vasculaire origine, cerebrale microinfarcten in de diepe grijze stof en hersenatrofie. In dit proefschrift werd gebruik gemaakt van data van de Second Manifestations of ARterial disease-Magnetic Resonance (SMART-MR) studie, een prospectief cohortonderzoek van het Universitair Medisch Centrum Utrecht onder patiënten met manifest arterieel vaatlijden.

Deel I van dit proefschrift richt zich op het bepalen van geavanceerde kenmerken van witte stofafwijkingen van vasculaire origine op MRI en hun relatie tot klinische uitkomsten. In de eerste studie (**Hoofdstuk 2**) worden deze geavanceerde kenmerken (volume, type en vorm) bepaald uit de MRI-scans van 999 patiënten middels een geautomatiseerd algoritme. Vervolgens werd het cross-sectioneel verband tussen deze kenmerken

en aanwezigheid van lacunes op MRI bepaald. Lacunes en witte stofafwijkingen van vasculaire origine zijn beide uitingen van CSVD, maar hun onderlinge relatie is onduidelijk. Lacunes bleken geassocieerd te zijn met grotere volumes en een meer irregulaire vorm van witte stofafwijkingen, kenmerken die correleren met uitgebreidere witte stofschade in histologische studies. Uit de tweede studie (**Hoofdstuk 3**) bleek dat grotere volumes en een meer irregulaire vorm van witte stofafwijkingen geassocieerd waren met een hogere kans op mortaliteit en het optreden van een herseninfarct gedurende follow-up. In de derde studie (**Hoofdstuk 4**) werden MRI fenotypes bepaald op basis van geavanceerde kenmerken van witte stofafwijkingen en overige afwijkingen van het hersenparenchym op MRI middels hiërarchische clusteranalyse, een techniek gebaseerd op kunstmatige intelligentie. Het risico op overlijden en het optreden van een herseninfarct bleek aanzienlijk te verschillen tussen de MRI fenotypes. Patiënten met een MRI fenotype bestaande uit hersenatrofie, lacunes en uitgebreide witte stofafwijkingen bleken het grootste risico op overlijden te hebben. Deze bevindingen suggereren dat geavanceerde kenmerken van witte stofafwijkingen en MRI fenotypes mogelijk in de toekomst gebruikt kunnen worden om bij individuele patiënten het risico op overlijden door vaatlijden in te schatten.

Deel II omvat studies die betrekking hebben op detectie, determinanten en relatie tot cognitief functioneren van microinfarcten in de diepe grijze stof op 7 tesla MRI. In de eerste studie (**Hoofdstuk 5**) werd geconstateerd dat microinfarcten en kleine infarctjes in de nucleus caudatus op 7 tesla MRI betrouwbaar gedetecteerd kunnen worden. Uit tweede studie (**Hoofdstuk 6**) bleek dat microinfarcten in de diepe grijze stof geassocieerd zijn met risicofactoren van zowel CSVD als LVD. Deze observatie suggereert dat de pathogenese van microinfarcten divers is. Daarnaast bleken microinfarcten in de diepe grijze stof geassocieerd te zijn met slechter algeheel cognitief functioneren, wat suggereert dat deze afwijkingen van klinische betekenis zijn.

Deel III van dit proefschrift richt zich op mogelijke risicofactoren voor progressie van hersenatrofie. In de eerste studie (**Hoofdstuk 7**) werd de relatie onderzocht tussen laaggradige carotisstenose op duplexonderzoek en veranderingen in hersenvolumes en cognitief functioneren over de tijd. De resultaten toonden dat laaggradige carotisstenose (vergeleken met afwezigheid van carotisstenose) geassocieerd was met meer hersenatrofie en cognitief verval, maar niet met veranderingen in volumes van witte stofafwijkingen. Toen de relatie tussen zijdigheid van carotisstenose en atrofie van afzonderlijke cerebrale hemisferen onderzocht werd (**Hoofdstuk 8**), bleek dat een ernstige carotisstenose geassocieerd was met meer atrofie van de cerebrale hemisfeer ipsilateraal aan de stenose. Tenslotte werd de relatie tussen cerebrale bloedflow (gemeten op MRI) en progressie van hersenatrofie onderzocht (**Hoofdstuk 9**). Uit de resultaten bleek dat een verlaagde cerebrale bloedflow geassocieerd was met meer hersenatrofie onafhankelijk van

cardiovasculaire risicofactoren. Deze bevindingen suggereren dat interventies gericht op carotisstenose en cerebrale bloedflow mogelijk kunnen leiden tot minder hersenatrofie.

De belangrijkste bevindingen van dit proefschrift waren dat 1) MRI fenotypes en kwantitatieve MRI markers van witte stofafwijkingen van vasculaire origine geassocieerd zijn met het risico op mortaliteit en het optreden van een herseninfarct, 2) lacunes op MRI geassocieerd zijn met kwantitatieve MRI markers van witte stofafwijkingen die correleren met uitgebreidere witte stofschade, 3) microinfarcten in de diepe grijze stof betrouwbaar gedetecteerd kunnen worden op 7 tesla MRI, geassocieerd zijn met markers van zowel CSVD als LVD, en mogelijk kunnen leiden tot slechter cognitief functioneren, en 4) een verlaagde cerebrale bloedflow en laaggradige carotisstenose risicofactoren kunnen vormen voor hersenatrofie en cognitief verval.

Acknowledgements (Dankwoord)

Dit proefschrift zou niet tot stand gekomen zijn zonder de bijdrage van een groot aantal mensen. Graag zou ik hierbij mijn dank willen betuigen aan hen.

Allereerst wil ik alle deelnemers aan de SMART-MR studie bedanken die vrijwillig tijd hebben doorgebracht in de 7T MRI scanner. Het was indrukwekkend om te zien hoeveel mensen hiertoe bereid waren. De talloze ontmoetingen en de mooie gesprekken die ik met de deelnemers heb gevoerd hebben mij doen beseffen waarom klinisch wetenschappelijk onderzoek zo ontzettend belangrijk is.

Beste professor Hendrikse, beste Jeroen, dank voor je vertrouwen in mij en de vrijheid die je mij gegeven hebt om het onderzoek naar eigen inzicht te verrichten. Ook wil ik je bedanken voor alle middelen die je zo vrijelijk beschikbaar stelde gedurende het promotietraject.

Beste professor van der Graaf, hartelijk dank voor uw bereidheid om mijn proefschrift te beoordelen en om aanwezig te zijn bij mijn verdediging, ondanks het feit dat u reeds met emeritaat bent gegaan.

Beste dr. Geerlings, beste Mirjam, jouw kritische blik en epidemiologische kennis zijn onmisbaar geweest om dit onderzoek tot een goede eind te brengen. Dank voor je enorme toewijding en je vertrouwen in mij. Het Amsterdam UMC boft met een toponderzoeker zoals jij, ik hoop dat je veel plezier zult beleven in je nieuwe baan in Amsterdam.

Beste dr. de Bresser, beste Jeroen, dank voor je begeleiding, enthousiasme en bovenal vooruitstrevende en innovatieve blik. Ik ben met name trots op onze samenwerking die geleid heeft tot een mooie paper in *Neurology* over witte stofafwijkingen. Ik hoop dat we in de toekomst als collega neuroradiologen samen zullen werken.

Beste Maarten, beste *cholo*, onze gedeelde humor en blik op de wereld heeft tot een mooie vriendschap geleid. Dank voor alle steun die je mij hebt gegeven, niet alleen tijdens de periode waarin we samen onderzoek deden in Utrecht maar ook erna.

Dear dr. Rissanen, dear Ina, I will never forget your tremendous help and dedication in getting my last papers published. I greatly enjoyed working with a great clinical scientist and above all a kind person like you. I wish you all the best in finishing your neurosurgical training, I'm sure you're going to be a great neurosurgeon!

Beste dr. Vonk, beste Jet, het is mij een genoegen geweest om samen te mogen werken met een toponderzoeker zoals jij. Ik heb enorm veel geleerd van jou wat betreft statistische modellen en programmeren in R. Hartelijk dank voor al je hulp en ik wens je een hele fijne tijd toe in Amerika!

Beste dr. Zuithoff, beste Peter, ik heb enorm veel geleerd van jou wat betreft statistiek en statistische modellen. Hartelijk dank voor de fijne samenwerking.

Beste Myriam, jouw technische know-how en skills zijn onmisbaar geweest voor de witte stofafwijking analyses. Ik wil je hartelijk bedanken voor de vruchtbare samenwerking en ik weet zeker dat je een mooie toekomst tegemoet gaat als technisch geneeskundige.

Beste dr. Kuijf, beste Hugo, hartelijk dank voor je onmisbare hulp bij de beeldverwerking van de talloze MRI scans in de SMART-MR studie.

Graag zou ik ook de leden van de SMART study group, de dames van de SMART office en het ICT team van divisie Beeld (in het bijzonder Kees van Kesteren) willen bedanken.

Geachte leden van de beoordelingscommissie, dank voor jullie bereidheid om mijn proefschrift te beoordelen.

Lieve mam en lieve Muska, oneindige dank voor jullie onvoorwaardelijke liefde, geduld, steun en toewijding. Jullie stonden altijd klaar voor me als ik even niet meer wist hoe ik verder moest. Lieve mam, jij hebt mij altijd gestimuleerd om het beste uit mijzelf te halen, ik weet zeker dat ik zonder jou nooit zo ver gekomen zou zijn.

Curriculum Vitae

Rashid Ghaznawi was born on August 6th 1988 in Kabul, Afghanistan. At the age of four, he migrated to the Netherlands with his family due to civil war in his homeland. After finishing secondary education in 2006 at the Gymnasium Haganum in The Hague, he studied medicine at the Leiden University. Upon graduation in 2013, he took the United States Medical Licensing Examination Step 1 exam, which he passed at the first attempt.

Thereafter, he worked for a short period as a Pathology resident at the Erasmus Medical Center Rotterdam. From 2014 to 2015, he gained valuable clinical experience as a Neurology resident at the Reinier de Graaf Gasthuis in Delft under the supervision of dr. H.J. Gilhuis.

In November 2015, he started as a PhD candidate at the department of Radiology of the University Medical Center Utrecht on the topic of brain parenchymal changes on MRI in cerebrovascular diseases. During this PhD program, he obtained a master's degree in clinical epidemiology from the Graduate School of Life Sciences (Utrecht University).

Since March 2019, Rashid is a Radiology resident at the Haga Hospital in The Hague with specialization in neuroradiology and thoracic imaging.

List of publications

Peer-reviewed publications

Ghaznawi R, Geerlings MI, Jaarsma-Coes M, Hendrikse J and de Bresser J. Association of White Matter Hyperintensity Markers on MRI and Long-term Risk of Mortality and Ischemic Stroke: The SMART-MR Study. *Neurology*. 2021; 96: e2172-e2183.

Ghaznawi R, de Bresser J, van der Graaf Y, Zwartbol MH, Witkamp TD, Geerlings MI and Hendrikse J. Detection and characterization of small infarcts in the caudate nucleus on 7 Tesla MRI: The SMART-MR study. *J Cereb Blood Flow Metab*. 2018; 38: 1609-1617.

Ghaznawi R, Geerlings MI, Jaarsma-Coes MG, Zwartbol MH, Kuijf HJ, van der Graaf Y, Witkamp TD, Hendrikse J and de Bresser J. The association between lacunes and white matter hyperintensity features on MRI: The SMART-MR study. *J Cereb Blood Flow Metab*. 2019; 39: 2486-2496.

Ghaznawi R, Zwartbol MH, Zuithoff NP, Bresser J, Hendrikse J and Geerlings MI. Reduced parenchymal cerebral blood flow is associated with greater progression of brain atrophy: The SMART-MR study. *J Cereb Blood Flow Metab*. 2021; 41: 1229-1239.

Ghaznawi R, Zwartbol MHT, de Bresser J, Kuijf HJ, Vincken KL, Rissanen I, Geerlings MI and Hendrikse J. Microinfarcts in the Deep Gray Matter on 7T MRI: Risk Factors, MRI Correlates, and Relation to Cognitive Functioning-The SMART-MR Study. *AJNR Am J Neuroradiol*. 2022; 43: 829-836.

Ghaznawi R, Rissanen I, de Bresser J, Kuijf HJ, Zuithoff NP, Hendrikse J, Geerlings MI. Carotid artery stenosis and progression of hemispheric brain atrophy. The SMART-MR study. *Cerebrovasc Dis*. 2022: 1-8.

Ghaznawi R, Vonk JMJ, Zwartbol MHT, de Bresser J, Rissanen I, Hendrikse J, Geerlings MI. Low-grade carotid artery stenosis is associated with progression of brain atrophy and cognitive decline. The SMART-MR study. *J Cereb Blood Flow Metab*. 2022: 271678x221133859.

Jaarsma-Coes MG, **Ghaznawi R**, Hendrikse J, Slump C, Witkamp TD, van der Graaf Y, Geerlings MI and de Bresser J. MRI phenotypes of the brain are related to future stroke and mortality in patients with manifest arterial disease: The SMART-MR study. *J Cereb Blood Flow Metab*. 2020; 40: 354-364.

Vonk JMJ, **Ghaznawi R**, Zwartbol MHT, Stern Y and Geerlings MI. The role of cognitive and brain reserve in memory decline and atrophy rate in mid and late-life: The SMART-MR study. *Cortex*. 2022; 148: 204-214.

Donahue MJ, Achten E, Cogswell PM, De Leeuw FE, Derdeyn CP, Dijkhuizen RM, Fan AP, **Ghaznawi R**, Heit JJ, Ikram MA, Jezzard P, Jordan LC, Jouvent E, Knutsson L, Leigh R, Liebeskind DS, Lin W, Okell TW, Qureshi AI, Stagg CJ, van Osch MJ, van Zijl PC, Watchmaker JM, Wintermark M, Wu O, Zaharchuk G, Zhou J and Hendrikse J. Consensus statement on current and emerging methods for the diagnosis and evaluation of cerebrovascular disease. *J Cereb Blood Flow Metab*. 2018; 38: 1391-1417.

Zwartbol MHT, Geerlings MI, **Ghaznawi R**, Hendrikse J and van der Kolk AG. Intracranial Atherosclerotic Burden on 7T MRI Is Associated with Markers of Extracranial Atherosclerosis: The SMART-MR Study. *AJNR Am J Neuroradiol*. 2019; 40: 2016-2022.

Scheer N, **Ghaznawi R**, van Walderveen MAA, Koot RW and Willems PWA. Evaluation of the yield of post-clipping angiography and nationwide current practice. *Acta Neurochir (Wien)*. 2019; 161: 783-790.

Blom K, Koek HL, Zwartbol MHT, **Ghaznawi R**, Kuijf HJ, Witkamp TD, Hendrikse J, Biessels GJ and Geerlings MI. Vascular Risk Factors of Hippocampal Subfield Volumes in Persons without Dementia: The Medea 7T Study. *J Alzheimers Dis*. 2020; 77: 1223-1239.

Zwartbol MHT, van der Kolk AG, **Ghaznawi R**, van der Graaf Y, Hendrikse J and Geerlings MI. Intracranial Vessel Wall Lesions on 7T MRI (Magnetic Resonance Imaging). *Stroke*. 2019; 50: 88-94.

Zwartbol MH, van der Kolk AG, Kuijf HJ, Witkamp TD, **Ghaznawi R**, Hendrikse J and Geerlings MI. Intracranial vessel wall lesions on 7T MRI and MRI features of cerebral small vessel disease: The SMART-MR study. *J Cereb Blood Flow Metab*. 2021; 41: 1219-1228.

Rissanen I, Lucci C, **Ghaznawi R**, Hendrikse J, Kappelle LJ and Geerlings MI. Association of Ischemic Imaging Phenotype With Progression of Brain Atrophy and Cerebrovascular Lesions on MRI: The SMART-MR Study. *Neurology*. 2021; 97: e1063-e1074.

Zwartbol MHT, van der Kolk AG, **Ghaznawi R**, van der Graaf Y, Hendrikse J and Geerlings MI. Intracranial atherosclerosis on 7T MRI and cognitive functioning: The SMART-MR study. *Neurology*. 2020; 95: e1351-e1361.

Zwartbol MH, Rissanen I, **Ghaznawi R**, de Bresser J, Kuijf HJ, Blom K, Witkamp TD, Koek HL, Biessels GJ, Hendrikse J and Geerlings MI. Cortical cerebral microinfarcts on 7T MRI: Risk factors, neuroimaging correlates and cognitive functioning - The Medea-7T study. *J Cereb Blood Flow Metab.* 2021; 41: 3127-3138.

Conference proceedings (first author only)

Ghaznawi R, de Bresser J, van der Graaf Y, Zwartbol MH, Witkamp TD, Geerlings MI and Hendrikse J. Detection and characterization of small infarcts in the caudate nucleus on 7 Tesla MRI: The SMART-MR study.

- *Oral pitch presentation, 8th International Society of Vascular Behavioural & Cognitive Disorders International Meeting: VASCOG 2016, Amsterdam, Netherlands. Nominated for Young Investigator Poster Award.*

Ghaznawi R, de Bresser J, van der Graaf Y, Zwartbol MH, Witkamp TD, Geerlings MI and Hendrikse J. Detection and characterization of small infarcts in the caudate nucleus on 7 Tesla MRI: The SMART-MR study.

- *Poster presentation, 3rd European Stroke Organisation Conference: ESOC 2017, Prague, Czech Republic.*

Ghaznawi R, de Bresser J, Kuijf HJ, Zuithoff NP, Hendrikse J, Geerlings MI. Sidedness of carotid artery stenosis and brain volume loss in the left and right hemisphere: The SMART-MR study.

- *Poster presentation, 3rd European Stroke Organisation Conference: ESOC 2017, Prague, Czech Republic.*

Ghaznawi R, Zwartbol MHT, de Bresser J, Kuijf HJ, Hendrikse J, Geerlings MI. Microinfarcts in the Deep Gray Matter on 7T MRI: Risk Factors, MRI Correlates, and Relation to Cognitive Functioning-The SMART-MR Study.

- *Poster presentation, Alzheimer's Association International Conference 2020, Amsterdam, Netherlands.*

